Transfert thermique et écoulement au sein d'un conteneur isotherme avec matériau à changement de phase pour le transport de produits alimentaires : approches expérimentales et de modélisation

Tanathep Leungtongkum

université PARIS-SACLAY

Heat transfer and airflow in an insulated box with phase change material for food transport: experimental and modelling approaches

Transfert thermique et écoulement au sein d'un conteneur isotherme avec matériau à changement de phase pour le transport de produits alimentaires : approches expérimentales et de modélisation

Thèse de doctorat de l'université Paris-Saclay

École doctorale n° 581, Agriculture, alimentation, biologie, environnement et santé (ABIES)
Spécialité de doctorat : Génie des procédés
Graduate School : Biosphera. Référent : AgroParisTech

Thèse préparée dans l'unité de recherche **FRISE** (Université Paris-Saclay, INRAE), sous la direction de thèse de **Onrawee LAGUERRE**, Directrice de recherche et la co-direction de **Denis FLICK**, Professeur

Thèse soutenue à Paris-Saclay, le 24 Octobre 2023, par

Tanathep LEUNGTONGKUM

Composition du Jury

Membres du jury avec voix délibérative

Laurence FOURNAISSON Directrice de recherche, INRAE (centre IdF-Jouy-en-Josas-Antony)	Présidente
Andrew EAST Professeur, Massey University (New Zealand)	Rapporteur & Examinateur
Michel HAVET Professeur, Oniris Nantes	Rapporteur & Examinateur
Hayat BENKHELIFA Maîtresse de conférences, AgroParisTech (Université Paris-Saclay)	Examinatrice

THESE DE DOCTORAT

NNT : 2023UPASB052

université PARIS-SACLAY

ÉCOLE DOCTORALE
Agriculture, alimentation, biologie, environnement, santé (ABIES)

Titre : Transfert thermique et écoulement au sein d'un conteneur isotherme avec matériau à changement de phase pour le transport de produits alimentaires : approches expérimentales et de modélisation

Mots clés : Caisson isotherme, Transport des denrées, Transfert de chaleur, Modélisation

Résumé : Les caissons isothermes équipées d'un matériau à changement de phase (PCM Phase Change Material) jouent un rôle important dans le transport des aliments en raison de leur faible coût et de leur flexibilité. Cependant, le maintien d'une température adéquate est complexe en raison de la variabilité des conditions de fonctionnement, ce qui peut entraîner une dégradation du produit. Une approche empirique est principalement utilisée dans la pratique pour choisir le caisson et le PCM pour des conditions spécifiques. Ainsi, des modèles physiques permettant de prédire l'évolution de la température des aliments pour de larges gammes de conditions de transport sont nécessaires. Le développement de tels modèles nécessite la compréhension des transferts de chaleur et des écoulements d'air.

En ce qui concerne l'étude bibliographique, plusieurs travaux ont considéré uniquement la conduction thermique dans l'air à l'intérieur de la caisse, certains travaux récents ont pris en compte la convection naturelle. A notre connaissance, aucune étude n'a inclus le rayonnement entre le produit et les surfaces de paroi et de PCM. De nombreuses études fondamentales concernent tous les modes de transfert de chaleur dans des cavités vides, elles imposent souvent deux températures de paroi différentes tandis que les autres parois sont adiabatiques. Certaines incluent la présence d'un objet solide ou d'un milieu poreux. Ces travaux ne peuvent pas être appliqués au transport alimentaire en caisson isotherme avec PCM.

Ainsi, ce travail de doctorat vise à développer des méthodologies expérimentale et numérique pour étudier les transferts de chaleur et les écoulements d'air dans cet équipement.

Dans un premier temps, deux types de mesures ont été entreprises : la température par thermocouples et la vitesse d'air par vélocimétrie par images de particules. Dans ces études, les caissons isothermes (45 litres) avaient un coefficient de transmission thermique de 0,9 $W \cdot m^{-2} \cdot K^{-1}$, le PCM était de la glace (point de fusion ~ 0°C, 3,5 kg) et le produit test était de la Tylose (16 kg) dont les propriétés thermo-physiques sont proches de celles de la viande. Les paramètres étudiés étaient : i) conditions de chargement (vide, chargé de polystyrène extrudé et chargé de produit test), ii) position du PCM (sur une paroi latérale et en haut), iii) forme géométrique de la boîte (hauteur/longueur ≈ 1 et 1,7), iv) température ambiante (10°C à 30°C), v) température initiale du produit (4°C et 10°C) et vi) espacement sous le produit (pas d'espace et 20 mm). Les résultats ont montré l'importance de la convection naturelle dans le caisson. Le PCM doit être placé en haut d'un caisson de faible rapport d'aspect (hauteur/longueur). Il faut éviter de charger des produits chauds. La quantité requise de PCM peut être estimée en fonction de la température ambiante.

Dans un second temps, trois modèles numériques ont été développés: a) le modèle global prédit la température moyenne du produit mais ne peut pas identifier les positions les plus chaudes/froides, b) le modèle zonal prend en compte les différents transferts de chaleur et l'écoulement d'air, il différencie les régions les plus chaudes et les plus froides et c) le modèle CFD décrit en détail les champs de température et de vitesse d'air, mais a recours à des ressources de calcul importantes. Ces modèles ont été validé en comparant avec les données expérimentales et ont montré un bon accord. Enfin, cette thèse montre comment utiliser ces modèles pour répondre à plusieurs questions pratiques telles que l'effet de la conception des caissons et des conditions de fonctionnement.

université PARIS-SACLAY

ÉCOLE DOCTORALE
Agriculture, alimentation, biologie, environnement, santé (ABIES)

Title: Heat transfer and airflow in an insulated box with phase change material for food transport: experimental and modelling approaches

Keywords: Insulated box, Food transport, Heat transfer, Numerical modeling

Abstract: Insulated boxes equipped with a Phase Change Material (PCM) play an important role in food transport due to low cost and flexibility. However, temperature control during the transport is complex due to the variation of operating conditions, which may lead to product degradation. An empirical approach is mainly used in practice to choose the box and PCM for some specific conditions. Thus, physical-based models allowing the prediction of food temperature evolution under wide ranges of transport conditions are necessary. The development of such models requires the understanding of heat transfer and airflow.

Regarding literature study, several works considered only heat conduction in the air inside the box, some recent works took natural convection into account. According to our knowledge, no study included radiation between product and wall/PCM surface. Many fundamental studies concern all heat transfer modes in empty cavities. They often imposed two different wall temperatures while the other walls were adiabatic. Some works included a small solid object or porous media. These works could not be applied to food transport in an insulated box with PCM.

This Ph.D. thesis aimed to develop an experimental and numerical methodologies to study heat transfer and airflow in this equipment.

First, two types of measurements were undertaken: temperature by thermocouples and air velocity by Particle Image Velocimetry. In these studies, the 45-L insulated boxes had a heat transmission coefficient of 0.9 $W \cdot m^{-2} \cdot K^{-1}$, PCM was ice (melting point ~ 0°C, 3.5 kg) and the test product was Tylose (16 kg) whose thermo-physical properties are close to ones of meat. The influence of several parameters was studied: i) loading conditions (empty, loaded with extruded polystyrene and loaded with test product), ii) PCM position (on a side wall and at the top), iii) aspect ratio of box (height/length ≈ 1 and 1.7), iv) ambient temperature (10°C to 30°C), v) initial test product temperature (4°C and 10°C) and vi) spacing beneath the test product (no space and 20 mm). The results showed the importance of natural convection in the box. PCM should be placed at the top of a box of low aspect ratio. Loading the product with high temperature should be avoided. The required amount of PCM can be estimated in function of ambient temperature.

Second, three numerical models were developed: a) lumped model predicts average product temperature but cannot identify the warmest/coldest positions, b) zonal model takes heat transfer and airflow into account, it differentiates the warmer and colder regions and c) CFD model describes in-depth temperature and air velocity fields, but high computing resources are inevitable. These models were validated by comparison with the experimental results and showed good agreement. Finally, this thesis demonstrates how to use these models to answer several practical questions such as the effect of box design and operating conditions.

Acknowledgement

First, I would like to sincerely thank Onrawee and Denis for the supervision of this Pd.D. thesis, your guidance for the thesis direction and the future professional advice, also the helps on the personal issues. The thesis could not be achieved without your contributions.

I would like to express also the gratitude to Steven, Minh and Anthony for their advices regarding to the review article, your help resulted in the great article with several citations, which will be of advantage for my future.

I would like to express my gratitude to the thesis progress committee and thesis defense committee for all your suggestions and advice for improving my work.

Thies work could not be operated as this smooth without the help of Nattawut, who is also my friend, he help reducing the time to develop the experimental protocol by his expertise in PIV technique. Regarding to this, I would like to thank all the TECHFRI team, Alain, Sébastian, Seydina, and Elyamin. Your help is really appreciated.

Apart from this Ph.D. thesis, I also got an opportunity to conduct a mobility research project at University of Iceland. First, I would like thank Olafur and Björn for accepting me to do this project there and supporting me during the stay. I am also appreciated the help and advice from Matis, Siguron and Hildur. I am also really grateful that ABIES, the doctoral school, provided the supplementary fund for this mobility.

Next, I would like to thank my family for supporting me to do whatever I think it fits the most with no resentment. Although we are far away, I have always been thinking of you all.

Of course, I could not survive the difficulty during Ph.D. thesis without my old friends, even though most of them are in Thailand and we rarely got a chance to meet in person but we are still connected and I am grateful for that.

My friend in the laboratory are also really nice no matter who they are, the interns, the Ph.D. students, the technician even the permanent researchers. I feel very welcomed staying in France. Walid, Dihia, Ahmad, Nada, Jordan, Damien, Maria-Aurely, Suveena and all other FRISE members that I did not mention their name.

I am really happy that I got a chance to meet new people while I am abroad, either in France or in Iceland, either Thai people or foreigners. All of the connections and conversation are well appreciated. Specifically, I would like to thank AETF, association of thai students in France, who allowed me to meet new people and do a lot of activities.

Next, I would like to thank Xavier, Benoît, Sohel and other foreigners friends I met here, you are all nice and help me get through this challenging period.

I would like to express my gratitude to Chulalongkorn University for agreeing to appoint me as a future lecturer, also OCSC who provide the fund covering all the necessary cost while studying here. I would like to thank the staff in OEA Paris for their support both documental and personal issues during the stay here.

CONTENT

LIST OF FIGURES

LIST OF TABLES

INTRODUCTION

BACKGROUND AND RESEARCH INTERESTS

Food security has become an urgent issue for several years. The estimation by the World Food Program indicated that 349 million people currently have no access to a healthy diet (Alleyne, 2023) and this number could reach 1.1 billion in 2050 (FAO, 2018). Recently, it was reported that about 28% of food is lost and wasted after harvest (FAO, 2019; United Nations Environment Programme, 2021). Thus, refrigeration to maintain food security by reducing food loss and waste is a subject of interest since the last decades.

Food loss and waste due to unsafe food and/or unacceptable quality are often caused by temperature abuse in cold chain. Too high temperature may result in foodborne infection and unacceptable organoleptic quality (Mercier et al., 2017; Ndraha et al., 2018). Too low temperature can cause undesirable quality in some foods, e.g. chilling injury in tropical fruit (Liu et al., 2019). Regarding frozen food, although products are kept within a suitable temperature range, temperature fluctuation allows ice recrystallization, yields bigger ice crystals and lowers the quality of the food product (Vicent et al., 2020). Hence, the cold chain must be well maintained at optimal storage temperature which depends on product nature, e.g. fish 0-2°C, fruit and vegetable 8°C (Grandison, 2011; Smith & Hui, 2004).

Transportation using insulated boxes equipped with passive cooling devices, i.e. without refrigerating equipment, such as Phase Change Material (PCM) is widely used (Robertson et al., 2017). Transport may involve a short distance (local food) or a long distance (East et al., 2009; Elliott & Halbert, 2008; Navaranjan et al., 2013) during which the ambient temperature can vary according to the season, e.g. -10°C in winter and 35°C in summer (East et al., 2009). Among the different links in the cold chain from the manufacturers to the consumers, the last mile transport to the consumers has been found to be one of the weakest. Laguerre et al. (2013) and Mercier et al. (2017) reported that this last step had the highest average temperature and the highest temperature variation. Accordingly, a cold storage system such as an insulated box with PCM could provide a solution to maintain an adequate product temperature, especially during delivery of temperature-sensitive products (Nie et al., 2020; Zhao et al., 2020a).

The main advantages of insulated boxes with PCM are low investment and operating costs, flexibility in storage temperatures, availability of several volumes, and ease of maintenance (Zhao et al., 2020a). However, two drawbacks emerge: the temperature in an insulated box is difficult to control, and temperature heterogeneity is often observed (Laguerre et al., 2008a; Margeirsson et al., 2012; Navaranjan et al., 2013). An empirical approach is mainly used in practice. It is challenging to establish physical-based models, which take into account various transport conditions (i.e. ambient

temperature and duration) for temperature prediction of various product types of different recommended storage temperatures.

There are several factors that impact the temperature of food in insulated boxes with PCM: box (insulation and geometry), PCM (melting point, position and mass), product (type and mass) and external ambient temperature. Several experimental and numerical studies reported that thermal insulation of the box exerts the most influence. The evaluation of the thermal performance of insulated boxes equipped with PCM was undertaken by different authors (Du et al., 2020; East & Smale, 2008; Navaranjan et al., 2013; Paquette et al., 2017).

In addition to the box's insulation, PCM position largely impacts temperature distribution inside insulated boxes. Placing PCM at the bottom generates the highest internal temperature and the highest temperature difference between the min. and max. values (Du et al., 2020; Laguerre et al., 2008a). For high-value products like vaccines, five or six PCM plates are placed on the internal box walls (Elliott & Halbert, 2005; Kacimi & Labranque, 2019) to compensate the heat losses through the walls during PCM melting. In this case, the useful volume for the product is significantly reduced, hence not suitable for food transport.

Understanding the physical phenomena is a key factor to optimize the operating conditions for food transport. Various phenomena are involved simultaneously in an insulated box equipped with PCM: conduction in product, solid PCM and box's wall, convection in air and melted PCM, radiation between product surface and internal wall, phase change during PCM melting and food quality evolution (Leungtongkum et al., 2022). According to the literature, several studies considered only heat transfer by conduction for model simplification (Du et al., 2020; Kozak et al., 2017; Margeirsson et al., 2012; Paquette et al., 2017; Xiaofeng & Xuelai, 2021). To better represent the real phenomena, some works include natural convection to predict the temperature profile and airflow pattern (Burgess et al., 2022; Calati et al., 2023; Rahimi-Khoigani et al., 2023). Baïri (2008) and Leporini et al. (2018) demonstrated the effect of radiation in an empty cavity. Heat exchanges in closed cavities via these three transfer modes are of the same order of magnitude; thus, it is necessary to take all of them into account (Laguerre & Flick, 2010).

In spite that natural convection in closed cavities filled with porous media or single solid objects (flat plate, cylinder and sphere) was extensively studied for various engineering applications (Miroshnichenko & Sheremet, 2018; Pandey et al., 2019), the knowledge acquired is not directly applicable in our case (e.g., meat, fruit and vegetables) with numerous product items whose dimensions are of the same order of magnitude as the cavity. Whereas there are several studies about temperature evolution in insulated boxes, there is a lack of data in literature about airflow in such boxes. The knowledge of airflow patterns and intensity is essential in natural convection because heat transfer and airflow are strongly related. This lack of airflow

data can be explained by the difficulty in measuring low air velocities as observed in natural convection (Miroshnichenko & Sheremet, 2018). The measurement of air velocity by optical techniques e.g. Laser Doppler Velocimetry (LDV) and Particle Image Velocimetry (PIV) has been successfully used to measure air velocity in several types of equipment used in the cold chain (Chaomuang et al., 2020; Pham et al., 2021). However, measurement of the air velocity in a loaded cavity such as an insulated box equipped with PCM for food transport has been investigated only rarely. The specificity in this case is that only one wall (PCM container) is at an almost constant temperature and all the other walls of the box are non-adiabatic. To our knowledge, no experimental studies combining temperature and air velocity measurements inside an empty and loaded insulated box with PCM has been conducted.

Various 2D and 3D CFD models of insulated boxes with PCM were developed (Du et al., 2020; Laguerre et al., 2018, 2019; Margeirsson et al., 2012; Paquette et al., 2017; Xiaofeng & Xuelai, 2021). These models allow the investigation in detail of the impact of design and operating conditions on temperature evolution in the space and with time. However, CFD models require a significant calculation time; for example, it took up to 8 h by using a computer with 32 GB of RAM to investigate a 3D heat transfer model of an insulated box containing food products (Paquette et al., 2017). Thus, it is not possible to apply a CFD model in real-time temperature prediction (Mercier et al., 2017). Moreover, the use of CFD software is complex and requires expertise in fluid mechanics. Hence, lumped and zonal models were also developed as a complementary approach (East et al., 2009; Laguerre et al., 2018, 2019). A lumped model assumes uniform product temperature and global heat resistances (Kozak et al., 2017; Laguerre et al., 2019) while a zonal model distinguishes warmer and colder regions (East & Smale, 2008). These models enable useful information (e.g., PCM melting duration and product temperature change during shipment) to be acquired as a function of the box design and usage conditions. However, they were often applied only for a specific box design and did not take all heat transfer modes into account although these heat transfer modes are of the same order of magnitude in terms of heat flux (Laguerre & Flick, 2004). It is to be highlighted that, the models cited above have different complexity levels, from simple to advanced. They need different kinds of input parameters and hypothesis, thus provide different outputs.

Various users are involved in the application of insulated boxes with PCM, i.e., researchers, manufacturers and stakeholders. They have different levels of expertise and their own practical questions. Hence, different numerical models (lumped, zonal and CFD model) are necessary to answer technical problems of the users in order to improve the thermal performance of food transport.

Introduction

Contexte

La sécurité alimentaire est devenue une question urgente depuis plusieurs années. Le programme alimentaire mondial indique que 349 millions de personnes n'ont actuellement pas accès à une alimentation saine (Alleyne, 2023) et ce nombre pourrait atteindre 1,1 milliard en 2050 (FAO, 2018). On estime qu'environ 28 % de la nourriture est perdue ou gaspillée après la récolte (FAO, 2019 ; Programme des Nations Unies pour l'environnement, 2021). C'est pourquoi la réfrigération qui permet de réduire les pertes et le gaspillage alimentaires est un sujet d'intérêt majeur depuis plusieurs décennies.

Les pertes et gaspillages alimentaires dus à des aliments insalubres et/ou de qualité inacceptable sont souvent causés par des températures excessives dans la chaîne du froid. Une température trop élevée peut entraîner des infections alimentaires et une qualité organoleptique inacceptable (Mercier et al., 2017 ; Ndraha et al., 2018). Une température trop basse peut entraîner un défaut de qualité de certains aliments, par ex. 'blessure' par le froid dans les fruits tropicaux (Liu et al., 2019). En ce qui concerne les aliments surgelés, bien que les produits soient conservés dans une plage de température appropriée, les fluctuations de température permettent la recristallisation de la glace ce qui produit des cristaux de glace plus gros et réduit la qualité du produit (Vicent et al., 2020). Par conséquent, la chaîne du froid doit être bien maintenue à une température optimale qui dépend de la nature du produit, par ex. le poisson 0-2°C, les fruits et légumes 8°C (Grandison, 2011 ; Smith & Hui, 2004).

Le transport à l'aide de caissons isothermes équipés de dispositifs de refroidissement passifs, c'est-à-dire sans équipement frigorifique, comme les matériaux à changement de phase (Phase Change Material: PCM) est largement utilisé (Robertson et al., 2017). Le transport peut impliquer une courte distance (nourriture locale) ou une longue distance (Elliott & Halbert, 2008 ; East et al., 2009 ; Navaranjan et al., 2013) sur laquelle la température ambiante peut varier selon la saison, par ex. -10°C en hiver et 35°C en été (East et al., 2009). Parmi les différents maillons de la chaîne du froid, des fabricants aux consommateurs, le transport des derniers kilomètres jusqu'aux consommateurs s'est révélé être l'un des plus faibles. Laguerre et al., (2013) et Mercier et al., (2017) ont rapporté que cette dernière étape avait la température moyenne la plus élevée et la variation de température la plus élevée. En conséquence, un système de stockage frigorifique tel qu'un caisson isolé avec PCM pourrait apporter une solution pour maintenir une température adéquate du produit, en particulier lors de la livraison de produits thermosensibles (Nie et al., 2020 ; Zhao et al., 2020a).

Les principaux avantages des caissons isothermes avec PCM sont les faibles coûts d'investissement et d'exploitation, la possibilité de choisir des PCM à différents points de fusion, la disponibilité de caissons de différents volumes et la facilité d'entretien (Zhao et al., 2020a). Cependant, deux inconvénients apparaissent : la température dans un caisson isotherme est difficile à contrôler et une hétérogénéité de température est souvent observée (Laguerre et al., 2008a ; Margeirsson et al., 2012 ; Navaranjan et al., 2013). Une approche empirique est principalement utilisée dans la pratique. Il est difficile d'établir des modèles basés sur la physique qui prennent en compte diverses conditions de transport (température ambiante, durée) pour des produits ayant différentes propriétés et températures de stockage recommandées.

Plusieurs facteurs impactent la température des aliments dans les caissons isothermes avec PCM : caractéristiques du caisson (isolation et géométrie), du PCM (point de fusion, position et masse), du produit (type et masse) et température ambiante extérieure. Plusieurs études expérimentales et numériques ont rapporté que l'isolation thermique du caisson a le plus d'influence. L'évaluation des performances thermiques de caissons isothermes équipées de PCM a été effectuée par plusieurs auteurs (Du et al., 2020 ; East & Smale, 2008 ; Navaranjan et al., 2013 ; Paquette et al., 2017).

En plus de l'isolation du caisson, la position du PCM a un impact important sur la distribution de température. Placer le PCM en bas génère la température interne la plus élevée et la différence min/max de température la plus élevée (Du et al., 2020 ; Laguerre et al., 2008a). Pour les produits de grande valeur comme les vaccins, cinq ou six plaques PCM sont placées sur les parois internes du caisson (Elliott & Halbert, 2005 ; Kacimi & Labranque, 2019) pour compenser directement les pertes de chaleur à travers les parois. Dans ce cas, le volume utile pour le produit est considérablement réduit, donc inadapté au transport alimentaire.

La compréhension des phénomènes physiques est essentielle pour optimiser les conditions opératoires du transport alimentaire. Différents phénomènes interviennent simultanément dans un caisson isotherme équipée de PCM : conduction dans le produit, dans le PCM solide et dans les parois du caisson ; convection dans l'air et le PCM fondu, rayonnement entre surfaces du produit et des parois internes ; changement de phase lors de la fusion du PCM et évolution de la qualité des aliments (Leungtongkum et al., 2022). Plusieurs études ont considéré uniquement le transfert de chaleur par conduction dans un souci de simplification du modèle (Du et al., 2020 ; Kozak et al., 2017 ; Margeirsson et al., 2012 ; Paquette et al., 2017 ; Xiaofeng & Xuelai, 2021). Pour être plus réalistes, certains travaux ont inclus la convection naturelle (Burgess et al., 2022 ; Calati et al., 2023 ; Rahimi-Khoigani et al., 2023). Bairi (2008) et Leporini et al. (2018) ont démontré l'effet du rayonnement dans une cavité vide. En réalité, les échanges thermiques dans des cavités fermées via ces trois modes de transfert sont du même ordre de grandeur ; il faut donc tous les prendre en compte (Laguerre & Flick, 2010).

Bien que la convection naturelle dans des cavités fermées remplies de milieux poreux ou d'objets solides uniques (plaque plate, cylindre et sphère) ait été largement étudiée pour diverses applications d'ingénierie (Miroshnichenko et Sheremet, 2018 ; Pandey et al., 2019), les connaissances ainsi acquises ne sont pas directement applicables dans notre cas (par exemple, viande, fruits et légumes) où on a de nombreux produits dont les dimensions sont du même ordre de grandeur que la cavité. Alors qu'il existe plusieurs études sur l'évolution de la température dans les caissons isothermes, la littérature manque de données sur les écoulements d'air dans ces caissons. La connaissance de la structure et de l'intensité des écoulements d'air est essentielle en convection naturelle car le transfert de chaleur et l'écoulement sont fortement liés. Ce manque de données aérauliques peut s'expliquer par la difficulté à mesurer les faibles vitesses d'air observées en convection naturelle (Miroshnichenko et Sheremet, 2018). La mesure de la vitesse de l'air par des techniques optiques, par ex. la vélocimétrie laser Doppler (LDV) et la vélocimétrie par images de particules (PIV) ont été utilisées avec succès pour mesurer la vitesse de l'air dans plusieurs types d'équipements utilisés dans la chaîne du froid (Chaomuang et al., 2020 ; Pham et al., 2021). Cependant, la mesure de la vitesse de l'air dans une cavité chargée telle qu'un caisson isotherme équipée de PCM pour le transport de denrées alimentaires n'a été que rarement étudiée. La spécificité dans ce cas est qu'une seule paroi (PCM) est à une température quasi constante et toutes les autres parois de la cavité sont non adiabatiques. À notre connaissance, aucune étude expérimentale combinant des mesures de température et de vitesse de l'air à l'intérieur d'une enceinte isotherme vide et chargée avec du PCM n'a été menée.

Différents modèles CFD 2D et 3D de caissons isothermes avec PCM ont été développés (Du et al., 2020 ; Laguerre et al., 2018 ; 2019 ; Margeirsson et al., 2012 ; Paquette et al., 2017 ; Xiaofeng & Xuelai, 2021). Ces modèles permettent d'étudier en détail l'impact de la conception du caisson et des conditions de fonctionnement sur l'évolution de la température en fonction de la position. Cependant, les modèles CFD nécessitent un temps de calcul important ; par exemple, il a fallu jusqu'à 8 h en utilisant un ordinateur avec 32 Go de RAM pour étudier un modèle de transfert de chaleur 3D d'un caisson isotherme contenant des produits alimentaires (Paquette et al., 2017). Ainsi, il n'est pas possible d'appliquer un modèle CFD dans la prédiction de température en temps réel (Mercier et al., 2017). De plus, l'utilisation des logiciels CFD est complexe et nécessite une expertise en mécanique des fluides. Par conséquent, des modèles globaux et zonaux ont également été développés comme approche complémentaire (East et al., 2009 ; Laguerre et al., 2018 ; 2019). Un modèle global suppose une

température uniforme du produit et des résistances thermiques globales (Kozak et al., 2017 ; Laguerre et al., 2019) tandis qu'un modèle zonal distingue les régions plus chaudes et plus froides (East & Smale, 2008). Ces modèles permettent d'obtenir des informations utiles (par exemple, durée de fusion du PCM et évolution de la température du produit) en fonction de la conception du caisson et des conditions d'utilisation. Cependant, ils ne s'appliquent souvent qu'à un caisson spécifique et ne prennent pas en compte tous les modes de transfert de chaleur bien qu'ils soient du même ordre de grandeur en termes de flux de chaleur (Laguerre & Flick, 2004). Il convient de souligner que les modèles cités ci-dessus ont des niveaux de complexité différents ; ils ont besoin de différents types de paramètres d'entrée et d'hypothèses ; et ils fournissent des sorties différentes.

Différents acteurs sont impliqués dans le domaine des caissons isothermes avec PCM : des chercheurs, des fabricants et des utilisateurs. Ils ont différents niveaux d'expertise et leurs propres questions pratiques. Ainsi, différents modèles numériques (modèles globaux, zonaux et CFD) sont nécessaires pour répondre aux problèmes techniques des utilisateurs afin d'améliorer les performances thermiques du transport alimentaire.

AIM AND SCOPE

Following the previous reasoning, the present Ph.D. thesis was conducted with two main objectives.

First, it aims to develop an experimental methodology to:

- Characterize natural convection, i.e., heat transfer and airflow, in an insulated box equipped with PCM. A non-intrusive technique, Particle Image Velocimetry (PIV), was implemented to address the air velocity field and thermocouples to address the temperature field.

- Study the influence of box configuration (PCM position and box geometry) and operating conditions (ambient temperature, initial product temperature and air gap underneath the product) on flow patterns and temperature distribution.

- Derive, from the experimental data, analytical equations to estimate, for example, the maximum storage time (under which the product temperature is always under a critical value) in function of PCM mass.

Second, it aims to develop three numerical tools from basic to advanced: lumped model, zonal model and CFD model, to predict temperature evolution in an insulated box with PCM loaded with products. The lumped model predicts average product temperature evolution regarding global heat resistances. The zonal model distinguishes warmer and colder regions by taking heat transfer and airflow into account. The CFD model describes detailed temperature and velocity fields. These models were compared in view of different practical questions (effect of box design and operating conditions) and of their capacities to contribute in the prediction of food quality and safety evolution.

Objectif de la thèse

Ce travail de doctorat a été menée avec deux objectifs principaux.

Premièrement, il vise à développer une méthodologie expérimentale pour :

- Caractériser la convection naturelle, c'est-à-dire le transfert de chaleur et l'écoulement d'air, dans un caisson isotherme équipée de PCM. Une technique non intrusive : vélocimétrie par image de particules (Particle Image Velocimetry : PIV), a été mise en place pour obtenir le champ de vitesse de l'air et des thermocouples pour le champ de température.

- Étudier l'influence de la configuration du caisson (position du PCM et géométrie du caisson) et des conditions de fonctionnement (température ambiante, température initiale du produit et espace laissé sous le produit) sur la structure de l'écoulement et la distribution de température.

- Déduire, à partir des données expérimentales, des équations analytiques pour estimer, par exemple, la durée maximale de stockage (sous laquelle la température du produit est toujours inférieure à une valeur critique) en fonction de la masse de PCM.

Deuxièmement, il vise à développer trois outils numériques : modèle global (lumped), modèle zonal et modèle CFD pour prédire l'évolution de la température dans un caisson isotherme avec PCM chargé de produits. Le modèle global prédit l'évolution de la température moyenne du produit en fonction des résistances thermiques. Le modèle zonal distingue les régions plus chaudes et plus froides en tenant compte des transferts de chaleur et de l'écoulement d'air. Le modèle CFD décrit en détail les champs de température et de vitesse. On cherche à comparer ces modèles en termes de réponses qu'ils peuvent donner à différentes questions pratiques et à illustrer leurs potentialités concernant l'évolution de la qualité et de la sécurité sanitaire des aliments.

STRUCTURE OF THE THESIS

The structure of the manuscript described briefly below includes 5 chapters, it is also presented in Figure 0.1.

Chapter I: Literature review presents the state of the art of previous studies involving insulated boxes with PCM. First, several experimental and numerical studies in the field of food transportation of various product types in insulated boxes equipped with PCM (approaches, techniques and main observations) are discussed. The influence of the food characteristics, insulating material, box design, PCM properties and the external ambient temperature was analyzed. Moreover, the studies related to PCM application in other cold equipment (refrigerated trucks, cold rooms, display cabinets and domestic refrigerators) are also presented. This literature review leads to Article 1 in 2022. From there, more studies on heat transfer and airflow in a closed cavity are reported. Finally, the originality of this thesis in comparison with the previous studies is discussed.

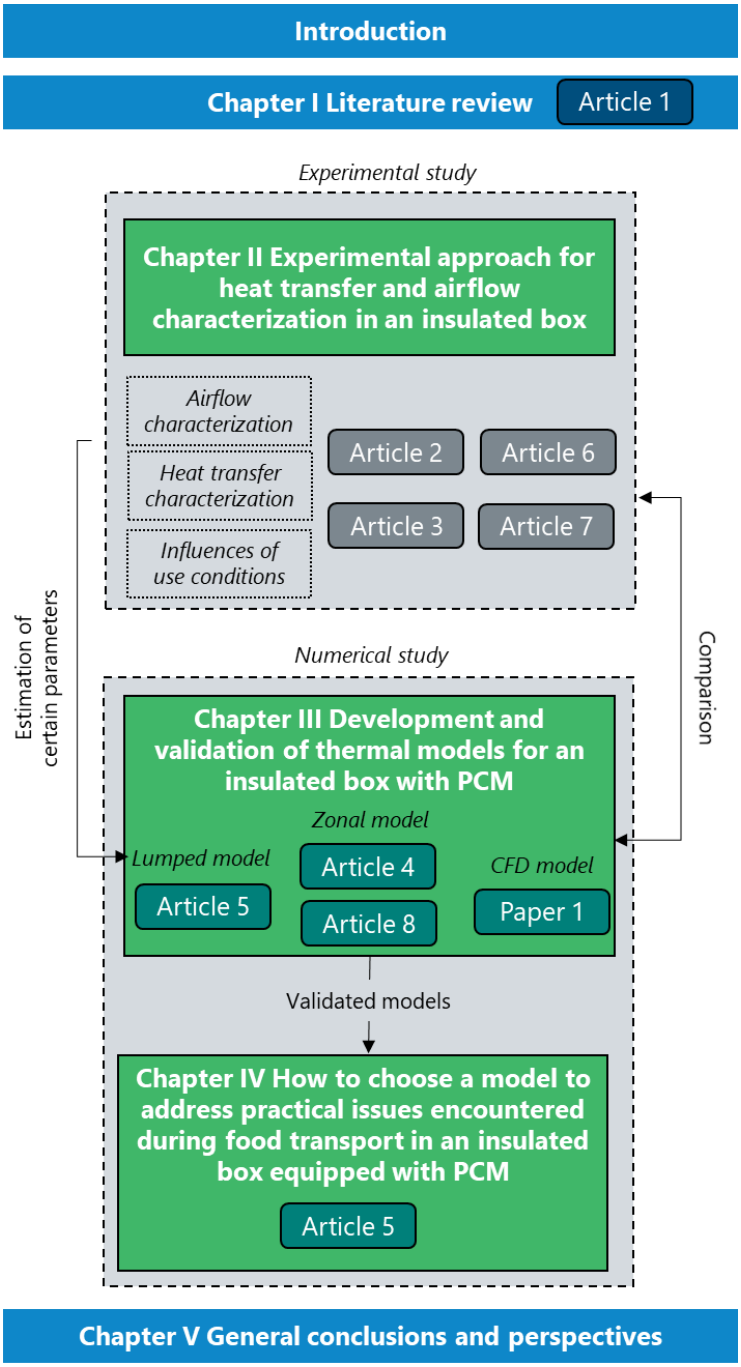

Figure 0.1 Structure of the thesis

Chapter II: Experimental approach for heat transfer and airflow characterization in an insulated box describes the developed experimental devices and protocols to characterize heat transfer and airflow in an insulated box with PCM, ice of melting point ~ 0°C in our case. It consists of temperature measurements by thermocouples and air velocity measurements by PIV technique with two challenges: low velocity (mm/s in some cases) and smog introduction in a non-isothermal system. The studying parameters were loading condition: no load, load with extruded polystyrene slabs (XPS - without heat exchange with air) and load with test product (Tylose). Next, several effects of box configurations and operating conditions were presented: effect of the

PCM position (on a sidewall and at the top), box geometry (height/width ≈ 1 and 1.7), ambient temperature (10°C to 30°C), initial test product temperature (4°C and 10°C), and spacing beneath the test product (no gap and a 20-mm gap). The availability of both temperature and velocity fields allowed a better understanding of the coupling between heat transfer and airflow in various operating conditions. Some practical outcomes were derived from the observations: estimation of maximum storage time for a given PCM mass and ambient temperature; influence of box insulation on temperature level and temperature heterogeneity. These outcomes could help the stakeholders to optimize food transport/storage using insulated boxes with PCM in terms of box insulation, mass and position of PCM to achieve the targeted storage time under a given ambient temperature. The experimental investigation has been published as articles 2 and 3 and data articles 6 and 7.

Chapter III: Development and validation of thermal models for an insulated box with PCM explains the development and validation of three modeling approaches: lumped model, zonal model and CFD model. The simple lumped model is first presented briefly (this model is presented more in detail in chapter IV). Then the hypotheses of the zonal model are presented and the validation by comparison with the experimental results are shown (Article 4 and Code Article 8). Finally, the CFD model development and validation is presented (Conference Paper 1).

Chapter IV: How to choose a model to address practical issues encountered during food transport in an insulated box equipped with PCM demonstrates how the validated thermal models (presented in chapter III) are useful to design the box and determine optimal conditions. It contains the numerical demonstrations of temperature variation under different cold chain scenarios and the estimation of the required PCM amount (for given time and ambient temperature). Then, the effect of box insulation, PCM and food characteristics (mass, properties, position) is discussed. Next, the coupling between thermal and microbiological models to predict microbial growth evolution is demonstrated. The work presented in chapter III and IV aims to propose several modelling approaches, with different complexity, for different users, to answer technical questions in food transport and storage in an insulated box with PCM. The comparison between the different approaches is presented as Article 5.

Finally, the conclusions and perspectives are provided in **Chapter V**. A list of literature cited throughout the thesis is summarized in **Reference**.

Structure de la thèse

Le manuscrit comprend 5 chapitres (cf Figure 0.1)

Le chapitre I : Etude bibliographique présente l'état de l'art des études antérieures impliquant des PCM lors du transport de produits alimentaires. Dans un premier temps, on résume plusieurs études expérimentales et numériques portant sur le transport de divers types de produits alimentaires dans des caissons isothermes équipées de PCM (approches, techniques et principaux constats). L'influence des caractéristiques des aliments, du matériau isolant, de la conception du caisson, des propriétés du PCM et de la température ambiante externe a été analysée. De plus, des études liées à l'utilisation de PCM dans d'autres équipements frigorifiques (camions frigorifiques, chambres froides, vitrines et réfrigérateurs domestiques) sont également présentées. Cette revue de la littérature (effectuée en début de thèse) a été publié en 2022 : article 1. Le chapitre I comporte en plus de cet article une analyse d'autres études sur le transfert de chaleur et les écoulements d'air dans des cavités fermées. Enfin, l'originalité de cette thèse par rapport aux études précédentes y est discutée.

Le Chapitre II : Approche expérimentale pour la caractérisation des transferts de chaleur et des écoulements d'air dans un caisson isotherme décrit les dispositifs et protocoles expérimentaux développés pour caractériser les transferts de chaleur et les écoulements d'air dans une enceinte isotherme avec PCM (glace de point de fusion ~ 0°C dans notre cas). Les mesures de température se font par thermocouples et les mesures de vitesse d'air par PIV avec deux défis : faible vitesse (mm/s dans certains cas), introduction de fumée dans un système non isotherme. Les paramètres étudiés concernent le chargement: pas de chargement (enceinte vide), chargement en polystyrène extrudé (XPS - sans échange de chaleur avec l'air) et chargement de produits test (Tylose). L'effet de la configuration du caisson et des conditions de fonctionnement sont présentés : effet de la position du PCM (sur un côté et en haut), géométrie du caisson (hauteur/largeur ≈ 1 et 1,7), température ambiante (10°C à 30°C), température initiale du produit à tester (4°C et 10°C) et espace laissé sous le produit (pas d'espace et espace de 20 mm). La disponibilité des champs de température et de vitesse a permis une meilleure compréhension du couplage entre les transferts de chaleur et l'écoulement d'air dans les différentes conditions de fonctionnement. Quelques résultats pratiques ont été dérivés des observations : estimation du temps de transport/stockage maximal pour une masse de PCM et une température ambiante données ; influence de l'isolation du caisson sur le niveau de température et l'hétérogénéité de la température. Ces résultats pourraient aider les parties prenantes à optimiser le transport/stockage des aliments à l'aide de caissons isothermes avec PCM en termes d'isolation des caissons, de masse et de position du PCM pour atteindre le temps de transport/stockage ciblé sous une température ambiante donnée. L'étude expérimentale a été publiée sous la forme deux articles 'conventionnels' : articles 2 et 3 et deux articles de données (data papers) : articles 6 et 7.

Le Chapitre III : Développement et validation de modèles thermiques pour un caisson isotherme avec PCM explique la construction et la validation de trois approches de modélisation : modèle global, modèle zonal et modèle CFD. Le modèle global, le plus simple, est d'abord présenté brièvement (ce modèle est présenté plus en détail au chapitre IV). Puis les hypothèses du modèle zonal sont présentées ainsi que sa validation par comparaison avec les résultats expérimentaux (Article 4 et Article de logiciel 8). Enfin, le développement et la validation du modèle CFD sont présentés (Communication à conférence, conference paper 1).

Le chapitre IV : Comment choisir un modèle pour répondre à des problèmes pratiques rencontrés lors du transport de denrées alimentaires dans un caisson isotherme équipée de PCM montre comment les modèles thermiques (présentés avec leur validation au chapitre III) sont utiles pour concevoir le caisson et déterminer les conditions optimales d'utilisation. Il présente des simulations numériques de l'évolution de température du produit selon différents scénarios de chaîne du froid. Il montre aussi comment estimer la quantité de PCM requise (pour un temps et une température

ambiante donnés). Ensuite, l'effet de l'isolation du caisson, des caractéristiques du PCM et des aliments (masse, propriétés, position) est discuté. Enfin, le couplage entre des modèles thermiques et microbiologiques pour prédire l'évolution de la croissance microbienne est exposé. Le travail présenté dans les chapitres III et IV vise à proposer plusieurs approches de modélisation, de complexité différente, pour divers utilisateurs, permettant de répondre à des questions techniques en matière de transport et de stockage alimentaire en caisson isotherme avec PCM. La comparaison entre les différentes approches est présentée à l'article 5.

Enfin, les conclusions et les perspectives sont fournies au **chapitre V**.

LIST OF PUBLICATIONS

In peer-reviewed journal

- Leungtongkum, T., Flick, D., Hoang, H. M., Steven, D., Delahaye, A., & Laguerre, O. (2022). Insulated box and refrigerated equipment with PCM for food preservation: State of the art. *Journal of Food Engineering*, *317*, 110874. https://doi.org/10.1016/j.jfoodeng.2021.110874 (Article 1)

- Leungtongkum, T., Laguerre, O., Flick, D., Denis, A., Duret, S., & Chaomuang, N. (2023). Experimental investigation of airflow and heat transfer by natural convection in an insulated box with a Phase Change Material using a Particle Image Velocimetry technique. *Journal of Food Engineering*, *336*, 111207. https://doi.org/10.1016/j.jfoodeng.2022.111207 (Article 2)

- Leungtongkum, T., Flick, D., Chaomuang, N., Denis, A., & Laguerre, O., (2023). Influence of Use Conditions on Heat Transfer in an Insulated Box Equipped with a Phase Change Material. *Journal of Food Engineering, 357,* 111644. https://doi.org/10.1016/j.jfoodeng.2023.111644 (Article 3)

- Leungtongkum, T., Laguerre, O., & Flick, D. (2023). Simplified heat transfer model for real-time temperature prediction in insulated boxes equipped with a phase change material. *International Journal of Refrigeration*. *149,* 286-298. https://doi.org/10.1016/j.ijrefrig.2023.02.009 (Article 4)

- Leungtongkum, T., Laguerre, O., Duret, S., & Flick, D. (n.d.). How to choose a model to answer practical questions of food transport in an insulated box equipped with PCM? (Article 5 – revision submitted to *Applied Thermal Engineering*)

Supplementary articles

- Leungtongkum, T., Laguerre, O., Flick, D., Denis, A., Duret, S., & Chaomuang, N. (2022). Dataset of experimental study investigation of airflow and heat transfer

in an insulated box equipped with a phase change material. *Data in Brief*, *45*, 108696. https://doi.org/10.1016/j.dib.2022.108696 (Article 6)

- Leungtongkum, T., Flick, D., Chaomuang, N., Denis, A., & Laguerre, O. (n.d.). Dataset of influence of Use Conditions on Heat Transfer in an Insulated Box Equipped with a Phase Change Material. (Article 7 – submitted to *Data in Brief*)

- Leungtongkum, T., Laguerre, O., & Flick, D. (2023). The code of simplified heat transfer model for temperature prediction in an insulated box equipped with phase change material. *Software Impact, 17,* 100538. https://doi.org/10.1016/j.simpa.2023.100538 (Article 8)

Conferences

- Leungtongkum, T., Flick, D., Chaomuang, N., Denis, A., & Laguerre, O. (2023, August 22). *CFD modelling of heat transfer and airflow in an insulated box equipped with Phase Change Material* [Oral presentation]. 26th International Congress of Refrigeration, Paris, France. https://doi.org/10.18462/iir.icr.2023.0556 (Paper 1)

- Leungtongkum, T., Flick, D., Hoang, H., Duret, S., Delahaye, A., & Laguerre, O. (2022, April 13). *Optimization of Food Transportation and Storage in an Insulated Box: Effect of Phase Change Material Position and Spacing Underneath the Load* [Oral presentation]. 7th IIR conference on Sustainability and the Cold Chain, Newcastle, UK [Online]. https://doi.org/10.18462/iir.iccc2022.1117

- Leungtongkum, T., Laguerre, O., & Flick, D. (2022, November 6). *Simplified heat transfer modelling for temperature prediction in an insulated box equipped with PCM* [Poster presentation]. 36th EFFoST 2022 International conference, Dublin, Ireland.

1 LITERATURE REVIEW

1.1 SUMMARY

This chapter summarizes the published studies related to insulated boxes with PCM for food transport. First, several articles investigating the use of PCM in insulated boxes and other cold equipment (refrigerated trucks, cold storage facilities, display cabinets and domestic refrigerators) are presented as shown in Article 1. As a complementary to Article 1, this chapter describes briefly the studies related to predictive models for food quality and safety, the studies dealing with transport phenomena (heat transfer and airflow) in a closed cavity. Finally, the conclusion stating the novelty of this thesis regarding the previous studies is explained.

Résumé

Ce chapitre fait un état de l'art des travaux publiées sur des caissons isothermes équipés d'un matériau à changement de phases (Phase Change Material : PCM) pour le transport alimentaire. Dans un premier temps, une synthèse des études portant sur l'utilisation de PCM dans des caissons isothermes mais aussi dans d'autres équipements frigorifiques (camions frigorifiques, entrepôts frigorifiques, vitrines et réfrigérateurs domestiques) est présentée sous la forme d'un article publié (article 1). En complément de cet article, ce chapitre décrit brièvement des études portant sur des modèles prédictifs de qualité et de sécurité des aliments et des études concernant les phénomènes de transport (transfert de chaleur et écoulement d'air) en cavité fermée. Enfin, la conclusion énonce les nouveautés de cette thèse par rapport aux études antérieures.

1.2 NOMENCLATURE

A	Area [m^2]
C_p	Heat capacity [$J \cdot kg^{-1}$]
d_c	Characteristic length [m]
$\vec{g}$	Gravitational acceleration = 9.81 $m \cdot s^{-2}$
Gr	Grashof number [-]
h	Convective heat transfer coefficient [$W \cdot m^{-2} \cdot K^{-1}$]
H	Height [m]
k	Thermal conductivity [$W \cdot m^{-1} \cdot K^{-1}$]
L	Length [m]
Nu	Nusselt number [-]
Pr	Prandtl number [-]
q	Heat flux [W]
Ra	Rayleigh number [-]
T	Temperature [°C or K]
T_f	Film temperature [°C or K]
T_∞	Fluid temperature [°C or K]
T_s	Surface temperature [°C or K]
x	Slab thickness [m]

Greek symbols

β	Thermal expansion coefficient [K^{-1}]
ε	Surface emissivity [-]
ρ	Density [$kg \cdot m^{-3}$]
μ	Dynamic viscosity [$kg \cdot m^{-1} \cdot s^{-1}$]
σ	Stefan-Boltzmann constant = 5.67 x 10^{-8} $W \cdot m^{-2} \cdot K^{-4}$

1.3 ARTICLE 1

Etat de l'art concernant les caissons isothermes et les équipements réfrigérés avec des matériaux à changement de phase pour la conservation des aliments

Résumé (version française de l'abstract de l'article 1)

L'utilisation de matériaux à changement de phase (phase change material : PCM) comme accumulateur de froid permet une meilleure préservation des aliments, accroit la sécurité sanitaire et améliore la gestion de l'énergie. Cependant, dans la pratique, l'utilisation de PCM se fait de façon empirique, en se basant sur l'expérience de l'utilisateur ou par essais/erreurs. De nombreuses études ont été réalisées sur des caissons isothermes et dans des équipements frigorifiques (camions frigorifiques, chambres froides, vitrines réfrigérées et réfrigérateurs domestiques). Elles ont analysé l'influence qu'ont différents paramètres tels que le point de fusion, la position et la masse du PCM, les propriétés et la masse de produit, le matériau d'isolation ainsi que la température extérieure sur les températures (air et produit) et la consommation d'énergie. Les paramètres les plus importants sont l'isolation des parois et la configuration du PCM. En raison des interactions complexes entre ces paramètres, ils doivent être considérés conjointement avec les conditions d'utilisation. Les relations entre échange thermique et flux d'air à l'intérieur de l'équipement doivent être étudiées plus en détail notamment en fonction de la position du PCM.

Insulated Box and Refrigerated Equipment with PCM for Food Preservation: State of the Art

Tanathep Leungtongkum[a, b], Denis Flick[b], Hong Minh Hoang[a], Duret Steven[a], Anthony Delahaye[a] and Onrawee Laguerre[a]

[a]Université Paris-Saclay, INRAE, FRISE, 92761, Antony, France
[b]Université Paris-Saclay, INRAE, AgroParisTech, UMR SayFood, 91300 Massy, France

Corresponding author e-mail: Tanathep.leungtongkum@inrae.fr

Abstract

The use of Phase Change Material (PCM) as a cold accumulator in refrigeration contexts leads to better food safety, food security and energy management. However, applying PCM in real usage still depends on the user's experience or a trial-and-error basis. Studies carried out on insulated boxes and in refrigerated equipment (refrigerated trucks, cold storage facilities, display cabinets and domestic refrigerators) were reported. The influence of the studied conditions such as PCM melting point, position, mass of PCM and load, insulation material, external temperature on air/product temperatures and energy consumption was analyzed. Important parameters enabling the application of PCM in boxes and refrigerated equipment are the wall insulation and PCM configuration cited previously. Because of the complex interactions between these parameters, they need to be considered together with the usage conditions. The relationships between heat exchange and airflow inside the equipment should be further studied notably in function to the PCM position.

Keywords: Phase change material, Food cold chain, Insulated box, Energy management

1. Introduction

The main concern during food transportation is the microbial safety of the food that could be compromised by high temperature and may result in food poisoning or foodborne infection (Mercier et al., 2017). However, products with unacceptable organoleptic quality (firmness, color), although still edible, may also be regarded as not sellable by retailers or inedible by consumers, thus leading to food waste (Ndraha et al., 2018). A temperature that is too low can also lead to undesirable quality in some foods, for example, chilling injury in tropical fruit (Liu et al., 2019). FAO (2019) reported that 1.3 billion tons per year or one-third of edible food consumed by humans is wasted worldwide. Each food product has a specific optimal storage temperature, since a storage temperature that is too high or too low can adversely affect the quality and/or safety of the food (East et al., 2009).

Regarding frozen food, although products are kept within a suitable temperature

range, temperature fluctuations can still impact their quality. Indeed, during frozen storage, ice recrystallization caused by temperature variations yields bigger ice crystals and lowers the quality of the food product (Oró et al., 2012a; 2012b; Phimolsiripol et al., 2008; Vicent et al., 2019, 2020).

Transportation using insulated boxes plays an important role in the cold chain, particularly when passive cooling devices such as Phase Change Material (PCM) are used, e.g. during shipment from the producer to the retailer, then to the consumer (Robertson et al., 2017). Transport may involve a short distance (a few kilometers for locally produced food) or long distances, e.g. from Glasgow to London (Elliott & Halbert, 2008), from Sydney to Melbourne (East et al., 2009), or from New Zealand to Singapore (Navaranjan et al., 2013). The ambient temperature during delivery can vary according to the season, e.g. -10°C in winter and 35°C in summer (East et al., 2009). Among the different links in the cold chain, the final transport to the consumer has been found to be one of the weakest. Laguerre et al. (2013) and Mercier et al. (2017) reviewed temperature abuse in the cold chain and reported that this last step had the highest average temperature and the highest temperature variation. Accordingly, a cold storage system such as a PCM could provide a solution that maintains the product temperature, especially during delivery of temperature-sensitive products (Nie et al., 2020; Zhao et al., 2020a; 2020b).

This review article investigates studies on the transport of food in insulated boxes with PCM knowing that such transport can also be used for pharmaceutical products (Yang et al., 2021). Despite the ease of use of this technology and its relatively low cost, temperature abuse can be observed, particularly due to insufficient PCM mass and inappropriate PCM position causing temperature heterogeneity inside the box. In fact, controlling the product temperature in a closed cavity is complex because of several simultaneous heat transfer modes: conduction, natural convection and radiation (Laguerre & Flick, 2010; Rincón-Casado et al., 2017; Shinoda et al., 2019). These transfer modes are of the same order of magnitude; thus, it is necessary to take all of them into account .

PCM is also used in other cold equipment such as refrigerated trucks, cold rooms, display cabinets and domestic refrigerators. Here, PCM plays an important role, not only in temperature control, but also in energy management (Schalbart et al., 2013; Sonnenrein et al., 2015b; Yilmaz et al., 2020). However, determining the optimal PCM position and mass is still the challenge in these applications (Azzouz et al., 2009; Pirdavari & Hossainpour, 2020; Schalbart et al., 2013; Yilmaz et al., 2020).

There are several review articles on PCM classification, properties and improvement (Oró et al., 2012a; 2012b; Rostami et al., 2020; Zhao et al., 2020a, 2020b). Many studies on PCM application in buildings, solar systems, or even in the food industry have been performed (Nie et al., 2020; Yang et al., 2021; Zhao et al., 2020a; 2020b). However, we have not found any review articles dedicated to the use of PCM to maintain the desired

food temperature throughout the entire cold chain equipment including insulated boxes. For instance, Zhao et al. (2020a) reviewed PCM application in refrigerated trucks, refrigerated containers and insulated boxes. Bista et al. (2018) alone reported the use of PCM in a refrigerator. It is important to investigate this subject throughout the entire cold chain in order to identify any research gaps and enhance the efficiency of the cold chain (Costa, 2020) since chilled and frozen products transport has expanded rapidly in all parts of the world in recent years. A comprehensive review devoted to all cold chain equipment would be useful for food manufacturers and logistics companies. Consequently, the objectives of this review article are firstly to present the state of the art in the field of food transportation of various product types in insulated boxes equipped with PCM (study approaches, techniques and main observations). The influence of the insulating material, box design, PCM properties and the external ambient temperature was analyzed. Secondly, the aim is to report on studies on the application of PCM in other refrigerated equipment: refrigerated trucks, cold rooms, display cabinets and domestic refrigerators where energy management is the main concern. Finally, a discussion highlights the potential and the limitations associated with the development of the use of PCM in the cold chain. Data gaps regarding the complex phenomena involving heat and mass transfer, the phase-change process and food engineering are also discussed.

2. Insulated box with PCM

There are various complex phenomena involved in an insulated box with PCM: heat conduction inside the product, PCM and the walls of the box, heat convection between the air and the product/PCM inside the box and between the external air and the box, radiation between walls, the phase change process and food quality evolution. Standard solutions cannot be widely applied as all these phenomena are impacted by the type of product itself, the operating conditions (external temperature and duration), the box dimensions, the type of PCM (latent heat, heat capacity and melting temperature), its quantity and its position in the box. The objectives of this section are to describe the existing studies in terms of the product quality (Section 2.1), type of product transported (Section 2.2), box design (Section 2.3), PCM characteristics (Section 2.4), operating conditions (Section 2.5) and influence of each factor in application and modeling (section 2.6) to identify the overall findings as well as the knowledge gaps.

2.1. Effect of PCM in insulated box on food quality

The interest of PCM application is to maintain low temperature and reduce temperature fluctuations during food transport, which leads to better food quality particularly for high perishable products. In the case of fresh fruit and vegetable, the product respires continuously during storage, which leads to heat generation. High respiration rate, a major factor contributing to the product loss, depends on product (e.g. strawberry respiration rate is 4 times higher than that of apple) and on storage

temperature (e.g. strawberry respiration rate at 15°C is 5 times higher than that at 0°C) (Chakraverty & Singh, 2001). Numerous studies have shown the interest of Modified Atmosphere Packaging (MAP) for the product shelf life extension because the gas composition in the headspace (O_2, CO_2) decreases the respiration rate. Zhao et al. (2019) studied fresh strawberry quality change using MAP in an expanded polystyrene box exposed to ambient temperature at 10°C and 20°C. Three PCM packs, previously frozen at -18°C for 24 h, were placed at the top of the box. The results were compared with the current package (air in headspace) and a control configuration where the product was directly in contact with ambient air (Figure 1.1). It was observed that MAP allowed product weight loss 30% lower than that in current package and about 160% lower than that of control after 4 days at 10°C, this effect was more significant at storage temperature at 20°C (Figure 1.1a). These authors also reported that the combination of MAP, PCM and the insulated box allows the strawberry quality preservation in terms of firmness, color, total soluble solids and global appearance (results not shown). The better quality preservation under this combination can be explained by first, MAP allows a reduction of product respiration rate (Figure 1.1b) and second, PCM allows low product temperature fluctuation. These results confirm the interest of the combination of MAP, PCM and the insulated box for delivery when the ambient temperatures are not well controlled. Gin & Farid (2010) stored frozen meat and ice cream in a domestic freezer without and with PCM (melting temperature -15.4°C). For meat, these authors reported the reduction of drip loss from 17% (without PCM) to 10% (with PCM) after 2-week storage and for ice cream, the average crystal size decreased from 70 µm - 80 µm (without PCM) to 40 µm -50 µm (with PCM). It is to be emphasized that the higher temperature fluctuation during frozen storage, the bigger the ice crystals, the lower the food quality (Oró et al., 2012a; 2012b; Phimolsiripol et al., 2008; Vicent et al., 2019, 2020).

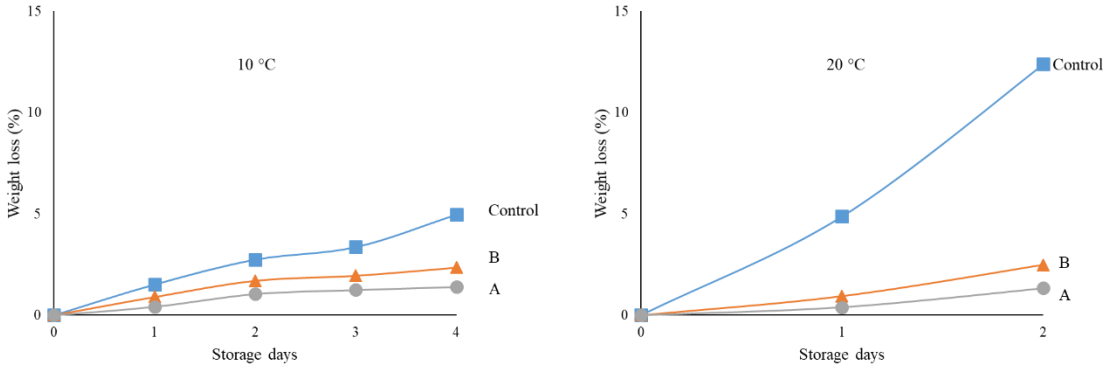

(a)

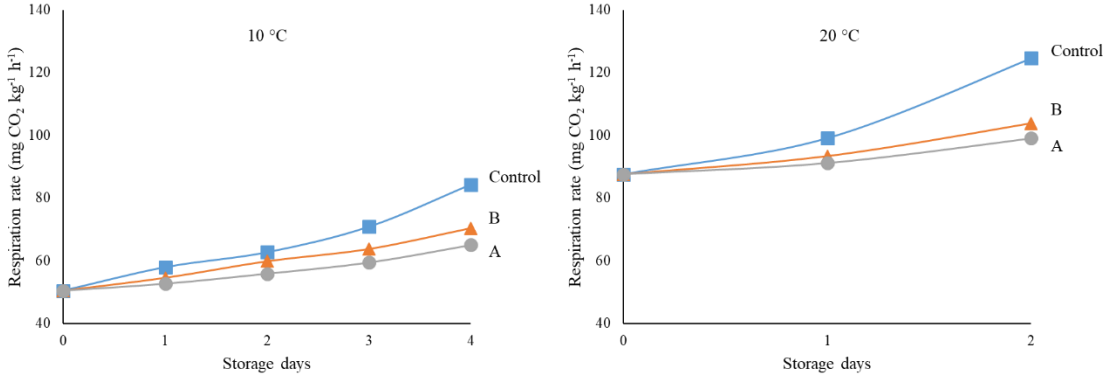

(b)

Figure 1.1 Evolution of (a) product weight loss and (b) product respiration rate of a strawberry packed in an expanded polystyrene box with PCM.

A = MA pack (10% O_2, 0% CO_2), B = air pack and C = Control (product directly in contact with ambient air). Adapted from Zhao et al. (2019)

2.2 Type of food product transported

Studies dealing with the transportation of different types of food products in insulated boxes with PCM are summarized in Table 1.1. Out of 16 studies, six of them focused on meat and fishery products since these products are extremely sensitive to temperature changes during transportation and storage. As PCM, ice packs were placed on top of the products in several experimental and numerical studies: haddock fillets (Margeirsson et al., 2011), cod fillets (Margeirsson et al., 2012), New Zealand terakihi (Navaranjan et al., 2013), horse mackerel (Laguerre et al., 2018), and sardine (Laguerre et al., 2019). Zhao et al. (2019) investigated strawberry fruit transportation using an insulated box with PCM. There were fewer studies dealing with fruit and vegetable transportation by means of insulated boxes equipped with PCM. This may be due to the fact that fruit and vegetable are not as perishable as meat products, thus, they are less sensitivity to temperature abuse (Committee, 2014). However, it could be valuable to investigate such applications as higher demand for fresh tropical produce from cold climate countries has emerged recently (ICI Business on behalf of Centre for

the Promotion of Imports from developing countries, 2020; Loria, 2021).

Delivery in an insulated box offers flexibility as it is possible to transport different types of products simultaneously (Ndraha et al., 2019). Paquette et al. (2017) studied a system with a mixed load containing food cans, vegetable packs and meat packs using gel packs, but the focus of this work was the temperature of meat and vegetables, as these products are more sensitive to temperature abuse than food cans. However, greater care is needed during transport of several types of perishable products in the same box since they require different optimal temperatures. Temperature abuse may affect the final quality of sensitive products (Paquette et al., 2017).

Kozak et al. (2017) and Paquette et al. (2017) investigated liquid foods such as bottles of water and beakers containing water, respectively. East & Smale (2008) and East et al. (2009) studied beverage cans because they could be considered as lump objects without internal heat transfer resistance via numerical modelling. These authors used numerical models for the box design optimization: the material and thickness of the box and dividers between the product and the PCM below, PCM type and thickness and initial product and PCM temperatures.

The two remaining studies were conducted on an empty box to clearly determine the impact of system design: insulating material, PCM position, melting point and compartment volume (Du et al., 2020; Xiaofeng & Xuelai, 2021). As shown in Figure 1.2, the more box surface covered by PCM, the longer warming time of air at the box center to increase from 0°C to 8°C (Du et al., 2020). This was due to greater heat exchange area between the PCM and internal air, thus, greater cooling capacity. It was observed that the PCM placed at the top and the bottom of the box gives almost the same warming time.

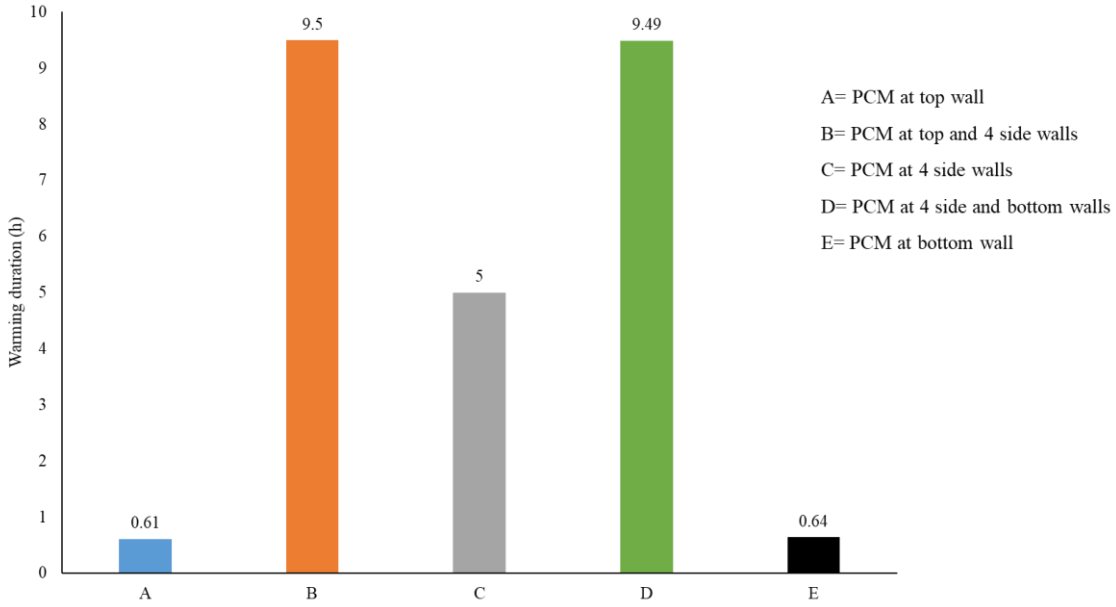

Figure 1.2 Influence of PCM position and surface area in an insulated box on warming duration defined as the duration during which the temperature at the center of the box rises from 0 °C to 8 °C. Adapted from Du et al. (2020) for a polyurethane box with PCM of 5°C melting point.

Some authors investigated the effect of product quantity on the thermal behavior of the box equipped with a PCM. Elliott & Halbert (2008) reported that a higher load quantity increases the thermal inertia, and thus generates a different temperature profile. It is to be emphasized that the load quantity and the arrangement were varied simultaneously in the experiments. Thus, it was difficult to highlight the influence of these parameters separately. Paquette et al. (2017) compared the temperature profile when one beaker of water and 4 beakers of water were placed in a box. They found that the rate of temperature increase was 20% lower in the box with 4 beakers, can be explained by the higher product inertia in comparison with 1 beaker. However, a higher load quantity may lead to a lower cooling rate if the load is not previously chilled before packing, and this causes deterioration in quality. Laguerre et al. (2018) indicated that the greater the thickness of a stack of fish in the box, the longer the cooling duration.

The load type also impacts the temperature profile because of different thermal properties. Kacimi & Labranque (2019) studied the effect of the load using an empty bag (lower thermal inertia) and a bag of water (higher thermal inertia). They noted that by using bags of water, the temperature could be maintained for a longer period of 131 h compared with 115 h for empty bags.

Table 1.1 Summary of studies using PCM in insulated boxes

Reference / Product	**PCM (melting point) / position**	**Box material (internal dimensions)**	**Type of the study**	**Main observation(s)**
Margeirsson et al. (2011) / Haddock fillets	Ice pack (0°C) / on top of the product	- Expanded polystyrene (EPS) (35.6 cm x 22.0 cm x 8.5 cm) - Corrugated plastic (CP) (37.0 cm x 23.0 cm x 8.0 cm)	Experimental and numerical (3D CFD)	- The warmest position was at the bottom corner - The coldest position was at the top center - After 6 h, the temperature increase in EPS and CP boxes was 8°C and 14°C, respectively - Ice pack decreased the product temperature by around 4°C but increased its heterogeneity (up to 8°C compared with 3°C in the box without an ice pack).
Margeirsson et al. (2012) / Cod fillets	Ice pack (-0.5°C to 0.5°C) / on top of the product	EPS with - Sharp corners (35.6 cm x 22.0 cm x 10.9 cm) - Rounded corners (35.6 cm x 22.0 cm x 9.0 cm)	Experimental and numerical (3D CFD)	- The warmest position was at the bottom corner - The coldest position was at the top center - Fillets in rounded box had a 2°C lower temperature difference and a shelf life that was 2 days longer.

Navaranjan et al. (2013) / New Zealand terakihi (*Nemadactylus macropterus*)	Ice pack (0°C) / in the center at the top of the box	6 Boxes with the same dimensions (55.0 cm x 37.5 cm x 12.0 cm) - 3 In-house EPS with 1.0 cm, 1.5 cm and 2.5 cm thickness (E10, E15 and E25) - 1 Commercial EPS box (CE) - 1 box-in-box using CP with 1.5 cm gap (B1) - 1 improved box-in-box with 2.1 cm gap and covered with aluminum foil (B2)	Experimental	- The warmest position was at the corner - The coldest position was at the center - Thermal resistance (R) of B2 is twice that of B1 but less than CE and it positively related to the thickness of in-house EPS box. - Fish quality estimated by time-temperature profile related to R value of the insulating material with a coefficient of determination > 0.80.
Paquette et al. (2017) / Water beaker, food can, meat pack, vegetable pack and fresh-cut lettuce pack	Gel pack (0°C) / at different locations in the box related to the meat pack: on the side, above, below and both above and below	Multilayer box in CP box (40.4 cm x 31.9 cm x 21.5 cm)	Numerical (3D heat transfer) with experimental validation	- Use of aluminum foil led to 13% and 10% lower meat and lettuce temperatures (in °C), respectively. - More gel packs prolonged the time needed for meat to reach 10°C: 6.0 h (without a gel pack) and 36.6 h (6 kg gel pack). - The configuration with the gel pack at the center was the most efficient.

				- Thermal conductivity of insulation had the most influence on product temperature.
Laguerre et al. (2018) / Horse mackerel (*Trachurus*)	Flaked ice (0°C) / top of fish stack	EPS box with 3 cm thickness	Experimental and numerical (1D analytical model and 2D CFD)	- The warmest position was at the bottom - The coldest position was at the top - 2D CFD could predict the cooling front in the box. - The cooling time of the bottom stack correlated with the fish stack's thickness.
Laguerre et al. (2019) / Sardine	Ice pack (-0.1°C to 0.1°C) / top of the fish stack	2 EPS box with different dimensions. A: 21.0 cm x 21.0 cm x 17.9 cm with 1.8 cm thickness B: 17.5 cm x 23.5 cm x 15.3 cm with 2.5 cm thickness	Experimental and numerical (1D analytical model and 3D Finite Element Method or 3D FEM)	- The warmest position was at the bottom corner - The coldest position was at the top - 1D analytical model could roughly predict melting time and highest product temperature. - 3D FEM could determine temperature profile more accurately, particularly under real conditions.

Zhao et al. (2019) / Strawberries	Commercial PCM (-2.0°C to -1.2°C) / top wall of the box	EPS (29.0 cm x 17.5 cm x 13.0 cm)	Experimental	- The stored sample packed in the box and PCM had a higher organoleptic quality than that without PCM. - The weight loss of the product decreased 3% and 10% while the respiration rate was reduced 22% and 17% under 10°C and 20°C conditions, respectively compared with no package.
Du et al. (2020) / No load	PCM (0°C, 2°C, 3°C, 4°C, 5°C and 8°C) / 5 configuration - 100% top (A) - 20% each side and top (B) - 25% each side (C) - 20% each side and bottom (D) - 100% bottom (E)	Polyurethane (PU) or vacuum insulated panels (VIPs) (35.5 cm x 21.5 cm x 26.5 cm)	Numerical (3D heat transfer model) with experimental validation	- A PU box + PCM with melting points of 2°C and 8°C gave the highest cooling time (9.6 h) and lowest cooling time (2.1 h), respectively. - Configuration B led to highest cooling time (9.6 h) while configuration A and E had the lowest values (around 0.6 h). - VIPs allowed a longer cooling duration than PU (up to 36.9 h).

Xiaofeng & Xuelai (2021) / No load	2 PCM type: A: 87% n-caprylic acid and 13% myristic acid (7.1°C) for chilled storage B: potassium sorbate solution (-2.1°C) for sub-zero storage/ 4 side walls and a bottom of each compartment	PU and VIP (145 cm x 75 cm x 65 cm) divided into 3 compartments for 1) ambient storage (no PCM), 2) chilled storage at 7°C to 10°C with PCM A, and 3) storage at -3°C to -1°C with PCM B with volume ratios of 1:1:1 and 1:2:2.	Numerical (3D unsteady model) with experimental validation	- The warmest position was at the top corner of first compartment - The coldest position was at the wall's surface between second and third compartment - In the box with 1:1:1 volume ratio, the temperature in the second and third compartments was maintained at the desired range for 15 h and 16.5 h, respectively. - But it was only 10.8 h, and 11.5 h, respectively in the box with 1:2:2 volume ratio.
Elliott & Halbert (2005) / Small boxes containing empty packages	Ice brix® frozen gel pack: 3, 4, 8 and 16 packs (charging at -20°C) / the wall of the box	Polystyrene (32.0 cm x 32.0 cm x 24.5 cm)	Experiment and transit test to maintain the temperature between 0°C and 8°C	- 3 gel packs gave the desired temperature range. - Placing PCM before product loading (for 4 h or 24 h) or preconditioning prevented storage conditions that were too cold. - Transporting with 3 gel packs resulted in acceptable temperature profiles in all

				seasons except in summer, when 4 gel packs were needed.
Elliott & Halbert (2008) / Small boxes containing empty packages	dry ice (CO_2: -78.5°C) / bottom of the box	EPS box (32 cm x 32 cm x 29.5 cm)	Experiment and transit test to maintain temperature below -10°C	- The warmest position was at the top - The coldest position was at the bottom - The preferable configuration was when dry ice was placed closer to the product with the highest temperature at -21.9°C. - All transit tests during real transport yielded good results.
Laguerre et al. (2008a) / Cartons of several product units	PCM (-0.5°C) / top, middle and bottom of the container	Corrugated cardboard insulated with polystyrene plates (108 cm x 72 cm x 137 cm)	Experimental and numerical (excitation-response model)	- The warmest position was at the middle of the side wall - The coldest position was at the bottom center - The model was validated and able to predict the product temperature inside the container exposed to a variable ambient temperature when the PCM was not completely melted.

Kacimi & Labranque (2019) / Empty packages and water bags	- Organic PCM (5°C) / all box faces - Inorganic PCM (21°C) / bottom, top and two opposite sides	VIPs with 15 L, 27 L, 40 L and 64 L	Experimental	- The warmest position was at the top - The coldest position was at the bottom - Organic PCM could withstand cold better than warm conditions when the inorganic PCM could perform better. - The boxes with 27 L and 40 L volumes were more efficient than the other two box sizes.
Kozak et al. (2017) / Water bottle	Salt solution (-10°C for small box or -33°C for big box) / in bottles placed inside the box	Cardboard box (external dimensions: 32 cm x 25 cm x 25 cm – small; and 50 cm x 50 cm x 50 cm – big) with insulating material fitted with the bottle	Experimental and numerical (1D analytical model)	- The warmest position was at the top - The coldest position was at the bottom - Changing Biot number from 1 to 4 did not markedly affect the melting time. - Melting time was affected by the ratio between the thermal conductivity of the liquid PCM and insulation.

East & Smale (2008) / Beverage cans	Ice pack (0°C), or commercial PCM (2°C and 5°C) / below the product	Polyurethane or polystyrene (28.7 cm x 28.7 cm x 13.2 cm)	Box design optimization (8 parameters) regarding the cost of the material, shipping and penalty due to temperature abuse by using zonal based heat transfer model coupled with a hybrid genetic algorithm	- The box thickness (about 150 mm), PCM type (ice pack) and PCM thickness (about 60 mm) were the factors that influenced optimization to the greatest extent. - The cost of the boxes is almost the same, whatever the design.
East et al. (2009) / Beverage cans	Same as East & Smale (2008)	Same as East & Smale (2008)	- Same optimization approach as East & Smale (2008) but for different climate conditions to obtain an optimal box design for summer only (22°C to 35°C, 24 h), only winter (-18°C to 10°C, 24 h), and both summer-winter (-18°C to 35°C, 48 h) transport. - These boxes were numerically tested against 1095 ambient temperature	- In winter, a 10 mm polystyrene box and a 10 mm of ice pack were proposed and caused 86% heat failure. - In summer, it required a polyurethane box thickness of 90 mm and 53.9 mm ice pack but led to 26% freezing failure. - Boxes for both summer and winter had 90 mm of polyurethane wall thickness and a 30.5 mm ice pack and caused only 0.5% of freezing failure. - The box for

			profiles that varied according to climate conditions.	winter climate conditions only is about twice as cheap as those used in summer only or both in summer and winter.

2.3 Insulating material and box design

Reducing heat flux by using an insulating material is essential (Singh et al., 2008a). Not only the temperature inside the box should be maintained within a desired range for the longest duration, but temperature fluctuations should also be reduced, especially when the external ambient temperature varies, as is often observed in the supply chain (Fioretti et al., 2016). Low thermal conductivity rigid materials have been used above all, for example, expanded polystyrene and polyurethane (East & Smale, 2008; Kacimi & Labranque, 2019; Margeirsson et al., 2011). Many studies have shown that a change in the insulating material significantly impacted the temperature profile and product quality (Du et al., 2020; East et al., 2009; East & Smale, 2008; Kozak et al., 2017; Margeirsson et al., 2011). For instance, Margeirsson et al. (2011) reported that the average rates of fish temperature rise were 0.51°C/h and 1.41°C/h using expanded polystyrene and corrugated plastic, respectively. Kozak et al. (2017) showed that an optimal configuration can be reached, which allows maximizing the melting time of the PCM. The ratios of insulation and PCM thicknesses and their thermal conductivities are the determining factor of this optimal condition (allowing longest period at low temperature).

The insulation is reinforced when vacuum panels are used (Kacimi & Labranque, 2019). This can be explained by the fact that the thermal conductivity of vacuum panels is very low, and these panels thus provide greater insulation capacity (Du et al., 2020). These authors compared the effects of polyurethane (PU) and Vacuum Insulated Panels (VIPs) used as insulating materials. The authors found that VIPs prolonged the warming duration (defined as the duration during which the temperature at the center of the box rises from 0°C to 8°C) 3.8-fold in comparison with PU. Another solution to reduce the overall heat transfer coefficient consists of covering the surfaces with a low-emissivity material which can decrease radiation. Paquette et al. (2017) showed that by covering the internal surface of the box with aluminum foil to decrease the emissivity from 0.8 (without foil) to 0.2 (with foil) reduced the product temperature by about 2°C. The combined effects of wall emissivity and wall thickness on box insulation was studied by Navaranjan et al. (2013). These authors pointed out that replacing perpendicular spacers (with a 15 mm air gap) with double fluted spacers (with a 21 mm air gap) and metallizing the surface led to 102% greater thermal resistance.

In addition to the thermal conductivity of the material, box insulation also depends on its design. Margeirsson et al. (2012) reported that using an expanded polystyrene box with rounded corners helped to decrease the temperature difference of 2.0°C between fish at the center and at the corners, while this difference was 4.4°C for sharp corners and it also led to extending the product shelf life for an additional 2 days. This may be due to a lower exchange area at the round corner in comparison with the sharp corner, so less heat exchange with the environment occurs. However, the box design should be optimized taking into account the usable volume in comparison with the total box volume and cost (East & Smale, 2008).

Heat flow resistance (R value – $m^2 \cdot K \cdot W^{-1}$) is a factor determining the insulation effectiveness of a box. Singh et al. (2008b) and Navaranjan et al. (2013) placed a known quantity of ice in a box, left it in a constant temperature chamber for a certain period to allow the ice to partially melt, then determined the amount of liquid water and calculated the R value. Navaranjan et al. (2013) pointed out that there was a good correlation between the R value and the quality of New Zealand terakihi fish stored in insulated packaging. Another method used to estimate heat flow resistance of a box is the use of an internal cooling or internal heating method (ATP, 2020). For the internal heating method, a heat resistance (with a known heating power) and temperature sensors are placed in an empty box at locations suggested in the guidelines and the temperature profile is recorded continuously. When steady state is reached, the difference between the internal/external air temperatures and the heating power allow the R value to be calculated.

The box can be composed of multiple partitions to allow delivery of various types of products with different recommended storage temperatures in the same box. Xiaofeng & Xuelai (2021) developed an insulated box with partitions making it possible to transport three different product categories: no PCM for ambient storage, with PCM with a melting point of 7.1°C (87% n-caprylic acid and 13% myristic acid) for chilled storage and with a PCM with a melting point of -2.1°C (potassium sorbate solution) for storage at temperatures below 0°C. They reported that this box could maintain the internal temperature within the expected range for each partition for up to 16 h.

2.4 PCM properties, position and usage

Apart from the insulating material, thermal energy storage using PCM is another key factor that maintains the temperature in a shipment (Yang et al., 2021). During transportation, a difference between recommended and real product temperatures may occur because of heat diffusion from the external ambient into the box, resulting in temperature abuse. PCM plays a significant role in cold storage as it offsets heat diffusion, particularly during its melting thanks to high PCM latent heat (East & Smale, 2008; Kacimi & Labranque, 2019; Laguerre et al., 2008a). Oró et al. (2012a, 2012b), Rostami et al. (2020) and Zhao et al. (2020a, 2020b) have classified the PCM and fully described its properties.

There are numerous thermal energy storage materials e.g. water, salt solution, paraffin (Oró et al., 2012a; 2012b). Various compounds were applied as PCMs in an insulated box, e.g. ice or an ice pack with a melting point ranging from -0.5°C to 0.5°C (East et al., 2009; East & Smale, 2008; Laguerre et al., 2018, 2019; Margeirsson et al., 2011, 2012; Navaranjan et al., 2013). To achieve a temperature range below 0°C, Kozak et al. (2017) used salt solutions with melting points of -10°C and -33°C while Elliott & Halbert (2008) studied the system with dry ice (CO_2: phase change temperature = -78.5°C). Elliott & Halbert (2005) used Icebrix® frozen gel packs which froze at -20°C. Commercially available PCMs with various melting points between -2°C and 21°C were also investigated (East et al., 2009; East & Smale, 2008; Kacimi & Labranque, 2019; Zhao et al., 2019).

Today, there is greater demand for produce from different regions in the world, hence, long transport duration and fluctuating ambient conditions are unavoidable (Loria, 2021). It is challenging to establish a common guideline for various types of products and transportation conditions, e.g. transportation ranged from 3 h to 96 h under extremely cold (-10°C) or hot (35°C) conditions (East et al., 2009; Laguerre et al., 2019; Zhao et al., 2019).

In some studies, a PCM was placed on the internal face of the box or in the layer between the internal and external walls to compensate for heat exchange with the ambient. East et al. (2009) and East & Smale (2008) placed PCM only at the bottom of the box. Kacimi & Labranque (2019) put PCM at top, bottom and side walls while Laguerre et al. (2008a) applied ice pack at top, middle and bottom layer of the box. Du et al. (2020) and Elliott & Halbert (2005) compared the effect of PCM position on temperature profile. Some studies recommended the position of the PCM on the top or side walls because this allows internal airflow by natural convection, thus generating a more uniform temperature. The PCM placed on the bottom leads to conduction alone along with greater temperature heterogeneity (Du et al., 2020; Laguerre et al., 2008a). In an insulated box with PCM at the top, middle and bottom, Laguerre et al. (2008a) indicated that PCMs on the top of the container completely melted within 32 h during an experiment on transport, while those at the bottom remained partially frozen for more than 72 h, while the product temperature reached 21.5°C at the level of the top layer.

A composite box wall with PCM was studied (Melone et al., 2012). Mixtures of paraffin (melting point 0°C to 10°C) and cellulose solutions with different concentrations (0%, 25% and 50% w/w) were prepared to obtain cellulose sheets with PCM. It was observed that the maximum cooling period of 87 minutes was achieved for the sample with a paraffin concentration of 50% w/w.

Some studies focused on maintaining the temperature of the load inside the box by placing the PCM close to the most sensitive product such as fish and meat (Elliott & Halbert, 2008; Laguerre et al., 2018, 2019; Margeirsson et al., 2011, 2012; Navaranjan

et al., 2013; Paquette et al., 2017). Paquette et al. (2017) showed that placing PCM at the center of the box provided better efficiency by comparing the duration required for the temperature of meat to increase from 3.5°C to 10.0°C. It was found that this temperature rise took 32.1 h with PCM at the center and 8.6 h with PCM on the side of the box. They also pointed out the decrease in the temperature of meat during the initial period when 1 kg of PCM was placed on top of the meat and another kg of PCM was placed on the bottom, whereas this phenomenon was not noticed when both parts of PCM was combined and added either at the top or at the bottom due to lower surface area for heat exchange. However, once the temperature went up, it rose faster and reached 18°C after a 48-h interval when the PCM was split into two layers compared with only 15°C when all the PCM was placed at the same position.

However, placing PCM in an inappropriate position may still lower the internal temperature, but causes significant temperature heterogeneity (Elliott & Halbert, 2008; Navaranjan et al., 2013; Paquette et al., 2017). For instance, Navaranjan et al. (2013) indicated that the temperature difference in a box with an ice pack on top of the product compared with a box with no ice pack was over 5°C. The load type and amount, the operating conditions and the transport constraints e.g. acceptable limit of product temperature, are the determining factors when designing the system.

The weight of the PCM influences the product temperature profile and should be optimized with respect to the size of the box. Kacimi & Labranque (2019) recommended that a moderate amount of PCM should be applied, since too little or too much PCM decreases the efficiency and causes undesirable outcomes i.e. temperature abuse and chilling injury. Xiaofeng & Xuelai (2021) increased the volume of the compartment by 25% while maintaining the same amount of PCM and found that the temperature rose faster in the compartment with a higher volume of PCM (the temperature increased from 0.24°C/h to 0.41°C/h). East et al. (2009) also reported that an inappropriate amount of PCM led to temperature abuse during delivery because the products were either too warm or frozen.

2.5 Effect of the external temperature

The influence of the ambient temperature was also investigated as an important factor e.g. greater numbers of PCM packs were required during delivery in summer (East et al., 2009; Elliott & Halbert, 2005; Kacimi & Labranque, 2019; Zhao et al., 2019). Although the difference in heat flux caused by different ambient temperatures is well-known, investigation of the influence of this factor on product quality is still necessary. East et al. (2009) optimized box design using different ambient temperature profiles from different seasons and were able to choose the box material, the wall thickness and the amount of PCM. Kacimi & Labranque (2019) studied two PCMs with different melting points under different ambient conditions and recommended that the PCM melting point should be matched with the ambient conditions. It is to be emphasized that the PCM was placed only on the side wall of the box in this study.

Many studies have investigated the influence of ambient temperature, either by temperature monitoring during real shipping or by temperature recording in a controlled-temperature test chamber. The latter case is easier to implement and requires fewer resources. Elliott & Halbert (2005) and Elliott & Halbert (2008) performed a shipping test using long-distance delivery in different seasons generating data from real situations. Margeirsson et al. (2012) recorded the ambient temperature during cod fillet transport from Dalvík to Reykjavík and further utilized this data for numerical model validation. Navaranjan et al. (2013) reproduced, in a test chamber, the ambient temperature obtained during airfreight from New Zealand to Singapore. The delivery between these two countries was considered as the route during which highest product spoilage rate was observed for international fish exports from New Zealand, and the fish shelf life was 4.76 days lower than that stored at 0°C.

Some ambient temperature profile databases are available for member at International Station Meteorological Climate Summary (ISMCS, https://ui.adsabs.harvard.edu/abs/1992 BAMS...731578J/abstract) or International Safe Transit Association (ISTA, https://ista.org/test_procedures.php) and could be useful for those with no available data (East et al., 2009; Kacimi & Labranque, 2019).

2.6 Influence of each factor in application and modeling

As mentioned above, there are numerous parameters influencing the temperature profiles in an insulated box with PCM such as the characteristics of box (dimensions, shape of the corners and type of insulating material), PCM (type, quantity and position), product (thermophysical properties, mass and arrangement) and operating conditions (ambient temperature and transport duration). In such complex situations, physical-based modeling tools can be useful to identify the most sensitive factor. Paquette et al. (2017) performed sensitivity analysis to determine the most significant factor (external convective heat transfer, emissivity of food, box and gel packs, the thermal conductivity and the heat capacity of the insulating material). They reported that the thermal conductivity of the insulating material affected the product temperature profile to the greatest extent. Consequently, this is the main criterion to take into account when designing the system. Different types of models can be developed. A 1D analytical model was utilized to gain a general perspective of the system and roughly predict useful responses, e.g. maximum temperature, PCM melting time (Laguerre et al., 2018, 2019). A zonal model which assumed that each zone has uniform and lumped properties is also used to acquire a thorough understanding with an acceptable calculation time for design optimization and temperature prediction (East et al., 2009; East & Smale, 2008). 2D and 3D heat transfer of a CFD model (in some cases, convection and/or radiation were neglected) are described in articles with extensive results such as temperature distribution and profile, PCM liquid fraction and air velocity, but this approach requires more computational time and resources (Du et al., 2020; Laguerre et al., 2018, 2019; Margeirsson et al., 2011, 2012; Paquette et al., 2017). A data-based model, which needs less background in physics, is simpler to use.

This model represents a simple relationship between the input parameters and the intended responses, for example, using the thermal resistance of the insulated box to predict food quality (Navaranjan et al., 2013).

This complexity also impacts system design. To find the best compromise between these constraints, the objectives must be clearly identified depending on the application. For example, one might consider that the criterion is the maximum temperature that can be attained inside the box after a defined duration or the temperature heterogeneity within the box. The choice of this objective might impact the design of the box and the PCM. For instance, if the box is designed to transport fruit and vegetables with an optimal temperature range (e.g. from 4°C to 10°C), the temperature heterogeneity might not be crucial. Hence, there will be more flexibility in the choice of the box material and the PCM position in the box. A specific design is required during transportation of highly temperature sensitive products e.g. superchilled food products (Kaale et al., 2011). These authors reported that temperature fluctuations lead to ice recrystallization and drip loss leading to product quality degradation. East et al. (2009) and East & Smale (2008) optimized insulated box design using a hybrid genetic algorithm to obtain the box with the lowest cost regarding material, transportation and penalty due to temperature abuse. They suggested that the boxes used in summer should have a thicker insulating material and a larger quantity of PCM to withstand the heat flux from ambient than that in winter while the other factors remained almost identical.

Among the studies examined in our review, several focused on how to improve the insulation of a classic box, i.e. a box made of expanded polystyrene, polyurethane, or a corrugated box by increasing the air gap, adding spacers, vacuum panels and metallizing the surface. The rounded corner box design was also suggested to deal with temperature heterogeneity. The methods used to determine insulation efficiency was developed by measuring the heat flow resistance (R) value and was tested in real application. The external temperature and load type and mass inside the box were also investigated. The effect of each factor was described and predicted by basic heat transfer equations. There was substantial evidence proving that the application of PCM could lower the temperature of the system and possibly improve thermal homogeneity. However, the PCM melting point, the amount of PCM and optimization of its position are still necessary to achieve the most efficient conditions for each system.

For food transport, there is a lack of field data on what happen to insulated boxes when they arrive the destination. For pharmaceutical transport, a survey revealed that 79% of customer consider that using reusable containers for delivery is more attractive than single use ones in spite of higher price (Biopharma cold chain logistic survey, 2019). This statistical data is in agreement with an increase of plastic waste recycling by 92% in Europe in 2020 due to the sake of cold chain sustainability (PlasticsEurope, 2019).

Concerning the box with PCM, it could be possible to apply a similar principle for reusable packaging by improving the logistic organization of return boxes and PCM from the end-user (retailer, final consumer) to the supplier (food distribution center). For example, the development of deposit locations and the collection by a transporter in order to minimize the logistic costs and environmental impact.

3. Cold chain equipment with PCM

Unlike in an insulated box, PCM in refrigerated equipment often enables energy management, temperature stabilization, etc. Many articles pointed out the capacity of PCM to reduce the compressor operating time, thus lowering energy consumption (Alzuwaid et al., 2015; Azzouz et al., 2008, 2009; Berdja et al., 2019; Ezan et al., 2017; Maiorino et al., 2019; Sonnenrein et al., 2015a; 2015b; Yilmaz et al., 2020). Several studies showed that PCM allows the extension of the cooling period following power failure (Ben-Abdallah et al., 2019; Oró et al., 2012b; Yilmaz et al., 2020). Use of PCM can also decrease the temperature of the system with greater homogeneity (Alzuwaid et al., 2015, 2016; Azzouz et al., 2009; Ben-Abdallah et al., 2019; Maiorino et al., 2019; Sonnenrein et al., 2015a).

3.1 PCM in refrigerated trucks

PCMs with various melting points were applied in the cooling unit or on truck walls, and the studies are summarized in Table 1.2. To obtain a very low melting point, different types of salts with different concentrations were used: an in-house inorganic salt solution with a melting point of -26.7°C (Liu et al., 2012), a NaCl solution with a melting point of -21.2°C, (Xiaofeng et al., 2017) and commercial blends of salts with melting points of -26°C, -29°C and -32°C, (Mousazade et al., 2020). For PCMs with higher melting points (7°C to 45°C) which are inserted between the external and internal walls, paraffin and salt hydrate were used (Ahmed et al., 2010; Copertaro et al., 2016; Fioretti et al., 2016).

To facilitate experimental implementation, several studies investigated stationary refrigerated trucks in a test chamber in which the ambient temperature alone was controlled. Liu et al. (2012) determined the period during which the internal temperature was below -15°C by using 136.8 kg of PCM salts in a tank connected to the truck evaporator when the ambient temperature was about 30°C. The authors predicted that 163% more PCM would be necessary for 10 h transportation during summer (maximum temperature = 41°C) in Adelaide, Australia. The same authors also pointed out that a phase change thermal storage unit could replace the cooling engine. This storage unit, charged at the distribution center before transportation, allows 51.0% - 86.4% cost savings depending on the COP of the system and the electricity tariff.

Fioretti et al. (2016) studied insulating walls with and without PCM exposed to solar radiation in a test room to simulate real conditions. They observed that the wall fitted with PCM resulted in an internal wall surface temperature that was 1.8°C lower.

Other studies dealt with stationary refrigerated trucks under real climate conditions i.e. ambient temperature, solar radiation. Ahmed et al. (2010) and Fioretti et al. (2016) investigated the efficiency of their systems with PCM under real conditions and reported that the truck equipped with PCM could decrease the total heat flux through the wall by 1.7% to 26.4%. This heat flux varied according to the angle between the wall and the radiation source.

Copertaro et al. (2016) developed a model in order to choose the PCM with the most suitable melting point to be inserted between the external and internal walls of refrigerated trucks. They recommended that with a melting point of 35°C for the truck operating under ambient temperatures varying from 20°C to 33°C as observed in various cities in Italy in summer.

Mousazade et al. (2020) conducted an experiment in a moving truck and pointed out that the speed needed optimization. In fact, a higher speed led to a greater distance covered and lowered the PCM cooling time due to higher heat exchange. This was probably due to a higher external convective heat transfer coefficient and more vibration. They reported that the longest PCM cooling period was 4.78 h in a truck moving at a speed of 81 km/h (distance covered: 387 km), but the longest distance covered was 491 km in the case of a truck moving at a speed of 110 km/h (4.46 h cooling period).

Table 1.2 Summary of studies using PCM in refrigerated trucks

Reference / Type of study	**PCM (melting temperature) / its location**	**Main observation(s)**
Ahmed et al. (2010) / Experimental (stationary empty truck container under real climate conditions)	Paraffin (7°C) / between the external wall and the internal wall	PCM decreased peak heat flux (11.3% to 43.8%) and total heat flux (1.7% to 26.4%) depending on the angle between the wall and the sun.
Liu et al. (2012) / Experimental (empty truck in laboratory) and numerical (Transient system simulation)	Inorganic salt solution (-26.7°C) / in the tank connected to the heat exchanger of the refrigerated space	- In the experiment, 136.8 kg of PCM stabilized the temperature below -15°C for 3 h. - From numerical results, 360 kg of PCM was suggested for 10 h transportation. - This system could save energy costs by 51.0% to 86.4% compared with the system using internal combustion engine cooling.
Copertaro et al. (2016) / Numerical (2D heat transfer model in empty refrigerated truck)	8 paraffins (27.5°C to 45°C) and 1 salt hydrate (46.5°C) / inside the	- Paraffin PCM was more efficient than salt hydrate: it reduced energy consumption by 4% on the average, whereas salt hydrate achieved a 2% reduction. - PCM with 35°C melting point was the most

with experimental validation	refrigerated truck wall made of steel.	efficient.
Fioretti et al. (2016) / Experimental (stationary empty truck container in laboratory test room and real climate conditions) and numerical study (2D heat transfer model)	Paraffin wax (35°C) / inside refrigerated truck wall made of steel	- The experiment demonstrated that PCM decreased heat flux (between 15 W/m^2 and 47.5 W/m^2 to between 13 W/m^2 and 25 W/m^2), decreased the external wall surface temperature (from 93.0°C to 80.0°C), and the internal wall surface temperature (from 11.8°C to 10.0°C). - From numerical results, comparing the PCM-equipped wall and no PCM with the thicker insulated wall, the former had less temperature variation (0.3°C and 0.7°C) but a slightly higher average temperature (around 0.15°C) than the latter.
Xiaofeng et al. (2017) / Numerical (3D CFD of empty refrigerated truck)	Eutectic NaCl solution (-21.2°C) / in a plate installed on the truck wall	- Higher climate temperature led to a shorter melting time (86 h and 73 h at 20°C and 30°C, respectively), higher heat transfer rate (1.9 W/h and 2.75 W/h at 20°C and 30°C, respectively) and a higher internal air temperature (0°C and 10°C at 20°C and 30°C ambient temperature, respectively). - The highest air velocity (0.035 m/s) was located near the lowest part of the PCM plate.
Mousazade et al. (2020) / Experimental (stationary and moving empty truck)	Commercial PCM containing various blends of salts (-26°C, -29°C and -32°C) / in a plate placed on the truck wall.	- PCM melting at -26°C showed the best cooling efficiency with the longest melting time (5.11 h and 4.78 h in stationary and 81 km/h truck, respectively). - Higher truck speed caused lower melting time but longer travelling distance where the maximum distance was 491 km in a truck with a speed of 110 km/h.

3.2 PCM in cold rooms

According to the authors' knowledge, only a few studies have been conducted on PCM application in cold storage facilities or warehouses, although it has been shown that higher product quality can be achieved using PCM (Pirdavari & Hossainpour, 2020; Schalbart et al., 2013). The difficulty in PCM charging and temperature control in a cold room may be one of the main obstacles to implementation. The application of PCM in cold storage facilities is summarized in Table 1.3.

PCM can be placed on the wall of the cold storage facility (Yang et al., 2017), in some locations inside the building (Schalbart et al., 2013), or near the product (Pirdavari & Hossainpour, 2020). For potatoes cold storage at temperatures above 0°C, Pirdavari &

Hossainpour (2020) considered PCM with a melting point between 8.5°C and 9.5°C. They optimized the melting point of the PCM, the ratio of the weight of PCM to the one of the potatoes and the insulation type. They indicated that a greater amount of PCM, a lower PCM melting point and a higher thermal resistance of the insulation triggered, a longer melting time and a lower product temperature. For icecream, Schalbart et al. (2013) optimized the melting point of the PCM between -23.3°C and -17.5°C. They showed that the use of PCM reduced ice crystal growth by 2.7% to 9.0% thanks to fewer temperature fluctuations.

Yang et al. (2017) and Pirdavari & Hossainpour (2020) reported that installing PCM fulfilled the gap in energy supply in the case of solar energy or a more economical electrical source, which are not available all day.

Table 1.3 Summary of studies using PCM in cold storage facilities

Reference / Type of study	**PCM (melting point) / its location**	**Main observation(s)**
Schalbart et al. (2013) / Numerical (1D finite difference equation system) of warehouse storage of ice cream for a period of 90 days with different PCM positions.	PCM with a melting point that was optimized depending on the location / post-evaporator, ceiling, wall, storage tank and product package	- From optimization, the melting point of the PCM was in the range of -23.3°C at the storage tank to -17.5°C at the walls. - Without PCM, the predicted final ice crystal size was 58 µm and there was ±1.0°C temperature fluctuation with 13.6 GJ energy consumption. - Predicted final ice crystal size was 53 µm with PCM at storage tank to 57 µm with PCM at the ceiling and the temperature fluctuation was only ±0.01°C with PCM at product package to ±0.76°C with the PCM at the ceiling. - PCM at post-evaporator and storage tank increased the energy consumption by 2.2 GJ and 0.7 GJ, respectively, while at other locations, energy consumption was almost the same as that without PCM.
Yang et al. (2017) / Numerical (3D CFD) of cold storage facility with a container of potatoes	Ice plate (0°C) / on each side of the wall, the floor and the roof	The upper part was 4°C warmer than the lower part due to external heat convection via the roof which had a heat transfer coefficient of 5 W/m^2 K.

Pirdavari & Hossainpour (2020) / Optimization via numerical study (1D simplified dynamic model which is validated by using experimental data from Azzouz et al. (2009)).	$LiClO_3 \cdot 3H_2O$ PCM capsule (8.5°C, 9.0°C and 9.5°C) / in a cylindrical column placed in the stack of potatoes in the cold room.	The greater the quantity of PCM, the lower the melting point of the PCM and the lower thermal conductivity of insulation led to a longer melting time and lower product temperature.

3.3 PCM in display cabinets

The application of PCM in display cabinets is summarized in Table 1.4. Pure ice placed near the evaporator was generally used (Alzuwaid et al., 2016; Ben-Abdallah et al., 2019; Ezan et al., 2017). Ice with an additive (melting point -6°C to -2°C) was placed either near the evaporator or below the cabinet shelves (Alzuwaid et al., 2015; Yilmaz et al., 2020). Oró et al. (2012b) applied commercial PCM (Climsel C-18 and Cristopia E-21), with melting point of -18 °C and -21.3 °C respectively, over evaporator tubes located at different shelves of a closed display cabinet. The authors reported that for empty closed display cabinet, the air temperature rose from -22 °C to 0 °C within 1.5 h (without PCM), 6.5 h (-18°C PCM) and 8 h (-21°C PCM). This period extended when display cabinet was loaded by test product: 11.5 h (without PCM), 15.6 h (-18°C PCM) and 21.5 h (-21°C PCM), as illustrated in Figure 1.3. These results demonstrated the interest of PCM to slow down the product temperature change when the display cabinet was turn off, due to machine failure for example.

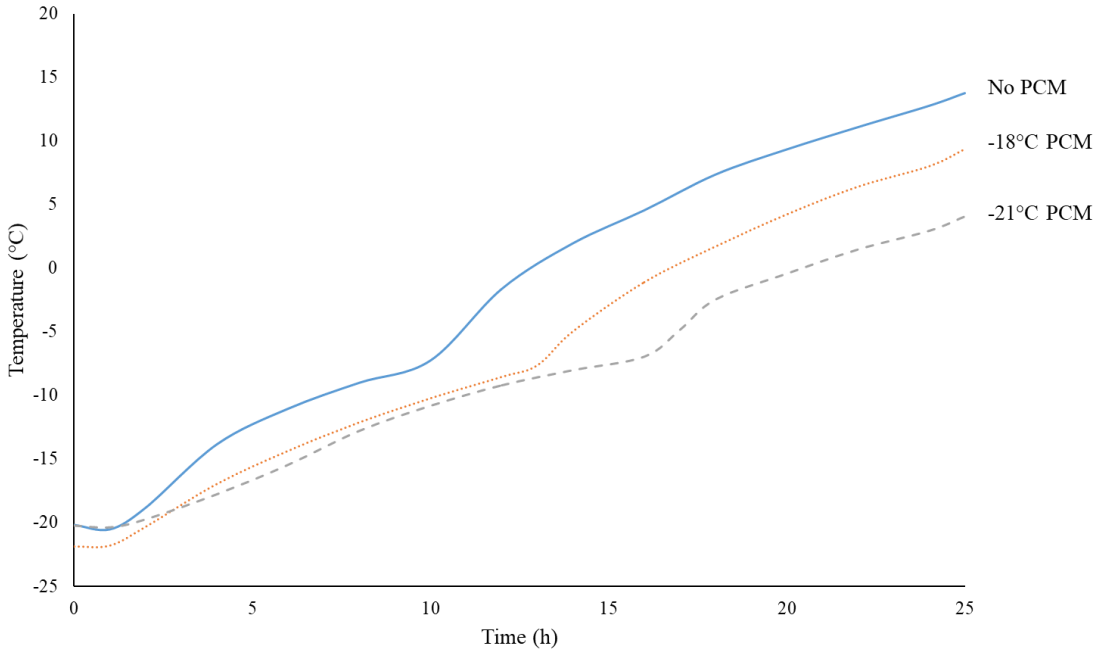

Figure 1.3 Test product temperature evolution during "turn off" closed display cabinet (Adapted from Oró et al. (2012b))

PCM decreased the compressor operating time by 4% to 10% and reduced energy consumption by 5.0% to 6.4% (Alzuwaid et al., 2015, 2016; Ezan et al., 2017). In fact, for a given average air temperature in a cold enclosure with and without PCM; the same quantity of heat has to be removed. However, the presence of PCM makes the temperature in the enclosure more stable, so, a slightly higher evaporator temperature can be used. Thus, the COP is increased and the electrical energy consumption is reduced. In this manner, the heat transfer efficiency of the cold enclosure can be improved. The amount of PCM or the thickness of the PCM slab had to be optimized (Ben-Abdallah et al., 2019). Ezan et al. (2017) compared the efficiency of PCMs with a thickness varying from 2 mm to 10 mm and reported that the compressor operating duration was the lowest with the 6-mm PCM thickness due to appropriate cooling capacity without significantly obstructing the airflow inside the equipment. The position of the PCM is another challenge in the application because PCM in an inappropriate place led to a worse outcome than in a context where no PCM was used. Yilmaz et al. (2020) reported that when a PCM was used at the back of a closed display cabinet, the system consumed 8% more energy than a system without a PCM due to the delay in cabinet temperature change detection of temperature sensor.

PCM was able to stabilize the display cabinet for 5 h to 14 h longer during a power outage (Oró et al., 2012b; Yilmaz et al., 2020). Ben-Abdallah et al. (2019) mentioned that the internal temperature increased by 1°C in the open display cabinet with PCM during the 2 h period during which the compressor was not operating compared with 2°C in the system without PCM. Adding load into the test system could prolong this period by 8 h to 12 h compared with the empty system as it increased thermal inertia (Oró et al., 2012b).

Table 1.4 Summary of studies using PCM in display cabinets

Reference / Type of study	**PCM (its phase change temperature) and its location**	**Main observation(s)**
Oró et al. (2012b) / Experimental (closed display cabinet freezer)	ClimSel C-18 (-18°C) or Cristopia E-21 (-21.3°C) / encapsulated in a stainless-steel thin plate placed on top of the evaporator tube	- For an empty display cabinet, the air temperature rose from -22°C to 0°C within 1.5 h (without PCM), 6.5 h (C-18) and 8 h (E-21). - The presence of load in the display cabinet enabled this period to be extended: 11.5 h (without PCM), 15.6 h (C-18) and 21.5 h (E-21).
Ezan et al. (2017) / Numerical (3D CFD) with experimental validation (closed display cabinet)	Ice (0°C) / placed behind rollbond evaporator at the rear of the empty cabinet	- The coldest area was at the bottom corner and the warmest area was located at the top with up to 7.5°C temperature difference. - Increasing PCM thickness explains the decreases of compressor run-time ratio: 36% (without PCM), 32% (2 mm PCM), 28% (4 mm), 26% (6 mm) 27% (8 mm) and 29% (10 mm). - PCM that was too thick obstructed the airflow with maximum velocity at 4.94 m/s (10 mm of PCM slab) and at 5.55 m/s (2 mm) and led to a higher ratio of compressor run-time.
Yilmaz et al. (2020) / Experimental (closed display cabinet)	Distilled water with a nucleating agent and thickening agent (-6°C) / either on the back wall or on the shelves	- PCM on the back wall generates minimum running cycles: 17 cycles (without PCM) to 11 cycles (PCM on shelves) and 9 (PCM on back wall) over 8 h running. - PCM on shelves is more efficient than that on the back wall: 888 kJ, 3.8 h “on” cycle (shelves) and 1003 kJ, 5.6 h, (backside) over 8 h running. - During power failure, the system with PCM had a longer cooling period with 6 h, 17 h, and 20 h, without PCM, with PCM at the back, and with PCM on the shelves, respectively.
Alzuwaid et al. (2015) / Experimental (open display cabinet)	Ice gel PCM (-2°C) / above evaporator	Adding PCM led to 5% energy savings, 70% longer defrost period, 2°C lower maximum cabinet temperature and more stable product temperature: Tmax-Tmin 7.33°C (without PCM) and 6.50°C (with PCM).

Alzuwaid et al. (2016) / Numerical study (2D CFD) with experimental validation (open display cabinet)	Pure-water ice PCM (0°C) / above the evaporator	- Installing PCM enabled 6.4% energy savings to be achieved and decreased the product temperature difference from 5.0°C (without PCM) to 4.2°C (with PCM). - The highest product temperature was at the front of the middle shelf and the lowest one was located at the back of top shelf.
Ben-Abdallah et al. (2019) / Experimental (open display cabinet)	Ice (0°C) / in a finned tube heat exchanger placed in the rear duct	- Adding PCM decreased the average air temperature from 8.4°C (without PCM) to 1.5°C (with PCM). - PCM is an airflow obstacle and lowered the airflow by 28%. - When the compressor stopped operating for 2 h, the product in the cabinet with PCM the temperature increase was only 1°C compared with a 2°C increase without PCM.

3.4 PCM in domestic refrigerators

Several studies have investigated PCM application in domestic refrigerators as summarized in Table 1.5. In most studies, the PCM was placed at the evaporator by using ice (Azzouz et al., 2009; Maiorino et al., 2019), a copolymer with a melting point of -4°C (Sonnenrein et al., 2015a), or an eutectic solution with a melting point between -9°C and -1°C (Azzouz et al., 2008, 2009). Sonnenrein et al. (2015a) and Sonnenrein et al. (2015b) applied ice, paraffin (melting point = 34°C) and a copolymer (melting point = 34°C to 35°C) at the condenser. Sonnenrein et al. (2020) studied the application of a copolymer PCM (melting point = 9°C) in the load compartment.
PCM decreased the temperature of the system and resulted in 17.6% to 32.5% less operating time, 10% to 17% less energy consumption and 5% to 15% greater COP (Azzouz et al., 2008; Berdja et al., 2019; Sonnenrein et al., 2015a). The selection of a PCM with an appropriate melting point was necessary to ensure the efficiency of the cooling system (Azzouz et al., 2008). Azzouz et al. (2009) reported that placing a eutectic plate (melting point = -3°C) at the evaporator lowered the internal temperature by up to 1.5°C. However, the compressor operating period was 0.4 h longer. Thus the COP was lower in comparison with the system using ice. Sonnenrein et al. (2015a) and Sonnenrein et al. (2015b) reported that paraffin and copolymer PCM (melting point = 34°C to 35°C) were more efficient than ice at the condenser since they allowed a temperature that was 5°C to 6°C lower to be achieved at the condenser, leading to 2% to 17% lower energy consumption. The thickness of the PCM slab should also be optimized to achieve the highest efficiency (Azzouz et al., 2008; Berdja et al., 2019).

PCM (melting point = 9°C) in the load compartment has proved to be useful in several commercialized domestic refrigerators by decreasing the cooling time (the time

required to reduce the product temperature from 25°C to 10°C) by 16% to 33%. It also makes it possible to increase the temperature rise period (the time required to raise the package temperature from 8°C to 11°C after turning off the cooling system) by 75% to 145% (Sonnenrein et al., 2020).

Frost formation on evaporator was still a challenge since it exerted a greater effect on airflow than the PCM due to higher thermal resistance (Berdja et al., 2019). Azzouz et al. (2008) pointed out that greater numbers of door openings led to lower PCM efficiency as the PCM did not completely melt by the time the compressor restarted and could not provide full cooling capacity. Maiorino et al. (2019) indicated that an ambient temperature that was 7°C higher raised energy consumption by 38.4% to 63.6% although PCM was applied in both conditions.

Table 1.5 Summary of studies using PCM in domestic refrigerators

Reference / Type of study	**PCM (melting point) / its location**	**Main observation(s)**
Azzouz et al. (2008) / Numerical study (1D simplified dynamic model) with experimental validation.	Eutectic aqueous PCM (-9°C, -7°C, -5°C, -3°C or -1°C) / on evaporator surface	- Adding PCM increased the COP by 5% - 15%, decreased operating time by 28.5% - 32.5% and prolonged the cooling period by 4 h – 8 h when the compressor was off. - Increasing the melting temperature of the PCM led to a higher COP but also a higher cabinet temperature. - Thicker PCM caused a shorter operating time because of the higher cooling capacity.
Azzouz et al. (2009) / Experimental	Ice (0°C) or eutectic mixture (-3°C) / on evaporator surface	- Eutectic mixture PCM led to 1.0°C to 1.5°C lower air temperatures but a 0.4 h longer compressor operating period. - The COP of the refrigerator with ice or with eutectic salt solution were not significantly different. - Increasing the PCM thickness did not improve the COP since it was not completely frozen.
Sonnenrein et al. (2015b) / Experimental	Paraffin (34°C), copolymer compound with 10% (w/w) graphite (34°C), or water (0°C) / condenser	- Paraffin PCM on the condenser led to a 5°C lower condenser temperature and 2% to 7% lower energy consumption compared with water (only sensible heat variation). - Copolymer compound PCM on the condenser generated up to 10% energy

		savings.
Sonnenrein et al. (2015a) / Experimental	- Copolymer PCM (-4°C) / evaporator - Another copolymer PCM (35°C) / on the condensers of 2 different refrigerator models	- PCM increased the evaporator temperature between 6°C and 8°C and decreased the condenser temperature by 6°C. - 12% to 17% less energy consumption and a more constant compartment temperature were observed in refrigerators with both types of PCM.
Berdja et al. (2019) / Experimental and numerical (1D analytical model)	PCM (-11°C) / covering the evaporator surface	- From the experiment, installing PCM resulted in 10% lower energy consumption, 17.6% lower compressor operating time, 5.05% greater COP and an evaporator temperature that was 1.89°C lower. - From numerical results, higher PCM slab thickness yielded a lower overall heat transfer coefficient (H). - Adding PCM led to longer periods during which the compressor was off, but also generated a higher air temperature. - H was more affected by frost formation and its thickness than by PCM slab thickness due to lower thermal conductivity of frost.
Maiorino et al. (2019) / Experimental	Ice (0°C) / above and below the evaporator rack tube	- PCM reduced and stabilized the product temperature. - Higher ambient temperature caused 0.1 h to 3.6 h lower compressor off period and 0 h to 3.4 h shorter cycle time. - More product yielded a 0.5 h to 1.1 h longer compressor off period and a 0.6 h to 1.4 h longer cycle time. - These effects were more pronounced at higher hysteresis. - Generally, the products at the higher level were colder, except in the system with high hysteresis.
Sonnenrein et al. (2020) / Experimental	Polymer-bound PCM (9°C) / in each load compartment	- PCM decreased 16% - 33% cooling time and increased 75% - 145% the temperature rise period. - Energy consumption was not significantly

		different.

4. General discussion

The application of PCMs in the cold chain has been widely studied with a wide variety of types of equipment. PCMs can be used in complement with cold production in refrigerated equipment or as alternative cooling systems. For example, when refrigeration equipment is not available or the ambient temperature during transportation is not appropriate, an insulated box with a PCM can be an alternative. It ensures a low, stable temperature, and thus preserves food quality.

The incorporation of PCM in refrigerated equipment is mostly performed for energy-management-related purposes. Many studies have been conducted on PCM in domestic refrigerators and display cabinets, but fewer studies have been performed on cold rooms. This may be due to difficulties related to the controlling and recharging of PCMs.

What clearly appears from the existing studies is the absence of an ideal general solution to apply PCM in equipment and boxes as it involves complex interactions between the parameters of the studied system such as the insulating material, the external temperature, the product load, the melting point and the quantity of the PCM.

To design such a system, experimentally validated numerical studies (CFD or zonal models) can be used to simulate other configurations. These models often consider heat transfer by conduction alone, although radiation and free convection can exert significant impacts in insulated boxes, especially in terms of temperature heterogeneity. Consequently, it is important to quantify heat flux by conduction, convection, and radiation since none of them can be neglected. Therefore, further studies are essential to better understand the relationship between heat transfer and airflow by natural convection. Studies on the effect of the load porosity on heat transfer by convection and conduction and on the impact of the emissivity of walls or product packages on heat transfer by radiation should be undertaken.

Other concerns in the application of PCMs are related to chilling injury, particularly when a PCM is directly in contact with sensitive products. To avoid this problem, some studies proposed, for instance, to precondition the PCM before product loading.

The use of PCMs in insulated boxes exerts environmental impacts because of the PCM production itself, the production of the insulating material and the energy consumption required for charging the PCM before each use, along with PCM waste etc. Consequently, additional specific studies on these issues may help evaluate the feasibility and sustainability of the use of PCMs. Some progress has been achieved in the development of new insulating materials with less environmental impacts. For example, Jiang et al. (2021) and Khalaf et al. (2021) fabricated cellulose-based and

chitosan-based insulating materials, respectively. Melone et al. (2012) also developed a composite cellulose and paraffin (melting point 0°C to 10°C) insulating material acting as phase change material for transporting perishable products.

5. Conclusions and suggested future research

Applying PCMs in the food cold chain provides several benefits: less temperature abuse, and thus better product quality and better energy management. To achieve these benefits, many factors should be considered: insulating material (thermal conductivity and thickness), PCM type (i.e. heat storage capacity and its melting point), its quantity and position, load characteristics (load nature, mass and arrangement), and operating conditions (i.e. ambient temperature and storage and transport duration). These factors significantly affect the efficiency of the system, especially when PCM is the only cold source (no refrigerating machine). Thus, optimization of these factors is necessary in order to design the best configuration for achieving the objective of each application.

Modeling is a complementary experimental approach but is more complicated to develop. By using modeling, the prediction of results under unexplored operating conditions is possible e.g. ambient temperature, transport/storage duration, load type and its initial temperature. Existing models could be improved by acquiring a better understanding of the instantaneous heat transfer and airflow in the cold equipment. Knowledge of airflow can be acquired by using innovative optical techniques such as Laser Doppler Velocimetry (LDV) and Particle Image Velocimetry (PIV). These techniques are already used for several types of refrigerated equipment (refrigerated trucks, display cabinets and domestic refrigerators) but are not yet applied to insulated boxes with PCM in which the air velocity is very low because natural convection is the driving phenomenon.

According to the authors' knowledge, an insulated box equipped with a fan has not yet been commercialized. This type of box would allow airflow by forced convection inside the box, and the temperature would thus be more homogeneous. A rechargeable battery should supply enough power to the fan in order to assure continuous fan running along the supply chain. After arrival at the end-user's premises, the box could be returned to the distribution center (or the departure site), then the battery could be recharged with optimal power prior to the following delivery. The rechargeable battery and fan design need future development.

Although there are many challenges in display cabinet operation such as exposure to light and door openings, few studies have investigated these effects in cold equipment with PCM, so studies focused on these aspects would be useful. Moreover, only a few studies on PCMs used in cold rooms have been published. Additional studies on this application would be valuable. Applying PCM in commercially available refrigerated

equipment ranging from refrigerated trucks to domestic refrigerators could attract interest within the industry.

For the sake of cold chain sustainability, the extensive use of polystyrene and polyurethane as insulating materials should be replaced by biodegradable materials (cellulose-based and chitosan-based for example), thus exerting less impact on the environment. Also, reusable boxes and a recycling logistic chain should be developed to a greater extent taking into consideration both the economic cost and the environmental impact.

1.4 COMPLEMENTARY OF ARTICLE 1

1.4.1 Predictive models for food quality and safety in food cold chain

Most of studies reviewed in Article 1 focused on spatial and temporal temperature evolution and temperature abuse. Other aspects to be considered in food cold chain are food safety and food quality. Directly measuring the quality parameters requires resource and good sampling techniques to get reliable representative values for the whole lot. Since the main factor changing during food cold chain is temperature, the kinetic models to predict quality evolution, as a results of bio-chemical reactions, can be coupled with measured/modelled temperature values. There are several works developing predictive models taking temperature into account. Some models describe transpiration rate of vegetables which leads to weight loss, thus affecting visual and other qualities (Kang & Lee, 1998; Kedia et al., 2021; Mahajan et al., 2008). Joshi et al. (2019) studied the weight loss of Modified Atmosphere Packaged strawberries by calculating transpiration rate, respiration reaction, film permeability and condensation. The chemical reaction models, e.g., the zero-order reaction or the first order-reaction, were examined and it was found that these models can describe several quality changes of fruits and vegetables, e.g. weight loss, reducing sugar content, color and firmness (Muley et al., 2022; Van Dijk et al., 2006). Other types of models (Weibull model and fractional conversion model) were also used for these qualities' change (Oliveira et al., 2012; Pinheiro et al., 2013). The Arrhenius equation was mainly selected to fit the effect of temperature on the reaction rate in these studies. Combining these models with thermal models makes it possible to predict quality evolution of food product in logistic chains (García et al., 2022; Matar et al., 2020; Onwude et al., 2022; Penchaiya et al., 2020).

Evolution of microorganisms in food is also essential for evaluating food quality and safety. Microbial growth is extensively modelled in function of time, temperature, pH, water activity, etc. (Duret et al., 2019). Modelling microbial growth is more complex than that of organoleptic quality change due to the variation of the growth factors with the growth stages: lag phase, exponential phase and stationary phase (Huang, 2016, 2018; Li et al., 2016). Some studies also included the competition between the targeted organism with background microbiota (Cheng et al., 2023; De Cesare et al., 2018; Jia et al., 2020). García et al. (2022) reviewed the coupling between thermal models and microbial growth models in fish.

1.4.2 Heat transfer and airflow characterization in a closed cavity

Three heat transfer modes have to be taken into account:

1. Heat conduction: the heat is transferred through the vibration of the molecules, dominant in rigid objects.

2. Heat convection: the heat is transferred due to the movement of the flowable medium, dominant in fluid (air in our case).

    2.1 Forced heat convection: this occurs when the fluid is forced to flow by blowing, pumping, etc.

    2.2 Natural heat convection: this occurs when a temperature difference causes the flow due to the difference in density (hotter fluid is generally lighter than colder one).

3. Radiation: the heat is transferred in the form of electromagnetic wave, so this can happen even though there is no medium (Singh et al., 2008a).

Heat conduction occurs inside the solid part of product, PCM and in the rigid wall of the box (Laguerre & Flick, 2010). Heat fluxes via conduction through one slab or a series of slabs of different materials is shown in Figure 1.4 and expressed by Equations 1.1 and 1.2.

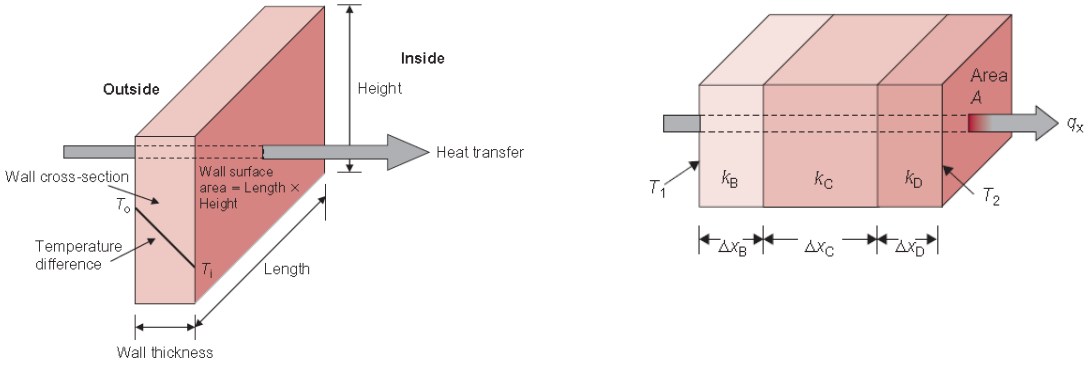

(a) (b)

Figure 1.4 Heat conduction through (a) a single slab and (b) a series of rectangular slabs (Singh et al., 2008a)

Heat conduction through a slab: $q_x = -kA\frac{dT}{dx}$ (1.1)

Heat conduction through a series of rectangular slabs: $q_x = \frac{A(T_2 - T_1)}{\sum_i \frac{\Delta x_i}{k_i}}$ (1.2) (Singh et al., 2008a)

Heat convection occurs between external air and box's wall, between internal air and box's wall or product surface, and in liquid PCM or product (Rincón-Casado et al., 2017). The general expression of heat convection is shown in Equation 1.3.

$q = hA(T_s - T_\infty)$ (1.3) (Singh et al., 2008a)

Only natural convection happens inside an insulated box with PCM (absence of

ventilation system), it can be characterized by the following dimensionless numbers (Equations 1.4 to 1.7) (Singh et al., 2008a).

- Grashof number (*Gr*): represents the ratio between buoyancy force and viscous force. This number is used to characterize the flow pattern; for example, the flow is laminar over a vertical plate when Gr is lower than 10^9.

$$Gr = \frac{{d_c}^3 \rho^2 g \beta \Delta T}{\mu^2} \quad (1.4)$$

where the thermophysical properties of the fluid are evaluated at film temperature

$$T_f = \frac{(T_s + T_\infty)}{2} \quad \text{(Singh et al., 2008a)}$$

- Prandtl number (*Pr*): represents the ratio between momentum diffusivity and heat diffusivity

$$Pr = \frac{\mu C_p}{k} \quad (1.5)$$

- Rayleigh number (*Ra*): is a result of the product of Grashof number and Prandtl number. *Ra* allows the characterization of the flow pattern i.e. laminar flow is considered when *Ra* is below 10^9 (Saury et al., 2011).

$$Ra = Gr \times Pr \quad (1.6)$$

- Nusselt number (*Nu*): represents the ratio between heat transfer rate by convection and conduction. It can be determined by either experiments or analytical solutions. The most widely used correlation is the relationship between *Nu* and *Ra* as shown in Eq. 1.7

$$Nu = \frac{h d_c}{k} = a Ra^m \quad (1.7)$$

Where a and m are coefficients depending on the studied geometry.

For example, in the case of natural convection beside a vertical plate (characteristic length or $d_c = L$), Nu can be calculated as below:

$Nu = 0.59 Ra^{1/4}$ (Cengel & Ghajar, 2020).

For an empty enclosure, empirical equations can be used to determine Nusselt number. For a vertical enclosure of height H with a gap between each vertical wall L (Figure 1.5a), the fluid flows downward near the cold surface because it exchanges heat and becomes colder, thus, higher density (Figure 1.5b). Then, it flows upward along the warmer opposite vertical wall to the top since its temperature increases and its density decreases. This generates a flow loop inside the enclosure (Cengel & Ghajar, 2020).

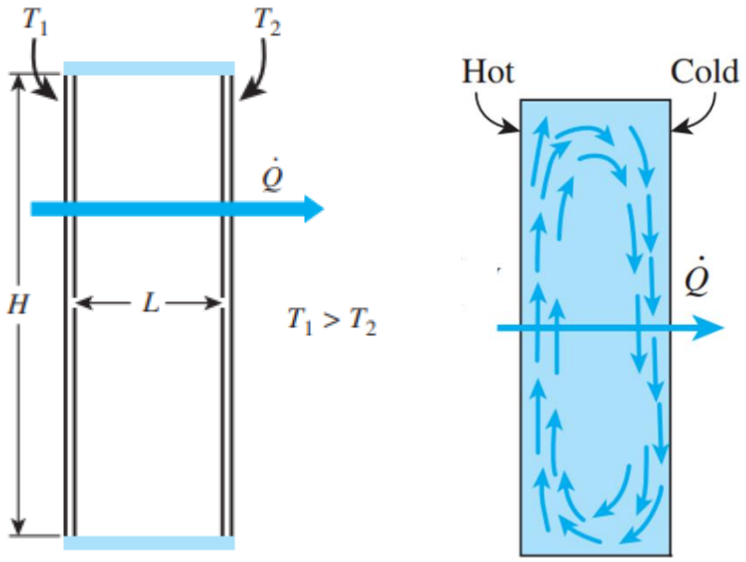

Figure 1.5 (a) A vertical enclosure with isothermal surfaces and adiabatic horizontal walls and (b) fluid flow pattern inside the enclosure (Cengel & Ghajar, 2020)

Catton (1978) proposed a correlation (Equation 1.8) for an enclosure with active vertical walls of $2 < H/L < 10$ and $Ra_L < 10^{10}$:

$$Nu = 0.22\left(\frac{Pr}{0.2+Pr}Ra_L\right)^{0.28}\left(\frac{H}{L}\right)^{-0.25} \qquad (1.8)$$

Inside an enclosure with cold top wall and warm bottom wall (Figure 1.6a), fluid flows in several cells (Figure 1.6b) and this is called Rayleigh-Bénard convection (Cengel & Ghajar, 2020).

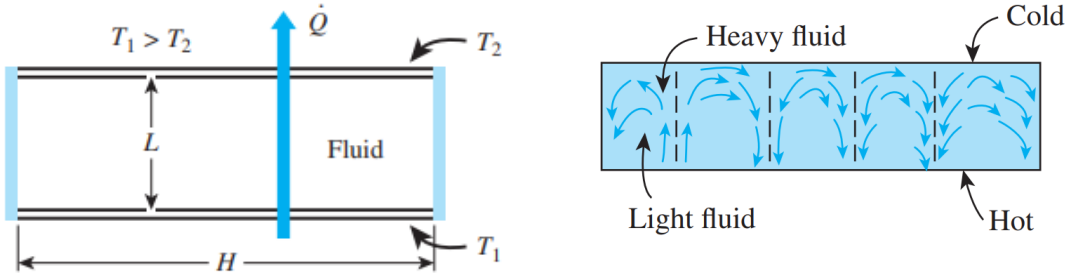

(a) (b)

Figure 1.6 (a) A horizontal enclosure with isothermal surfaces and adiabatic vertical walls and (b) fluid flow pattern inside an enclosure (Cengel & Ghajar, 2020)

For a horizontal enclosure, Hollands et al. (1976) proposed a correlation (Equation. 1.9).

$$Nu = 1 + 1.44\left[1 - \frac{1708}{Ra_L}\right]^{+} + \left[\frac{Ra_L^{\frac{1}{3}}}{18} - 1\right]^{+} \qquad (1.9)$$

where $[\,]^{+}$ indicates that if the value inside the bracket is negative, it is assumed to be zero.

Radiation occurs from the surrounding to an object or between two surfaces, e.g., at the external wall, between product surface and internal wall, product surface and PCM surface (Shinoda et al., 2019). It can be described as Equations 1.10 and 1.11.

Radiation to an object from surrounding: $q = \varepsilon\sigma A\left(T_1{}^4 - T_2{}^4\right)$ (1.10)

Where T_1 is temperature of surrounding

T_2 is temperature of an object (Geankoplis, 1993).

Radiation between two infinite parallel plates (view factor = 1):

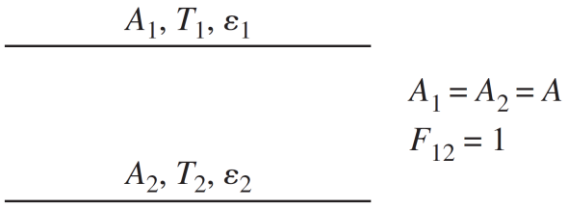

Figure 1.7 Radiation between two infinite parallel plates (Cengel & Ghajar, 2020)

$$q = \frac{\sigma A\left(T_1{}^4 - T_2{}^4\right)}{\frac{1}{\varepsilon_1} + \frac{1}{\varepsilon_2} - 1} \qquad (1.11)$$ (Cengel & Ghajar, 2020)

Understanding the relying physical phenomena inside a cavity with heated and/or cooled surfaces is necessary for the cavity design. A thermal performance cavity allows low average temperature and temperature homogeneity, which is essential for food transport in an insulated box with PCM.

Experimental approach for heat transfer and fluid flow characterization

The driving force of heat transfer is temperature difference, so measurement of temperature at various positions in the cavity is essential to characterize this phenomenon. Thermocouples are usual sensors used by several works as they are easy to implement with a good accuracy (Baïri, 2008; Jevnikar & Siddiqui, 2019; Labihi et al., 2017; Leporini et al., 2018; Moreno et al., 2020; Zhang et al., 2015). However, the compromise between the resolution of measured temperature field and the number of thermocouples (and its positions) should be taken in consideration. In fact, the presence of thermocouples in a cavity disturbs fluid flow (Miroshnichenko & Sheremet, 2018). As an alternative, Ataei-Dadavi et al. (2019) proposed Liquid Crystal

Thermography (LCT) with less flow obstruction to determine temperature field in a cavity (Figure 1.8a). This technique involves introducing a low quantity of tracers, for instance, micro-encapsulated liquid crystal tracer of which its hue is correlated to temperature. Then, the pictures of a cavity filled with tracers are captured and analyzed to establish the temperature field. This technique requires robust calibration between temperature and hue.

Once temperature measurement has been achieved, heat transfer characterization can then be done by distinguishing heat flux by conduction, radiation, and convection. Conductive flux in a cavity occurs at the walls, hence it can be determined by calculating or measuring heat flux through these walls (Ataei-Dadavi et al., 2019; Baïri, 2008). Radiative flux in a cavity could be determined by radiosity method as conducted in Baïri (2008). It computes the flux via surfaces' emissivity and shape factor between each surface. Finally, convective flux is obtained by subtracting the total heat flux with conductive and radiative flux. It is to be highlighted that calculating precisely radiative flux is complex, so many works neglected this flux. To compare convective flux, Rayleigh numbers is first calculated (Equation 1.6) knowing the temperature of hot and cold walls from measurement, then, Nusselt can be calculated which allows the estimation of convective heat transfer coefficient (Equation 1.7).

Fluid flow pattern and its velocity is also important to understand the physical phenomena in a cavity, and to identify the position with high and low heat flux. However, the hot-wired anemometer cannot be applied to the cavity where natural convection takes place because the fluid velocity is too low in comparison to the apparatus precision. Hence, non-intrusive optical techniques, e.g., Particle Image Velocimetry (PIV), are used (Ataei-Dadavi et al., 2019; Jevnikar & Siddiqui, 2019; Leporini et al., 2018; Zhang et al., 2015). The visualization of the fluid flow pattern is possible by the scattering of tracers, for example, oil-based smoke or silver coated particles, during laser pulses. An example of PIV experimental set up is shown in Figure 1.8b.

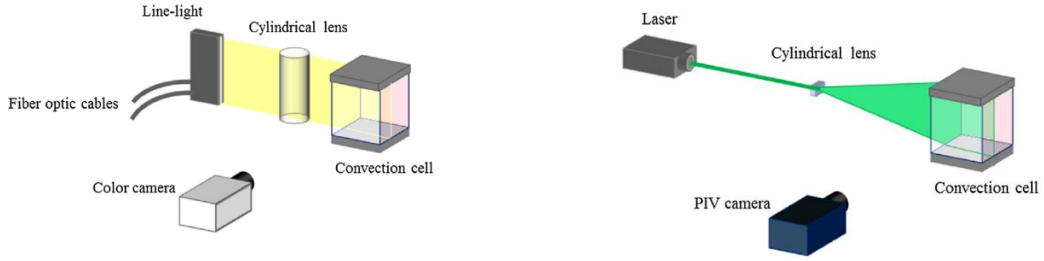

(a) (b)

Figure 1.8 Experimental setup for (a) temperature field measurement by LCT and (b) velocity field measurement by PIV (Ataei-Dadavi et al., 2019)

Numerical approach for heat transfer and fluid flow characterization

Experimentally measuring fluid flow in a cavity is a challenging task because of its extremely sensitive behaviors to experimental and boundary conditions (Miroshnichenko & Sheremet, 2018). Some numerical studies investigated a close cavity and used their own experimental data for model validation (Baïri, 2008; Leporini et al., 2018) or the ones from literature (Aitlahbib & Chehouani, 2015; Dalal & Das, 2006; Lee et al., 2016; Pirmohammadi & Ghassemi, 2009; Rincón-Casado et al., 2017).

Computational Fluid Dynamics (CFD) model is widely used for studying fluid flow in a cavity because the flow can be complex even under low Rayleigh numbers depending on the position of the cold and warm walls, aspect ratio (H/L) and inclination angle. The Finite Volume method is the most common strategy to solve heat transfer and fluid flow problems. The Finite Element Method could still be used but it has less specificity to the fluid flow problem where non-linearity is high.

CFD simulations allow researchers to investigate the effect of radiation on heat transfer in a cavity as it is complicated to experimentally determine radiative flux as mentioned previously. Leporini et al. (2018) compared numerical results applying convection with or without radiation in an empty cavity filled with air under several tilting angles. They reported that radiation significantly impacted the numerical results of some configurations with up to 8% difference of average air velocity.

Since the cavities related to insulated boxes with PCM for food transport usually have low Rayleigh number ($Ra < 10^9$) because the boxes have relatively small dimensions (< 1 m) and low temperature differences, the laminar airflow inside a cavity can be assumed (Saury et al., 2011). This explains the absence of the discussion on the turbulence models in this section.

One limitation of CFD model using finite volume method is that the input geometry needs to be clean, e.g., smooth surface, no overlapping surface, well-connected geometry. These defects could lead to error in meshing; thus in simulation results. Hence, additional steps for repairing the geometry are essential. The conventional mesh is shown in Figure 1.9a and the Immersed Boundary Method (IBM) in Figure 1.9b. IBM is often used to deal with complex geometries (Kim et al., 2001) in which all domains are considered as fluid, then meshes are generated.

(a) (b)

Figure 1.9 Comparison between (a) conventional mesh and (b) mesh for IBM for a 2D cavity with a circular cylinder (Bansal, 2015)

Recently, the Lattice-Boltzmann method is getting more interest from CFD researchers. It solves Navier-Stokes equations based on 'particles' interactions. It includes collision and propagation of the particles throughout the simulating domain (Aniello et al., 2022). It has been used to study heat transfer and airflow in a closed cavity with internal bodies by Jami et al. (2007) and Jami et al. (2008).This method requires less computing time and resource with better accuracy than finite volume method but it has less flexibility (Shardt, 2020).

Although CFD is widely used for heat transfer and fluid flow simulation as it has high flexibility and is suitable for several applications, e.g., buildings, chemical reactors, heat exchangers, it requires licensed software and high computing resources. It is also not suitable for real-time analysis and prediction which is crucial for monitoring transport in insulated boxes with PCM (Mercier et al., 2017). Thus, the zonal model is an alternative. It requires fewer computing resources but still gives the information of spatial and temporal temperature variation in a box. These data are necessary to control product quality and safety. East & Smale (2008) developed a zonal model for an insulated box with PCM loaded by liquid food cans (Figure 1.10). This model takes into account conduction and convection, however, it is based on specific assumptions for example, identical boundary conditions and load geometry, thus, it can only be applied to some configurations.

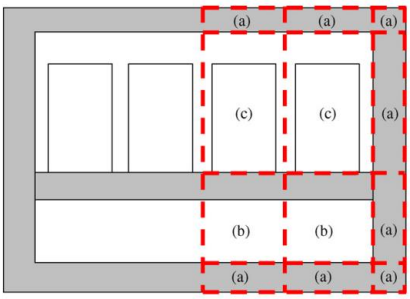

Figure 1.10 Schematic for zonal heat transfer modelling. Zone definition: (a) box's insulation, (b) PCM and the divider between PCM and product and (c) food product and air gap (East & Smale, 2008)

1.4.3 Factors affecting heat transfer and fluid flow in a closed cavity

Several factors impacting heat transfer and fluid flow in a closed cavity are presented in this sub-section.

Rayleigh number

As mentioned previously, Rayleigh numbers determine fluid flow regime. Although this thesis discusses only laminar flow ($Ra < 10^9$), Rayleigh numbers are still an essential factor in heat transfer and fluid flow characterization in a cavity. They can define the dominant heat transfer mode (Baïri, 2008; Dalal & Das, 2006; Pirmohammadi & Ghassemi, 2009), fluid flow pattern (Ha et al., 2002; Rincón-Casado et al., 2017) and time-dependent characteristic of flow patterns (Ha et al., 2002; Lee et al., 2013; 2016). Figure 1.11 illustrates isotherms and streamlines in an empty cavity with vertical warm wall and cold wall and adiabatic horizontal walls for $Ra = 10^3$ and 10^6 by changing temperature difference between warm wall and cold wall. It can be seen that higher Rayleigh number leads to more thermal stratification at the top and more distorted flow patterns.

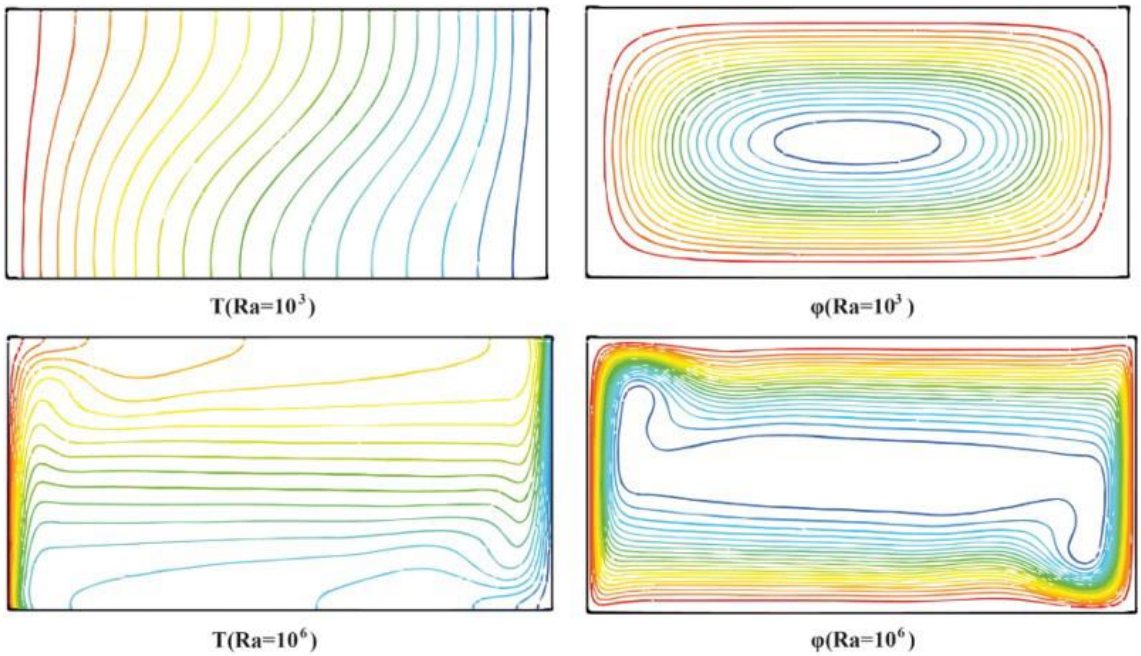

Figure 1.11 Isotherms (left) and streamlines (right) of an empty cavity with vertical warm and cold wall and adiabatic horizontal walls (Rincón-Casado et al., 2017)

High Rayleigh numbers also induces 3-dimensional flow patterns, especially in cavities with internal bodies. In the case of a cavity with hot circular cylinder located close to the bottom wall and cold side walls (adiabatic front and rear walls), Choi et al. (2015) found that the flow patterns changed from 2D to 3D when Rayleigh number increased from 10^3 to 10^6.

Apart from 3D behavior, higher Rayleigh number also induces time-dependent

behavior. Lee et al. (2013) studied the airflow in a cavity with a circular cylinder and reported that at *Ra* = 10^4, the flow was steady but it became time-dependent when *Ra* = 10^6 (Figure 1.12).

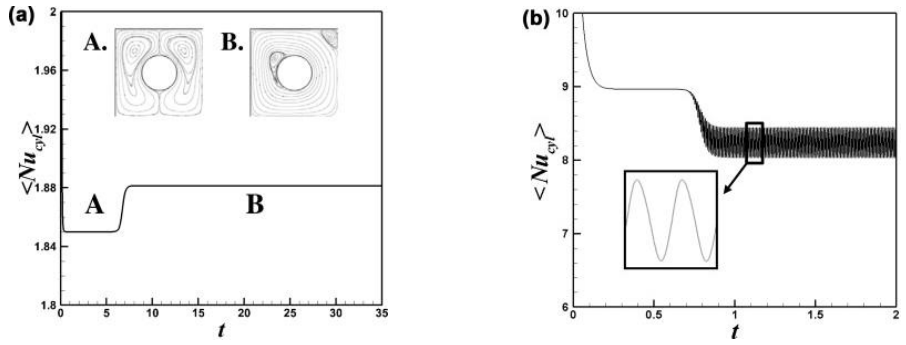

Figure 1.12 Time history (using dimensionless time value) versus surface-averaged Nusselt number of a heated cylinder in a cavity with heated bottom wall and top cold wall at (a) Ra = 10^4 and (b) Ra = 10^6 (Lee et al., 2013)

Rayleigh number also influences the effect of other parameters on heat transfer and fluid flow in a cavity, e.g., the effect of aspect ratio on Nusselt number (Ataei-Dadavi et al., 2019; Lee et al., 2013; Rincón-Casado et al., 2017).

Aspect ratio of a cavity

Dalal & Das (2006) mentioned that aspect ratio (H/L) of a cavity affects the convective heat transfer. In an empty cavity with vertical cold and warm walls, higher H/L led to higher maximum velocity and higher Nu at the side wall, lower Nu at the top wall and no effect on the bottom wall. The same findings were reported by Cesini et al. (1999) for an enclosure with a circular cylinder.

Cavity inclination

The configuration with opposite cold and warm walls can be varied by changing the tilting angle of the cavity. Baïri (2008) investigated the impact of cavity inclination on fluid flow patterns and temperature in an empty cavity (Figure 1.13a). They also reported the average Nusselt number of each angle (Figure 1.13b). The lowest Nusselt number was observed when the tilting angle was 270° or -90°. This configuration represented the warm wall at the top and the cold wall at the bottom, so, pure conduction occurred. Then, when the warm and cold walls were vertically aligned at 0°, the flow became one loop with thermal stratification. The highest average Nusselt number was found when the inclination angle was 90°, i.e., when the warm wall was at the bottom and the cold wall was at the top. In this case, Rayleigh-Bénard convection took place in the cavity.

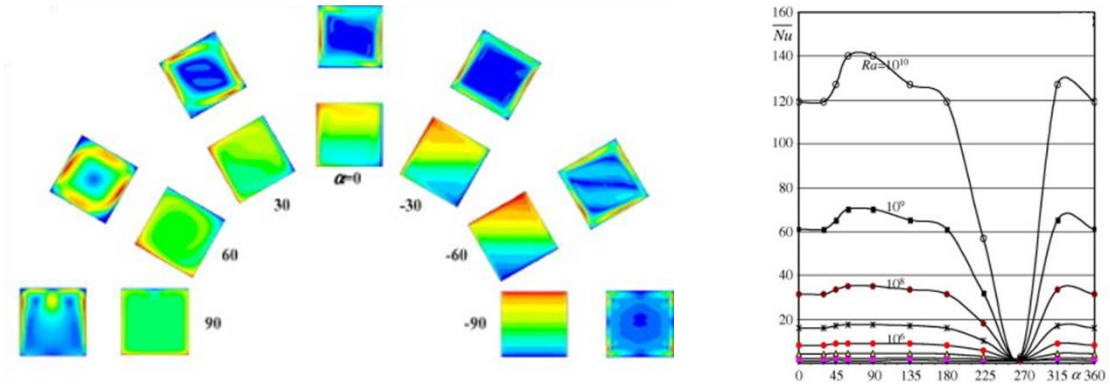

(a) (b)

Figure 1.13 Effect of inclination angle of a cavity on (a) velocity map (on the outer radius) and temperature map (on the inner radius) and (b) average Nusselt number versus inclination angle for various Rayleigh number (Baïri, 2008)

Internal bodies

The presence of internal bodies in a cavity obstructs heat transfer and fluid flow and often leads to lower heat transfer coefficient (Ha et al., 2002). The internal body's position and its thermal boundary conditions (e.g., cold, warm, adiabatic) are the main factors that several works focused on. Jami et al. (2008) found that when they moved a heated circular cylinder far away from isothermal hot wall, Nusselt number of this wall decreased. They also reported that moving this body closer to cold wall led to higher Nusselt number of this wall (Figure 1.14).

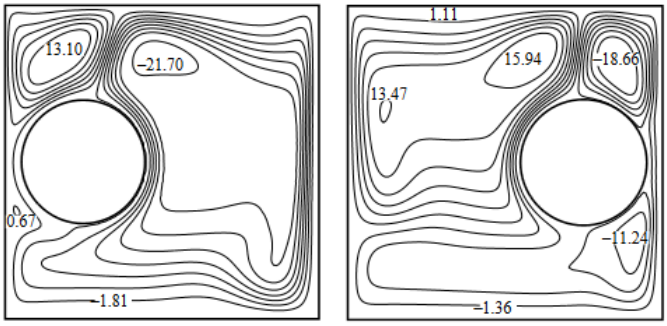

(a) (b)

Figure 1.14 Effect of position of a heated circular cylinder on streamlines in a cavity (hot wall on the left and cold wall on the right) at Ra = 10^6 with (a) cylinder on the left and (b) cylinder on the right (Jami et al. 2008)

For food transport in an insulated box, the load can sometimes be assumed as a porous body (Laguerre et al., 2008b) i.e. presence of a lot of small product items compared to the cavity. The impact of the presence of a porous medium on temperature and fluid flow in a cavity were experimentally measured by Ataei-Dadavi et al. (2019). They studied the effects of packed spheres in a cavity by varying its material, size and packing patterns on temperature field and fluid flow. They found that Nusselt number depends on spheres' size and thermal conductivity at low Rayleigh number, but only the sphere thermal conductivity had a significant effect under high Rayleigh number as shown in Figure 1.15.

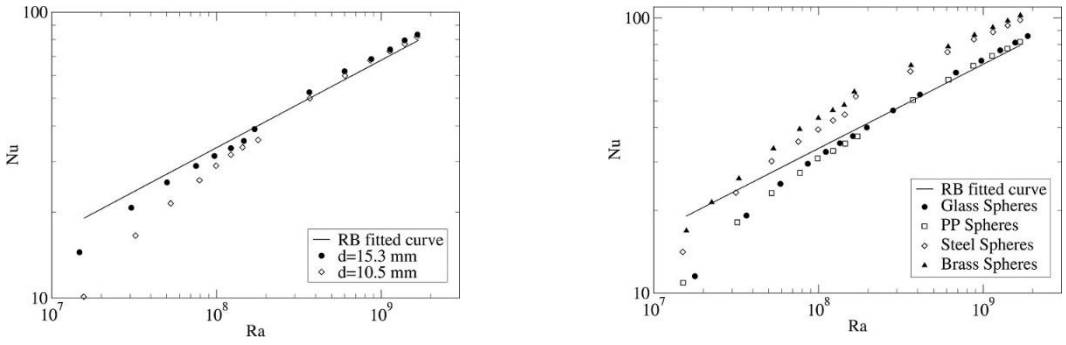

(a) (b)

Figure 1.15 Effect of (a) size of glass sphere and (b) sphere's material at d = 15.3 mm on average Nusselt number in a cavity - RB fitted curve represents the case when Rayleigh-Bénard (RB) convection takes place in the cavity (Ataei-Dadavi et al., 2019)

Presence of PCM

Since PCM acts as thermal energy storage in transport with an insulated box, thermal performance of PCM is necessary to determine the appropriate amount of PCM. Jevnikar & Siddiqui (2019) and Kamkari et al. (2014) demonstrated the evolution of heat transfer inside PCM during melting process. When PCM slab is placed vertically, these authors reported three main periods: conduction, strong convection and weak convection. Initially, conduction heat transfer dominated when most parts of the PCM was solid (Figure 1.16a) during which Nusselt number was the lowest. Then, PCM melted and turned to liquid, which recirculated along the cavity height and this allowed the increase in Nusselt number (Figure 1.16b). When most part of PCM was liquid, there was a thermal stratification, i.e., liquid at the top became stagnant and led to lower Nusselt number (Figure 1.16c). It is to be emphasized that these three periods were observed when the heat responsible to PCM temperature increase comes from one vertical wall.

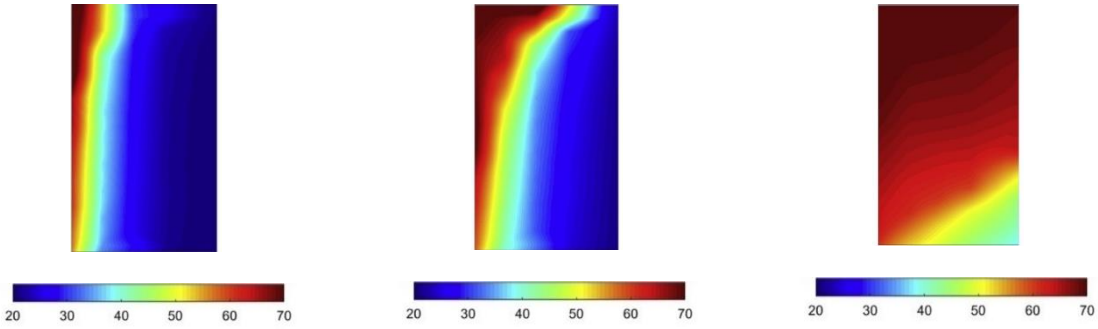

(a) (b) (c)

Figure 1.16 Temperature field in a melting PCM (paraffin waxes – T_m = 55.0°C) at (a) 40 min, (b) 80 min and (c) 600 min (Jevnikar & Siddiqui, 2019)

Kamkari et al. (2014) found that when PCM was placed horizontally and the heat responsible to PCM temperature increase comes from bottom wall. In this case, only two periods were observed: conduction and strong convection. This can be explained by the fact that this configuration did not allow thermal stratification (Figure 1.17). They also mentioned that melting time of horizontal PCM was shorter than vertical one (Figure 1.18).

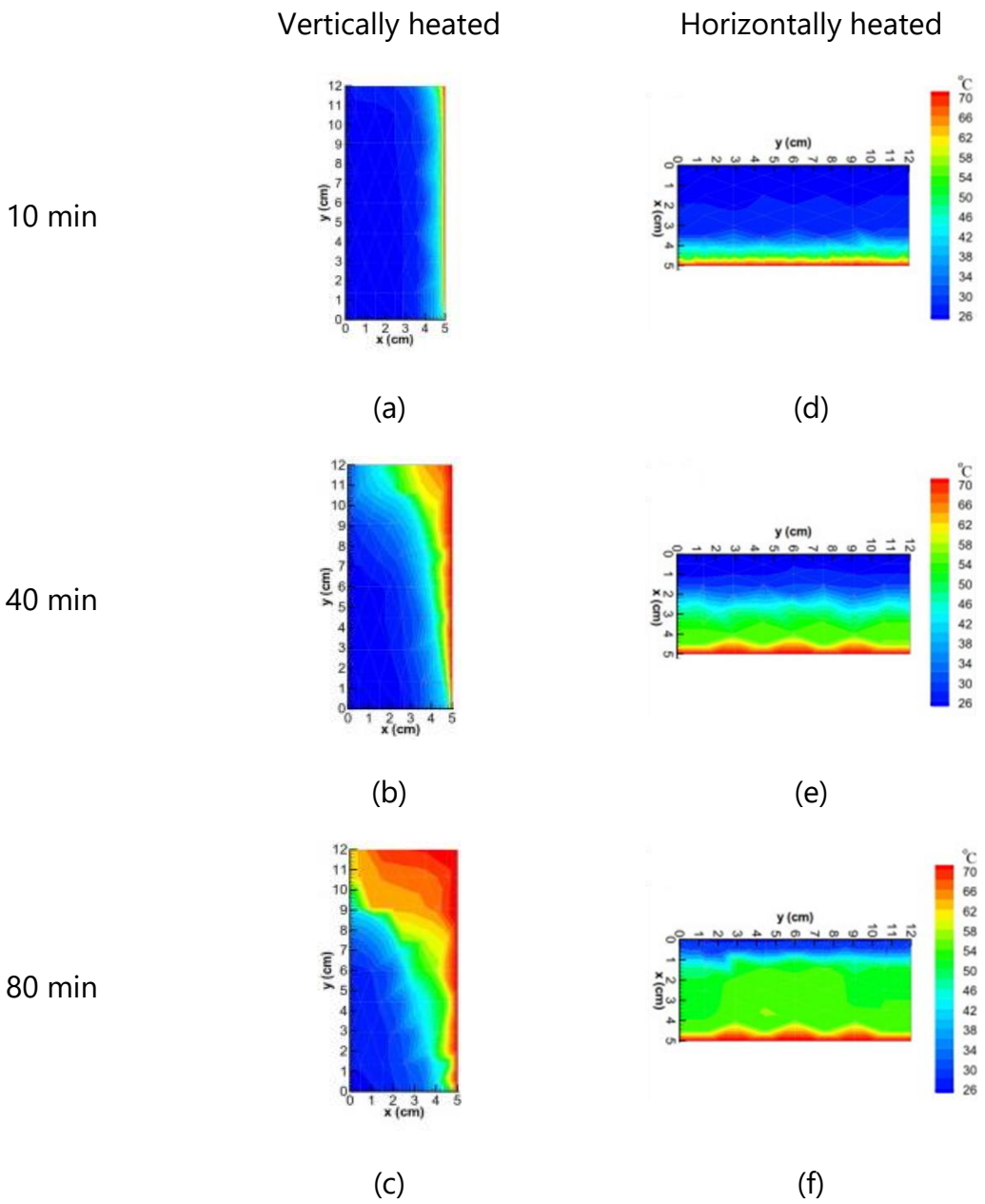

Figure 1.17 Temperature contour at middle plane of melting PCM (Lauric acid – T_m = 43.5 to 48.2°C) (a – c) vertically heated (d – f) horizontally heated at 10, 40 and 80 min. (Kamkari et al., 2014)

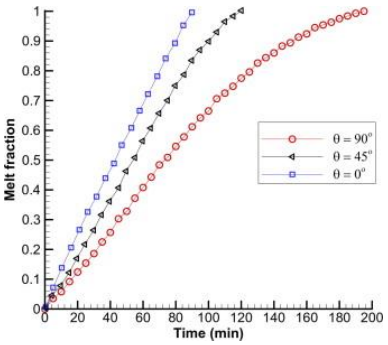

Figure 1.18 Effect of inclination angle of a PCM cavity on melt fraction evolution – θ = 0° is horizontally PCM and θ = 90° is vertically PCM (Kamkari et al., 2014)

The aim of food transport in an insulated box is to maintain an optimal temperature as long as possible. PCM as thermal energy storage allows the increase in thermal performance by taking advantage of its latent heat (Aitlahbib & Chehouani, 2015; Moreno et al., 2020). Figure 1.19 compares the temperature evolution in a cavity with and without PCM, it can be seen that PCM allows maintenance of low temperature in a cavity as long as PCM is not completely melted.

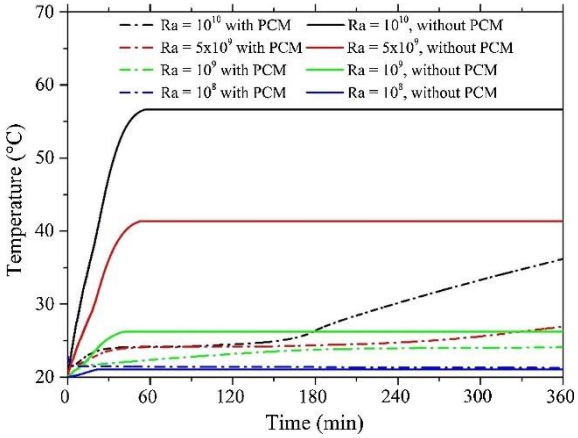

Figure 1.19 Temperature evolution in a cavity without and with PCM (PureTemp29X – T_m = 28.6 – 29.4°C) at various Rayleigh number (Moreno et al., 2020)

The challenges for studying a cavity with PCM were uneven PCM surface temperature and PCM density change during melting (Labihi et al., 2017; Moreno et al., 2020). Thus, assuming constant temperature at the surface and/or constant density during melting process may lead to significant error of numerical results. However, simulating the phase change process including density change requires adaptative mesh and largely increases simulation time. To reduce simulation time, Labihi et al. (2017) and Moreno et al. (2020) used effective density for PCM to calculate heat transfer during phase change.

1.5 CONCLUSIONS

The literature study showed the benefits of applying PCM in food cold chain: less temperature abuse, and thus better product quality and better energy management. To achieve these benefits, many factors should be considered: insulating material, PCM type, its quantity and position, load characteristics, and operating conditions. Thus, optimization of these factors is necessary in order to design the best configuration for achieving the objective of each application.

Since there are several commercialized box designs and operating conditions in real transport, modeling is an interesting tool to optimize these factors for wider range of applications since the results can be predicted within a short time and low cost in comparison to experimental approach. A better understanding of the instantaneous heat transfer and airflow in an insulated box with PCM can improve existing models. Innovative optical techniques such as Laser Doppler Velocimetry (LDV) and Particle Image Velocimetry (PIV) could be used for investigating airflow in a closed cavity where natural convection takes place. In the previous studies about free convection in cavities the boundary conditions are usually assumed isothermal or adiabatic. In practice, PCM surface temperature can be uneven and time-dependent during phase change and the other walls are imperfectly insulated. In addition, there is also a transient heat exchanges between internal air and load. This type of configuration is rarely studied.

This thesis has developed a protocol to determine temperature and air velocity in an insulated box with PCM and investigated them experimentally to get better understanding of the physical phenomena in the box. Then, they were used for thermal model development for model validation. Ultimately, this thesis presented tools (experiment and models) to optimize the box design and the operating conditions to maintain appropriate food temperature during transport, thus minimize food loss and waste.

Conclusions

L'étude bibliographique a montré les avantages de l'utilisation de PCM dans la chaîne du froid alimentaire : moins de dépassements de température recommandée, et donc une meilleure qualité des produits, ainsi qu'une meilleure gestion de l'énergie. Pour bénéficier de ces avantages, de nombreux facteurs doivent être pris en compte : le matériau isolant, le type de PCM, sa quantité et sa position, les caractéristiques du chargement et les conditions ambiantes. Pour chaque application, il conviendrait d'optimiser les paramètres d'action.

Comme il existe de très nombreuses conceptions de caissons et conditions de fonctionnement, la modélisation est un outil intéressant d'optimisation de ces facteurs pour une large gamme d'applications puisque les résultats peuvent être prédits rapidement et à faible coût par rapport à l'approche expérimentale. Une meilleure compréhension des transferts de chaleur et des écoulements d'air dans un caisson isotherme avec PCM peut améliorer les modèles existants. Des techniques optiques innovantes telles que la vélocimétrie laser Doppler (LDV) et la vélocimétrie par images de particules (PIV) pourraient être utilisées pour étudier l'écoulement d'air par convection naturelle dans des enceintes fermées. Dans les études antérieures sur la convection libre dans les cavités, les conditions aux limites sont généralement supposées isothermes ou adiabatiques. Dans notre cas, la température de surface du PCM peut être hétérogène et dépendante du temps lors du changement de phase et les autres parois sont imparfaitement isolées. De plus, il y a aussi un échange de chaleur transitoire entre l'air intérieur et le chargement. Ce type de configuration est rarement étudié.

Dans ce travail de thèse, nous avons développé un protocole expérimental pour déterminer la température et la vitesse d'air dans un caisson isotherme équipé de PCM afin de mieux comprendre les phénomènes physiques en jeu. Ces résultats ont été utilisés pour le développement de modèles thermiques et pour leur validation. En résumé, cette thèse présente des outils (expériences et modèles) pour optimiser la conception de caissons isothermes et leurs conditions de fonctionnement afin de maintenir une température appropriée des aliments pendant le transport, minimisant ainsi les pertes et le gaspillage alimentaires.

2 EXPERIMENTAL APPROACH FOR HEAT TRANSFER AND AIRFLOW CHARACTERIZATION IN AN INSULATED BOX

2.1 SUMMARY

This chapter explains the experimental approach for measuring heat transfer (by thermocouples) and airflow (by Particle Image Velocimetry) in an insulated box with PCM. Loading conditions of progressive complexity were used to characterize physical phenomena: no load, load with extruded polystyrene slabs (XPS - without heat exchange with air) and load with test product (Tylose). Next, several effects of box configurations and operating conditions were discussed: PCM position (on a sidewall and at the top), box geometry (height/width ≈ 1 and 1.7), ambient temperature (10°C to 30°C), initial test product temperature (4°C and 10°C), and spacing beneath the test product (no gap and 20-mm gap). This chapter also provides the estimation of maximum storage time for a given PCM mass and a given ambient temperature. The experimental results in this chapter were published in Article 2 and 3 and whole data in Article 6 and 7 (data papers, see appendix).

Résumé

Ce chapitre porte sur la caractérisation expérimentale des transferts thermiques (par thermocouples) et des écoulements d'air (par Vélocimétrie par Images de Particules) dans un caisson isotherme avec PCM. Des conditions de chargement de complexité progressive ont été étudiés : pas de chargement, chargement en polystyrène extrudé (XPS - sans échange de chaleur avec l'air) et chargement avec le produit modèle (Tylose). Ensuite, les effets de plusieurs paramètres ont été analysés : position du PCM (sur un côté et en haut), géométrie du caisson (hauteur/largeur ≈ 1 et 1,7), température ambiante (10°C à 30°C), température initiale du produit à tester (4°C et 10°C) et espacement sous le produit à tester (pas d'espace et espace de 20 mm). Ce chapitre fournit également une estimation de la durée maximale de stockage pour une masse de PCM et une température ambiante données. Les résultats de ce chapitre ont été publiés dans les articles 2 et 3 et l'ensemble des données dans les articles de données (data paper) 6 et 7 (voir annexe).

2.2 ARTICLE 2

Étude expérimentale de l'écoulement d'air et des transferts de chaleur par convection naturelle dans un caisson isolé équipé d'un matériau à changement de phase à l'aide d'une technique de vélocimétrie par images de particules

Résumé (version française de l'abstract de l'article 2)

L'écoulement et les transferts de chaleur par convection naturelle dans un caisson isolé équipé d'un matériau à changement de phase (phase change material : PCM) ont été étudiés expérimentalement par vélocimétrie par images de particules (particle image velocimetry PIV) et par des mesures de température. L'effet de la position du PCM (paroi latérale ou couvercle) sur l'écoulement et la distribution de température ont été étudiés dans des conditions de caisson vide et chargé. Deux chargements ont été considérées pour étudier l'effet d'obstacle et l'influence des échanges thermiques avec l'air. Quelle que soit la position du PCM, un écoulement laminaire a été observé et le nombre de Rayleigh correspondant était d'environ 10^7. Un écoulement ascendant a toujours été observé près des parois latérales de la boîte. Lorsque le PCM était sur le côté, un flux descendant se produisait le long du PCM ; dans le cas vide, le flux était presque 2D mais est devenu 3D en présence du chargement. Lorsque le PCM était sur le couvercle, l'air se refroidissait au contact du PCM, s'en détachait et coulait vers le bas. Dans le cas vide, le flux descendant était instable, et avec le chargement l'air suivait des chemins préférentiels. Le type de chargement n'a montré que peu d'effet sur la structure de l'écoulement, ainsi, un chargement plus simple (polystyrène extrudé) peut être utilisée en première approche. La vitesse maximale était d'environ 0,1 $m.s^{-1}$, la convection naturelle ne peut donc pas être négligée par rapport à la conduction. La position du PCM montre peu d'influence en termes de température du produit du moment que des espaces sont laissés entre le chargement et les parois ou le PCM.

Experimental investigation of airflow and heat transfer by natural convection in an insulated box with a Phase Change Material using a Particle Image Velocimetry technique

Tanathep Leungtongkum[a], Onrawee Laguerre[a], Denis Flick[b], Alain Denis[a], Steven Duret[a] and Nattawut Chaomuang[c]*

[a]Université Paris-Saclay, INRAE, FRISE, 92761 Antony, France
[b]Université Paris-Saclay, INRAE, AgroParisTech, UMR SayFood, 91300 Massy, France
[c]Department of Food Engineering, School of Engineering, King Mongkut's Institute of Technology Ladkrabang, Bangkok, Thailand 10520

***Corresponding author:** Nattawut Chaomuang, Tel: +66 (0) 2 329 8356 Ext. 21, e-mail: nattawut.ch@kmitl.ac.th

Abstract

Airflow and heat transfer via natural convection in an insulated box with Phase Change Material (PCM) were experimentally investigated using Particle Image Velocimetry (PIV) and temperature measurements. The effects of PCM positions (side wall and lid) on flow pattern and temperature distribution were studied under empty and loaded conditions. Two loads were considered to study the obstacle effect and the influence of heat exchange with air. When PCM was either at the side wall or at the lid of the box, laminar flow was observed and the corresponding Rayleigh number was about 10^7. Upward flow was always observed near the side walls of the box. When PCM was on the side, downward flow occurred along the PCM; in the empty case, flow was almost 2D but became 3D when the load was added. When PCM was on the lid, the air cooled in contact with PCM, detached from it and flowed downwards. In the empty case, downward flow was unstable, and with the load, it followed preferential pathways. The type of load exerted little effect on flow patterns at thermal steady state. Thus, a simpler load (extruded polystyrene) can be used in the first approach. The maximum velocity was about 0.1 $m \cdot s^{-1}$, so free convection cannot be neglected compared with conduction. Regarding temperature performance, PCM on the side and on the lid showed no substantial difference if gaps were left between the load and the walls or PCM.

Keywords: Airflow, Heat Transfer, Natural convection, Insulated box, Phase Change Material

Nomenclature

A Aspect ratio [-]
c_p Specific heat [$J \cdot kg^{-1} \cdot K^{-1}$]
g Acceleration due to gravitation [$m \cdot s^{-2}$]
Gr Grashof number [-]
H Height [m]

L Length [m]
Ra Rayleigh number [-]
Pr Prandtl number [-]
t Time [s]
T Temperature [°C or K]
ΔT Temperature difference [°C or K]
U Overall heat transfer coefficient [$W \cdot m^{-2} \cdot K^{-1}$]
v Velocity magnitude [$m \cdot s^{-1}$]
W Width [m]
x, y, z Coordinates [m]

Greek letters

α Thermal diffusivity [$m^2 \cdot s^{-1}$]
β Thermal expansion coefficient [K^{-1}]
λ Thermal conductivity [$W \cdot m^{-1} \cdot K^{-1}$]
ε Emissivity [-]
ρ Density [$kg \cdot m^{-3}$]
μ Dynamic viscosity [$kg \cdot m^{-1} \cdot s^{-1}$]
υ Kinematic viscosity [$m^2 \cdot s^{-1}$]

Subscripts

a air
c cold
g glass
h hot
s surface
th thermal
w wall
∞ free stream

Abbreviations

CFD Computational Fluid Dynamics
PCM Phase Change Material
PIV Particle Image Velocimetry
TYL Tylose
XPS Extruded Polystyrene

1. Introduction

Insulated boxes equipped with Phase Change Material (PCM) have been widely used in the transport of various temperature-sensitive products such as meat and fishery products (Paquette et al., 2017), fruit and vegetables (Zhao et al., 2019), and

pharmaceutical products (Robertson et al., 2017). The advantages of insulated boxes with PCM include low investment and operating costs, flexibility in storage temperatures and volumes, and ease of maintenance (Zhao et al., 2020a). However, two drawbacks emerge: the temperature in an insulated box is difficult to control, and temperature heterogeneity is often observed, with a low temperature in the vicinity of the PCM and a high temperature further away from the PCM (Laguerre et al., 2008a; Margeirsson et al., 2012; Navaranjan et al., 2013). This problem can result in the degradation of product quality, for instance chilling/freezing injury (a temperature that is too low leads to cell damage) and pose a safety risk (a temperature that is too high leads to bacterial growth) (Laguerre et al., 2019). As reviewed by Leungtongkum et al. (2022), numerous experimental and numerical studies have been conducted to evaluate the thermal performance of insulated boxes equipped with PCM. Choi & Burgess (2007) developed simplified heat transfer models based on an ice melting test for the estimation of heat flow resistance (R-value) which is a factor generally used to determine the insulation performance of the box. Later, Singh et al. (2008b) applied this method and reported the R-values of insulated boxes made of various insulating materials with different wall thicknesses and box dimensions. Various 2D and 3D Computational Fluid Dynamics (CFD) models of insulated boxes with PCM were developed to study the influences of different factors on the evolution of air/product temperatures (Du et al., 2020; Laguerre et al., 2018, 2019; Margeirsson et al., 2012; Paquette et al., 2017; Xiaofeng & Xuelai, 2021). These factors included box characteristics (dimensions, shape of inner corners, types and thicknesses of insulating materials, internal surface emissivity), PCMs (types, mass, and position in a box), products (types, initial temperature, mass, and arrangement in a box), and operating conditions (ambient temperature and transport duration) (Leungtongkum et al., 2022). To reduce computational time, analytical and zonal models were also developed as a complementary approach (East et al., 2009; Laguerre et al., 2018, 2019). These models enable useful information (e.g., PCM melting duration and product temperature change during shipment) to be acquired as a function of the box design and usage conditions. Xiaofeng & Xuelai (2021) developed an insulated box with multiple partitions for delivery of various products, which require different preservation temperatures (ambient, chilled, and frozen temperatures) in the same box. Despite these efforts, there is still no universal optimal condition that can be applied to control the air/product temperatures in an insulated box.

All heat transfer modes can occur simultaneously in an insulated box with PCM: conduction (inside the product, PCM and the walls of the box), natural convection (between air and product/PCM in the box), natural/forced convection (between external air and the box), and radiation (between the walls and product/PCM in the box) (Leungtongkum et al., 2022). For model simplification, most numerical studies consider heat transfer by conduction, and sometimes also by radiation, while natural convection inside the box tends to be neglected (Du et al., 2020). In fact, all heat transfer modes can be of the same order of magnitude, and natural convection can

exert significant impacts, especially on temperature heterogeneity in the insulated box (Laguerre & Flick, 2010).

Natural convection in closed cavities occurs in a wide range of engineering applications and has been extensively studied with both experimental and numerical approaches (Miroshnichenko & Sheremet, 2018; Pandey et al., 2019). The configurations commonly studied are air or water in a rectangular cavity of which two opposite (horizontal/vertical) walls are maintained at different constant and uniform temperatures (hot and cold) while the other walls are perfectly insulated (adiabatic). Many studies also introduce porous medium or solid objects (flat plate, cylinder and sphere) in the cavity to observe their effects on heat transfer and airflow (Ataei-Dadavi et al., 2019; Lee et al., 2016). The knowledge acquired using a cavity filled with porous media can be applied to the case of small products such as cereal grains (ratio between characteristic lengths of product and cavity ≤ 0.02). However, the models are limited in the case of larger products (e.g., meat, fruit and vegetables) where the ratio is much higher (> 0.1) (Laguerre et al., 2008b). Moreover, the configuration of a product-loaded insulated box with PCM is more complex because all walls are subjected to heat loss and the wall equipped with PCM (cold wall) has a non-uniform temperature as PCM melts more rapidly at some positions (Jevnikar & Siddiqui, 2019). Several experimental and numerical studies were conducted to investigate heat transfer and airflow in air-filled cavities with PCM at one wall. Aitlahbib & Chehouani (2015) developed a two-dimensional numerical model to evaluate the thermal performance of an insulated container with one vertical wall equipped with PCM, the opposite one kept at higher temperature while other walls were well-insulated. The results demonstrated that the container with PCM wall achieved superior thermal performance than the one without. The same cavity configuration was numerically studied by Labihi et al. (2017). The effect of volume expansion of the PCM during solidification was considered in the model. Better predictions were obtained when this effect was taken into account. Moreno et al. (2020) developed a transient 2D-CFD model to describe the airflow and the heat transfer in an air-filled cavity with a PCM wall. The numerical results revealed flow patterns similar to ones observed in experiment during melting process. The temperature stratification was intensified after the liquid fraction of the PCM started to predominate (> 50%). Orozco et al. (2021) further performed a numerical study with the same cavity configuration but this time the PCM wall was segmented into small volumes. The results showed that the segmentation of the PCM wall had no significant effect on the flow patterns and the temperature distributions in the air-filled cavity. Both flow topology and temperature stratification in the cavity with the segmented PCM wall were similar to those in the cavity with the non-segmented PCM wall. However, for the same requirement of thermal retention duration, the amount of the PCM could be reduced by dividing the PCM container into segments. These mentioned studies essentially dedicated to the use of PCM to enhance the energy efficiency of buildings. Only the temperature measurements were used for the model validation (no air velocity measurement). To our best knowledge, no experimental studies combining

temperature and air velocity measurements inside an empty and loaded insulated box with PCM have been conducted.

The present study attempted to bridge this research gap. The objective was to investigate experimentally the airflow and heat transfer due to natural convection in an insulated box with PCM. The influence of the PCM position and that of the presence of a load on flow patterns and temperature distribution in the insulated box were examined in the study. A non-intrusive technique, Particle Image Velocimetry (PIV), was implemented to characterize the air velocity field. The originality of this study lies in a) the implementation of PIV measurement for low air velocity and b) the analysis of both velocity and temperature fields in different configurations of an insulated box with PCM under a real use condition of food transport i.e., all walls of the box subjected to heat losses and the presence of loads in the box. The obtained knowledge would be useful to suggest the optimal practices for handling insulated boxes used for food transport. The experimental results obtained in this study enable deep knowledge in the exchange phenomena. They will be used to develop CFD and simplified thermal models, which will be presented in the future. These numerical approaches enable the prediction of product temperature change with time at different positions in an insulated box exposed to variable ambient temperatures as in a real shipment.

2. Materials and methods

2.1 Experimental device

Two insulated boxes were used. Box A was a commercially manufactured box which was used for the thermal study (temperature measurement by thermocouples). Box B was the same box in which two walls were replaced with triple-glazed windows ensuring almost the same insulation, and it was used for the momentum study (air velocity measurement by a PIV system). As shown in Figure 2.1a, the wall structure of Box A is composed of an expanded polystyrene foam layer (thickness: 25 mm, λ = 0.029 W·m^{-1}·K^{-1}) sandwiched between two polypropylene plastic layers (thickness: 3.5 mm, λ = 0.12 W·m^{-1}·K^{-1}, ε = 0.97). The inner gap between the polypropylene layers is 35 mm so that an air layer (thickness: 5 mm, λ = 0.025 W·m^{-1}·K^{-1}) is also present. The internal dimensions of the box were 310 mm (W) × 500 mm (L) × 300 mm (H), corresponding to about 0.05 m^3 in volume. Box B had the same dimensions and wall structure, but two vertical walls were replaced by triple-glazed windows. They were composed of three glass layers (λ = 1.4 W·m^{-1}·K^{-1}) each with a thickness of 4 mm and two 10-mm argon gaps (λ = 0.018 W·m^{-1}·K^{-1}), as shown in Figure 2.1b. In addition, the panes were coated with a low-emissivity material (ε = 0.03, manufacture data) to avoid the transmission of infrared radiation. In this manner, the overall heat transfer coefficient of the glass wall was almost identical to that of the unmodified commercially manufactured box: $U_g \cong U_w$ = 0.9 W·m^{-2}·K^{-1}. This makes it possible to consider that heat losses occurring in Boxes A and B were almost the same; thus, the momentum results obtained experimentally from Box B can be compared with the

thermal results obtained from Box A.

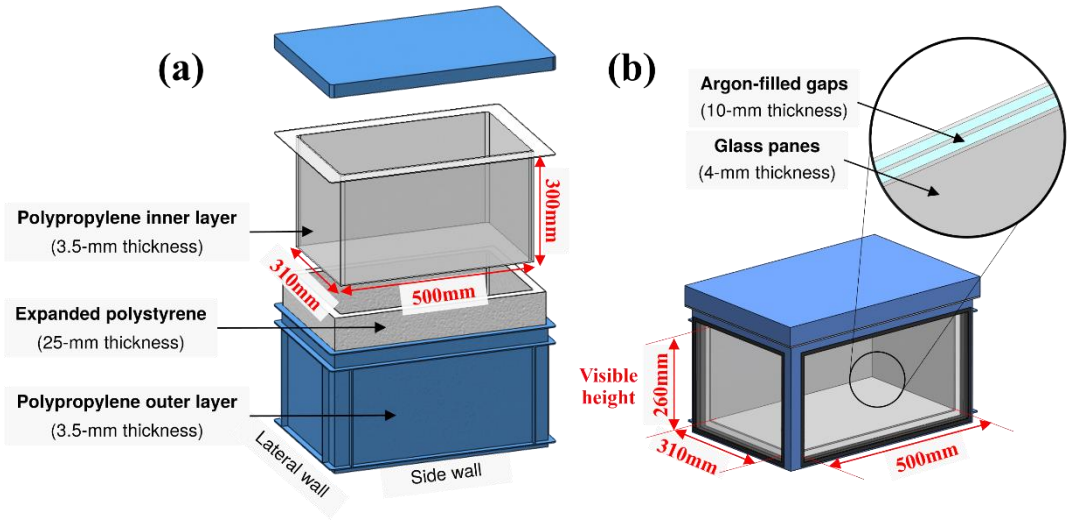

Figure 2.1 Insulated boxes: (a) commercially manufactured box for temperature measurement (Box A); and (b) box with two walls replaced with triple-glazed windows for velocity measurement (Box B).

Tap water (melting point of -0.2°C, latent heat of 334 kJ/kg) filled in a polypropylene recipient (280 mm × 460 mm × 50 mm) was used as a PCM for both thermal and momentum studies. The PCM was prepared (solidification) by placing horizontally in a freezer (-2.0°C set point) for at least 48 h before being used in each experiment to ensure that it was completely frozen at a temperature close to the melting point. Depending on the experimental conditions, the PCM was placed either on the top wall (lid) or on a vertical (side) wall of the box.

Two types of loads were used in the experiment: 4 inert blocks made of extruded polystyrene (XPS, dimensions 200 mm × 400 mm × 50 mm) and 16 packs of test product made of tylose (TYL, dimensions of a pack 200 mm × 100 mm × 50 mm). The presence of XPS blocks made it possible to study the influence of obstruction (without heat exchange with air) on the airflow pattern, while the presence of TYL packs made it possible to study the combined influence of obstruction and heat exchange with air. The use of XPS blocks made it possible to reach a thermal steady state (low thermal inertia) rapidly. Both types of loads were arranged so they had the same stack dimensions: 200 mm × 400 mm × 200 mm. The TYL packs were previously stored in a laboratory refrigerator and their initial core temperature was 5.0 ± 1.0°C before being used in the experiment. The 1.0°C temperature variation is related to the position of the pack in the refrigerator during preparation. It is to be emphasized that due to the large variety of food products and their thermophysical properties, the test product employed in the standard tests of refrigeration equipment was used. The properties of this test product (called Tylose) are close to those of meat product as shown in Table 2.1.

Table 2.1 Thermophysical properties of materials used in the study

Material	Density [kg·m^{-3}]	Specific heat [J·kg^{-1}·°C^{-1}]	Thermal conductivity [W·m^{-1}·K^{-1}]	Reference
Extruded polystyrene	35	1210	0.029	Cengel & Ghajar (2020)
Polypropylene	910	1925	0.120	Cengel & Ghajar (2020)
Tylose	1070	3372	0.510	Icier & Ilicali (2005)
Water (liquid)	1000	4217	0.561	Cengel & Ghajar (2020)
Water (solid)	920	2040	1.880	Cengel & Ghajar (2020)

To facilitate interpretation of the results, the boxes (for both the thermal and momentum studies) were placed on small supports (with a height of 50 mm) placed on a table (with a height of 700 mm), thereby ensuring homogeneous airflow around the box (including underneath it). The experimental device was placed in a test chamber (dimensions: 340 cm × 340 cm × 250 cm) in which the ambient temperature was controlled at 20.0 ± 1.0°C throughout the experiments. The humidity in the room was not controlled. The relative humidity measured by using a hygrometer (Testo 174H, accuracy ±3%rh) was in the range of 45-65%, corresponding to the humidity ratio of 0.006–0.009 kg of water vapor/kg dry air.

2.2 Thermal study

Temperature measurements were performed in Box A using calibrated T-type thermocouples (200 µm diameter, ± 0.2°C accuracy) connected to a data logger (Agilent 34972A). The protocols for the measurements under empty and loaded conditions are described hereafter.

2.2.1 Experimental protocol under empty conditions

The temperature measurements were conducted on a middle plane (x = 250 mm) of the box as shown in Figure 2.2a. Twelve thermocouples were installed on a portable stand at intervals varying from 5 mm (near the top and bottom) to 35 mm (mid-height) and were used to measure the air temperatures across the cavity. Another twelve thermocouples were fixed on the surfaces of the box walls and the PCM in order to measure their surface temperatures. Three thermocouples were also installed at three positions inside the PCM.

To establish the temperature profiles, several temperature measurements were carried out by moving the stand from one position to another across the plane. The stand was positioned at a distance of 5 mm from the walls for the initial measurement. The measurement began at least 90 min. after the box closure (steady state had been reached) and lasted for a duration of 5 min. with recording intervals of 15 s. The box

was re-opened in order to move the stand to the next position and then was closed rapidly to limit the effects of external air ingress (total duration of this operation: < 1 min). Then, temperature measurement was undertaken 15 min. after closure (steady state had been reached again). To address the temperature profile in the boundary layer, fine incremental steps of 5 mm were applied for the first five positions near the wall, then coarser incremental steps (up to 50 mm) were used (eighteen y-positions). The temperature at each position was averaged over 5 min. and the reported temperature profiles were based on these average values.

It needs to be emphasized that the phase change process of the PCM is a transient phenomenon and the real steady state never exists. The "pseudo" steady state stipulated in this study indicate the duration in which the air temperatures at different positions in the cavity were relatively constant. Preliminary experiments showed that "pseudo" steady state was reached after 90 min. Then, the standard deviations over 3 h of the air temperatures at eight positions in the box never exceeded 0.3°C.

2.2.2 Experimental protocol under loaded conditions

The stack of TYL packs was carefully placed in the center of the box, which corresponded to a loading percentage (including the PCM) of almost 50% by volume. In this case, all air and load temperatures (core and surface) were simultaneously measured throughout the experiment without intermittent openings. Figure 2.2b shows the positions of the thermocouples used to measure the air temperatures on the middle (x = 250 mm) and the lateral (x = 15 mm) planes of the box as well as the core and surface temperatures of four TYL packs. Thermocouples were also installed at three positions inside the PCM. Measurements were undertaken 90 min. after the closure of the box and lasted until the PCM was completely melted (i.e. all measured PCM temperatures started to increase). A recording interval of 30 s was set for the experiment. The air and product (core and surface) temperatures at each point were averaged over 200 min. during which the PCM was melting. These time-averaged values were used to establish the temperature field in the loaded box.

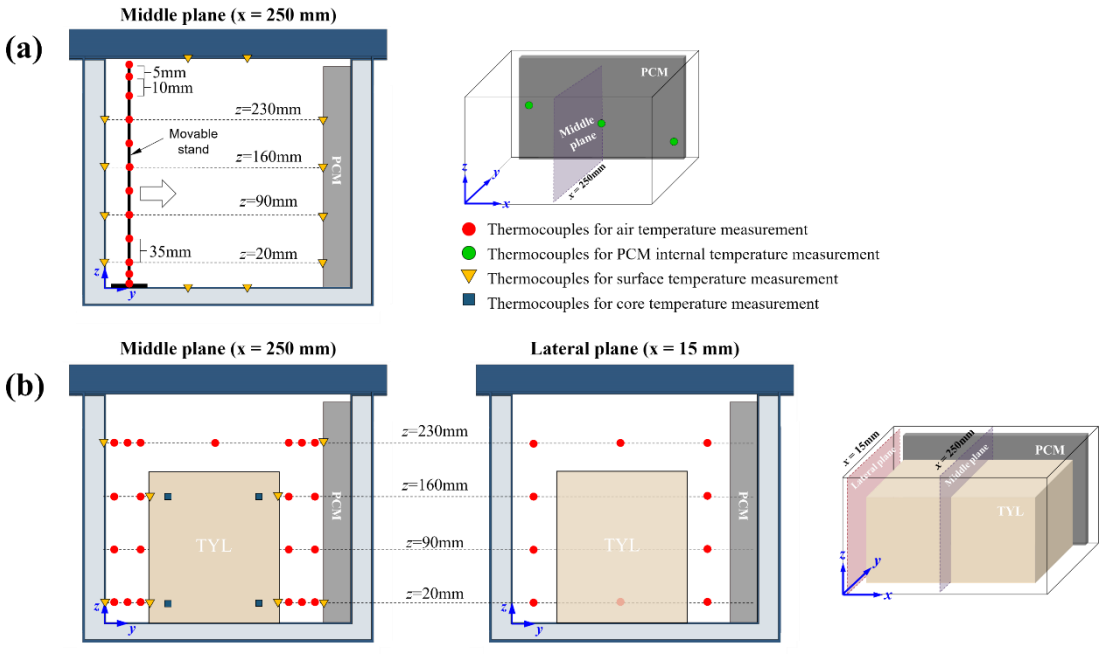

Figure 2.2 Diagram showing the experimental setup for temperature measurement for PCM located on the side wall of (a) empty box, and (b) loaded box. TYL = Tylose packages.

2.3 Momentum study

Figure 3 shows the overall view of experimental setup for the air velocity measurements in the insulated box (Box B) using a PIV system which requires tracer particles (oil smoke in our case) for the measurement. The box was connected to a smoke container using a flexible duct in which four small PCM packs were used to precool the smoke before entering the box. A small fan was used to assist the introduction of precooled smoke (~10°C) into the box and its flow rate was controlled by a valve on the connecting duct.

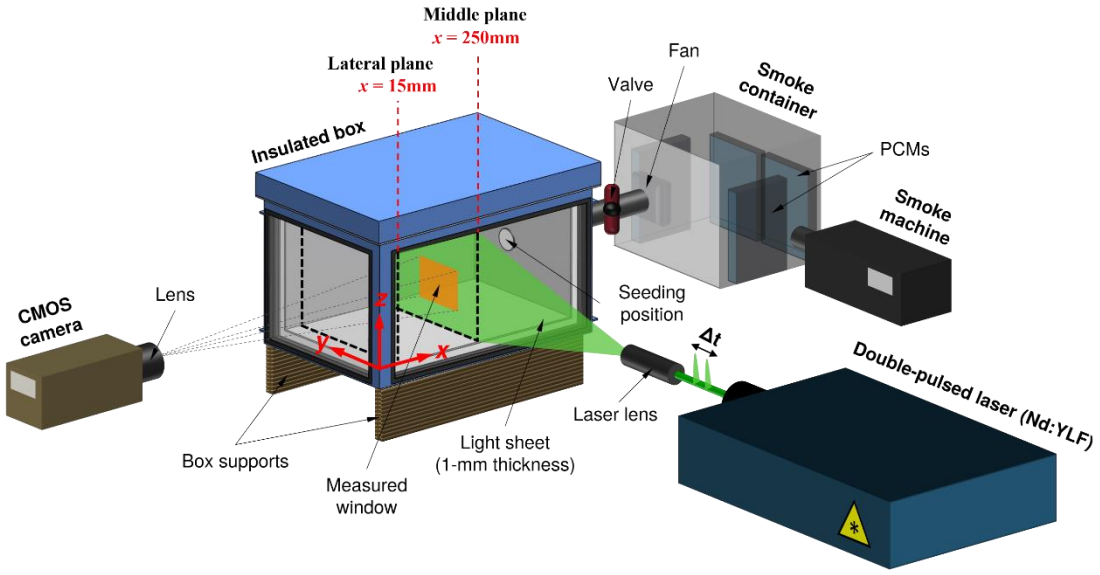

(a)

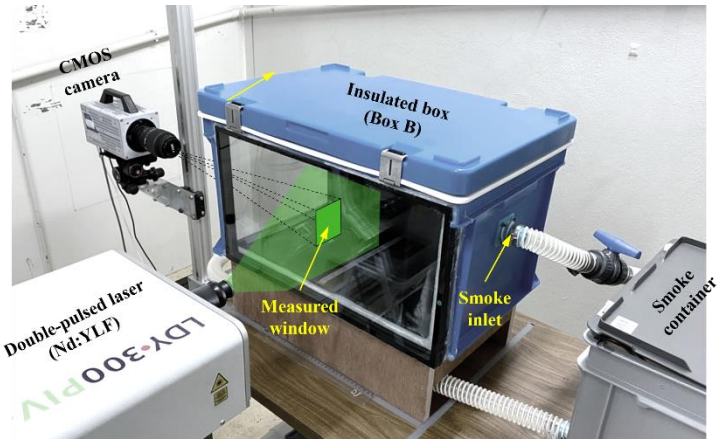

(b)

Figure 2.3 Diagram (a) and photograph (b) showing the PIV setup.

2.3.1 PIV system

A 2D-PIV system (LaVision, FlowMaster 2D) was used to visualize the flow pattern and to measure air velocity in the box. The system is composed of three main components: a double-pulsed Nd:YLF laser (527 nm wavelength, 10 mJ pulse energy), a high-speed 12-bit CMOS video camera (Photron, FASTCAM SA3; 1024 ×1024 pixels in resolution) mounted with a lens (Sigma; 105 mm, f/1:2.8), and a programmable timing unit (PTU-X) for the synchronization of the device. For light scattering, a smoke machine (Antari, F-80Z) was used to generate oil particles (Levenly, Smoke Standard; mean diameter of 0.3 µm). Image acquisition and post-processing were performed using DaVis 10.2 interfaced software. The camera and the laser were installed on a three-dimensional displacement system (displacement precision ± 1 mm) and aligned in such a manner that the field of the camera view was perpendicular to the light sheet (thickness of 1 mm).

2.3.2 Image acquisition

The PIV measurements under both unloaded and loaded conditions were performed on the same plane as the temperature measurement under loaded conditions: the middle plane (x = 250 mm) and the lateral plane (x = 15 mm). Based on the image calibration using a ruler and the DaVis software, the magnification factor of 0.113 mm/pixel was determined and it corresponded to an image size of approximately 115 mm × 115 mm. For each measurement plane, several measured windows with a partial overlap between them were used to cover the entire area of the plane. Figure 4 shows the position and its corresponding number of measured windows on the measurement plane for different experimental conditions (unloaded/loaded and PCM on the side/lid). The position of the measured windows was changed by using a displacement system.

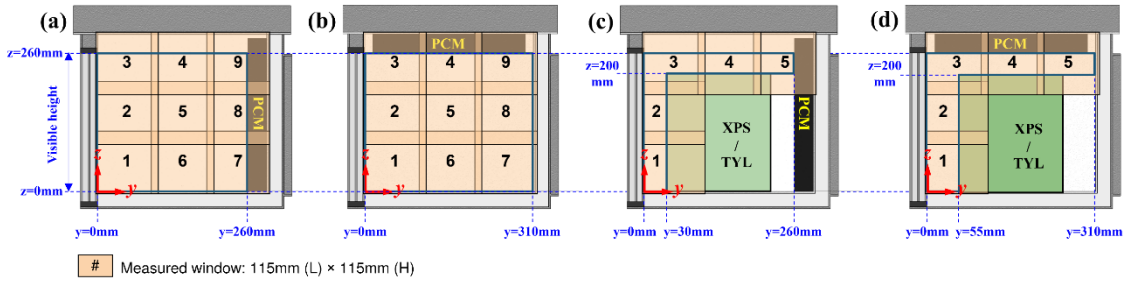

Figure 2.4 Position of measured windows for the PIV measurement: (a) empty box/PCM on the side wall, (b) empty box/PCM on the lid, (c) loaded box/PCM on the side wall, and (d) loaded box/PCM on the lid.

For each measured window, 500 pairs of images were recorded every 20 ms with a time interval (Δt) between two paired images (two pulsed laser illuminations) of 900 µs, and the total measurement duration was 10 s. Based on the preliminary experiment, the measurement duration should not exceed 10 s to avoid heat generation by the laser which caused an increase in wall temperature, thereby affecting airflow. This time interval was considered as an optimal value for a velocity estimation in our case, because it allowed a mean particle displacement of less than a quarter of the smallest width of interrogation window (Keane & Adrian, 1992).

2.3.3 Image post-processing

A multi-pass correlation algorithm was used to process instantaneous vector calculation. The cross-correlation between individual paired images was performed with decreasing interrogation window sizes: 64 × 64 pixels with 50% overlap for the first passes and 32 × 32 pixels with 75% overlap for the final passes. Given the interrogation dimensions of the final pass, the spatial resolution of the vector field (distance between two vectors) was 8 pixels (about 0.9 mm) in both vertical and horizontal directions. After 500 instantaneous vector fields were obtained, the mean velocity field (v: 2D velocity magnitude) was then calculated as follows

$$v = \frac{1}{N}\sum_{i=1}^{N}\sqrt{v_{y,i}^2 + v_{z,i}^2} \quad (2.1)$$

where N is the total number of measured windows (N = 500 in our case), v_y and v_z are the horizontal and vertical velocity components expressed in m·s^{-1}, respectively.

The mean velocity fields of all measured windows were then connected to establish the velocity field of the entire measurement plane. It should be emphasized that the out-of-plane regions and the regions near high reflection surfaces in the images (e.g. the surfaces of PCM, wall, and load) were deleted and excluded prior to the vector calculation.

The DaVis software uses the correlation statistics method (a-posteriori approach) to quantify the uncertainty of the PIV measurement. Based on the statistical analysis (Wieneke, 2015), the uncertainty of the mean air velocity reported in this study was less than 5% for v > 0.04 m·s^{-1} and less than 10% for 0.02 < v < 0.04 m·s^{-1}.

2.3.4 Experimental protocol

Air velocity measurements were carried out under steady state conditions which were achieved 90 min. after the PCM was introduced into the box. At steady state, the precooled smoke was introduced into the box until its concentration was sufficient. To ensure flow stabilization, the PIV measurement was performed about 30 min. after the smoke introduction. Nine and five measured windows of 500 paired images were captured for the experiments under empty and loaded conditions, respectively. Table 2.2 summarizes all experimental conditions for the temperature and the velocity measurements.

Table 2.2 Experimental conditions for thermal (temperature measurement) and momentum (air velocity measurement) studies.

Conditions	**PCM position**	**Temperature measurement**	**Numbers of windows for air velocity measurement [window number]**	
			Middle plane	**Lateral plane**
Unloaded	Side wall	Yes	9 [1-9]	9 [1-9]
	Lid	Yes	9 [1-9]	9 [1-9]
Loaded (XPS)	Side wall	No	5 [1-5]	9 [1-9]
	Lid	No	5 [1-5]	9 [1-9]
Loaded (TYL)	Side wall	Yes	5 [1-5]	9 [1-9]
	Lid	Yes	5 [1-5]	9 [1-9]

XPS is a stack of four extruded polystyrene blocks (block dimensions = 200 mm × 400 mm × 50 mm); TYL is a stack of 16 Tylose packs (pack dimensions = 200 mm × 100 mm × 50 mm); the window number is referred to that in Figure 2.4.

3. Results and discussion

3.1 Air velocity and temperature profiles under the empty condition

The experiment was firstly performed under empty conditions to gain an understanding of underlying momentum and energy transport phenomena inside the insulated box equipped with PCM. The influence of PCM positions (side wall and lid) on these phenomena were investigated and the results are presented as follows.

3.1.1 PCM on a side wall of the box

When the frozen PCM was placed on a side wall of the box, the apparent width (W') of the box was reduced to 260 mm and accordingly the aspect ratio ($A = H/W'$) of the box was about 1.15. Based on the temperature difference between the inner surfaces of the PCM and the walls ($\Delta T = T_h - T_c$ = 7.9°C), the Rayleigh (Ra) number based on the box height as defined in Equation 2.2 was approximately 2.8×10^7. Thus, the air flow in the box was in the laminar regime (< 10^9) (Saury et al., 2011).

$$Ra = Gr \cdot Pr = \frac{g\beta(T_h - T_c)H^3}{\upsilon^2} \cdot \frac{c_p \mu}{\lambda} \qquad (2.2)$$

The thermal properties of air were calculated at the mean air temperature in the box (T_{mean} = 7.7°C) by using the correlations proposed by McQuillan et al. (1984). The calculated values are summarized in Table 2.3.

Table 2.3 Thermophysical properties* of air used for the Ra estimation.

Parameter	Unit	Value	
		T_a = 6.2°C	T_a = 7.7°C
ρ	kg·m^{-3}	1.264	1.258
υ	m^2·s^{-1}	1.387×10^{-5}	1.400×10^{-5}
c_p	J·kg^{-1}·K^{-1}	1006	1006
λ	W·m^{-1}·K^{-1}	0.0245	0.0247
β	K^{-1}	0.0036	0.0036

*calculated at the average air temperature (T_a) from the correlations proposed by McQuillan et al. (1984)

Figure 2.5 shows the air velocity profiles on the middle (x = 250 mm) and the lateral (x = 15 mm) planes of the box equipped with the PCM on the side wall. For comparison purposes, the color scale was limited to 0.13 m·s^{-1} over which the maximum value recorded among all experimental conditions never exceeded. Large (red) arrows were drawn over the velocity field in order to provide better visualization of flow patterns represented by velocity vectors originally generated from the PIV software.

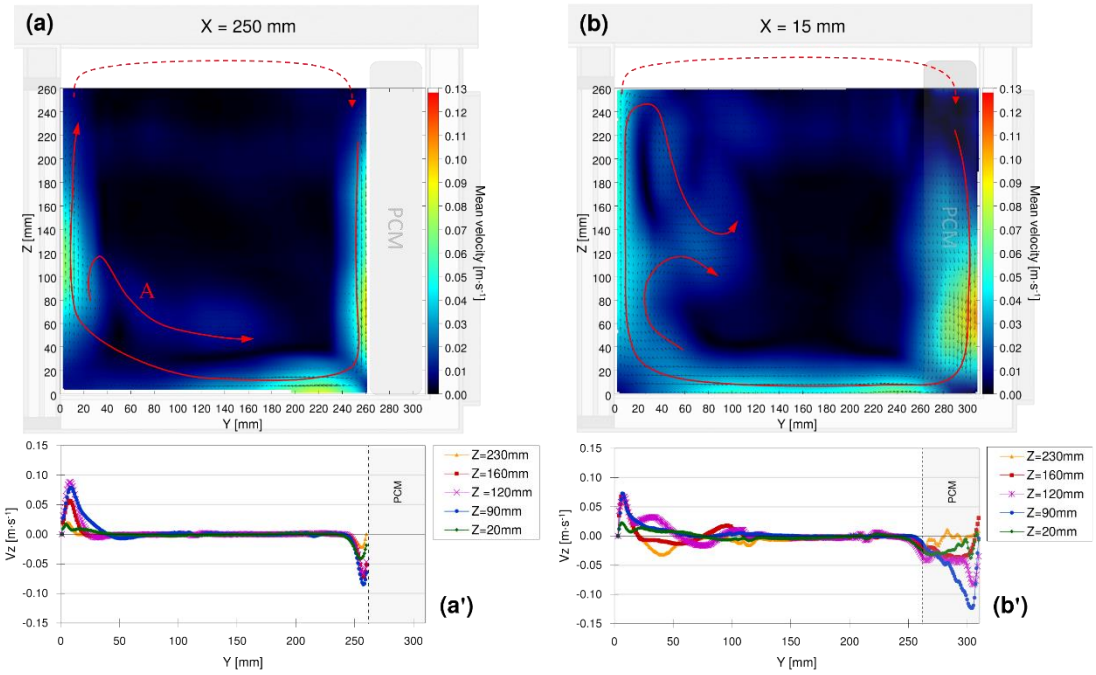

Figure 2.5 Air velocity fields on (a) the middle (x = 250 mm) and (b) the lateral (x = 15 mm) planes of the box with PCM on the side wall. (a') and (b') are the profiles of the vertical velocity component (v_z) at 4 heights on the middle and the lateral planes, respectively.

As shown in Figure 2.5a, the airflow on the middle plane exhibits a flow pattern similar to the simple case, largely documented in the literature, of a rectangular cavity with opposite isothermally hot and cold vertical walls and well-insulated horizontal walls (Lee & Lin, 1996): upward and downward flow streams adjacent to the vertical surfaces of the side wall and the PCM, respectively. These flow streams moved horizontally along the bottom and the top walls, respectively, thus forming a recirculation cell. However, due to the technical limitations of the experimental device, the visible height was limited to z = 260 mm; thus, the complete flow recirculating cell could not be visualized in our study (dashed-line arrow in Figure 2.5a).

A secondary flow was also detected (see arrow A on Figure 2.5a): the air at a distance of about 30 mm from the box wall changes its direction from upward to downward and flows toward the cold wall. This could result from the heat transfer through the bottom wall of the box. The airflow near the 'warm' bottom wall has a slightly ascending slope (this is not the case for an adiabatic bottom wall). The air located about 30 mm from the walls is entrained by the main recirculation flow, but it is relatively colder than the air nearer to the wall; thus, at a given point, its trajectory leaves the main cell and becomes downwards.

As illustrated in Figure 2.5a', the vertical velocity component (v_z) near the box wall tended to increase from bottom to mid-height (z = 120 mm) reaching almost 0.09 m·s^{-1}. Beyond this height (z > 120 mm), the velocity started to decease. A similar trend was observed near the PCM, but in the opposite manner. The vertical velocity component

($|v_z|$) steadily increased from the top until roughly z = 90 mm reaching almost 0.08 $m \cdot s^{-1}$, then the velocity began to decrease, conceivably because the flow 'turned' at the corner. The flow pattern on the lateral plane (Figure 2.5b) was almost identical to that on the middle plane, but the maximal velocity magnitude was higher (0.12 $m \cdot s^{-1}$). Note that the velocity field on the lateral plane (x = 15 mm) was extended to the region of the PCM because the PCM was symmetrically placed in the box, thereby allowing the PIV measurement in the gap between the lateral wall and the PCM (x > 20 mm).

On both planes, there is a zone of stagnant air in the core region of the box. However, this region on the lateral plane was smaller than that on the middle plane. Three-dimensional flow due to additional heat gain through the side wall could explain this difference.

Figure 2.6a shows the air temperature field on the middle plane (x = 250 mm) of the box with PCM on the side wall. This temperature field was plotted by interpolation from 252 measurement points over this plane by using MATLAB. The temperature field shows the thermal boundary layers. Due to heat conduction from the exterior, the air temperature increases constantly while it flows along the box walls, and the boundary layer thickness increases. Then, the air is cooled down along the PCM. This is coherent with the flow pattern (recirculation cell) observed by the PIV measurement. Overall stratification was observed: colder air near the bottom, and warmer air near the top. The maximum air temperature was about 10°C at the top corner on the side wall and the minimum air temperature was observed at the bottom corner on the PCM side. The surface temperature of the PCM container varied from 0.5°C at the bottom (z = 20 mm) to around 3.5°C at the top (z = 230 mm). Thermal boundary layers at different heights are illustrated in Figure 2.6b. As expected, their thickness was close to hydrodynamic thicknesses (Figure 2.5a') since the Prandtl number is relatively close to 1 (Pr = 0.71).

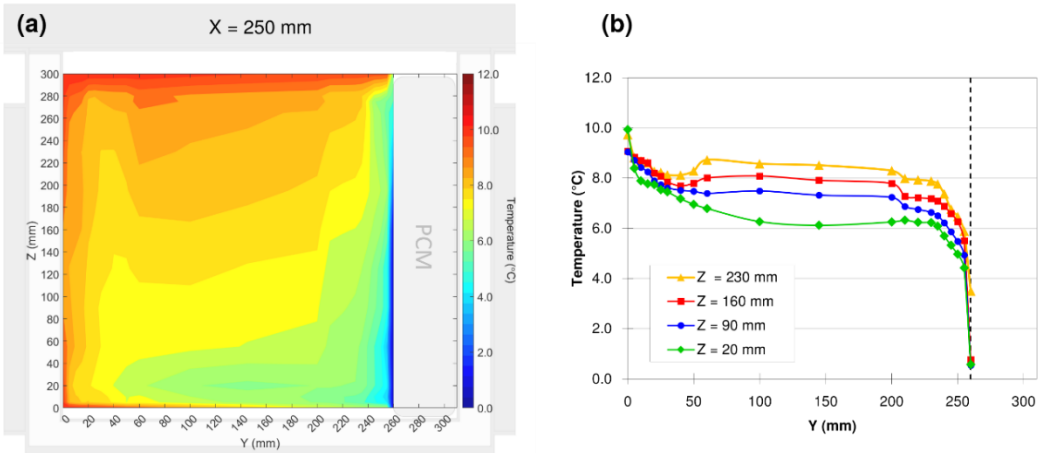

Figure 2.6 (a) Air temperature field on the middle plane (x = 250 mm) of the box with PCM on the side wall and (b) temperature profiles at four different heights.

3.1.2 PCM on the lid of the box

The apparent height was H' = 250 mm; thus, the aspect ratio of the box with PCM on the lid ($A = H'/W$) was about 0.81 and the Ra number was 2.4×10^7 (ΔT = 6.8°C). As in the case of PCM on the side wall, the airflow was laminar. The values of thermal properties of air are summarized in Table 2.3 (T_{mean} = 6.2°C).

Figure 2.7 shows the air velocity profiles on the middle (x = 250 mm) and the lateral (x = 15 mm) planes of the box with PCM on the lid. It was found from Figure 2.7a that there were two almost symmetric, counterrotating air-flow cells. This result qualitatively agrees with the numerical solution obtained by Corcione (2003) who also observed such a two-cell flow pattern in a rectangular cavity with one cold top wall, one hot bottom wall and two hot side walls (A = 0.5 and Ra = 10^6 in his study). As shown in Figure 2.7a', the positive vertical velocity components were detected along the side walls (y < 50 mm and y > 260 mm) while the negative ones were mostly in the core region. On the middle plane, the absolute values of the vertical velocity components never exceeded 0.08 m·s^{-1}. The upward flow along the side walls was induced by the relatively high air temperature in these regions as a result of heat conduction through the box walls. Accordingly, these flow streams converged on the top where air was cooled down via the PCM. Becoming heavier, the air then flowed downward in the center region.

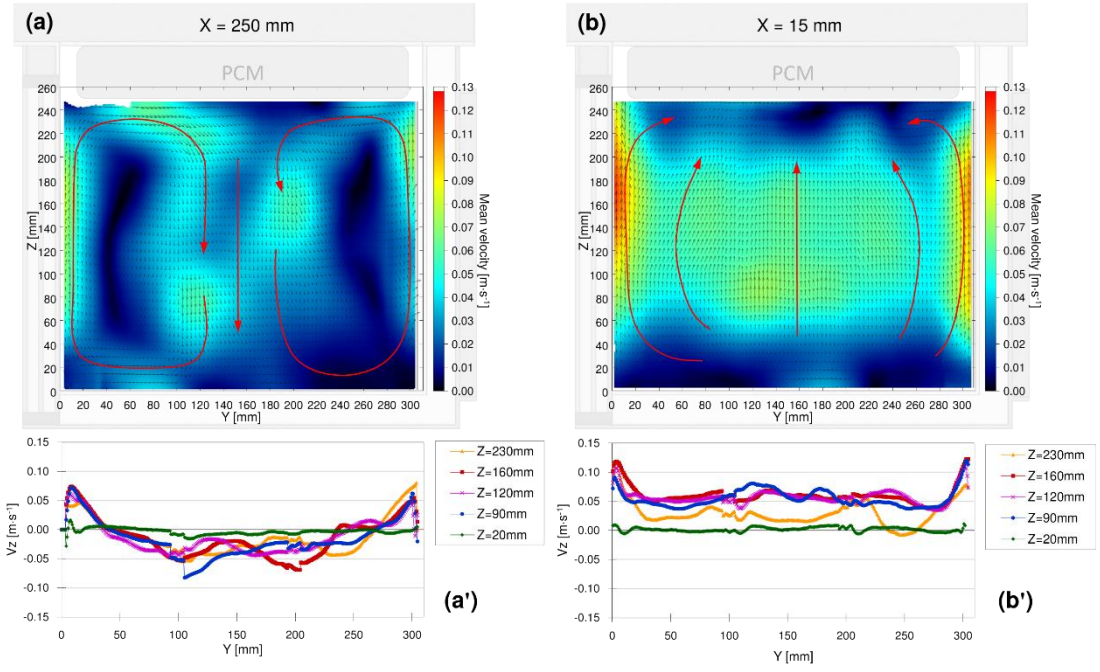

Figure 2.7 Air velocity fields at (a) the middle (x = 250 mm) and (b) the lateral (x = 15 mm) planes of the box equipped with PCM on the lid. The profiles of the z-component of the velocity at 4 heights on (a') the middle and (b') the lateral planes.

Near the lateral wall (x = 15 mm, Figures 2.7b and b'), the flow is almost everywhere upwards as is the case near the side wall (v_z > 0 for y = 15 mm in Figure 2.7a'). In fact, one would expect a similar 2D cell flow pattern in x-z plane ($y = W/2$) as that observed in the y-z plane ($x = L/2$, Figure 2.7a). Overall, air flows upwards along the lateral and side walls, whereas it flows downward in the central region (3D flow). Near the corners (junction of lateral and side walls e.g. x = 15 mm, y = 15 mm) the heat flow by conduction through the walls is the highest, and this explains why the vertical velocity is also the highest in these positions: 0.12 m·s^{-1}.

It should be borne in mind that the presented velocity fields are time-averaged over 10 s and are composed of 9 windows recorded at different times (typically at 2 min. intervals taking into account the time needed to move the camera and save the recorded data). Direct observation of smoke in the middle plane showed that the flow was not stable (it was unsteady) in the central region: the downward flow oscillated in the y direction. This explains why the velocity observed in Figure 2.7a is not strictly symmetric and that there are some 'jumps' between the 3 parts (3 windows in the y direction) of the profiles in Figure 2.7a. This type of instability has been observed also for free convection in domestic refrigerators (Laguerre et al., 2005).

Figure 2.8 shows the air temperature field on the middle plane of the box. As expected, the cold region was in the center where downward flow was observed, while the warm region was near the side walls where upward flow was observed. The maximum air temperature was about 9°C near the top of the side walls and the minimum air temperature was observed just below the PCM (top of central region); the surface of the PCM container was at a temperature of around 1-2°C.

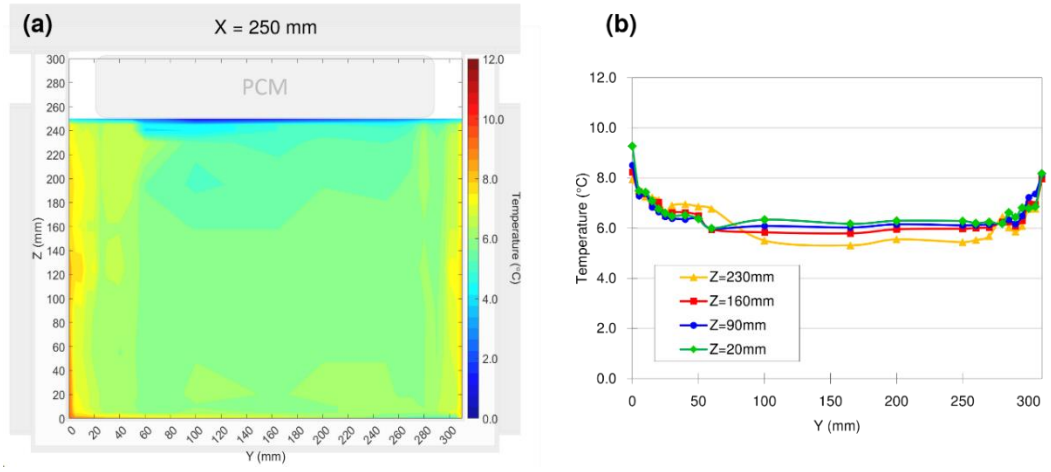

Figure 2.8 Air temperature field on the middle plane (x = 250 mm) of the box with PCM on the lid.

3.1.3 Comparison between PCM on the lid or on the side

In comparison with the case of PCM on the side wall, the box with PCM on the lid exhibited a lower maximal temperature: 9.3°C (lid)/10.5°C (side). This high temperature was observed near the walls. In fact, the product should not touch the walls and should even be placed outside the boundary layers whose thickness was around 30 mm. If we exclude the boundary layer zone, the mean temperature (in the middle plane) was lower for PCM on the lid: T_{mean} = 6.2°C (lid) and 7.7°C (side) and the temperature distribution was also more homogeneous for PCM on the lid: $T_{max} - T_{min}$ = 1.7°C (lid) and 2.7°C (side).

As mentioned previously, flow fluctuations were visually observed in the central region where the PCM was placed on the lid. To a lesser extent, fluctuations were also observed near the bottom of the PCM when it was placed on the (right) side. Figure 2.9 presents the instantaneous velocity evolution during 10 s at two positions (near the center and near the bottom/right corner). This confirms that the airflow was more stable in the case of PCM on the side. Velocity variations of up to 0.10 m·s^{-1} were detected at the center of the box with PCM on the lid (Figure 2.9b).

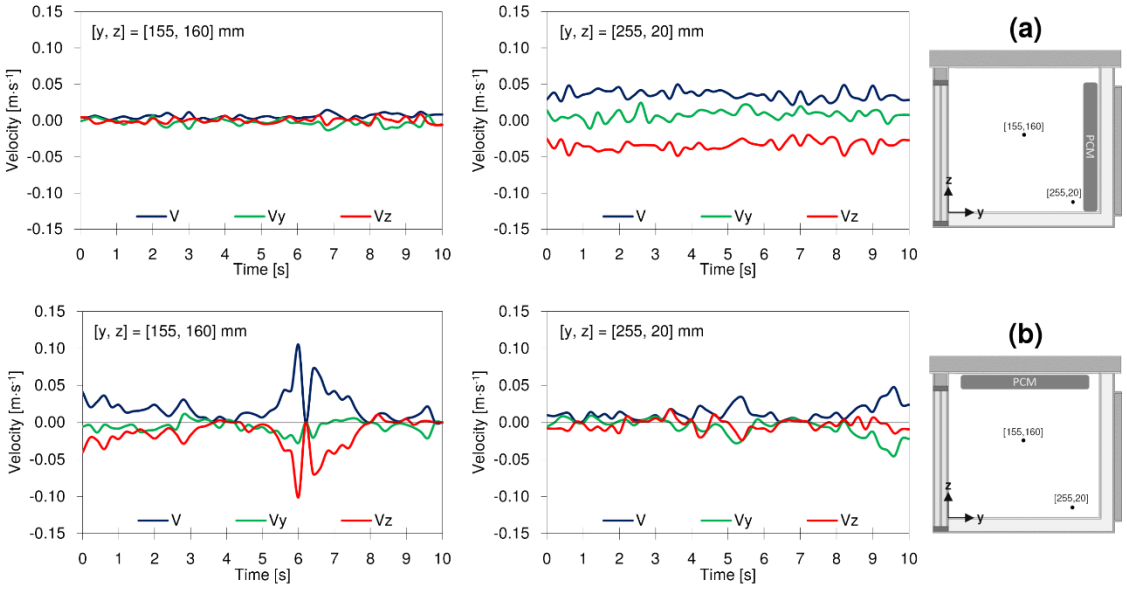

Figure 2.9 Velocity variations of the air at the same two positions in the box with PCM on (a) the side wall and (b) the lid.

The convective heat transfer coefficients can be estimated from the measured temperature profiles. Very near to the wall, the air velocity is close to zero. So, the heat flux (W·m^{-2}) along y-direction can be given by

$$\lambda_a \frac{\partial T}{\partial y} = h_z (T_w - T_\infty) \qquad (2.3)$$

where T_w and T_∞ are the temperatures of the wall and the air outside the boundary layer (free stream), respectively, λ_a is the thermal conductivity of the air, and h_z is the

local convective heat transfer coefficient at a given height (z) which can be approximately estimated from

$$h_z = \frac{\lambda_a(\partial T/\partial y)}{T_w - T_\infty} \quad (2.4)$$

For example, when the PCM was at the side wall, at the mid height (z = 160 mm), the temperature at the PCM wall, at 5 mm from the wall and outside the boundary layer were 0.8°C, 5.5°C and 7.2°C, respectively. The slopes ($\partial T/\partial y$) of the tangent line to the temperature profile near the PCM wall was thus approximately 1°C/mm. Accordingly, the local convective heat transfer coefficient at PCM wall could be estimated around 4 $W{\cdot}m^{-2}{\cdot}K^{-1}$. In the same way, the heat transfer coefficient at the vertical internal box walls (warm walls) could be estimated between 2 and 3 $W{\cdot}m^{-2}{\cdot}K^{-1}$.

Despite low heat transfer coefficients, convection cannot be neglected compared to conduction in air because the maximum air velocities observed in the box were around 0.1 $m{\cdot}s^{-1}$, corresponding to the Peclet number (Pe) of more than 100.

The Peclet number (Pe) is defined as

$$Pe = \frac{v_a L_c}{\alpha_a} \quad (2.5)$$

For the empty box, the value was approximately 1500, given the characteristic length (height of the box) of 0.3 m, the air velocity of 0.1 $m{\cdot}s^{-1}$, and the air thermal diffusivity of about 2×10^{-5} $m^2{\cdot}s^{-1}$.

3.2 Air velocity and temperature profiles under loaded conditions

The experiments were performed under loaded conditions. The experiment was firstly conducted with inert blocks (XPS) that made it possible to study the obstacle-effect alone on the flow pattern. Then, an experiment with the test packs (TYL) was performed to study both the obstacle-effect and the influence of heat exchange with air. Due to the presence of the obstacles, the light sheet was restricted; thus, the velocity field behind the load was not available.

3.2.1 PCM on the side wall of the box

As shown in Figure 2.10, the airflow in the loaded box, regardless of obstacle types, exhibited similarities with that in the empty box: upward and downward flow streams close to the vertical surfaces of the side wall and the PCM, respectively. However, under loaded conditions, the upward flow on the middle plane did not result from a two-dimensional recirculation cell (located in this plane) but instead from a three-dimensional flow pattern as illustrated in Figure 2.11. At State 1, the air flowed downward (-z direction) in the space between the PCM and the load. Once approaching the bottom wall (State 2), the air flowed rather horizontally (+/- x direction) toward the lateral walls of the box. At the edge of the load (State 3), the air

turned and flowed between the lateral wall and the load (-y direction). This is confirmed in Figures 2.10b and 2.10d (lateral plane, x = 15 mm) where a strong flow from the right to the left was observed in the bottom region. When it reached the bottom of the side wall (State 4), the air moved both horizontally to occupy the entire gap between the side wall and the load and upwards because it became warmer and warmer (heat exchange with the walls). Finally, starting from State 5, it recirculated to the PCM.

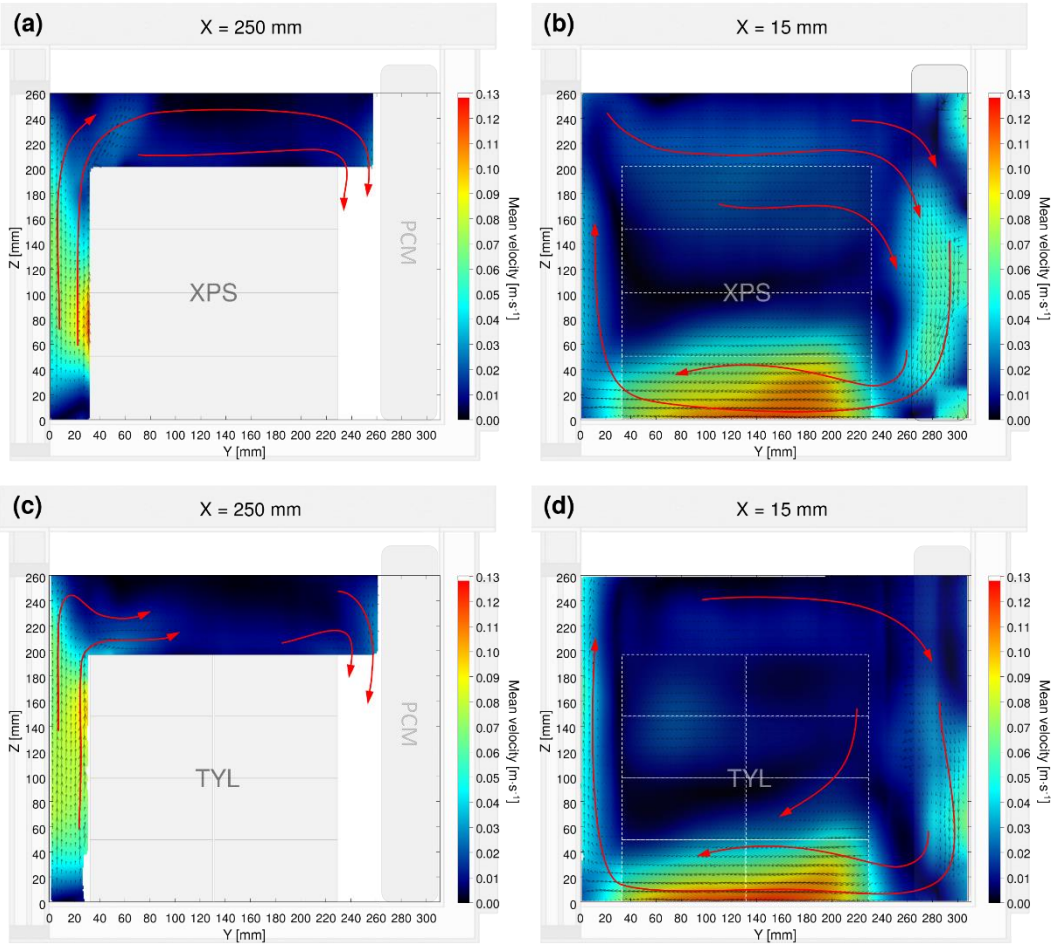

Figure 2.10 Air velocity fields at (a and c) the middle (x = 250 mm) and (b and d) the lateral (x = 15 mm) planes of the box with the PCM on the side wall.

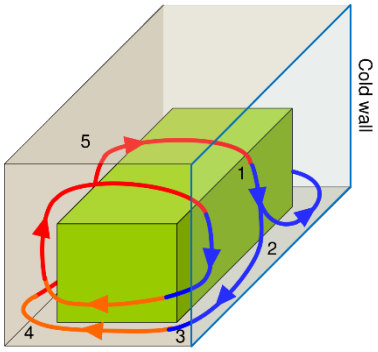

Figure 2.11 Illustration of three-dimentional flow in a box with PCM on the side wall. Numbers indicate the states of the flow.

The velocity fields obtained with inert blocks (XPS) and with test products (TYL) were very similar. This is because thermal steady state was practically reached in both cases (the test products were introduced practically at the equilibrium temperature and the measurement began after 2 h). In this manner, thermal inertia became negligible. For XPS (with very low thermal conductivity) the air temperature was expected to be relatively homogeneous in the gaps between the load and the lateral wall or the PCM. For TYL, due to conduction, the load surface temperature was lower than the air temperature in the wall-side gap but higher in the PCM-side gap (as shown hereafter in Figure 2.12a). This could diminish free convection, but the results showed a minor effect ($Pe \sim 150$, L_c (gap) = 30 mm). This means that (steady state) flow characterization can be carried out with inert blocks (XPS), which is much simpler. Certainly, if warm products were introduced in the box initially, the flow pattern would have been substantially altered.

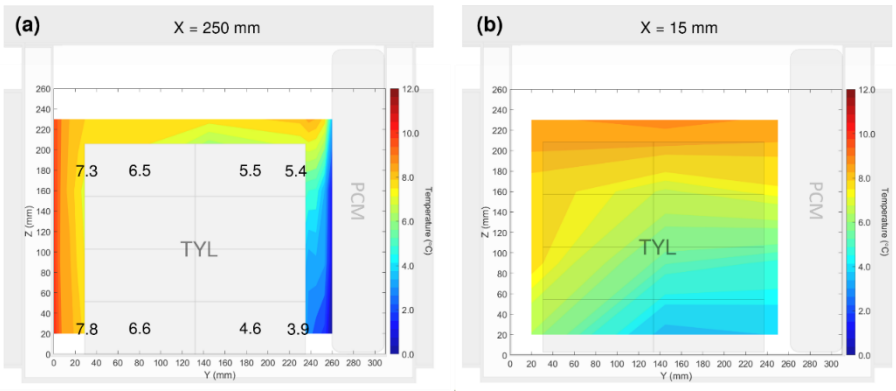

Figure 2.12 Air temperature field on (a) the middle (x = 250 mm) and (b) the lateral (x = 15 mm) planes of the box with PCM on the side wall. Values indicate the time-averaged core and surface temperatures of the test products.

Figure 2.12 shows the temperature field on the middle (x = 250 mm) and the lateral (x = 15 mm) planes of the box with PCM on the side wall and TYL load. The temperature field was coherent with the flow pattern: air was cooled down along the PCM and warmed up along all the box walls. It is obvious that the cold air near the PCM resulted in relatively low load temperatures on this (right) side. Conversely, the warmer air near the wall resulted in relatively high load temperatures on the opposite (left) side. Conduction in the load was not sufficient to homogenize the load temperature. The highest load temperature, 7.8°C, was reached near the side wall (opposite the PCM location). The average load temperature was 6.0°C and the maximum difference was 3.9°C. Air temperature stratification was observed on the lateral plane of the box (Figure 2.12b).

3.2.2 PCM on the lid of the box

A complex flow pattern was observed in the loaded box with PCM on the lid as shown in Figure 2.13. On the middle plane (x = 250 mm, Figures 2.13a and 2.13c), regardless of load types, cold air coming from the top (near the PCM) flowed downward in the center of the (left) gap between the side wall and the load. Then, air flowed upwards along the side wall and the load surface. An explanation for the upward flow along the side wall is that the air near this wall is warmed up by conduction through the wall (as in the empty case). The flow direction along the load surface is logically upwards if the surface temperature is higher than the average air temperature in the gap. This was the case for the XPS load because radiation from the wall to the load surface tended to increase the load surface temperature. For the TYL, in addition to radiation, conduction also occurred inside the load. This could explain why upward flow occurred all along the XPS load but occurred only along the upper part of the TYL load. This difference appeared also on the lateral plane (x = 15 mm): there were more upward flow regions in the case of the XPS load. However, the easier experiments with the XPS load gave a good approximation of the flow pattern in the presence of load in the box.

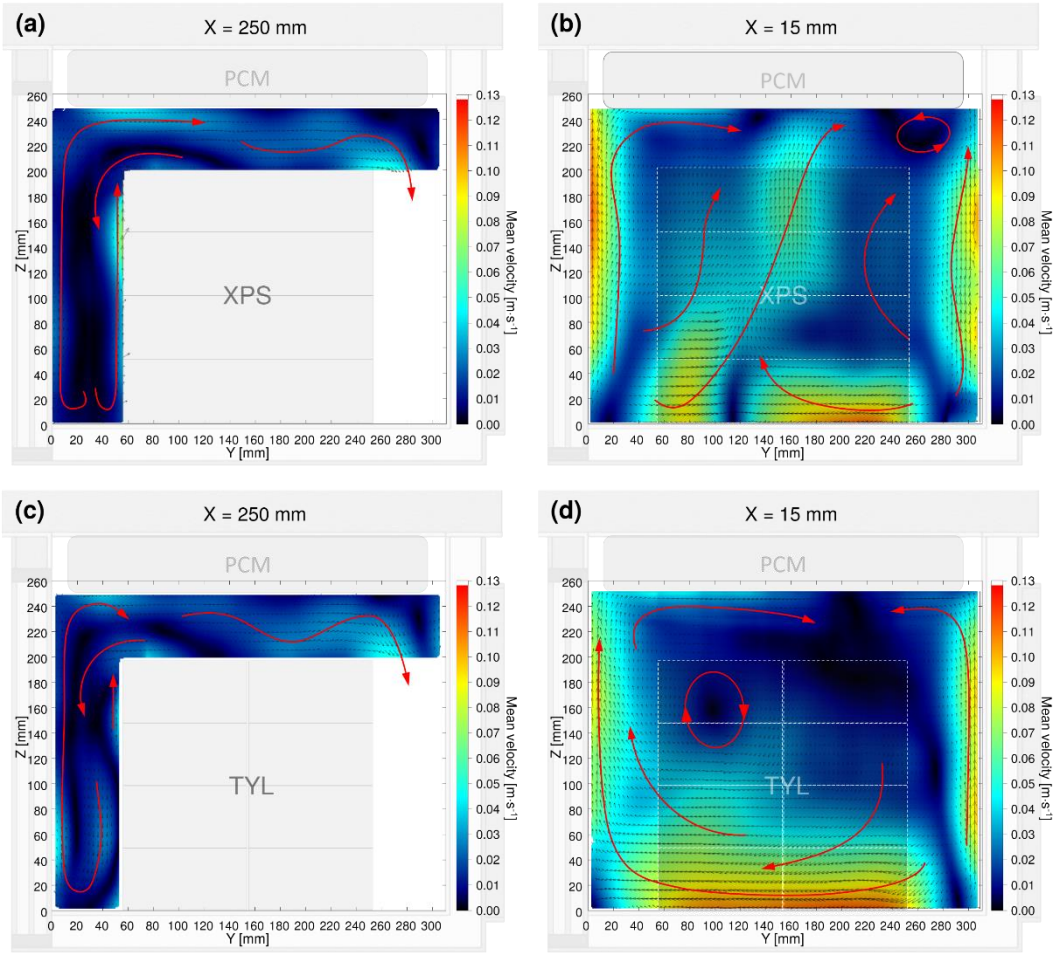

Figure 2.13 Air velocity fields on (a and c) the middle (x = 250 mm) and (b and d) the lateral (x = 15 mm) planes of the box equipped with PCM on the lid.

Due to the limitations of the PIV technique, velocity measurement was not possible in the (right) gap. A similar flow pattern could be expected due to symmetry. However, in fact, flow was not symmetrical above the load: it seemed that a stronger cold air stream flowed down in the right gap than in the left gap. Such dissymmetry was already observed in the empty case (PCM on the lid) where instability was induced by oscillations of downward flow. It seemed that in the loaded case, the flow 'chose' one or another preferential pathway (through the left or right gap). This is related to the non-linear term in the flow equations (Navier-Stokes) which is responsible for a break in symmetry (even before turbulence). This dissymmetry was also confirmed by Figures 2.13b and 2.13d (lateral plane, x =15 mm) where flow from the right to the left was observed in the lower part of the box. The small difference in heat transfer coefficient between the left (insulated wall) and the right (triple-glazed windows) can also induce dissymmetry.

Figure 2.14 presents the temperature field on the middle (x = 250 mm) and the lateral (x = 15 mm) planes of the box with PCM on the lid and TYL load. It shows the thermal boundary layers along the side wall (which explains upward flow along the walls). However, the load surface temperature seemed very close to the adjacent air temperature. At the center of the gap (where downward flow was observed) the air rapidly warmed up (the temperature was well above the PCM surface temperature). This can explain the weak velocity observed in the gap. Dissymmetry was also observed: the right gap had a lower average air temperature than the left gap which in turn affected the load temperature. This also seemed to be due to a stronger cold air stream from the PCM toward the right gap (see the red arrow in Figure 2.14). For temperature measurements, the dissymmetry cannot be imputed to a difference in insulation (Box A was used). This configuration did not allow stratification since the cold PCM container was placed at the top.

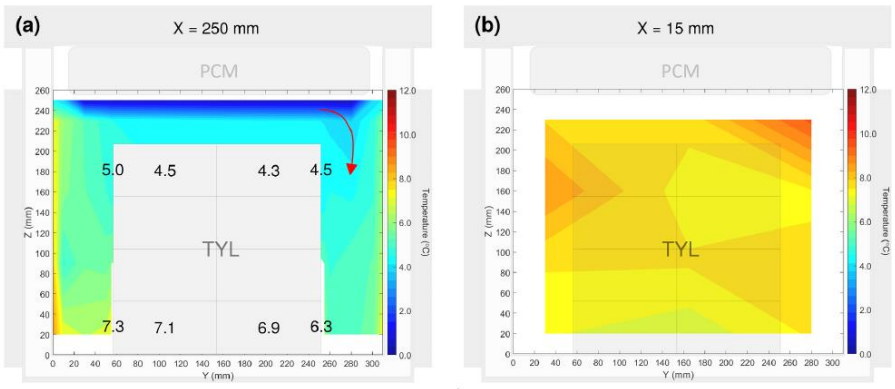

Figure 2.14 Air temperature field on (a) the middle (x = 250 mm) and (b) the lateral (x = 15 mm) planes of the box with PCM on the lid. Values indicate the time-averaged core and surface temperatures of the test packs.

In the case of PCM on the lid, the highest load temperature, 7.3°C (7.8°C for PCM on the side) was reached near the bottom (opposite the PCM location). The average load temperature was 5.7°C (6.0°C for PCM on the side), and the maximum difference was 3.0°C (3.9°C for PCM on the side). So, there was little apparent difference between the two configurations. These findings suggested that the PCM can be placed either at the side wall or at the lid without compromising the quality and safety of food products if spaces between the PCM and the load and between the side walls and the load are reserved. According to our estimation, the insulated box with ice as a PCM is feasible for the transport of food products in the temperature range of 4-8°C for about 10 h. The experimental results obtained by this study will be used for the development of CFD and simplified thermal models to predict product temperature evolution along a logistic chain. This evolution makes possible the prediction of product quality thanks to a relation with the product temperature. In this manner, the product shelf life under different logistic scenarios can be predicted. The thermal and quality modelling would help the supply chain management to optimize the logistic conditions to reduce food loss and waste.

4. Conclusions

The present study was carried out to characterize the airflow and the heat transfer due to natural convection in an insulated box equipped with PCM by using PIV technique and temperature measurement. The influence of the PCM position on the flow pattern and temperature distribution was investigated. The study was conducted in a progressively more complex manner: empty, loaded with extruded polystyrene (low conductivity and almost no thermal inertia), and loaded with tylose (thermal properties close to those of food). The key findings are summarized as follows:

Whatever the configuration, the highest observed air velocities were around 0.1 $m \cdot s^{-1}$; therefore, convection cannot be neglected compared to conduction in air (Peclet number > 100). Numerical simulations with either CFD or simplified models should include free convection.

When the PCM is on the side wall, the flow pattern is simple to predict. Air flows downwards along the PCM surface and upwards along the side walls. In the empty case, the flow pattern can be approximated by a 2D recirculation cell, but the presence of the load leads to a 3D flow pattern. When the PCM is on the lid, after cooling down in contact with the PCM, a cold air stream detaches from the PCM surface and flows downwards. This cold air stream is unstable in the empty case and shows preferential pathways (symmetry breaking) in the loaded case. The flow pattern is less predictable. In all cases, after cooling down near the PCM, the air temperature increases progressively along the trajectories until returning close to the PCM. The product surface temperatures are close to the temperature of the adjacent air. At steady state, conduction in the load has a minor effect on the flow pattern which can be approximated by replacing the real load with an obstacle of low conductivity.

From a practical point of view, it is recommended to leave a space between the PCM and the load (to promote free convection) and between the side walls and the load (to allow evacuation of heat from the ambient via conduction through the walls). The gap should be at least of the order of the boundary layer thicknesses: 2-3 cm. Further experiments without such gaps would be useful.

At thermal steady state, there was no significant difference in terms of maximum product temperature and heterogeneity between the PCM on the lid or at the side. The study showed the coldest and warmest zones in both cases, suggesting the best location for products that are sensitive to bacterial growth or chilling injury.

Further studies are planned in order to compare these results with CFD simulations and to develop a simplified model that enables prediction of temperature evolution (at different locations) as a function of the box, the product and PCM properties, along with ambient temperature changes.

2.3 ARTICLE 3

Influence des conditions d'utilisation sur les transferts de chaleur dans un caisson isotherme équipé d'un matériau à changement de phase

Résumé (version française de l'abstract de l'article 3)

Un caisson isolé équipé d'un matériau à changement de phase (phase change material : PCM - glace, point de fusion ~ 0 ° C) et chargée par un produit modèle (Tylose) a été étudiée expérimentalement pour analyser l'effet de la position du PCM, de la forme géométrique de la boîte (aspect ratio : AR = hauteur / largeur) du caisson, de la température ambiante, de la température initiale du produit et d'un éventuel espace laissé sous le produit. La température et la vitesse de l'air mesurées respectivement par thermocouples et vélocimétrie par images de particules (PIV) ont été analysées dans des conditions stables. La température maximale du produit était plus faible pour le PCM placé sous le couvercle (6,6 °C, AR ≈ 1) que pour le PCM placé sur le côté (7,7 °C, AR ≈ 1) et augmentait avec AR (9,9 °C, AR ≈ 1,7). Une relation non linéaire entre la température ambiante et la température du produit a été observée avec une température maximale du produit variant de 5,2 °C (10 °C ambiant) à 9,1 °C (30 °C ambiant). L'influence de l'espace laissé ou non sous le produit était négligeable malgré des différences en termes de structure d'écoulement d'air. Des équations simples ont été proposées pour prédire la durée maximale de stockage et la température moyenne dans la boîte. Elles permettent de prédire l'influence de la masse de PCM et de produit, du point de fusion du PCM, de l'isolation du caisson et de la température ambiante.

Influence of Use Conditions on Heat Transfer in an Insulated Box Equipped with a Phase Change Material

Tanathep Leungtongkum[a, b]*, Denis Flick[b], Nattawut Chaomuang[c], Alain Denis[a] and Onrawee Laguerre[a]

[a]Université Paris-Saclay, INRAE, FRISE, 92761 Antony, France
[b]Université Paris-Saclay, INRAE, AgroParisTech, UMR SayFood, 91120 Palaiseau, France
[c]Department of Food Engineering, School of Engineering, King Mongkut's Institute of Technology Ladkrabang, Bangkok, Thailand 10520

***Corresponding author:** Tanathep Leungtongkum, e-mail: Tanathep.leungtongkum@inrae.fr

Highlights

- Temperature and air velocity fields (by PIV) in insulated boxes with PCM were shown
- The effect of box configurations and operating conditions was studied
- PCM at the top allows 1.1°C lower maximum product temperature than that on the side
- An air gap of 20 mm below the product does not change the temperature profile
- Results can be used for optimizing the box and the condition for food transport

Abstract

An insulated box with Phase Change Material (PCM – ice, melting point ~ 0°C) and loaded by test product (Tylose) was investigated experimentally to study the effect of the PCM position, Aspect Ratio (AR = height/width) of box, ambient temperature, initial test product temperature and spacing beneath the test product. The temperature and the air velocity measured by thermocouples and Particle Image Velocimetry (PIV), respectively, were analyzed under stable conditions. The maximum product temperature was lower for PCM at the top (6.6°C, AR ≈ 1) than for PCM on a sidewall (7.7°C, AR ≈ 1) and increased with AR (9.9°C, AR ≈ 1.7). A non-linear relation between ambient temperature and product temperature was observed with the maximum product temperature from 5.2°C (10°C ambient) to 9.1°C (30°C ambient). The influence of spacing beneath the product was negligible despite different airflow patterns. Simple equations were proposed to predict the maximum storage time and mean temperature in the box enabling us to study the influence of PCM and product mass, melting point, box insulation and ambient temperature.

Keywords: Insulated box, Phase Change Material, Airflow, Heat Transfer, Food Cold Chain

Nomenclature

A	Exchange area [m^2]
AR	Aspect ratio of box = height/width [-]
C_p	Specific heat [$J \cdot kg^{-1} \cdot K^{-1}$]
e	Wall thickness [m]
h	Convective heat transfer coefficient [$W \cdot m^{-2} \cdot K^{-1}$]
L	Characteristic length [m]
L_f	Latent heat of fusion of PCM [$J \cdot kg^{-1}$]
$\dot{m}$	Mass flow rate of air [$kg \cdot s^{-1}$]
m	Mass [kg]
t	Time [s]
t_{max}	Maximum storage time [s]
T	Temperature [°C]
T_m	Melting temperature of PCM (~ 0°C)
T_{amb}	Ambient temperature [°C]
T^*	Dimensionless temperature $= \frac{T - T_m}{T_{amb} - T_m}$ [-]
ΔT	Largest temperature difference [°C]
U	Overall heat transfer coefficient between ambient and product surface through box insulation [$W \cdot m^{-2} \cdot K^{-1}$]
x, y, z	Coordinate [m]

Greek letters

α_c	Dimensionless heat transfer coefficient at cold wall $= exp\left(-\frac{A_c h_c}{\dot{m} C_{p,air}}\right)$ [-]
α_w	Dimensionless heat transfer coefficient at warm walls $= exp\left(-\frac{A_w U}{\dot{m} C_{p,air}}\right)$ [-]
β	Ratio of thermal resistance at cold and at warm walls $= \frac{A_w U}{A_c h_c}$ [-]
ρ	Density [$kg \cdot m^{-3}$]
τ	Thermal time constant [s]
λ	Thermal conductivity [$W \cdot m^{-1} \cdot K^{-1}$]

Subscript

air	Air
ave	Average value
c	Cold surface/walls
ini	Initial value
max	Maximum value
min	Minimum value
p	Product
pcm	Phase change material
w	Warm surface/walls

1. Introduction

Insulated boxes equipped with a Phase Change Material (PCM) are attracting particularly for the last mile delivery of small quantities of temperature-sensitive food and pharmaceutical products. This is due to the simple implementation, low cost and flexibility related to several box designs with different volumes ranging from 5 L to more than 300 L. Several parameters have an influence on the internal temperature profiles such as box characteristics (dimensions, aspect ratio, insulation), PCM (melting point, mass, position), product (thermal properties, mass, compactness) and operating condition (ambient temperature, transport duration). Because of the complex interactions between these parameters, they need to be considered together to avoid temperature abuse during delivery.

The temperature evolution inside an insulated box equipped with PCM loaded by real food/food model was investigated experimentally and numerically by several authors and summarized in Leungtongkum et al. (2022). In general, the product located at the corners of the box has the highest temperature (Laguerre et al., 2018; Margeirsson et al., 2012). Du et al. (2020) have compared the effect of PCM at the top, bottom, and all sidewalls on internal temperature evolution. The authors found that placing PCM at the bottom generated the highest internal temperature and the highest temperature difference between the min and max values. For high-value products like vaccines, five or six PCM plates are placed on the box walls to directly compensate the heat losses through the walls by PCM melting. This allows assuring the preservation of the recommended temperature (Kacimi & Labranque, 2019) but the useful volume for the product is significantly reduced, thus, this practice may not be suitable for low value products like food.

For simplification purposes, several studies assumed conduction only in the air, the product and the wall (Du et al., 2020; Paquette et al., 2017; Xiaofeng & Xuelai, 2021). To represent the real phenomena, Rincón-Casado et al. (2017) developed a numerical model considering conduction and natural convection to predict the temperature profile and airflow pattern in an empty cavity while (Leporini et al., 2018) also took radiation into account. Recently, some numerical studies considered natural convection of internal air and of melted PCM (Burgess et al., 2022; Calati et al., 2023; Rahimi-Khoigani et al., 2023).

Various phenomena are involved simultaneously in an insulated box equipped with PCM: conduction inside the product, the PCM and the walls of the box, convection between air and product/PCM, and between the external air and the box, radiation between walls, phase change during PCM melting and food quality evolution. Under natural convection as that in an insulated box, these three heat transfer modes (conduction, convection and radiation) are of the same order of magnitude in terms of heat flux (Laguerre & Flick, 2004). However, only a few studies considered all of them according to the difficulty in measuring low air velocities (Miroshnichenko &

Sheremet, 2018). In fundamental studies of natural convection in a closed cavity, two walls are generally at imposed temperatures (cold and warm) while the other walls are adiabatic, and most of them investigated empty cavities (Leporini et al., 2018; Zhang et al., 2015). PCM was used as a thermal energy storage in an empty cavity (Labihi et al., 2017; Moreno et al., 2020). Choi et al. (2015) and Lee et al. (2016) conducted numerical studies of a rectangular cavity filled with a circular cylinder (cylinder diameter/cavity size = 0.125). Some studies have investigated cavities filled with a porous medium (particle diameter/box width < 0.01), e.g., Ataei-Dadavi et al. (2019). The results of these studies cannot be applied to our case where only one wall (PCM container) is at almost constant temperature and all the other walls of the box are non-adiabatic. Moreover, a porous medium approach is not appropriate to our study, since the ratio between product diameter and box width is ≥ 0.1, thus, different airflow patterns will exist.

The strength of our work is that it is the first experimental study concerning the measurement of airflow patterns and air velocity in an insulated box with PCM at different locations by using an optical technique (PIV). Some results were already presented in a previous article (Leungtongkum et al., 2023a) for a limited number of configurations. The present article investigates many more parameters: aspect ratio, ambient temperature, initial product temperature and air gap underneath the product. From a practical point of view, this article also proposes simple equations to predict the maximum storage time, the equilibrium temperature and temperature heterogeneity at thermal stable condition enabling to study the influence of PCM mass, melting point, box insulation and ambient temperature. These equations are easy to use and they would be useful for stakeholders, for example, to choose the box insulation and the PCM mass according to the product to transport, duration and ambient temperature during the supply chain.

It is to be emphasized that certain experimental data presented in this article were used for a thermal model development based on the zonal approach. This model takes into account conduction, convection and radiation inside an insulated box (Leungtongkum et al., 2023b).

2. Material and methods

The material and methods described in detail in Leungtongkum et al. (2023a) are presented succinctly below.

2.1 Experimental setup

For thermal study, the box is a 45-L commercialized multilayer insulated box (Manutan SA, Gonesse, France). In fact, commercialized boxes are available in various sizes (from less than 5 L to more than 300 L). For meat, a highly perishable food, the boxes generally do not exceed 50 L. To be close to real situations, we chose a 45-L box in our study. For airflow study, the box has the same dimensions and wall structure as the

one for thermal study, but two side walls are replaced by triple-glazed windows (3 glass panes each with a thickness of 4 mm, 2 argon-filled 10-mm gaps) to allow the entrance of laser sheet and the image capture by a camera. The overall heat transfer coefficient of the walls of these two boxes is almost the same (0.89 $W \cdot m^{-2} \cdot K^{-1}$).

The PCM container, made of polypropylene (3.5-mm thickness), had external dimensions 460 mm x 280 mm x 50 mm and was filled with 3.5 kg of tap water (melting point ~ 0°C). The thermophysical properties of PCM (water in this study), in both liquid and solid state along with its enthalpy of melting is shown in Table 2.4. Since the form of food is diverse, Tylose packs are used as test product (dimensions of a pack 200 mm x 100 mm x 50 mm) as that used in standard tests for thermal performance of cold equipment. The physical properties of this test product are close to the ones of meat (Table 2.4). This configuration (compact load with air gaps between load and box walls) was studied by several authors (Ohkawara et al., 2012; Zhao et al., 2019).

Table 2.4 Thermophysical properties of materials

Material	ρ ($kg \cdot m^{-3}$)	C_p ($J \cdot kg^{-1} \cdot K^{-1}$)	λ ($W \cdot m^{-1} \cdot K^{-1}$)	Reference
Liquid water	1000	4217	0.561	Cengel & Ghajar (2020)
*Ice	920	2040	1.880	Cengel & Ghajar (2020)
Test product (Tylose)	1070	3372	0.510	Icier & Ilicali (2005)

*Enthalpy of melting of ice (L_f) is 333700 J/kg with melting temperature (T_m) at 0°C

The box can be placed horizontally (*AR*, height/width ≈ 1) or vertically (*AR* ≈ 1.7), making it possible to study the effect of the aspect ratio on heat transfer and the airflow pattern. The effect of the air space underneath the product was studied by placing the test product on a perforated support made of galvanized steel (length x width x height = 350 x 150 x 20 mm and 150 x 150 x 20 mm for a horizontal and a vertical box, respectively). An example of experimental setup for a horizontal box with PCM on a side wall is shown in Figure 2.15.

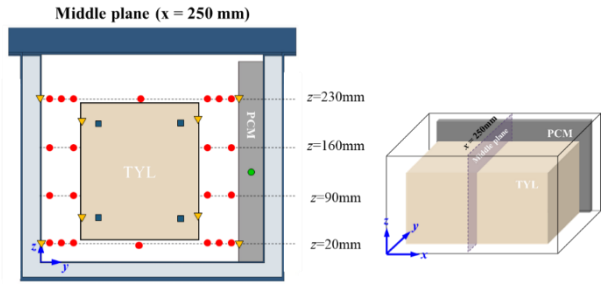

Figure 2.15 Experimental setup and thermocouple positions in the horizontal box with PCM on a side wall and loaded with the test product (Tylose, TYL). Note: Similar setup and measured positions were applied for the vertical box.

2.2 Thermal study

To assure the homogeneous initial PCM temperature, a PCM slab was placed horizontally in a freezer set at a temperature of -2°C for at least 48 h before each experiment. To assure the homogeneous initial product temperature, sixteen packs of test product were placed in a polystyrene box and stored in a domestic refrigerator set at a temperature of 4°C or 10°C for at least 24 h before each experiment. In this manner, the product temperature is not influenced by the air temperature fluctuation due to "on" and "off" compressor working cycles.

Temperatures of PCM, air, and test product in the loaded box (Figure 2.15) were measured at 35 positions located in the middle plane (x = 250 mm) every 30 s from 400 min. to 600 min. after closing the box to assure the stabilization of temperature during the measurement. The temperature contour map was drawn by MATLAB by interpolation from 30 measured points. More detail on temperature measurements can be found in Leungtongkum et al. (2023a).

It is to be emphasized that the T-type thermocouples were previously calibrated at -10°C, 0°C, 10°C, 20°C and 30°C and allowed the measurement precision of ± 0.2°C.

Table 2.5 describes the experimental conditions (cf. the detailed description in Section 2.4). Conditions 1, 2, 9 and 10 were done twice to verify the repeatability of the results. These conditions are notified by "*" in Table 2.5. Since the result repeatability was observed in these conditions (standard deviation ~ 0.2°C), the other ones reported in this Table were done only once allowing a large number of experimental conditions to be fulfilled.

Table 2.5 Experimental conditions

Condition	1*	2*	3	4	5	6	7	8	9*	10*
	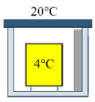	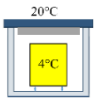	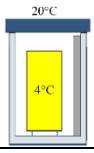	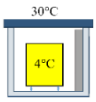	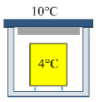	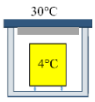	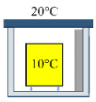	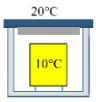	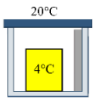	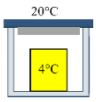
PCM position	Side	Top	Side	Side	Top	Top	Side	Top	Side	Top
Aspect ratio	~1	~1	1.7	~1	~1	~1	~1	~1	~1	~1
Ambient temperature (°C)	20	20	20	30	10	30	20	20	20	20
Initial test product temperature (°C)	4	4	4	4	4	4	10	10	4	4
Spacing beneath test product (mm)	20	20	20	20	20	20	20	20	0	0

* with two replications

2.3. Airflow study

Non-intrusive air velocity measurements were achieved by PIV (Particle Image Velocimetry). The PIV device is constituted of three components: a double-pulsed Nd:YLF laser (527 nm wavelength, 10 mJ pulse energy), a high-speed 12-bit CMOS video camera (Photron, FASTCAM SA3; 1024 × 1024 pixels in resolution) fitted with a lens (Sigma; 105 mm, f/1:2.8) and a programmable timing unit (PTU-X) to ensure synchronization of the laser and the camera. Visualization of the airflow pattern is possible by the scattering of smoke particles during laser pulses. Oil-based particles (mean diameter 0.3 µm) were generated using a smoke machine (Antari, F-80Z). Based on our calibration, the image size was 115.5 mm x 115.5 mm. The positions of the measured windows partially overlapped with the neighboring one using the displacement system. Finally, the air velocity field over the whole area of the plane could be developed.

For each measured window, 500 pairs of images were recorded every 20 ms with a time interval of 900 µs between two images of the same pair (between two laser pulses) with the total measurement duration of 10 s. After capturing all the images, instantaneous airflow vectors were calculated using a cross-correlation method with a multi-pass correlation algorithm (Raffel et al., 2007). The distance between two vectors was around 0.9 mm in both horizontal and vertical directions. After 500 instantaneous vector fields had been attained, the mean velocity field of each measured window was calculated. More detail on PIV system, image acquisition, image post-processing and experimental protocol can be found in Leungtongkum, et al. (2023a).

2.4 Experimental conditions

Table 2.5 summarizes the investigated experimental conditions: position of PCM, aspect ratio of the box, ambient temperature, initial test product temperatures and its position. The pictograms were introduced for further reference. The studied conditions (except PCM position) are new in comparison to the ones presented in Leungtongkum et al. (2023a).

3. Results and discussions

In addition to the results presented in our previous work (Leungtongkum et al., 2023a), this article focuses on the influence of box designing and operating parameters on temperature and air velocity fields: box aspect ratio and PCM position (Figure 2.16), external and initial product temperatures (Figure 2.17), space beneath the test product (Figure 2.18). These influences on the average, min and max temperatures of product core/surface and air at stable condition are summarized in Table 2.6. To complete the data at stable condition, the time-temperature evolutions at different positions are presented in Figure 2.19, the analysis of the time to reach stable condition (thermal time constant) quantitatively shows the importance of heat fluxes by conduction and

convection. The experimental results shown in Figure 2.20 show the effect of the amount of PCM on product temperature. Finally, simple equations are proposed to predict the maximum storage time in function of box insulation, PCM mass, melting point, product mass, ambient temperature.

3.1 Effect of the aspect ratio

Figure 2.16 shows the airflow pattern and the temperature field on the middle plane of horizontal and vertical loaded boxes with PCM on the right side. The absence of air velocity in the gap between the test product and PCM of the horizontal box can be explained by the impossibility of laser sheet projection in this zone, thus, no PIV measurement. The same reason explains the absence of air velocity in the gap below the test product of the vertical box.

Air velocity field

Temperature field

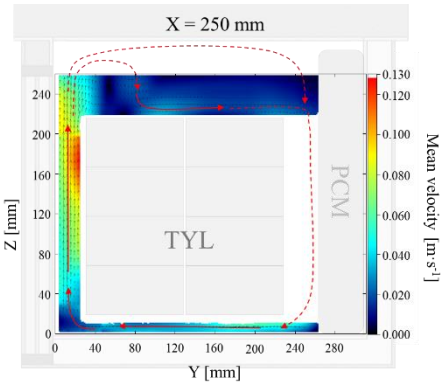

(a)

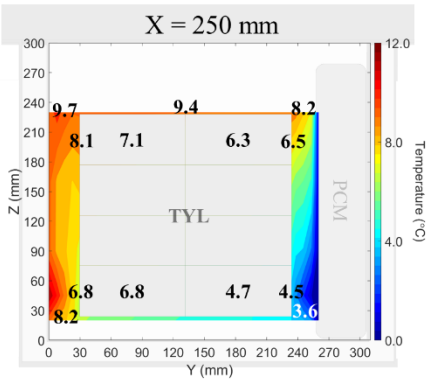

(a')

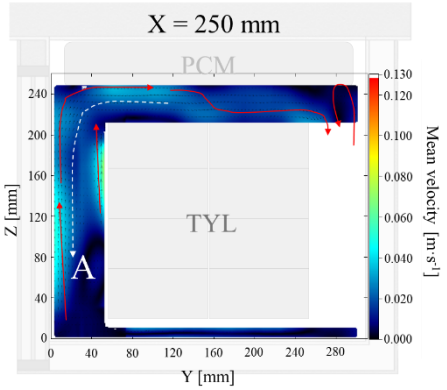

(b)

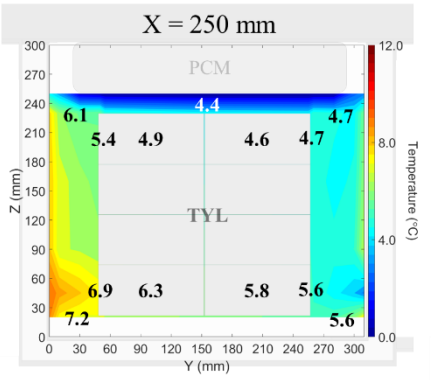

(b')

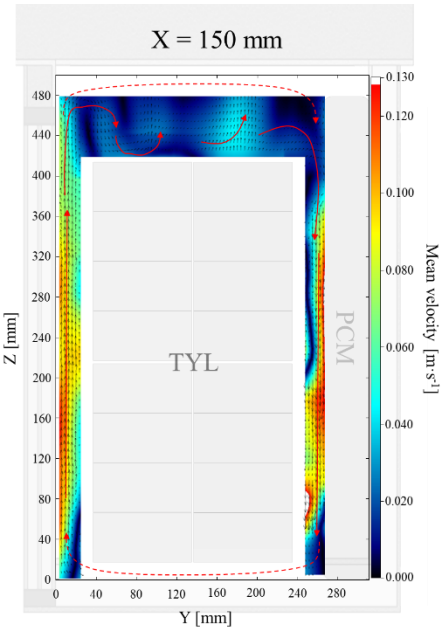

(c)

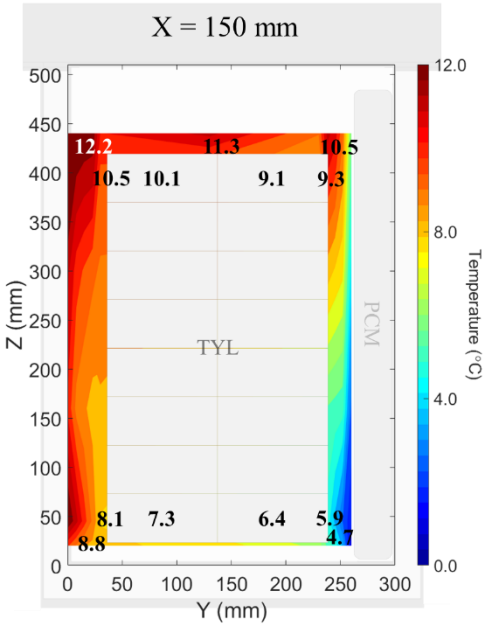

(c')

Figure 2.16 Measured air velocity field on the middle plane of a loaded box with (a) PCM on the side of the horizontal box – condition 1; (b) PCM at the top of the horizontal box – condition 2; and (c) PCM on the side of the vertical box – condition 3. (a'), (b') and (c') are corresponding measured temperature fields (for one of the replications)

When PCM was on the side (Figures 2.16a and 2.16c), air flows downwards close to PCM and flows upwards close to the opposite vertical wall. In the gap between the test product and the box wall (left side), the upward maximal velocity was similar in both cases (~ 0.11 $m \cdot s^{-1}$, with an uncertainty of 3 x 10^{-3} $m \cdot s^{-1}$). Comparison is not possible in the gap between the PCM and the test product. However, in the vertical box, the maximal downward velocity (0.13 $m \cdot s^{-1}$, with an uncertainty of 3 x 10^{-3} $m \cdot s^{-1}$) was higher than the maximal upward velocity (0.11 $m \cdot s^{-1}$, with an uncertainty of 3 x 10^{-3} $m \cdot s^{-1}$). This is because downward flow occurs only along the PCM, whereas upward flow occurs not only along the opposite wall but also along the two other vertical box walls (results not shown).

Regarding the temperature field (Figures 2.16a' and 2.16c'), increasing the height of the box did not change the coldest and warmest positions. The coldest spot was located at the bottom close to the PCM surface and the warmest spot was at the top close to the opposite side wall.

Table 2.6 summarizes the average temperatures observed between 400 and 600 min. considered as a stable period. In the pictograms, the cold/warm spot locations for air and the product are shown. This table distinguishes the temperature of air, of the product surface and of the product core in terms of average, maximum and minimum values. In the following section, we will focus on the average product core value, $T_{pc,\ ave}$ and the maximum product temperature (core or surface), $T_{p,\ max}$, because of the importance for product quality and the sanitary risk (on the average and for the highest temperature location). Indeed, the minimum product temperature was always positive (no freezing risk) since PCM was initially at a temperature of -2°C and melted near 0°C. To complement these findings, we will also consider the air temperature heterogeneity: $\Delta T_{air} = T_{air,\ max} - T_{air,\ min}$. Since the standard deviation (SD) between replicates for average product (core or surface, 4 positions each) temperatures is around 0.2°C (see Table 2.6), we should consider that a difference of less than about 0.5°C does not exert a significant impact on product quality evolution.

Increasing the height of the box significantly led to higher product temperatures and greater air temperature heterogeneity:

<u>Horizontal box:</u> $T_{pc,\ ave}$ = 5.8°C, $T_{p,\ max}$ = 7.7°C, ΔT_{air} = 6.0°C, SD of T_{air} = 2.2°C
<u>Vertical box:</u> $T_{pc,\ ave}$ = 7.8°C, $T_{p,\ max}$ = 9.9°C, ΔT_{air} = 7.5°C, SD of T_{air} = 3.0°C

A higher aspect ratio (height/width) leads to larger temperature differences between the top and the bottom. Thus, it is recommended to limit the height of insulated boxes.

In fact, increasing the height should increase convective heat transfer between PCM and air (according to Nu-Ra correlations) but the air pathway along the box walls is longer and thermal stratification is stronger. Finally, under conditions close to ours, these different phenomena lead to higher average temperature and temperature heterogeneity for higher aspect ratio.

Table 2.6 Test product core, surface and internal air temperatures for all experimental loaded conditions.

Note: the reported values are the average of the temperatures measured between 400 min. and 600 min. considered as the stable thermal condition.

Condition	***1	***2	3	4	5	6	7	8	***9	***10	**SD
*Pictogram			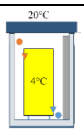								
Core temperature											
Average	5.8 (5.6,6.0)	5.4 (5.3,5.4)	7.8	7.4	4.3	7.2	9.3	8.0	5.8 (5.7,5.8)	5.6 (5.4,5.7)	0.19
Minimum	4.5 (4.2,4.8)	4.6 (4.5,4.6)	6.2	5.4	3.5	6.2	7.4	7.2	4.5 (4.4,4.6)	4.2 (4.1,4.3)	-
Maximum	6.8 (6.6,7.1)	6.4 (6.3,6.4)	9.5	9.4	4.9	8.4	10.9	9.1	6.5 (6.4,6.6)	7.0 (6.8,7.1)	-
Surface temperature											
Average	6.3 (6.1,6.5)	5.5 (5.3,5.7)	8.1	8.5	4.6	7.6	9.0	8.1	6.0 (6.1,5.9)	5.7 (5.6,5.8)	0.22
Minimum	4.3 (4.1,4.5)	4.6 (4.4,4.7)	5.8	5.2	3.9	5.9	6.0	6.9	3.7 (3.4,3.9)	4.4 (4.2,4.5)	-
Maximum	7.7 (7.3,8.1)	6.6 (6.4,6.9)	9.9	10.7	5.2	9.1	11.0	9.2	7.5 (7.2,7.8)	7.2 (7.0,7.3)	-
Internal air temperature											
Average	6.6 (6.2,7.0)	5.7 (5.7,5.7)	8.5	10.0	4.7	9.1	8.7	8.0	6.4 (6.0,6.7)	5.6 (5.5,5.7)	0.38
Minimum	2.6 (1.5,3.6)	4.5 (4.4,4.6)	4.7	4.6	3.5	5.2	4.1	6.3	1.6 (1.2,2.0)	4.4 (4.4,4.4)	-
Maximum	8.6 (7.7,9.6)	7.0 (6.9,7.2)	12.2	13.3	5.2	10.0	10.7	9.1	8.9 (8.9,8.9)	7.0 (6.9,7.0)	-
**SD	2.2	1.1	3.0	3.0	0.5	1.6	2.3	0.9	2.5	1.0	-

*▼and ▼ represent the coldest and warmest locations in the test product, respectively while ● and ● signify the coldest and warmest locations in the air, respectively.

** SD = Standard Deviation (°C). For a given condition (each column), SD represents the variation of air temperature among 13 measurement positions. For a given temperature (same row), SD represents the variation of temperature measured between 2 replications.

*** The values in parenthesis were the results of each replication.

3.2 Effect of the PCM position

The effect of PCM position on temperature and air velocity fields of a horizontal box are shown in Figure 2.16. For PCM at top, upward flow was observed near the left box wall and also near the top of test product but only a very weak downward flow (dashed arrow A in Figure 2.16b) was noticed in the left gap. In fact, flow was asymmetric: under the PCM, cold air flows preferentially towards the right gap where downward flow certainly dominates, whereas upward flow dominates in the left gap.

The temperature distribution on the middle plane (Figure 2.16b') also shows a dissymmetry of air and product temperatures. Air was at a temperature of around 5.2°C in the right gap and around 6.6°C in the left gap. This confirms the hypothesis of asymmetric airflow.

Placing PCM at the top allowed lower average temperature and lower air temperature heterogeneity:

PCM on the side: $T_{pc,\,ave}$ = 5.8°C, $T_{p,\,max}$ = 7.7°C, ΔT_{air} = 6.0°C, SD of T_{air} = 2.2°C
PCM at the top: $T_{pc,\,ave}$ = 5.4°C, $T_{p,\,max}$ = 6.6°C, ΔT_{air} = 2.5°C, SD of T_{air} = 1.1°C

Hence, placing PCM at the top is more appropriate for food transport and this configuration was used for further study of the influence of ambient and initial test product temperatures.

3.3 Effect of ambient temperature

Figure 2.17 presents the temperature field of the loaded box with a 20-mm air gap underneath and PCM at the top under ambient temperatures of 10°C (Figure 2.17a), 20°C (Figure 2.17b) and 30°C (Figure 2.17c). To compare the effect of different ambient temperatures on measured temperatures, the dimensionless temperature T^* was defined (Equation 2.6).

$$T^* = \frac{T - T_m}{T_{amb} - T_m} \qquad (2.6)$$

where T is the average value of the temperatures measured between 400 min. and 600 min.

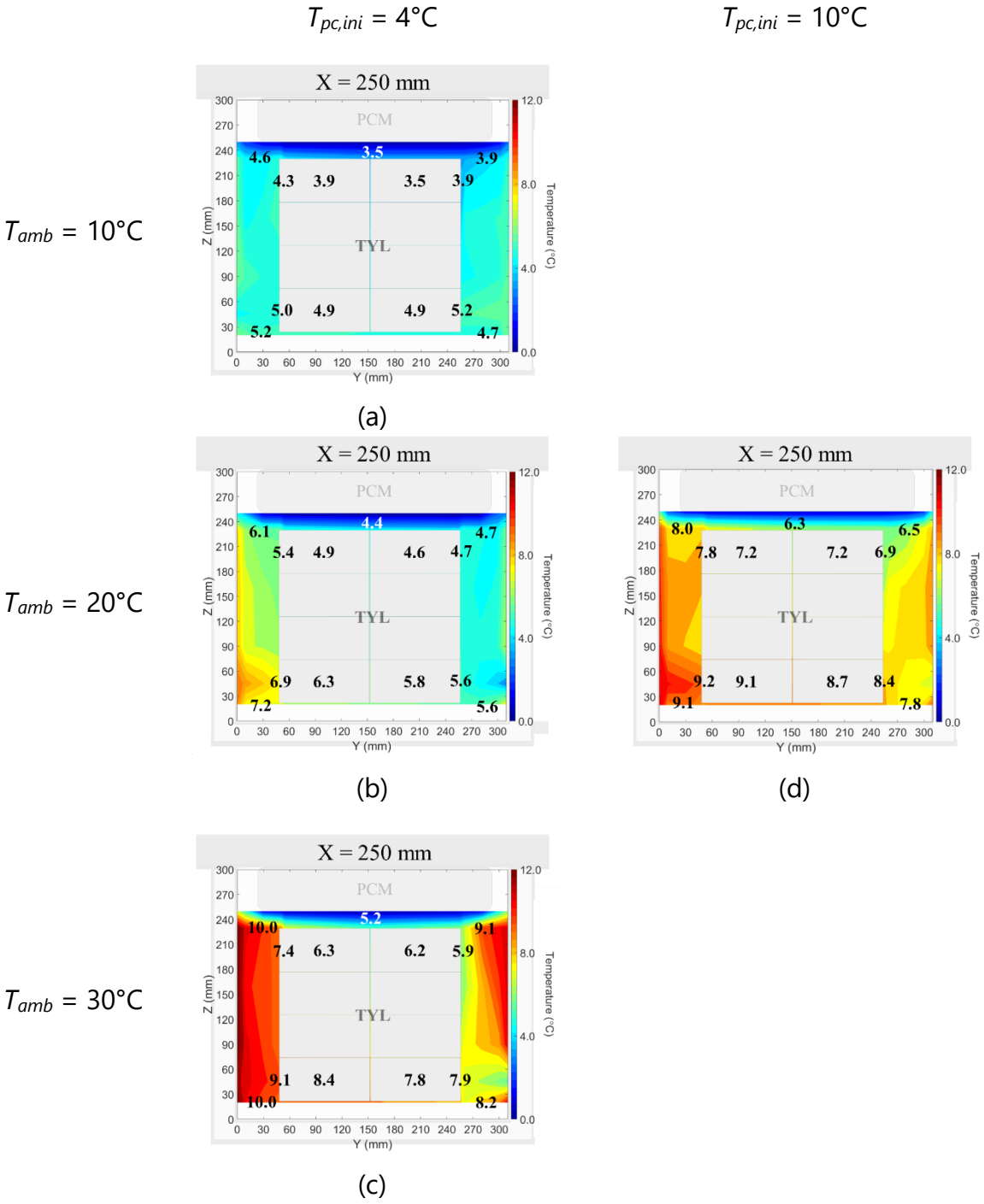

Figure 2.17 Measured temperature field on the middle plane of a loaded box with PCM at the top and a product initial temperature of 4°C under (a) 10°C ambient temperature – condition 5; (b) 20°C ambient temperature – condition 2; (c) 30°C ambient temperature – condition 6; and (d) product initial temperature of 10°C – condition 8 under 20°C ambient temperature

Logically, increasing ambient temperature led to a higher product temperature and greater air temperature heterogeneity:

$\underline{T_{amb} = 10°C}$: $T_{pc,\,ave}$ = 4.3°C ($T^*_{pc,\,ave}$ = 0.43), $T_{p,\,max}$ = 5.2°C, ΔT_{air} = 1.7°C, SD of T_{air} = 0.5°C
$\underline{T_{amb} = 20°C}$: $T_{pc,\,ave}$ = 5.4°C ($T^*_{pc,\,ave}$ = 0.27), $T_{p,\,max}$ = 6.6°C, ΔT_{air} = 2.5°C, SD of T_{air} = 1.1°C
$\underline{T_{amb} = 30°C}$: $T_{pc,\,ave}$ = 7.2°C ($T^*_{pc,\,ave}$ = 0.24), $T_{p,\,max}$ = 9.1°C, ΔT_{air} = 4.8°C, SD of T_{air} = 1.6°C

The positions of the coldest and warmest spots were the same for all ambient temperatures. One could expect that in terms of dimensionless temperature, the results would be the same, but this is not the case when applied to the average core temperature (T^* varying between 0.43 and 0.24). This can be due to the non-linearity of heat fluxes versus temperature difference in free convection: fluid flow and consequently the convective heat transfer coefficient which depends on the temperature difference. This was effectively observed with more noticeable downward airflow at an ambient temperature of 30°C (result not shown). This can also be due to the influence of the initial product temperature which is different in dimensionless terms for the three ambient temperatures (thermal inertia effect). Thus, a simple linear extrapolation cannot be applied for different ambient temperatures. For example, a 50% increase in the difference between the ambient temperature and the PCM melting temperature does not necessarily lead to a 50% higher product temperature. Similar results were obtained for PCM on the side (see Table 2.6, conditions 1 and 4). Physical-based models, e.g. zonal model or CFD, could be used to analyze the effect of ambient temperature on temperature heterogeneity and temperature evolution.

3.4 Effect of the initial test product temperature

Figure 2.17d presents the temperature field for an initial test product temperature of 10°C and PCM at the top under ambient conditions of 20°C. By comparing Figures 2.17b and 2.17d, it was observed that a higher initial test product temperature led to a higher product temperature:

$\underline{T_{pc,\,ini} = 4°C}$: $T_{pc,\,ave}$ = 5.4°C ($T^*_{pc,\,ave}$ = 0.27), $T_{p,\,max}$ = 6.6°C, ΔT_{air} = 2.5°C, SD of T_{air} = 1.1°C
$\underline{T_{pc,\,ini} = 10°C}$: $T_{pc,\,ave}$ = 8.0°C ($T^*_{pc,\,ave}$ = 0.40), $T_{p,\,max}$ = 9.2°C, ΔT_{air} = 2.8°C, SD of T_{air} = 0.9°C

Theoretically, the same results would be expected under steady state conditions, whatever the initial test product temperature if the same ambient temperature and PCM melting point are applied. This means that even after 8 h (on an averaged basis between 400 and 600 min.), steady state was not reached. This is highlighted in Section 3.6.

Similar results were obtained for PCM on the side (see Table 2.6, conditions 1 and 7). Concerning application aspects, placing a load with a high initial temperature in packaging is not recommended for food transport because PCM should only serve to maintain the product temperature, not to cool it.

3.5 Effect of a space beneath the test product

Figure 2.18 illustrates the air velocity field for the box with PCM at the top and on the side with a 20-mm gap underneath the test product (Figure 2.18a and Figure 2.18c) and without a gap (Figure 2.18b and Figure 2.18d). This gap is expected to ensure better air circulation and avoid direct heat conduction from the bottom wall to the product.

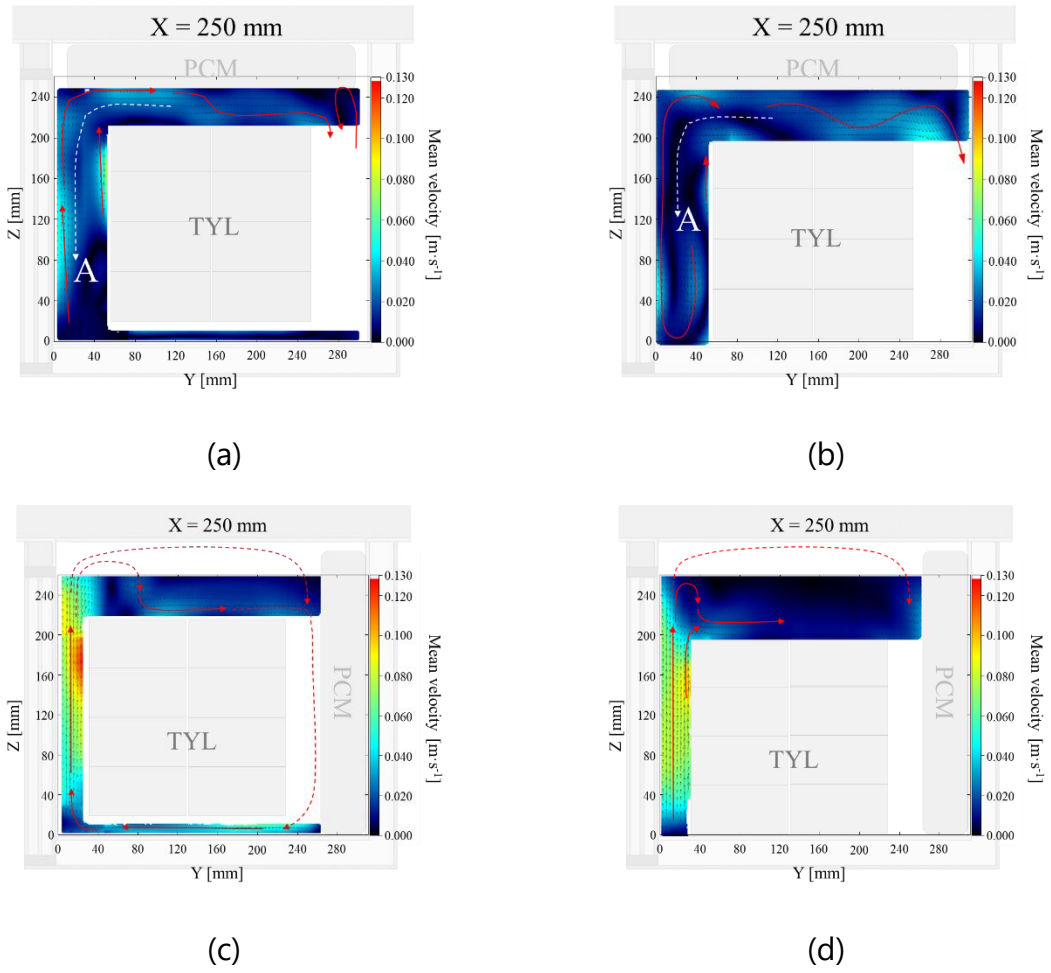

Figure 2.18 Measured air velocity field on the middle plane of a loaded box (a) PCM at the top, 20-mm gap underneath the test product – condition 2, (b) PCM at the top, without gap – condition 10, (c) PCM on the side, 20-mm gap underneath the test product – condition 1 and (d) PCM on the side, without gap – condition 9

When PCM was at the top (Figures 2.18a and 2.18b), the airflow pattern was quite similar with and without gap. From Table 2.6, for PCM at the top, it appears that the influence of gap beneath the test product on the product temperature is not significant.

With a 20-mm gap: $T_{pc,\,ave}$ = 5.4°C, $T_{p,\,max}$ = 6.6°C, ΔT_{air} = 2.5°C, SD of T_{air} = 1.1°C
Without gap: $T_{pc,\,ave}$ = 5.6°C, $T_{p,\,max}$ = 7.2°C, ΔT_{air} = 2.6°C, SD of T_{air} = 1.0°C

When PCM was on the side (Figure 2.18c and 2.18d), the maximum air velocity was slightly higher with the gap (0.13 $m \cdot s^{-1}$, with an uncertainty of 3 x 10^{-3} $m \cdot s^{-1}$ and 0.10 $m \cdot s^{-1}$, with an uncertainty of 9 x 10^{-3} $m \cdot s^{-1}$ in the box with 20-mm gap underneath and without a gap, respectively). In spite that the presence of gap led to better air circulation, the influence on product temperature was not obvious. From Table 2.6, for PCM on the side:

With a 20-mm gap: $T_{pc,\,ave}$ = 5.8°C, $T_{p,\,max}$ = 7.7°C, ΔT_{air} = 6.0°C, SD of T_{air} = 2.2°C
Without gap: $T_{pc,\,ave}$ = 5.8°C, $T_{p,\,max}$ = 7.5°C, ΔT_{air} = 7.3°C, SD of T_{air} = 2.5°C

Since the presence of gap has insignificant influence on product temperature, it is more practical to load the product directly onto the bottom of the box without providing a gap.

3.6 Temperature evolution

Figure 2.19 presents the temperature evolution at several positions in a loaded horizontal box with PCM on the side after the lid was closed. The internal wall (TC1), internal air (TC2, TC5 and TC8) and PCM surface temperatures (TC9) decreased rapidly over a period of around 60 min. before gradually increasing, while the surface and core temperatures of the test product (TC3, TC4, TC6 and TC7) increased slowly over a period of 1100 min. (18 h).

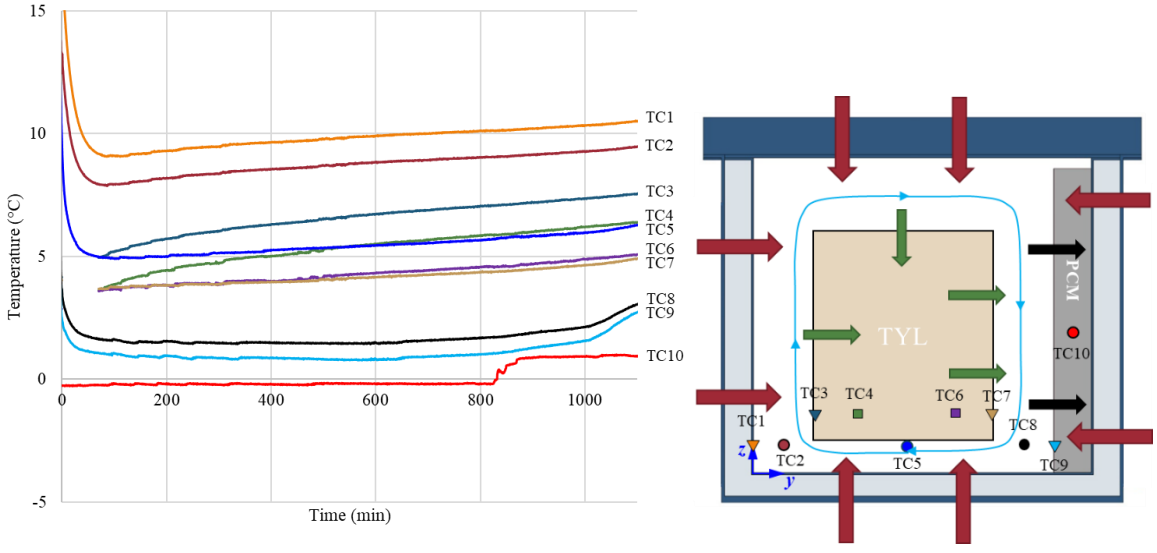

Figure 2.19 Temperature evolution at the bottom of the box during experiment No. 1 (ambient temperature = 20°C and initial test product temperature = 4°C) with heat flow (red arrows – from ambient, green arrows – between the internal air and the test product, and black arrows – from the internal air to the PCM). Airflow shown using blue arrows

The difference in temperature evolution of the walls of the box and the test product can be explained by their thermal inertia, diffusivity and convective heat exchange with air. The Biot number (*Bi*) was used to compare the effect of the internal and external thermal resistance of these materials, as defined in Equation. 2.7:

$$Bi = \frac{hL}{\lambda} \quad (2.7)$$

where *L* is the characteristic length represented by the thickness of the inner polypropylene layer (3.5 mm) for a wall of the box (considering that heat exchanged only with one side) and by the half thickness of the test product (100 mm). Due to natural convection inside the box, the order of magnitude of the heat transfer coefficient is approximately 5 $W \cdot m^{-2} \cdot K^{-1}$.

Consequently, the Biot number is 0.146 for polypropylene and 0.98 for the test product. Hence, the thermal resistance of the internal wall could be neglected, while that of the test product is of the same order of magnitude as the external thermal resistance.

The thermal time constant related to conduction can be estimated by Equation. 2.8 (Bergman, 2011).

$$\tau_{conduction} = \frac{\rho C_p L^2}{\lambda} \quad (2.8)$$

Similarly, the thermal time constant related to convection can be estimated by Equation. 2.9 (Bergman, 2011).

$$\tau_{convection} = \frac{\rho C_p L}{h} \quad (2.9)$$

For the internal wall, the thermal time constants for conduction and convection are 179 s (3 min.) and 1230 s (20 min.), respectively. It can be concluded that the delay in temperature evolution of the internal walls was mainly caused by convection between adjacent air and the walls.

For the test product, the thermal time constants of conduction and convection are 70800 s (> 19 h) and 72200 s (> 20 h), respectively. Thus, both heat conduction and convection play an important role in the temperature evolution, and this explains the temperature difference between the core, the surface of test product and the adjacent air.

The thermal time constants of the test product are much longer than those of the internal wall and this results in a different rate of temperature evolution.

According to Figure 2.19, the internal temperature of PCM (TC10) increased after 800 min. (~13 h) indicating that PCM was melted. The temperature of the other components thus increased. In view of the thermal time constant for the product, PCM

is melted before the product reaches thermal equilibrium, so there was no steady state in this condition. One could consider a hypothetical equilibrium temperature which would be reached after a long period by assuming that PCM is still at the melting temperature everywhere. Roughly, for horizontal boxes, for PCM either at the top or on the side:

$T_{pc,\,ini}$ = 4°C: after 8 h, $T_{pc,\,ave}$ is at around 5.5°C and the temperature is still rising
$T_{pc,\,ini}$ = 10°C: after 8 h, $T_{pc,\,ave}$ is at around 8.5°C and it is still decreasing

Therefore, the equilibrium temperature should be around 7°C.

In practice, to be able to compare the performances of insulated boxes equipped with PCM, the experiments should be carried out under the same loading conditions (mass and initial temperature), ambient temperature and duration of temperature measurement.

3.7 Effect of the amount of PCM on the test product temperature evolution and maximum storage time

This section describes a comparison of the experimental test product core temperature evolution (average of four measurements at different locations) for 3 amounts of PCM: 0 kg, 1.7 kg (about 10% of the product mass), and 3.5 kg (about 20% of the product mass) (Figure 2.20a). This experiment was undertaken for PCM located on a sidewall of a horizontal box loaded with the test product at an initial temperature of 4°C and 20°C ambient temperature. The higher amount of PCM lowered the rate of temperature increase. For example, during the first 2 h, this rate was 1.13°C·h^{-1}, 0.58°C·h^{-1} and 0.34°C·h^{-1}, for 0 kg, 1.7 kg and 3.5 kg of PCM, respectively.

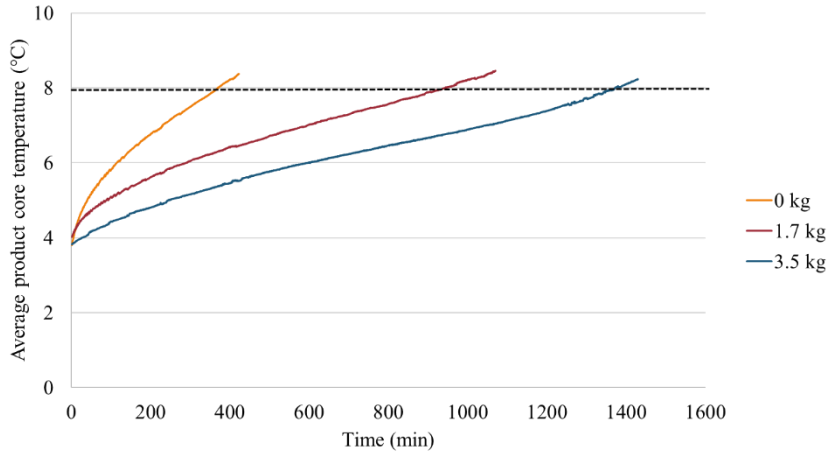

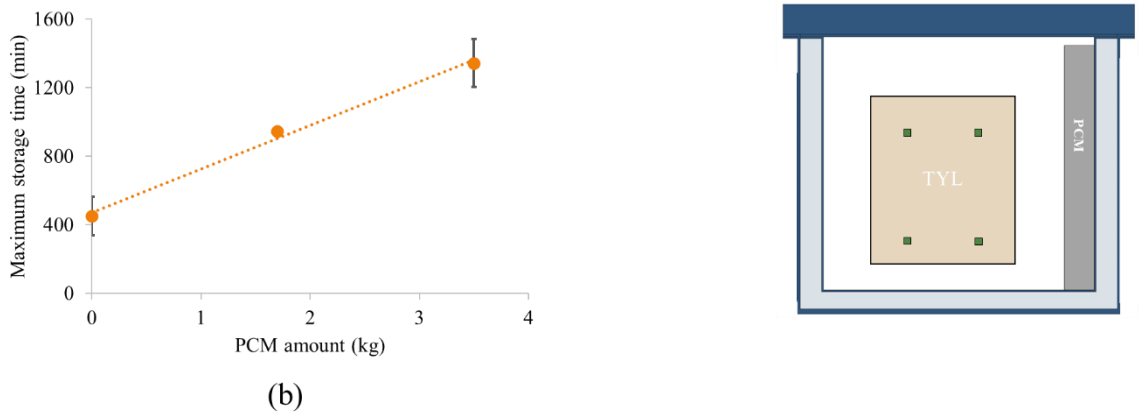

Figure 2.20 Effect of the amount of PCM on (a) test product core temperature evolution; and (b) maximum storage time, t_{max}. Error bars represent the standard deviation of 2 replications. The experiment was conducted under condition 4: loaded box with PCM on a sidewall with an ambient temperature of 20°C, 4°C initial product temperature, 20 mm gap beneath the test product (Tylose, TYL)

Figure 2.20b presents the relationship between the maximum product storage time (t_{max}) and the amount of PCM. This maximum storage time is defined as the duration during which the product remains below $T_{p,max}$ = 8°C, which is the maximum temperature value for the storage of certain chilled foods. The higher the amount of PCM, the higher the maximum storage time: 370 min. (for 0 kg), 944 min. (for 1.7 kg) and 1373 min. (for 3.5 kg). The results obtained in terms of product temperature evolution and maximum storage time confirm the benefit of PCM for food preservation as reported by Zhao et al. (2019) for strawberries. These authors showed that the use of PCM allowed less weight loss and greater product firmness in comparison with the case where PCM was not used.

To determine approximately the maximum storage time as a function of the amount of PCM, the following heat balance equation can be used:

$$m_p C_{p,p}\left(T_{p,max} - T_{p,ini}\right) + m_{pcm} L_f = UA\left(T_{amb} - \frac{T_{p,ini} + T_{p,max}}{2}\right) t_{max} \qquad (2.10)$$

where U is the overall heat transfer coefficient of the box [$W \cdot m^{-2} \cdot K^{-1}$]
and A is the exchange area [m^2]

The overall heat transfer coefficient of the box can be related to the thicknesses (e_k) and conductivities (λ_k) of the box wall materials (of index k) as shown in Equation 2.11 (assuming negligible convective heat transfer resistances).

Thus, $U = \frac{1}{\sum_k \frac{e_k}{\lambda_k}}$ (2.11)

Equation 2.10 assumes that PCM is completely melted when $T_{p,max}$ is reached and that the internal temperature is close to the average test product temperature.
Based on these assumptions, Equation 2.10 becomes:

$$t_{max} = t_{max,0}\left(1 + \alpha \frac{m_{pcm}}{m_p}\right) \qquad (2.12)$$

where $t_{max,0}$ is the maximum storage time of the box without PCM defined as

$$t_{max,0} = \frac{m_p C_{p,p}(T_{p,max} - T_{p,ini})}{UA\left(T_{amb} - \frac{T_{p,ini} + T_{p,max}}{2}\right)} \quad [s]$$

and $$\alpha = \frac{L_f}{C_{p,p}(T_{p,max} - T_{p,ini})} \quad [-]$$

This indicates a linear relationship between the maximum storage time and the amount of PCM as shown in Figure 2.20b.

In practice, for all types of boxes, it is suggested that this type of experiment should be conducted, at a fixed ambient temperature, without and with a given amount of PCM to determine $t_{max,0}$ and α. The influence of other parameters could be approximated according to Equations 2.10 and 2.12. For example, it is expected that the maximum storage time is inversely proportional to the difference between the ambient temperature (T_{amb}) and the internal temperature considered as the average test product temperature ($\frac{T_{p,ini} + T_{p,max}}{2}$).

3.8 Expected influence of insulation on temperature level and heterogeneity

The present study considered only one insulation configuration. This section aims to predict the effect of changing the insulation by using a basic approach. This effect is the determining factor for the temperature distribution in insulated boxes equipped with PCM (Paquette et al., 2017). To illustrate the influence of the box insulation, the analysis presented below concerns the box with PCM on the side where a higher temperature level and greater heterogeneity were observed.

As a first approach, the steady state mean temperature in the box (T_{mean}) could be

obtained from the following energy balance (Equation 2.13):

$$A_c h_c (T_{mean} - T_m) = A_w U (T_{amb} - T_{mean}) \qquad (2.13)$$

where A_c and A_w are the surface area of warm (insulated) and cold (PCM) walls [m^2],

h_c is the heat transfer coefficients between product and PCM surface [$W \cdot m^{-2} \cdot K^{-1}$],

U is the overall heat transfer coefficient between ambient and product surface through box insulation [$W \cdot m^{-2} \cdot K^{-1}$] and

T_m and T_{amb} are the melting temperature of the PCM and the external temperature, respectively [°C].

When the box is horizontal, in our case $\beta = (A_w U)/(A_c h_c) \approx 0.54$ with T_m = 0°C, T_{amb} = 20°C and $T_{mean} \approx$ 7°C. Since A_w/A_c = 4.3 and $h_c/U \approx 8$; therefore, if insulation is improved by 30%, (i.e., U divided by 1.3), the mean temperature should decrease from 7°C to 5.9°C.

To obtain an estimation of temperature heterogeneity, it can be assumed that air flows, with a mass flowrate $\dot{m}$, first along the PCM, where its temperature decreases to T_{min}, then along the warm walls, where the temperature rises to T_{max}. The following equations characterize these heat exchange phenomena (Equations 2.14 and 2.15):

$$T_{air,min} - T_m = \alpha_c (T_{air,max} - T_m) \qquad (2.14)$$

where $\alpha_c = exp\left(-\frac{A_c h_c}{\dot{m} C_{p,air}}\right)$

$$T_{amb} - T_{air,max} = \alpha_w (T_{amb} - T_{air,min}) \qquad (2.15)$$

where $\alpha_w = exp\left(-\frac{A_w U}{\dot{m} C_{p,air}}\right) = {\alpha_c}^{\beta}$

Therefore; $T_{air,max} - T_{air,min} = \frac{(1-\alpha_c)(1-\alpha_w)(T_{amb} - T_m)}{(1-\alpha_c \alpha_w)} \qquad (2.16)$

For the academic case of a square cavity with one vertical cold wall (T_c), one vertical warm wall (T_w) and adiabatic horizontal walls, Raithby & Hollands (1998) found that $T_{air,max} - T_{air,min} \approx 0.5(T_w - T_c)$ for the cavity with a low aspect ratio (AR < 40) which is often the case of insulated boxes (T_w and T_c are the temperature of warm wall and cold wall, respectively). If our basic approach is applied to this case, it can be estimated that $\alpha_c \approx 1/3$.

In our case ($\beta \approx 0.54$), it was calculated that $T_{air,max} - T_{air,min} \approx$ 7.4°C which is comparable to the observed values. If insulation is improved by 30% for example (β divided by 1.3), the temperature heterogeneity should decrease from 7.4°C to 6.1°C.

This basic approach does not take into account the interaction with the test product especially during the unsteady period, radiation, complex flow etc., but it allows a rough estimation of the influence of insulation. It also highlights the influence of the air mass flowrate ($\dot{m}$) and the heat transfer (h_c) along the PCM on the temperature level and heterogeneity.

4. Conclusion and perspectives

This study investigated airflow and temperature fields inside an insulated box equipped with PCM loaded with test product (Tylose slabs). PCM position significantly affected airflow patterns, air temperature profile, product temperature homogeneity, and average product temperature. When PCM was on a sidewall, the coldest position was at the bottom, close to the PCM surface, and the warmest one was at the top close to the opposite vertical wall. When PCM was at the top, the lowest product temperature was located at the top, while the highest one was at the bottom, and slightly lower air and product temperatures were observed. Increasing the box aspect ratio (higher box) led to a higher product temperature and greater temperature heterogeneity (at least for PCM on the side). The non-linear correlation between ambient temperature and product temperature can be explained by the non-linearity of free convection and the product thermal inertia. An insignificant influence of the initial product temperature on the airflow pattern and air velocity profile was observed. The presence and absence of a space underneath the product led to similar temperatures, despite the difference in airflow pattern in the case of PCM on the side.

It is recommended that the PCM should be placed at the top of the box in order to reduce temperature stratification. This configuration has been previously investigated in an empty cavity and this work confirms, by experiment, that it can be applied for the loaded cavity as well. The box should not be too high to avoid a high temperature and large temperature heterogeneity. The effect of aspect ratio is complex as higher boxes allow higher convective heat transfer and also higher thermal stratification. Thus, CFD model is suggested to analyze in detail the influence of aspect ratio on temperature distribution. To maintain the product temperature along a supply chain, PCM could be placed on all walls (top, bottom, sidewalls); however, the available volume would be significantly reduced and the logistic cost per kg of product would be higher. Our study demonstrates that it is possible to place PCM only at one wall (top or side) if an appropriate PCM mass is used. This mass depends on the ambient temperature in the supply chain, which directly impacts airflow and product temperature. Hence, the ambient temperature is an important factor for the system design, i.e., box wall material, PCM type and mass. However, linear extrapolation from one ambient to another is not recommended because of non-linear behavior, thus physical based models taking natural convection into account should be used to analyze the impact of ambient temperature on product temperature in an insulated box with PCM. Loading a product at a high temperature should be avoided since it takes more than 10 hours to cool it down according to its high thermal inertia. Adding a 20-mm air

space beneath the test product neither reduces the test product temperature nor increases homogeneity although this gap allows slightly better air circulation. Future studies are required to determine the influence of the other air gaps: between PCM and load, between lateral and top walls and load. The use of PCM can delay the internal temperature evolution and the amount of PCM linearly correlates with the maximum storage time of the insulated box. The influence of other parameters like the amount of product and the emissivity of box walls will be studied.

The experimental velocity and temperature fields obtained in different conditions can further be used to validate CFD models. They should confirm that when PCM is at top, although the configuration is symmetric, the velocity and temperature fields can be asymmetric. In practice, there are many other possible box designs and operating conditions and the interactions between the different factors are complex. Thus, numerical models are necessary for investigating the influence of these factors on temperature distribution and evolution in a wide variety of configurations (e.g., smaller/larger boxes, improved insulation). The experimental results presented in the present article can contribute to validate these models.

3 DEVELOPMENT AND VALIDATION OF THERMAL MODELS FOR AN INSULATED BOX WITH PCM

3.1 SUMMARY

This chapter presents the development and validation of three thermal models: lumped, zonal and Computational Fluid Dynamic (CFD). The lumped model considers uniform product temperature and global thermal resistances. The model description is presented briefly in this chapter (more detail of lumped model development and validation is in chapter IV). The zonal model distinguishes warmer and colder regions inside the insulated box, it takes airflow, heat conduction, convection and radiation into account. The detail of zonal model is shown in Article 4 and the code written in python was published in an Open access code paper (article 8 see appendix). Finally, CFD model, providing thorough understanding of airflow and heat transfer, is presented in a conference paper 1.

Résumé

Ce chapitre présente le développement et la validation de trois modèles thermiques : global (lumped), zonal et CFD. Le modèle global considère une température uniforme du produit et différentes résistances thermiques. Une brève description de ce modèle est donnée dans ce chapitre, plus de détails seront donnés au chapitre IV. Le modèle zonal distingue des régions plus chaudes et plus froides dans le caisson, il prend en compte l'écoulement d'air, la conduction thermique, la convection et le rayonnement. Le détail du modèle zonal est présenté dans l'article 4 (le code python a été publié dans l'article 8 donné en annexe). Enfin, le modèle CFD, fournissant une compréhension approfondie de l'écoulement d'air et des transferts de chaleur, est présenté dans la communication à congrès (paper 1).

3.2 BRIEF DESCRIPTION OF LUMPED MODEL

The product is assumed to be a lumped object characterized only by its average temperature which exchange heat with the ambiance and with the PCM through thermal resistances by using electrical analogues shown in Figure 3.1. The model predicts only the evolution of the average product temperature and of the mass of melted PCM.

Details of the model will be presented in chapter IV (Article 5).

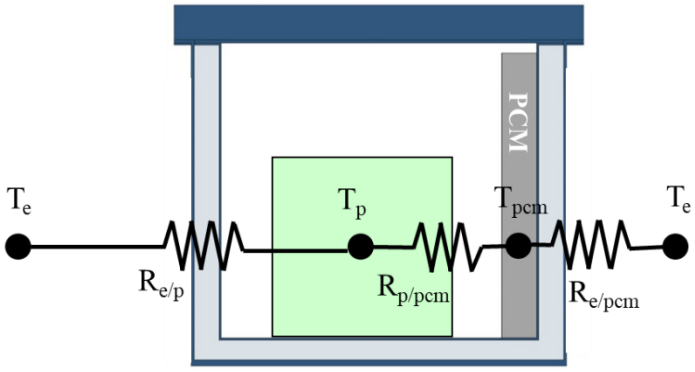

Figure 3.1 Lumped model structure

3.3 ARTICLE 4

Modèle de transfert thermique simplifié pour la prédiction en temps réel des températures dans un caisson isotherme équipé d'un matériau a changement de phase

Résumé (version française de l'abstract de l'article 4)

Un modèle simplifié de transfert de chaleur a été développé pour prédire les variations spatiales et temporelles de température dans des caissons isothermes chargés de produits (Tylose) et équipées d'un matériau à changement de phase sur une paroi latérale (point de fusion ~ 0°C). Ce modèle, basé sur l'approche zonale, considère le produit comme quatre blocs où l'on distingue le cœur et la surface. Il prend en compte les flux d'air, les échanges thermiques par conduction, convection et rayonnement. Le modèle a été validé en comparant les températures prévues avec celles mesurées à 24 positions (sur les parois, à cœur et en superficie du produit, au niveau de l'air intérieur). Le modèle a d'abord été validé en régime permanent (à des températures ambiantes de 10°C et 20°C), et il a montré un bon accord avec les valeurs mesurées avec une erreur quadratique moyenne de 0,60°C et 0,88°C pour 10°C et 20°C de température ambiante respectivement, et avec une pente de régression entre les courbes numérique et mesurée proche de 1 (0,89 et 0,98 pour une température ambiante de 10°C et 20°C, respectivement). Le modèle a ensuite été validé en régime transitoire (à 4°C et 10°C de température initiale du produit, 20°C de température ambiante) et il a fourni une bonne prédiction de l'évolution de la température de la superficie et du cœur du produit. Ce modèle pourrait être un outil utile pour les professionnels car il leur permettrait d'étudier l'effet de la configuration du caisson (isolation) et des conditions de fonctionnement (température ambiante) sur l'évolution de la température dans des scénarios réels. En combinant ce modèle avec un modèle de qualité et un modèle microbiologique, l'évolution de la qualité et de la sécurité sanitaire d'un produit alimentaire pourrait être prédite.

Simplified heat transfer model for real-time temperature prediction in insulated boxes equipped with a phase change material

Tanathep Leungtongkum[a,b*], Onrawee Laguerre[a] and Denis Flick[b]

[a]Université Paris-Saclay, INRAE, FRISE, 92761 Antony, France
[b]Université Paris-Saclay, INRAE, AgroParisTech, UMR SayFood, 91120 Palaiseau, France

***Corresponding author:** Tanathep Leungtongkum, e-mail: tanathep.leungtongkum@inrae.fr, tel: (+33) 1 40 96 61 48

Highlights

- A simplified model was developed for insulated boxes with a PCM.
- The model considered airflow, conduction, convection and radiation.
- The model predicts spatial and temporal temperature variations.
- The model was validated under various ambient and product initial temperatures.
- Linking the model with quality and microbiological models could give indications about food quality and safety along supply chains.

Abstract

A simplified heat transfer model to predict spatial and temporal temperature variations was developed for insulated boxes equipped with a phase change material (melting point ~ 0°C) on a sidewall and loaded with a test product (Tylose). This model, based on the zonal approach, considers the product as four blocks with shell and core regions. It takes into account airflow, heat exchange by conduction, convection and radiation. The model was validated by comparing the predicted temperatures with those measured at 24 positions (on the walls, on the product surface, shell and core, and internal air). The model was first validated under steady state (at 10°C and 20°C ambient temperatures), and it showed good agreement with the measured values with a root mean square error of 0.60°C and 0.88°C for 10°C and 20°C ambient temperatures respectively, and with a regression slope between the numerical and measured curves close to 1 (0.89 and 0.98 for 10°C and 20°C ambient temperature, respectively). The model was then validated under transient state (at 4°C and 10°C initial product temperatures, 20°C ambient temperature) and it provided a good prediction of the wall and product core temperature evolution. This model could be a useful tool for stakeholders as it enables them to study the effect of the box configuration e.g. box insulation and operating conditions e.g. the ambient temperature on temperature evolution in real scenarios. By combining this model with a quality and a microbiological model, the quality and safety evolution of a food product could be predicted.

Keywords: Insulated box, Phase change material, Simplified model, Heat transfer, Temperature

Nomenclature

A	Area [m^2]
C	Length of the cross-section of the product block [m]
C_p	Specific heat capacity [$J \cdot kg^{-1} \cdot K^{-1}$]
e	Thickness [m]
g	Gravitational acceleration = 9.81 $m \cdot s^{-2}$
Gr	Grashof number [-]
h	Convective heat transfer coefficient [$W \cdot m^{-2} \cdot K^{-1}$]
ΔH_{fus}	Latent heat of fusion [$J \cdot kg^{-1}$]
K	Heat transmission coefficient of insulation [$W \cdot m^{-2} \cdot K^{-1}$]
L	Length of the product block or wall [m]
M	Mass [kg]
MC_p	Thermal inertia [$J \cdot K^{-1}$]
$\dot{m}$	Mass flow rate [$kg \cdot s^{-1}$]
Nu	Nusselt number [-]
Pr	Prandtl number [-]
q_r	Radiative heat exchange [W]
R	Thermal resistance [$K \cdot W^{-1}$]
Ra_L	Rayleigh number [-]
T, T'	Temperature [°C or K]
T_m	Melting temperature of PCM [°C]
ΔT	Temperature difference between surface temperature and bulk fluid temperature [°C or K]
t	Time [s]
v	Velocity [$m \cdot s^{-1}$]
v^*	Dimensionless velocity [-]
x	Position along the vertical surface [m]
y	Distance from the vertical surface [m]
y^*	Dimensionless y-position [-]
Z	Height of the wall [m]

Greek symbols

α	Dimensionless heat transfer coefficient (between the air and the product shell or wall) [-]
β	Thermal expansion coefficient [K^{-1}]
ε	Surface emissivity [-]
λ	Thermal conductivity [$W \cdot m^{-1} \cdot K^{-1}$]
φ	Ice fraction [-]
ρ	Density [$kg \cdot m^{-3}$]

σ Stefan-Boltzmann constant = 5.67 x 10^{-8} W·m^{-2}·K^{-4}
τ Characteristic time [s]
μ Dynamic viscosity [kg·m^{-1}·s^{-1}]
κ, κ' Dimensionless constants defined in equations and 3.35 and 3.37

Subscripts

a Air
c Core
cw Cold wall
exp Experimental value
ext External
i Zone number (see Figure 3.2)
j Index of material composing the insulated wall of the box
ini Initial
max Maximum value
min Minimum value
n Data index
num Numerical value
p Product
pcm Phase Change Material
pp Polypropylene (material of the internal layer of the wall and the PCM container)
s Surface
sh Shell
w Wall
ww Warm wall

1. Introduction

To avoid temperature abuse during delivery of temperature-sensitive products, insulated boxes equipped with a Phase Change Material (PCM) have been commonly used in the food cold chain (Nie et al., 2020; Zhao et al., 2020a). They are often used in the last mile delivery of small product quantities when refrigeration equipment is not available (East et al., 2009; Elliott & Halbert, 2008; Navaranjan et al., 2013; Robertson et al., 2017). Although food transport in an insulated box is practical and cost-effective, insufficient PCM mass and inappropriate PCM positioning may cause temperature abuse (Du et al., 2020; Elliott & Halbert, 2005). Spatial and temporal temperature variations were observed (Laguerre et al., 2013; Mercier et al., 2017) and an empirical approach is still mainly used in practice. It is challenging to establish physical-based models for temperature prediction which fit various types of products (different recommended storage temperatures) and take into account various transport conditions (e.g. ambient temperature and duration).

During food transport in an insulated box, conduction (in the walls of the box, unmelted PCM and products), natural convection (between air and walls/product

surface) and radiation occur (Laguerre & Flick, 2010; Rincón-Casado et al., 2017; Shinoda et al., 2019). The heat exchanges via these transfer modes are of the same order of magnitude; thus, it is necessary to take all of them into account (Laguerre & Flick, 2010).

Experimental and numerical studies on insulated boxes equipped with PCM and loaded with food were reviewed by Leungtongkum et al. (2022). These studies often considered heat conduction in the air inside the box alone, while heat transfer by natural convection and radiation were neglected (Du et al., 2020; East et al., 2009; East & Smale, 2008; Ge et al., 2014; Kozak et al., 2017; Margeirsson et al., 2011, 2012; Paquette et al., 2017; Xiaofeng & Xuelai, 2021).

To understand the real phenomena in the system, Computational Fluid Dynamic (CFD) models can be used to predict the temperature field and its evolution with time. This approach consists of meshing the system and solving the Navier-Stokes and energy partial differential equations (Söylemez et al., 2021). This requires a significant amount of calculation time; for example, it took from 45 min. to 8 h, depending on the cell numbers and the quantity of PCM, using a computer with 32 GB of RAM to investigate a 3D heat transfer model of an insulated box containing food products (Paquette et al., 2017). Thus, it is not possible to apply a CFD model in real-time temperature prediction (Mercier et al., 2017). Moreover, the use of CFD software is complex and requires expertise in fluid mechanics.

In order to propose an alternative, the aim of this work was to establish a simplified heat transfer model based on a zonal approach to predict spatial and temporal temperature variations in an insulated box equipped with PCM. This model considers the same phenomena as those where CFD is applied, i.e. conduction in solids, convection between circulating air and solid surfaces, radiation between surfaces and PCM melting.

The temperature field and its variation with time were predicted for an insulated box (with PCM on one side) exposed to several ambient and initial product temperatures. For the model validation, these results were compared with those measured in a controlled ambient test room. Finally, the model could be used to numerically study the influence of input parameters, i.e. box insulation, PCM melting point, on the product temperature evolution for different time-temperature scenarios in a supply chain. It would be possible to link the thermal model and a food quality and a microbiological model enabling evaluation of product quality and safety in a supply chain. It should be emphasized that according to our best knowledge, there are no such models for insulated boxes equipped with PCM for food transport applications.

2. Simplified heat transfer model development

2.1 Main structure

As an initial approach, PCM was located on one side wall of an insulated box and loaded with the test product (Tylose). In this configuration, airflow and heat transfer occur mainly in two dimensions (*y* and *z* directions in Figure 3.2). Other configurations could be modelled in a similar manner with the modification of airflow pattern and related heat transfers. This model considers that there is a temperature difference between the air, the product surface, and the product core, between the top and the bottom, and between the cold side (near the PCM) and the warm opposite side wall (Figure 3.2). For a given zone number *i*, $T_{a.i}$ and $T'_{a.i}$ are the temperature of the air before heat exchange with the product and after, respectively.

The model considers heat exchange by convection between internal air and the product surface as well as by conduction inside the product. van der Sman (2003) proposed an approach to distinguish the shell and core temperatures. This approach better represents the real phenomena than a lumped approach, which considers the overall temperature of the product. In our model, the product was divided into four square blocks, and each block had a length *C* with shell (*C/4* length) and core (*3C/4* length). A two-dimensional model is proposed; first, air flows downward near the PCM surface as cold air has a higher density than warm air, then it flows upward near the opposite box wall because of decreasing density.

Convective heat fluxes occur between the different surfaces (product, PCM and box walls) and the adjacent air. Heat conduction occurs inside product blocks and insulation. Heat radiation occurs between the product surface and box walls or PCM surface. Figure 3.2 summarizes the control volumes and heat fluxes considered.

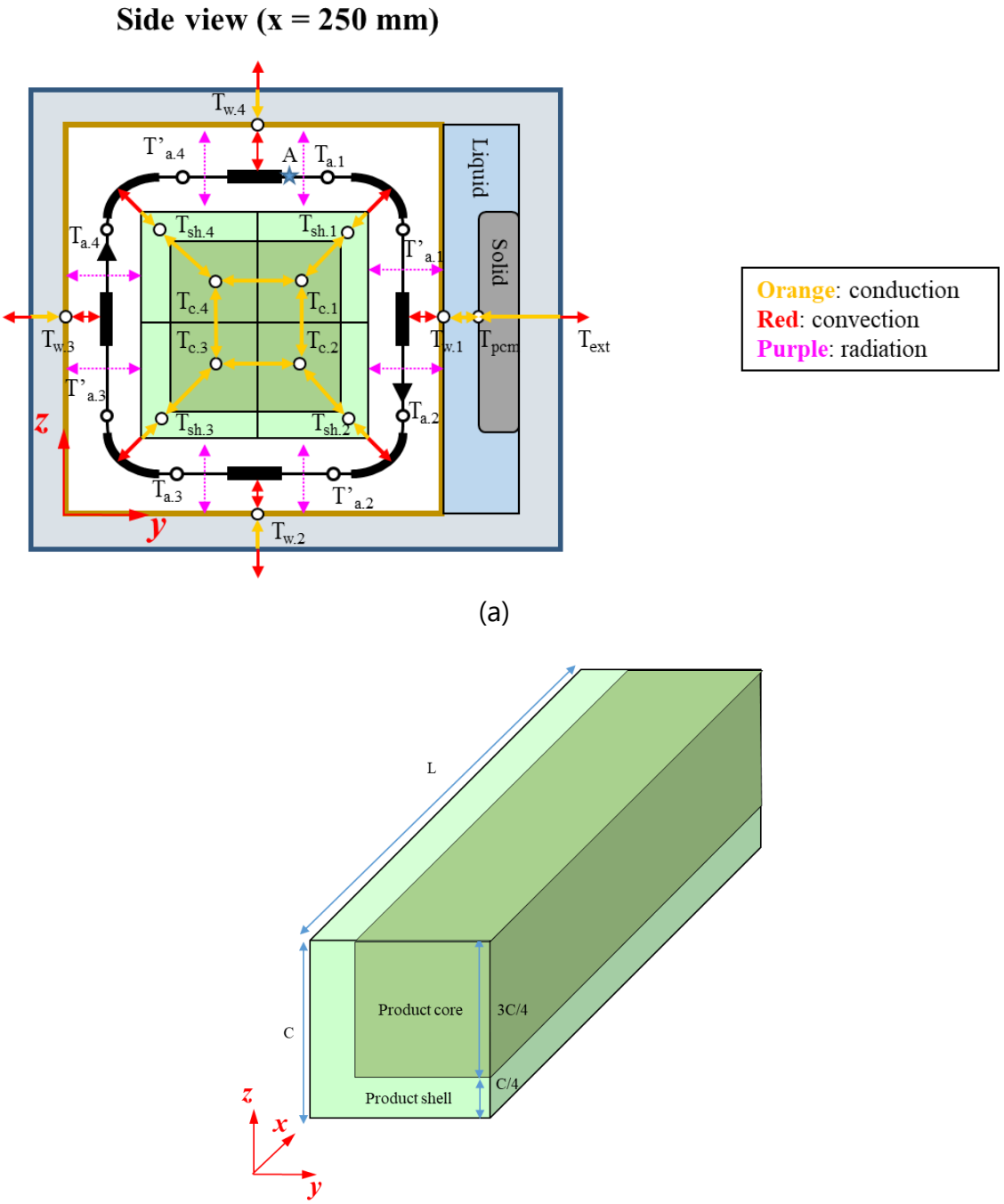

Figure 3.2 Simplified heat transfer and airflow diagram in a 2D insulated box with PCM on a side wall (a) Side view and (b) Perspective view of a quarter of test product

The following state variables describe the system at a given time:

- Air temperature in °C or K: $T_{a.i}$, $T'_{a.i}$ when $i \in [1,4]$
- Average temperature in product shell in °C or K: $T_{sh.i}$ when $i \in [1,4]$
- Average temperature in product core in °C or K: $T_{c.i}$ when $i \in [1,4]$
- Wall temperature in °C or K: $T_{w.i}$ when $i \in [1,4]$ where $T_{w.1}$ is the PCM surface temperature

- PCM temperature in °C or K: T_{pcm} (if the PCM is partially melted, $T_{pcm} = T_m$ at the liquid/solid interface)
- Solid fraction in melting PCM (fraction of ice): φ

2.2 Thermal resistances and inertia

Four thermal resistances in $K \cdot W^{-1}$ between the internal air, the product surface, the product shell and the product core can be defined, given *C* as the length of the cross-section of the product block [m] and *L* as the length of the product block [m] (Equations 3.1 to 3.4):

- from internal air to product surface:

$$R_{a.s} = \frac{1}{h_p A_{p.s}} \qquad (3.1)$$

where $A_{p.s} = 2CL$ (the external area of product block) [m^2]
and h_p is the heat transfer coefficient between internal air and the product surface [$W \cdot m^{-2} \cdot K^{-1}$]

- from the surface to the middle of the product shell:

$$R_{s.sh} = \frac{1}{8} \frac{C}{\lambda_p A_{p.s}} \qquad (3.2)$$

Where λ_p is the thermal conductivity of the product [$W \cdot m^{-1} \cdot K^{-1}$]

- from the product shell to the product core:

$$R_{sh.c} = \frac{3}{8} \frac{C}{\lambda_p A_{p.c}} \qquad (3.3)$$

where $A_{p.c} = \frac{3}{2} CL$ (the external area of product core) [m^2]

- between adjacent product cores:

$$R_c = \frac{3}{4} \frac{C}{\lambda_p A_c} \qquad (3.4)$$

where $A_c = \frac{3}{4} CL$ (the contact area between one product core and another) [m^2]

For each wall, two thermal resistances can also be defined as described in Equations 3.5 and 3.6. Index 1 corresponds to the PCM surface, while 2, 3 and 4 correspond to the bottom wall, the opposite side wall and the top wall of the box, respectively.

- from internal air to the internal wall:

$$R_{a.w.i} = \frac{1}{h_w A_{w.i}} \text{ when } i \in [1,4] \qquad (3.5)$$

where $A_{w.i}$ is the area of wall i [m^2]
and h_w is the heat transfer coefficient between the internal air and the internal wall, which is assumed to be the same value for all walls [$W \cdot m^{-2} \cdot K^{-1}$].

- from the internal wall to the external (ambient) air:

$$R_{w.ext.i} = \frac{1}{KA_{w.i}} \text{ when } i \in [1,4] \quad (3.6)$$

where $K = \frac{1}{\sum_j \frac{e_j}{\lambda_j}}$ (3.7)

and e_j and λ_j are the thickness [m] and the thermal conductivity [$W \cdot m^{-1} \cdot K^{-1}$] of the insulation materials of the wall, respectively.

Within a supply chain, PCM changes from the completely frozen (solid) state, to the melting (solid-liquid mixture) state, then to the completely melted (liquid) state, successively. The heat transfer from the PCM to its container wall (wall 1) involves different phenomena depending on the period (conduction in the solid and conduction and natural convection in the liquid).

The melting period is the most important, during this period, T_{pcm} is considered as the melting temperature T_m present at the solid/liquid interface, and the thermal resistance is estimated from the liquid-PCM conductivity (λ_{pcm} in $W \cdot m^{-1} \cdot K^{-1}$) and the PCM thickness (e_{pcm} in m) (Equation 3.8). This resistance is low compared with that between the PCM container wall and the internal air. Thus, its exact value is not of utmost importance. Therefore, the estimation of Equation 3.8 was considered whatever the period, and the PCM temperature was obtained from a heat balance for completely frozen or completely melted PCM (cf. the detailed description in Section 2.5).

$$R_{pcm.w1} = \frac{e_{pcm}}{\lambda_{pcm} A_{w.1}} \quad (3.8)$$

where $A_{w.1}$ is the area of wall 1 – PCM surface [m^2]

Regarding the contact between PCM surface and internal wall, since there was not a perfect contact, an additional thermal resistance should be added to $R_{w.ext.1}$. This resistance is difficult to estimate precisely. Nevertheless, considering for example, a 2-mm air gap between PCM surface and box wall, it would increase $R_{w.ext.1}$ value by less than 10% in our case, thus this thermal resistance was neglected.

For the purposes of model simplification, the thermal inertia (mass multiplied by the heat capacity) of air is considered as negligible compared with that of the product and box walls.

Different thermal inertias (MC_p in $J \cdot K^{-1}$) are considered as shown in Equations 3.9 to

3.12 with ρ_p as the density of product [kg·m^{-3}], C as the length of the cross-section of the product block [m], L as the length of the product block [m] and $C_{p.p}$ as the specific heat capacity of product [J·kg^{-1}·K^{-1}].

- for the core of a product block:

$$MC_{p.c} = \rho_p \left(\frac{3}{4}C\right)^2 LC_{p.p} \qquad (3.9)$$

- for the shell of a product block:

$$MC_{p.sh} = \rho_p \left(C^2 - \left(\frac{3}{4}C\right)^2\right) LC_{p.p} \qquad (3.10)$$

- for each wall in contact with the adjacent air:

$$MC_{p.w.i} = \rho_{pp} e_{pp} A_{w.i} C_{p.pp} \qquad (3.11)$$

where ρ_{pp} is the density of polypropylene (internal layer of the wall) [kg·m^{-3}]
e_{pp} is the thickness of internal polypropylene layer [m]
$A_{w.i}$ is the area of wall i [m^2]
$C_{p.pp}$ is the specific heat capacity of polypropylene [J·kg^{-1}·K^{-1}]

- for completely frozen or completely melted PCM:

$$MC_{p.pcm} = M_{pcm} C_{p.pcm} \qquad (3.12)$$

where M_{pcm} is the mass of PCM [kg]
The value of $C_{p.pcm}$ [J·kg^{-1}·K^{-1}] is different for the frozen or the melted state.

2.3 Air temperature estimation from product shell and wall temperatures

Since air moves clockwise in the box, the air at the top of the box (position A in Figure 3.2) successively exchanges heat with the shell of product block 1, then with wall 1 (PCM surface), with the shell of product block 2, and so on. Its temperature changes from $T_{a.1}$ to $T'_{a.1}$, then to $T_{a.2}$, to $T'_{a.2}$, respectively.

The equation governing the heat balance between the adjacent air and wall 1 (surface of the PCM) can be written in the same manner as that in a heat exchanger. According to Figure 3.2, the air with an inlet temperature $T'_{a.1}$ exchanges heat with wall 1 ($T_{w.1}$) with a convective heat transfer coefficient h_w. This exchange leads to an outlet air temperature $T_{a.2}$, given $C_{p.a}$ as the specific heat capacity of air [J·kg^{-1}·K^{-1}] and $\dot{m}_a$ as the mass flow rate of air [kg·s^{-1}].

So, $\dot{m}_a C_{p.a} dT_a = h_w (T_{w.1} - T_a) dA$

$ln\left(\frac{T_{a.2}-T_{w.1}}{T'_{a.1}-T_{w.1}}\right) = -\frac{h_w A_{w.1}}{\dot{m}_a C_{p.a}}$

Since $\frac{h_w A_{w.1}}{\dot{m}_a C_{p.a}} = \frac{1}{R_{a.w.1}\dot{m}_a C_{p.a}}$

Finally, $(T_{a.2} - T_{w.1}) = \alpha_{w.1}(T'_{a.1} - T_{w.1})$ (3.13)

with $\alpha_{w.1} = exp\left(-\frac{1}{R_{a.w.1}\dot{m}_a C_{p.a}}\right)$

Where $\alpha_{w.1}$ is the dimensionless convective heat transfer coefficient between internal air and internal wall 1 [-]

$R_{a.w.1}$ is the thermal resistance between internal air and internal wall 1 [K·W^{-1}]

The same approach is applied to the heat exchange between the internal air and the shell of product block 1, which gives rise to Equation 3.14.

$(T'_{a.1} - T_{sh.1}) = \alpha_p(T_{a.1} - T_{sh.1})$ (3.14)

with $\alpha_p = exp\left(-\frac{1}{R_{a.sh}\dot{m}_a C_{p.a}}\right)$

and $R_{a.sh} = R_{a.s} + R_{s.sh}$

Where α_p is the dimensionless overall heat transfer coefficient between internal air and product shell [-]

$R_{a.sh}$ is the thermal resistance between internal air and product shell [K·W^{-1}]

$R_{a.s}$ is the thermal resistance between internal air and product surface [K·W^{-1}]

$R_{s.sh}$ is the thermal resistance between product surface and product shell [K·W^{-1}]

These approaches are used to formulate eight equations involving eight air temperatures. They can be expressed in a matrix form:

$A \cdot T_a = B$

So, $T_a = A^{-1} \cdot B$ (3.15)

Where $A = \begin{bmatrix} -\alpha_p & 1 & 0 & 0 & 0 & 0 & 0 & 0 \\ 0 & -\alpha_{w.1} & 1 & 0 & 0 & 0 & 0 & 0 \\ 0 & 0 & -\alpha_p & 1 & 0 & 0 & 0 & 0 \\ 0 & 0 & 0 & -\alpha_{w.2} & 1 & 0 & 0 & 0 \\ 0 & 0 & 0 & 1 & -\alpha_p & 1 & 0 & 0 \\ 0 & 0 & 0 & 0 & 0 & -\alpha_{w.3} & 1 & 0 \\ 0 & 0 & 0 & 0 & 0 & 0 & -\alpha_p & 1 \\ 1 & 0 & 0 & 0 & 0 & 0 & 0 & -\alpha_{w.4} \end{bmatrix}$

$T_a = \begin{bmatrix} T_{a.1} \\ T'_{a.1} \\ T_{a.2} \\ T'_{a.2} \\ T_{a.3} \\ T'_{a.3} \\ T_{a.4} \\ T'_{a.4} \end{bmatrix}$ and $B = \begin{bmatrix} (1-\alpha_p)T_{sh.1} \\ (1-\alpha_{w.1})T_{w.1} \\ (1-\alpha_p)T_{sh.2} \\ (1-\alpha_{w.2})T_{w.2} \\ (1-\alpha_p)T_{sh.3} \\ (1-\alpha_{w.3})T_{w.3} \\ (1-\alpha_p)T_{sh.4} \\ (1-\alpha_{w.4})T_{w.4} \end{bmatrix}$

2.4 Radiative heat exchange

The radiative heat exchange between the lateral surface of product block 1 ($T_{s.1}$ in K) and wall 1 (PCM surface, $T_{w.1}$ in K) is shown in Equation 3.16.

$$q_{r.s1.w1} = \varepsilon_{w.1}\sigma\left({T_{s.1}}^4 - {T_{w.1}}^4\right)CL \qquad (3.16)$$

Where $q_{r.s1.w1}$ is the radiative heat exchange between surface of product block 1 and wall 1 [W]

$\varepsilon_{w.1}$ is the surface emissivity of wall 1 [-]

σ is the Stefan-Boltzmann constant = 5.67 x 10^8 W·m^{-2}·K^{-4}

C is the length of the cross-section of the product block [m]

L is the length of the product block [m]

The surface temperature of product block 1 is a weighted average of its shell temperature ($T_{sh.1}$) and the average temperature of the adjacent air ($T_{a.1}$ and $T'_{a.1}$) (Equation 3.17).

$$T_{s.1} = \frac{R_{s.sh}\left(\frac{T_{a.1}+T'_{a.1}}{2}\right) + R_{a.s}T_{sh.1}}{R_{a.s} + R_{s.sh}} \qquad (3.17)$$

The same approaches are applied for seven other radiative heat fluxes as shown in Figure 3.2.

2.5 Temperature evolution of product, walls, and PCM, and PCM ice fraction evolution

Equations 3.18 and 3.19 are the unsteady heat balance equations for the shell ($T_{sh.1}$) and the core of product block 1 ($T_{c.1}$).

$$MC_{p.sh}\frac{dT_{sh.1}}{dt} = \dot{m}_a C_{p.a}(T_{a.1} - T'_{a.1}) + \frac{T_{c.1}-T_{sh.1}}{R_{sh.c}} - q_{r.s1.w1} - q_{r.s1.w4} \qquad (3.18)$$

$$MC_{p.c}\frac{dT_{c.1}}{dt} = \frac{T_{sh.1}-T_{c.1}}{R_{sh.c}} + \frac{T_{c.2}-T_{c.1}}{R_c} + \frac{T_{c.4}-T_{c.1}}{R_c} \qquad (3.19)$$

Where MC_p is the thermal inertia [J·K^{-1}]

$\dot{m}_a$ is the mass flow rate of air [kg·s^{-1}]

$C_{p.a}$ is the specific heat capacity of air [J·kg^{-1}·K^{-1}]

q_r is the radiative heat exchange [W]

R is the thermal resistance [K·W^{-1}]

The same approach was applied to the three other blocks.

The unsteady heat balance equations of the internal walls giving their temperature evolution are shown in Equations 3.20 and 3.21.

- for wall 1 (PCM surface in contact with adjacent air):
$$MC_{p.w1}\frac{dT_{w.1}}{dt} = \dot{m}_a C_{p.a}(T'_{a.1} - T_{a.2}) + \frac{T_{pcm}-T_{w.1}}{R_{pcm.w1}} + q_{r.s1.w1} + q_{r.s2.w1} \qquad (3.20)$$

- for wall 2 (internal bottom box wall):
$$MC_{p.w2}\frac{dT_{w.2}}{dt} = \dot{m}_a C_{p.a}(T'_{a.2} - T_{a.3}) + \frac{T_{ext}-T_{w.2}}{R_{w.ext.2}} + q_{r.s2.w2} + q_{r.s3.w2} \qquad (3.21)$$

The same approach was applied for walls 3 (internal vertical box wall) and 4 (internal top box wall).

Equations 3.22 and 3.23 show the evolution of PCM temperature and ice fraction, respectively.

- if PCM is completely frozen ($T_{PCM} < T_m$ and $\varphi = 1$) or completely melted ($T_{PCM} > T_m$ and $\varphi = 0$);
$$MC_{p.pcm}\frac{dT_{pcm}}{dt} = \frac{T_{w1}-T_{pcm}}{R_{pcm.w1}} + \frac{T_{ext}-T_{pcm}}{R_{w.ext.1}} \qquad (3.22)$$

- if PCM is partially melted ($T_{pcm} = T_m$ and $0 < \varphi < 1$);
$$M_{pcm}\frac{d\varphi}{dt}\Delta H_{fus} = \frac{T_{w1}-T_{pcm}}{R_{pcm.w1}} + \frac{T_{ext}-T_{pcm}}{R_{w.ext.1}} \qquad (3.23)$$

Where φ is the ice fraction of PCM [-]

ΔH_{fus} is the Latent heat of fusion [J·kg^{-1}]

2.6 Model input parameters

The model was solved for a 45-L commercial insulated box loaded with 16 kg of Tylose, which was used for experimental validation (cf. the detailed description in Section 3.1). Table 3.1 shows the thermophysical properties of each material, and Table 3.2 presents all the input parameters of the model along with their determination methods. For the heat transmission coefficient (K), the heat transfer coefficient (h_w and h_p) and the mass flow rate of air ($\dot{m}_a$), the calculation is presented in Sections 2.2, 2.6.1 and 2.6.2, respectively.

Table 3.1 Thermophysical properties of materials

Material	ρ (kg·m^{-3})	C_p (J·kg^{-1}·K^{-1})	λ (W·m^{-1}·K^{-1})	Reference
Polypropylene	910	1925	0.120	Cengel & Ghajar (2020)
Test product (Tylose)	1070	3372	0.510	Icier & Ilicali (2005)
Liquid water	1000	4217	0.561	Cengel & Ghajar (2020)
Ice	920	2040	1.880	Cengel & Ghajar (2020)
Air (5°C)	1.269	1006	0.024	Cengel & Ghajar (2020)
Extruded polystyrene	35	1210	0.029	Cengel & Ghajar (2020)

*Enthalpy of melting of ice (ΔH_{fus}) is 333700 J/kg with melting temperature (T_m) at 0°C

Table 3.2 Values of input parameters in the simplified heat transfer model

Parameter	Value	Unit	Means of determination
Convective heat transfer coefficient between internal air and internal wall (h_w)	3	W·m^{-2}·K^{-1}	Estimation from experimental temperature profile
Convective heat transfer coefficient between internal air and product surface (h_p)	3	W·m^{-2}·K^{-1}	Assumed to be equal to h_w
Heat transmission coefficient of insulation (K)	0.9	W·m^{-2}·K^{-1}	Calculation
Length of product block (C)	0.100	m	Measurement
Length of test product (L)	0.400	m	Measurement
Product surface area ($A_{p.s}$)	0.080	m^2	Measurement
Product external core area ($A_{p.c}$)	0.060	m^2	Measurement

Contact area of each product core with another core (A_c)	0.030	m^2	Measurement
PCM surface area ($A_{w.1}$)	0.120	m^2	Measurement
Vertical wall area ($A_{w.3}$)	0.120	m^2	Measurement
Horizontal wall area ($A_{w.2}$ and $A_{w.4}$ – bottom and top wall area, respectively)	0.104	m^2	Measurement
PCM thickness (e_{pcm})	0.040	m	Measurement
Mass flow rate of air ($\dot{m}_a$)	3.26×10^{-4}	$kg \cdot s^{-1}$	Calculation
Emissivity of polypropylene ($\varepsilon_{w.i}$)	0.97	-	Vavilov & Burleigh (2020)

A sensitivity study was performed in order to investigate the influence of the heat transfer coefficient (h_w and h_p), the mass flow rate of air ($\dot{m}_a$) and the heat transmission coefficient of box (K) by using the values in Table 3.2 as reference values. The influence of the reference values ± 10% and ± 20% on the product core temperature was studied.

2.6.1 Convective heat transfer coefficient estimation (h_w and h_p)

As per our previous work (Leungtongkum et al., 2023a), the convective heat transfer coefficient between internal air and the wall surface in an insulated box with PCM on a side wall was about 3 $W \cdot m^{-2} \cdot K^{-1}$ (estimated using measured temperature profiles).

2.6.2 Air mass flow rate estimation ($\dot{m}_a$)

According to our knowledge, there is no correlation in the literature allowing the estimation of the air flow rate ($\dot{m}_a$) in a cavity as a function of the four different wall temperatures. Therefore, it is proposed to relate h_w and $\dot{m}_a$ in a simple well-known situation: the case of an empty cavity with a cold vertical wall, a warm vertical wall and adiabatic horizontal walls. A model constructed on the basis of this simple case would also consider circular airflow with a mass flow rate of $\dot{m}_a$. Firstly, air flows along the cold wall (T_{cw}), and its temperature decreases to $T_{a.min}$, then it flows along the warm wall (T_{ww}), and its temperature rises to $T_{a.max}$. The following equations characterize these heat exchanges (Equations 3.24 and 3.25).

At the level of the cold wall;

$$(T_{a.min} - T_{cw}) = \alpha(T_{a.max} - T_{cw}) \qquad (3.24)$$

At the level of the warm wall;

$$(T_{a.max} - T_{ww}) = \alpha(T_{a.min} - T_{ww}) \qquad (3.25)$$

with $\alpha = exp\left(-\frac{h_w A}{\dot{m}_a C_{p.a}}\right)$

Where α is the dimensionless convective heat transfer coefficient between internal air and internal wall [-]

Equations 3.24 and 3.25 lead to:

$$\frac{T_{a.max} - T_{a.min}}{T_{ww} - T_{cw}} = \frac{1-\alpha}{1+\alpha} \qquad (3.26)$$

Raithby & Hollands (1998) reported that for the cavity with a vertical cold wall and a vertical warm wall with a low aspect ratio (height/width < 40), the air temperature difference ($T_{a,max} - T_{a,min}$) is about the half of the temperature difference between the cold and warm walls ($T_{ww} - T_{cw}$).

So, $\frac{T_{a.max} - T_{a.min}}{T_{ww} - T_{cw}} = \frac{1}{2}$ (3.27)

Based on Equations 3.26 and 3.27, $\alpha = exp\left(-\frac{h_w A}{\dot{m} C_{p.a}}\right) = \frac{1}{3}$

Thus, $\dot{m}_a = \frac{h_w A}{ln(3) C_{p.a}}$ (3.28)

This means that the air mass flow rate is proportional to the heat transfer coefficient and the cold wall area. For our loaded box, the same relationship was applied. Hence, with a heat transfer coefficient of 3 $W \cdot m^{-2} \cdot K^{-1}$ and a cold wall area of 0.120 m^2, the estimated mass flow rate of air is 3.26 x 10^{-4} $kg \cdot s^{-1}$. It should be highlighted that this estimation is based on the assumption of constant PCM shape and thickness but in reality, they slightly change during melting.

To verify the assumption of the linear relationship between h_w and $\dot{m}_a$, we considered the dimensional analysis and similarity model of the fluid flow and heat exchange along a vertical surface by laminar free convection as for the PCM surface or the opposite wall of the box.

Natural convective heat transfer of air along a vertical surface can be characterized as below.

For laminar flow or $10^4 < Ra_L < 10^9$; $Nu = \frac{hZ}{\lambda} = 0.59 {Ra_L}^{1/4}$ (Cengel & Ghajar, 2020)

where $Ra_L = Gr \cdot Pr$ and $Pr = \frac{C_{p.a}\mu}{\lambda}$ which equals to 0.71 for air thus,

$$Nu = \frac{hZ}{\lambda} = 0.54 Gr^{1/4} \qquad (3.29)$$

with $Gr = \frac{g \beta \Delta T Z^3}{\left(\frac{\mu}{\rho}\right)^2}$ (3.30)

where Z is the height of the wall [m]

Padet (2010) characterized the velocity profile of laminar free convection along the vertical surface as below.

$$v^* = f(y^*, Pr) \qquad (3.31)$$

with $$v^* = \frac{v}{\sqrt{g\beta\Delta Tx}} \qquad (3.32)$$

and $$y^* = \frac{y}{x} Gr^{1/4} \qquad (3.33)$$

Mass flow rate of fluid can be obtained by integrating the velocity profile over a cross section.

$$\dot{m} = \int_0^\infty \rho v L dy \qquad (3.34)$$

where L is the length of the wall [m]

From Equation 3.31; $$\dot{m} = \rho L\sqrt{g\beta\Delta TZ}\int_0^\infty f(y^*, Pr)dy$$

$$\dot{m} = \rho L\sqrt{g\beta\Delta TZ}\int_0^\infty f(y^*, Pr)xGr^{-1/4}dy^*$$

$$\dot{m} = \rho L\sqrt{\frac{g\beta\Delta TZ^3}{\left(\frac{\mu}{\rho}\right)^2}}\left(\frac{\mu}{\rho}\right)Gr^{-1/4}\int_0^\infty f(y^*, Pr)dy^*$$

The maximal flow rate is obtained for $x = Z$ (the height of the vertical wall in m)

Defining $\kappa = \int_0^\infty f(y^*, Pr)dy^*$ [-] which is constant for air (Pr = 0.71)

Thus, $$\dot{m} = \kappa\mu L Gr^{1/4} \qquad (3.35)$$

Combining Equations (3.29) and (3.35) leads to

$$\dot{m} = \kappa\mu L Gr^{1/4} = \frac{\kappa\mu L h Z}{0.54\lambda} = \frac{\kappa}{0.54}\frac{C_{p.a}\mu}{\lambda}\frac{hLZ}{C_{p.a}}$$

So, $$\dot{m} = \kappa'\frac{hA}{C_{p.a}} \qquad (3.36)$$

where $$\kappa' = Pr\frac{\kappa}{0.54} \qquad (3.37)$$

Equation 3.36 confirms that mass flow rate of air can be considered as approximately proportional to the heat transfer coefficient for free convection as assumed previously. However, this proportional relation is based on a very simplified approach. A finer analysis, integrating for example the channeling effect of the load, could lead to a non-linear relationship between mass flow rate of air and heat transfer coefficient.

2.7 Numerical solving

At a given time t, firstly, the eight air temperatures were deduced from the wall and product shell temperatures, then the eight radiative heat fluxes were calculated. Finally, the thirteen heat balance equations, i.e. 4 wall temperatures, 4 product shell temperatures, 4 product core temperatures and 1 PCM (temperature or ice fraction) were applied with an explicit scheme with 5 s time intervals (shorter time intervals led to the same results). The code was implemented using Python.

3. Experimental study

The measurement of the air, product (surface, shell and core), PCM and wall temperatures was carried out in order to enable comparison with the predicted values obtained from the model.

3.1 Materials

A commercialized multilayer insulated box (Manutan SA, Gonesse, France) with 500 mm x 310 mm x 300 mm internal dimensions was used (Figure 3.3a). The walls were made of expanded polystyrene (25 mm thickness), polypropylene (inner and outer layers of 3.5 mm thickness) and an air gap was present between the expanded polystyrene and the inner layer (estimated thickness: 5 mm).

The box was placed on a wooden support with a height of 50 mm to ensure uniform heat exchange with the ambient around the box. This box was placed on a table (0.7 m height) positioned in the center of the test room measuring 3.4 m x 3.4 m x 2.5 m in which the ambient temperature was controlled. The PCM container, made of polypropylene (3.5-mm thickness) and filled with 3.5 kg of tap water (melting point ~ 0°C), had external dimensions of 460 mm x 280 mm x 47 mm (the thickness of the PCM slab was not uniform and ranged from 35 mm to 50 mm). The test product consisted of Tylose slabs (with 200 mm x 100 mm x 50 mm pack dimensions). Tylose contains 23% methylhydroxyethylcellulose, 76.4% water and 0.5% NaCl (Refrigeration Development and Testing Ltd., North Somerset, UK). A perforated support made of galvanized steel (350 mm x 150 mm x 55 mm) was used to allow a gap below the test product for air circulation. Two extruded polystyrene (XPS) slabs (260 mm x 280 mm x 50 mm) were placed on each lateral wall (Figure 3.3b). In this manner, heat transfer and airflow can be considered as almost 2D. Indeed, these XPS slabs prevented air from flowing along the lateral walls and drastically reduced heat loss through them. Table 3.1 indicates the thermophysical properties of each material.

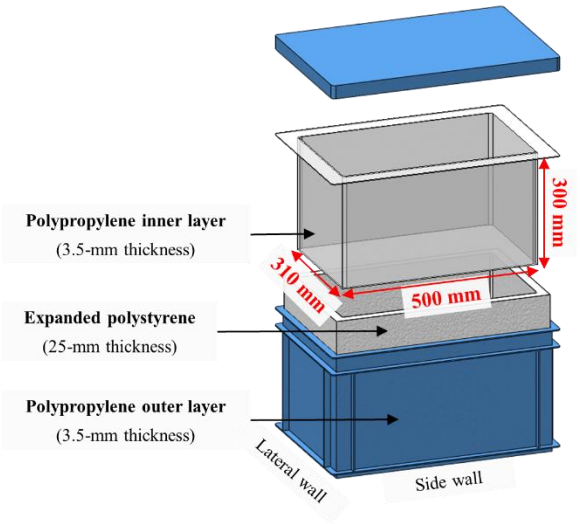

(a)

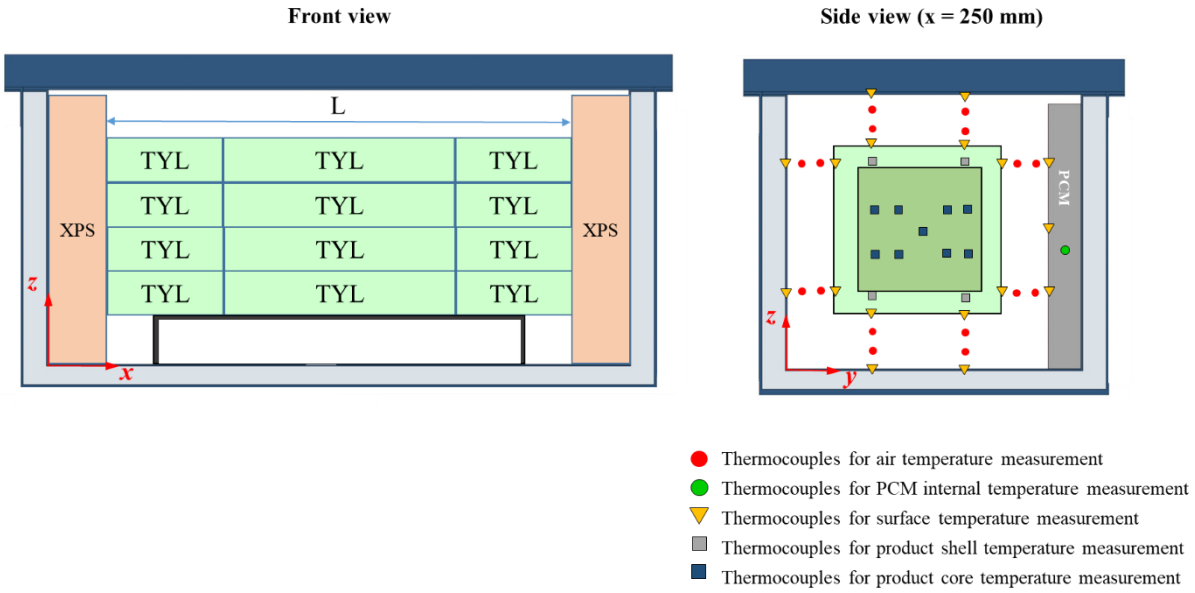

(b)

Figure 3.3 (a) Insulated box; and (b) experimental set-up of a box loaded with the test product (Tylose, TYL) and 50-mm extruded polystyrene plates (XPS) on the lateral walls to prevent airflow, and thermocouple positions

3.2. Instrumentation

The temperature was measured using type T thermocouples connected to an Agilent 34972A data acquisition unit (Agilent Technologies, CA, USA). The thermocouples were previously calibrated at -10°C, 0°C, 10°C, 20°C and 30°C with a precision of ± 0.1°C.

3.3 Experimental protocol

Before conducting each experiment, the PCM was frozen in a freezer set at a temperature of -2°C for at least 48 h, and the test products were stored in a polystyrene box in a domestic refrigerator set at a temperature of 4°C or 10°C for at least 24 h. This box prevented product temperature fluctuations caused by the working cycle of the compressor of the refrigerator.

The thermocouples were placed inside the PCM, on the surface of the PCM, on internal wall surfaces, on the product (surface, shell and core) and in internal air as shown in Figure 3.3b.

Prior to the measurement process, the thermocouples, the PCM and the 16 test product slabs were positioned in the box. Then all the temperatures were recorded once per minute. The measurements were conducted in two manners. First, the equilibrium temperature profile inside the box in steady state was determined (ideal case where the PCM was still melting, $T_{PCM} = T_m \sim 0$°C). To achieve the steady state, the PCM slab was constantly replaced (every 12 h) with a completely frozen one, while the measurements were conducted continuously over a period of 72 h. Second, the temperature evolution inside the box in transient state was monitored. To achieve the transient state, only one completely frozen PCM slab was loaded into the box and left for 24 h.

Table 3.3 presents the experimental conditions: the ambient temperature and the initial test product temperature were varied.

Table 3.3 Conditions in the experimental study

Condition	State	Ambient temperature (°C)	Initial test product temperature (°C)
1*	Steady	20	4
2	Steady	10	4
3*	Transient	20	4
4	Transient	20	10

*Reference condition

3.4 Model validation

In order to validate the model, twenty-four experimental temperature measured at steady state were compared with the numerical ones from the model. The Root Mean Square Error (*RMSE*) and the regression slope ($a_{num/exp}$) between the numerical ($T_{num.n}$) and experimental values ($T_{exp.n}$) were calculated as follows:

$$RMSE = \sqrt{\frac{\sum_{n=1}^{N}(T_{exp.n} - T_{num.n})^2}{N}} \qquad (3.38)$$

$$a_{num/exp} = \frac{\sum_{n=1}^{N}(T_{num.n}T_{exp.n})}{\sum_{n=1}^{N}(T_{exp.n})^2} \quad (3.39)$$

4. Results and discussion

4.1 Comparison between numerical and experimental temperatures in steady state

Firstly, a comparison was made under steady state conditions in order to verify the assumptions of the model and the energy balance equations to predict spatial variations in an insulated box equipped with PCM. This steady state was considered to have been reached when the average product shell and the core temperature varied less than 0.1°C. After the steady state was reached, the experimental values of the air, product (surface, shell and core) and wall temperatures were averaged over 600 min. and then compared with the predicted values (Figure 3.4) for 20°C ambient temperature (reference condition) and 10°C ambient temperature.

From Figure 3.4, overall, the model predicted well wall, air and product temperatures with an *RMSE* lower than 1°C (0.88°C and 0.60°C under 20°C and 10°C ambient temperatures, respectively) and with a regression slope $a_{num/exp}$ of the experimental temperature (T_{exp}) versus numerical temperature (T_{num}) curve close to 1 (0.98 and 0.89 under 20°C and 10°C ambient temperatures, respectively). The spatial temperature heterogeneity was correctly simulated with the lowest air and product temperatures at the bottom close to the PCM surface (in the zone surrounded with blue lines) and the highest temperatures at the top opposite the PCM surface (in the zone surrounded with red lines). It can be seen that the model clearly describes the air temperature evolution along the airflow course: the air temperature decreases from the top to the bottom along the PCM and increases along the other walls.

In general, the discrepancies between the measured and predicted air temperatures can be explained by the fact that the air temperature was measured at a given point (Figure 3.3b) whereas the predicted air temperature was a bulk value, which is the velocity-weighted average temperature over a cross-section. The highest discrepancy was noticed at the top with around 1.1°C and 1.5°C lower than the measured values at ambient temperatures of 10°C and 20°C respectively. This could be due to a strong stratification effect of warm air at this position. This local effect was not completely considered in the model.

T_{ext} = 20°C (Reference condition)

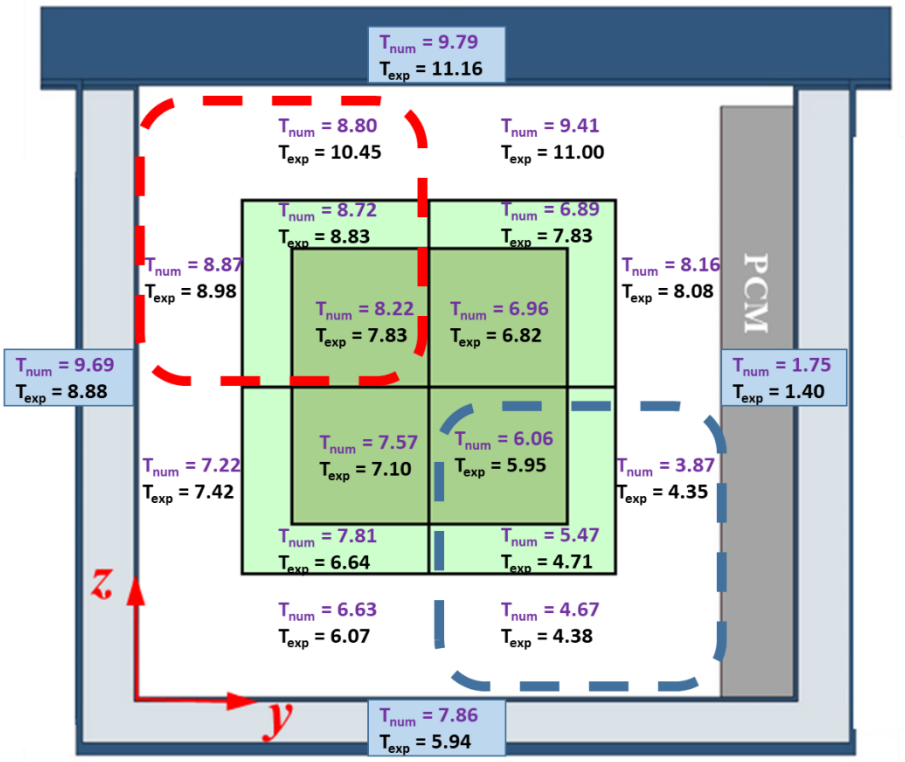

X = 250 mm

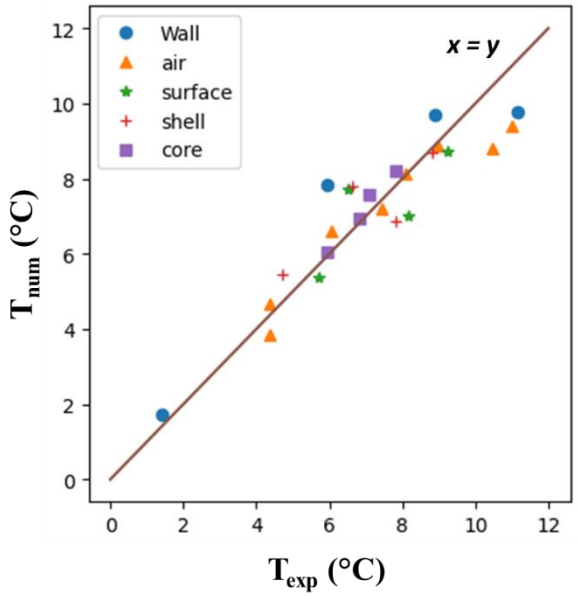

(a)

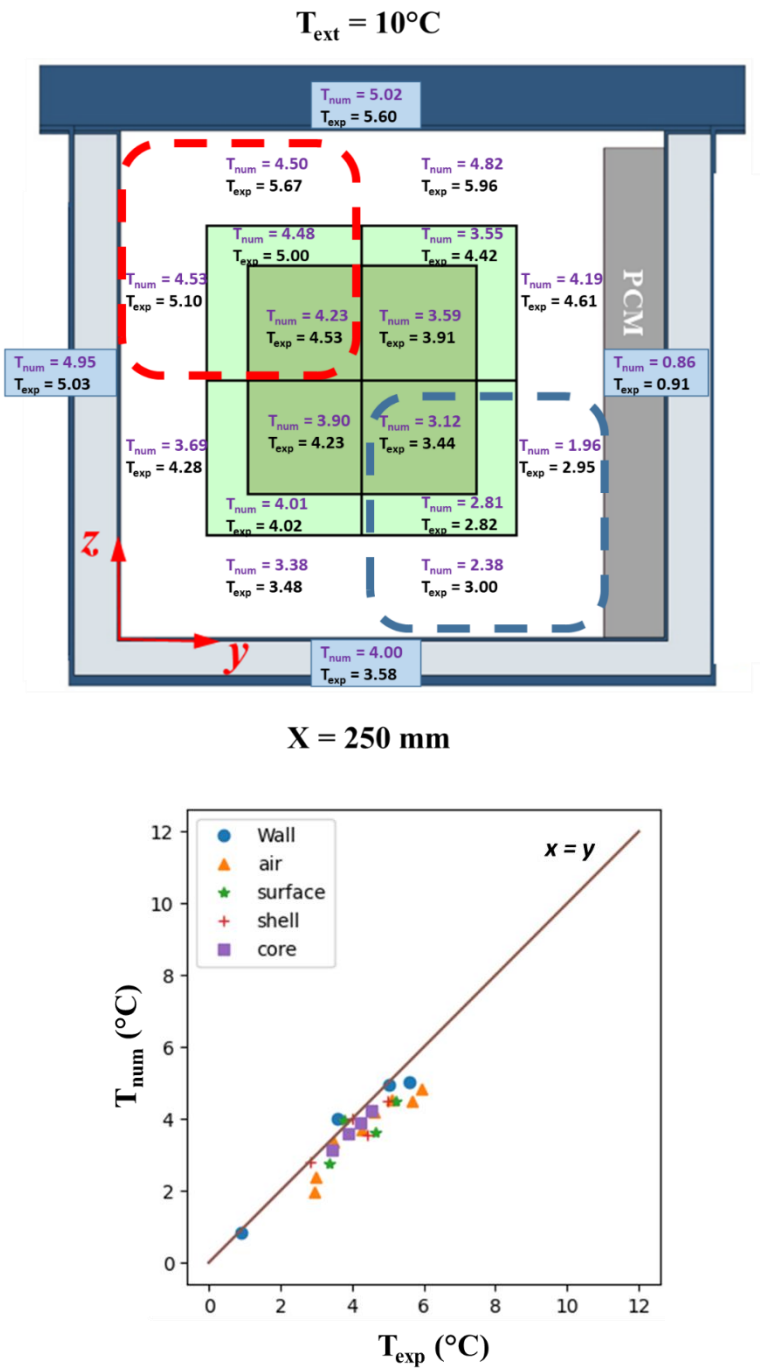

(b)

Figure 3.4 Comparison between the numerical and experimental values of temperature at steady state in an insulated box equipped with PCM on one side with an ambient temperature of (a) 20°C (reference condition) and (b) 10°C. The zones with the lowest and highest temperatures are surrounded in blue and red lines, respectively.

4.2 Sensitivity study

The input parameters should be as precise as possible, but measurement/estimation is sometimes difficult, so a sensitivity study was undertaken numerically. It aims to investigate the effect of the heat transfer coefficient (h_w and h_p), the mass flow rate of air ($\dot{m}_a$) and the heat transmission coefficient of box (K) on the product core temperature under steady state conditions. These input parameters were varied by ± 10% and ± 20% compared with the reference values (parameter value divided by the reference value varying from 0.8 to 1.2). Two criteria were used to evaluate the effect of the precision of these parameters, *RMSE* and the regression slope ($a_{num/exp}$). The results shown in Figure 3.5 lead to the conclusion that the box heat transmission coefficient K is the factor that exerts the greatest influence on the model precision. In fact, increasing the K value by 20% (i.e. reducing the insulation thickness by 20%) led to an increase in the product core temperature of about 1.5°C. From Figure 3.5, it can be seen that the reference value (0.9 $W \cdot m^{-2} \cdot K^{-1}$) gave the best agreement with the experimental value with the lowest *RMSE* at 0.88°C and $a_{num/exp}$ at 0.98 which was close to 1. Therefore, this parameter is the main factor to be taken into consideration when designing the box so as to preserve the product at a recommended temperature throughout the supply chain.

The influence of the h_w, h_p and $\dot{m}_a$ values on the predicted core temperature and the model precision is weak. From Figure 3.5, increasing h_w by 20% tended to decrease all the product temperatures by around 0.3°C. Indeed, the exchange with the PCM is enhanced by 20% as thermal resistance is inversely proportional to h_w. The exchange with the ambient air also increased, but only by 4% because the thermal resistance is mainly due to insulation (the overall resistance is proportional to $\frac{1}{K} + \frac{1}{h_w}$). Increasing $\dot{m}_a$ tended to decrease only the highest product temperature (T_{c4}), thus, temperature is more homogenous. This can be explained by the fact that a higher airflow rate leads to slow down the rate of air temperature increase along the air circulation loop. Changing h_p had almost no effect on the product temperature because the product had reached thermal equilibrium with the adjacent air during steady state, so there was almost no heat exchange.

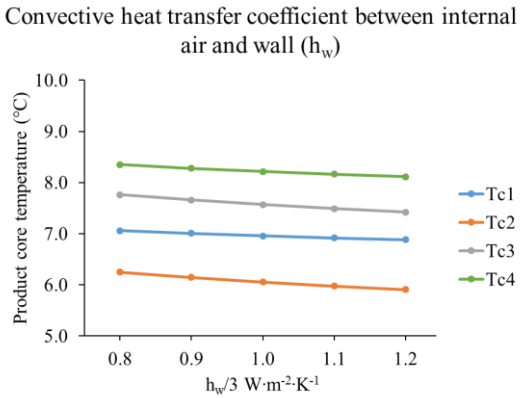

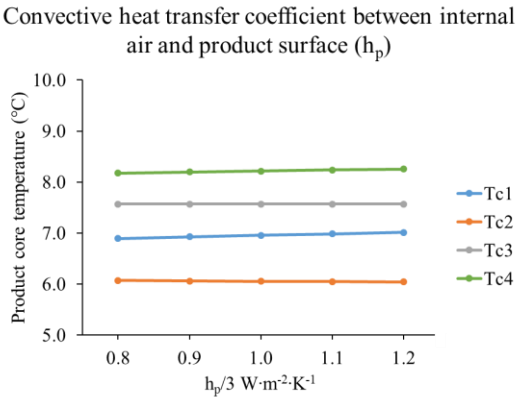

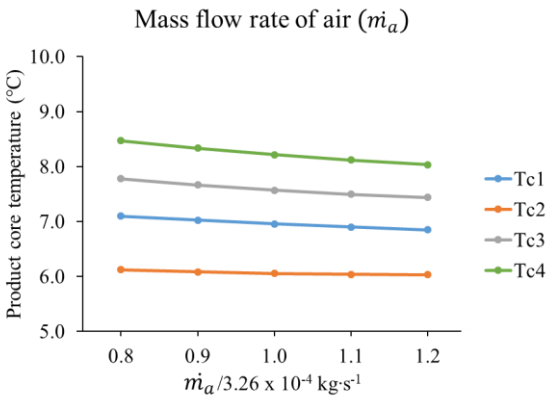

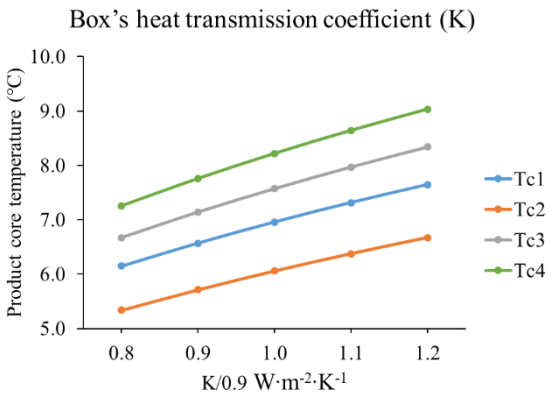

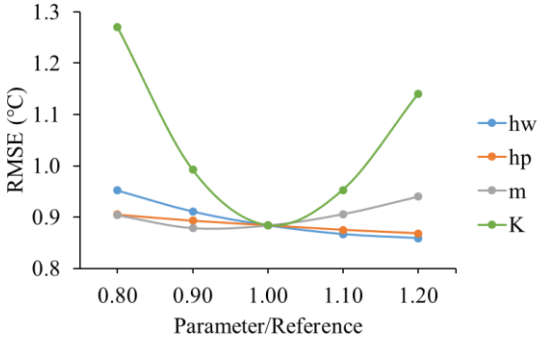

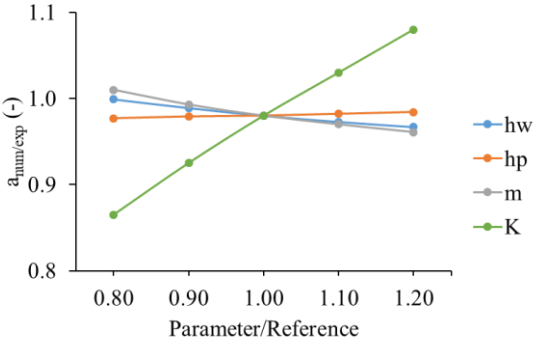

Parameter	Reference value
h_w (W·m^{-2}·K^{-1})	3
h_p (W·m^{-2}·K^{-1})	3
$\dot{m}_a$ (kg·s^{-1})	3.26 x 10^{-4}
K (W·m^{-2}·K^{-1})	0.9

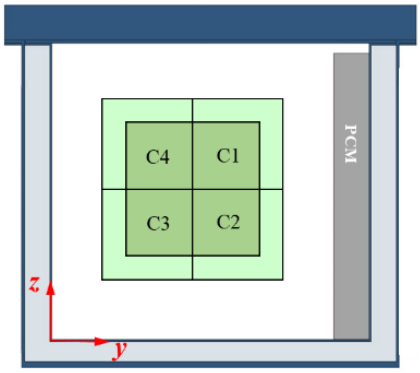

Figure 3.5 Sensitivity study showing the influence of the value of the input parameters (± 10%, ± 20% of reference values) on the variation in the product core temperature, *RMSE* and regression slope. The results were obtained at steady state for an insulated box with PCM on one side under 20°C ambient conditions for four input parameters: convective heat transfer coefficient between internal air and the wall (h_w), between internal air and product surface (h_p), mass flow rate of air ($\dot{m}_a$) and the heat transmission coefficient of the box (K).

4.3 Comparison between numerical and experimental temperatures in transient state

The model was used to predict the wall and product core temperature evolution in an insulated box equipped with PCM under 20°C ambient temperature at two initial test product temperatures: 4°C (reference condition) and 10°C. The results are shown in Figure 3.6.

For both conditions, the temperature inside the PCM increased very rapidly from -2°C to the melting temperature of 0°C (result not shown). The PCM container wall ($T_{w.1}$) also rapidly reached an almost constant temperature around 1.5°C higher than the melting temperature, indicating that the effect of PCM thermal resistance - $R_{pcm.w1}$ is small but not negligible.

At the beginning of the experiment, the wall temperatures, initially at the ambient temperature of 20°C, decreased rapidly. These walls exchange heat with the internal air with a heat transfer coefficient (h_w) of 3 $W \cdot m^{-2} \cdot K^{-1}$ and with the external ambience with a heat transmission coefficient (K) of 0.9 $W \cdot m^{-2} \cdot K^{-1}$. Their superficial inertia ($e_{pp}\rho_{pp}C_{p.pp}$) is 6130 $J \cdot m^{-2} \cdot K^{-1}$. So they tend toward a weighted average of internal air and ambient temperature $\frac{h_w T_{air} + K T_{ext}}{h_w + K}$ with a characteristic time interval τ_w given by Equation 3.40.

$$\tau_w = \frac{e_{pp}\rho_{pp}C_{p.pp}}{h_w + K} = 1570\ s \sim 26\ min \qquad (3.40)$$

This value corresponds to the order of magnitude of the initial period during which the wall temperature decreased.

After this initial period, the wall temperatures slowly increased (for $T_{p.ini}$ = *4°C*) or decreased (for $T_{p.ini}$ = *10°C*) toward their equilibrium (steady state) values. This slow variation is dictated by the thermal inertia of the product.

At the beginning, a quick temperature increase in all product core positions was experimentally observed for both initial conditions. For $T_{p.ini}$ = *10°C*, a similar trend was observed by the model for positions 3 and 4, but with slower dynamics. For the other cases, the model did not follow this trend. This quick increase is due to the fact that the walls are initially at ambient temperature and remain relatively warm during the first hour. Therefore, initially, the internal air temperature is higher than the

equilibrium temperature. This is taken into account by the model. In addition, during loading, the surface of the test product blocks is exposed to ambient air, so its temperature increases. This is not taken into account by the model and explains the model/measurement discrepancies.

Nevertheless, after this initial period, the model predicts relatively well the product core temperature evolution for both initial conditions. For $T_{p.ini}$ = *4°C*, the product temperatures slowly increased toward the equilibrium (steady state) values (7°C ± 1°C) and for $T_{p.ini}$ = 10°C, they decreased with the same dynamic toward these equilibrium values. The model correctly predicted the warmest and coldest zones and also the temperature increase/decrease rate.

The product cores exchange heat with the internal air through two thermal resistances in series: $R_{a.sh}$ = *4.47 K·W*$^{-1}$ (from air to shell) and $R_{sh.c}$ = *1.23 K·W*$^{-1}$ (from shell to core). As their thermal inertia ($MC_{p.c}$) is 8120 J·K^{-1}, the characteristic time of core temperature evolution is given by Equation 3.41.

$$\tau_p = MC_{p.c}(R_{a.sh} + R_{sh.c}) = 46300\ s \sim 13\ h \qquad (3.41)$$

This value corresponds to the order of magnitude observed in Figure 3.6 (for a simple first order dynamic, it is expected that when $t = \tau_p \sim 13\ h$, $T_p - T_{p.eq}$ is about 1/e or 0.37 of $T_{p.ini} - T_{p.eq}$).

In summary, during the first hour, the temperature evolution is affected by the initial temperature of the box wall, then the product temperature slowly tends toward the equilibrium value (with a characteristic time interval of around 13 h for our test product) as long as the PCM is not completely melted. Here, we consider only this case because PCM loses its effects when it is completely melted.

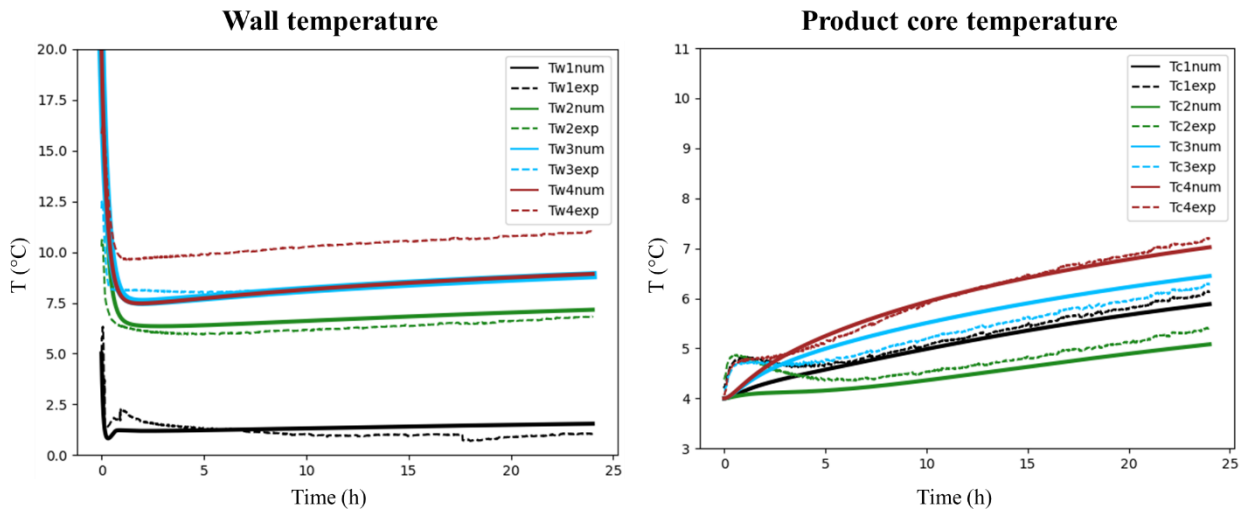

(a)

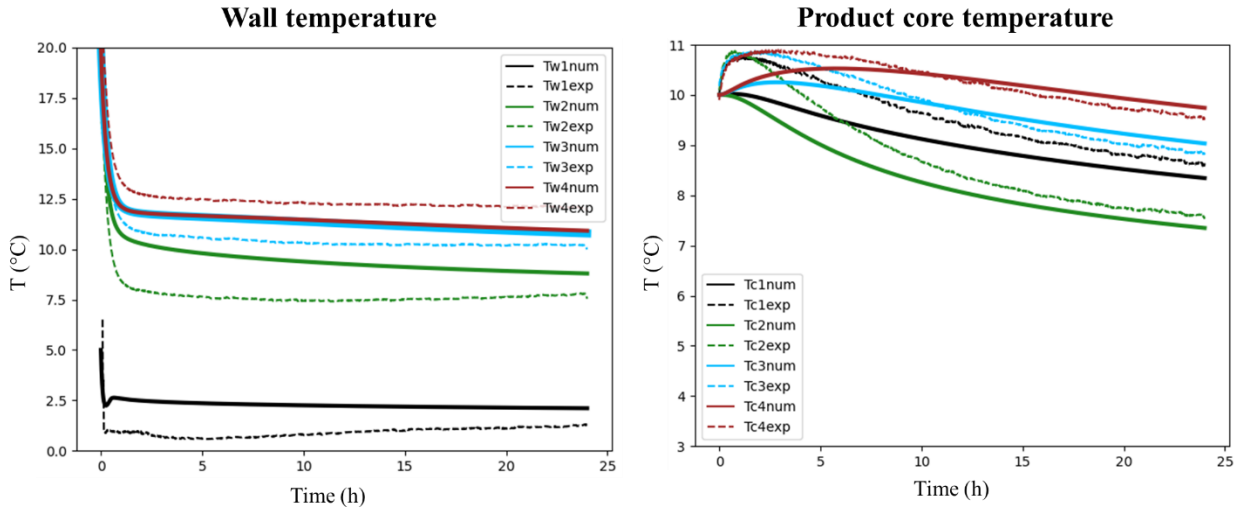

(b)

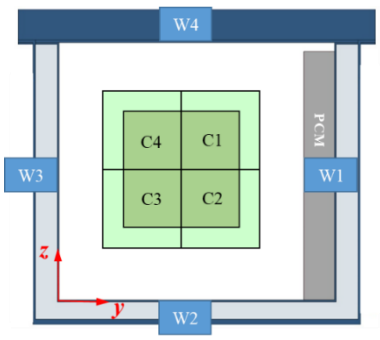

Figure 3.6 Comparison between numerical results and the experimental values of the temperature evolution during 24 h at the level of the wall and the product core in an insulated box equipped with PCM on one side during transient state with an ambient temperature of 20°C and an initial test product temperature of (a) 4°C (reference condition) and (b) 10°C

5. Conclusion and suggested future studies

In this study, a simplified heat transfer model based on a zonal approach was developed for an insulated box equipped with PCM (ice with melting point ~ 0°C) on a side wall and loaded with a test product (Tylose). The model considered that the product is composed of 4 blocks with a shell and a core in each block. The model was validated by comparing the predicted temperatures with those measured at different positions in the box exposed to two ambient temperatures and with two initial product temperatures. The comparison under steady and transient states demonstrates good agreement in terms of spatial and temporal temperature variation. This model shows good practical applicability with a short calculation time (less than 10 s using a computer with 64 GB of RAM) and it could predict the effects of different parameters such as box insulation (heat transmission coefficient or *K*), emissivity of internal walls and PCM melting temperature. There are still some discrepancies from experimental values as the model is simplified but it does not require high computing resource like detailed CFD model.

It can predict the product temperature evolution for different time-temperature scenarios (variable external temperature) in a supply chain depending on the position of the product inside the box. It would be possible to link the thermal model with a food quality and a microbiological model enabling the evaluation of product quality and safety evolution along a real supply chain. It is important to emphasize that precaution must be taken while coupling this simplified thermal model with quality or microbiological models. As this thermal model is based on the zonal approach, only the zone with the highest risk of spoiled and unsafe product could be predicted but not the exact time neither the precise position.

3.4 PAPER 1

Modélisation numérique (Computational Fluid Mechanics : CFD) des transferts de chaleur et de l'écoulement d'air dans un caisson isotherme équipé d'un matériau à changement de phase

Résumé (version française de l'abstract du paper 1)

Les caissons isothermes équipés de matériau à changement de phase (Phase Change Material : PCM) sont principalement utilisés pour la livraison de nourriture sur le dernier kilomètre, car ils sont simples à utiliser et peu coûteux. Cependant, la température moyenne y est parfois assez élevée avec une importante hétérogénéité. Ce travail présente une étude numérique des transferts thermiques et de l'écoulement d'air à l'intérieur d'un caisson isotherme (coefficient global de transfert thermique 0,9 $W \cdot m^{-2} \cdot K^{-1}$) équipée de PCM (glace, point de fusion ~ 0°C). Trois configurations ont été étudiées : caisson vide, caisson chargé de polystyrène extrudé et une caisson chargé de produit modèle (Tylose). Les simulations numériques ont été réalisées avec le logiciel ANSYS FLUENT. Les résultats numériques des champs de température et de vitesse ont été comparés aux valeurs expérimentales mesurées respectivement par thermocouples et vélocimétrie par images de particules. Un bon accord a été obtenu entre les résultats numériques et expérimentaux, avec une différence maximale de 1,5°C et 0,03 $m \cdot s^{-1}$.

CFD modelling of heat transfer and airflow in an insulated box equipped with Phase Change Material

Tanathep LEUNGTONGKUM*[a,b], Onrawee LAGUERRE[a], Nattawut CHAOMUANG[c], Alain DENIS[a] and Denis FLICK[b]

[a] Université Paris-Saclay, INRAE, FRISE, 92761 Antony, France
[b] Université Paris-Saclay, INRAE, AgroParisTech, UMR SayFood, 91120 Palaiseau, France
[c] Department of Food Engineering, School of Engineering, King Mongkut's Institute of Technology Ladkrabang, Bangkok, Thailand 10520
*Corresponding author: Tanathep.leungtongkum@inrae.fr

Abstract

Insulated boxes equipped with Phase Change Material (PCM) are primarily used for the last mile food delivery, as they are simple to use and low-cost. However, these boxes maintain high average temperature and significant temperature heterogeneity in transport. This work presents a numerical study to predict the heat transfer and airflow inside an insulated box (overall heat transfer coefficient 0.9 $W \cdot m^{-2} \cdot K^{-1}$) equipped with PCM (ice, melting point 0°C). Three configurations were studied: an empty box, a box loaded with Extruded Polystyrene (XPS slabs), and a box loaded with test product (Tylose slabs). Computational Fluid Dynamic simulations were performed by ANSYS FLUENT. The numerical results of temperature and velocity fields were compared with experimental values measured by thermocouples and Particle Image Velocimetry, respectively. Good agreement was obtained between the numerical and experimental results, with the maximum difference of 1.5°C and 0.03 $m \cdot s^{-1}$.

Keywords: Insulated boxes, PCM, Airflow, Heat transfer, CFD

1. INTRODUCTION

Insulated boxes equipped with Phase Change Material (PCM) have been widely used in the last-mile delivery of temperature-sensitive products, mainly when refrigeration equipment is unavailable (East et al., 2009). However, spatial and temporal temperature variation during a supply chain currently limit their use (Du et al., 2020; Laguerre et al., 2013). Accurate physical-based models can predict the temperature in a box in which conduction (in walls, unmelted PCM, and products), natural convection (between air and walls/product surface), and radiation occur (Rincón-Casado et al., 2017; Shinoda et al., 2019). These three heat transfer modes are of the same order of magnitude; although several studies reviewed in Leungtongkum et al. (2022) often considered only heat conduction, all three need to be considered (Laguerre & Flick, 2010).

This paper develops a Computational Fluid Dynamic (CFD) model that applies airflow and all heat transfer modes for an insulated box equipped with PCM. The simulation allows the prediction of the temperature field and its evolution with time inside the box for two PCM positions (top and sidewall) and three loading conditions: no load,

loaded with insulating material (extruded polystyrene slabs), and with test product (Tylose slabs). The second condition highlights the effect of the inert load as an obstacle on airflow (without heat exchange), while the third represents the realistic food transport conditions. The numerical results of different studied conditions are compared with the experimental ones for validation.

The model developed in this paper can be used to predict the effect of box characteristics such as insulation type, wall thickness, box geometry, and operating conditions such as ambient temperature, load type, and product initial temperature. By combining this model with quality and safety models, product evolution along the supply chain can be assessed.

2. Experimental study

2.1 Materials

Measurement of temperature and air velocity required two different boxes (Figure 3.7). Box A was used for the thermal study; it was a commercialized multilayer insulated box (Manutan SA, Gonesse, France) with 500 mm x 310 mm x 300 mm internal dimensions and 570 mm x 380 mm x 370 mm external dimensions. Its walls were made of expanded polystyrene (25 mm thickness), polypropylene (inner and outer layers of 3.5 mm thickness with ε = 0.97 (Vavilov & Burleigh, 2020)), and an air gap between the expanded polystyrene and the inner layer (estimated thickness 5 mm). Box B was used for the airflow study; it had the exact dimensions and wall structure except two side walls made of triple-glazed windows (3 glass panes of 4 mm thickness each, wall emissivity ε = 0.03 (manufacturer data), two argon-filled 10-mm gaps). The overall heat transfer coefficient of these two walls (insulated wall and triple-glazed window) is about 0.90 $W \cdot m^{-2} \cdot K^{-1}$. This value was obtained by calculation based on the thickness and thermal conductivity of the materials used for building the walls, which are listed in Table 3.4.

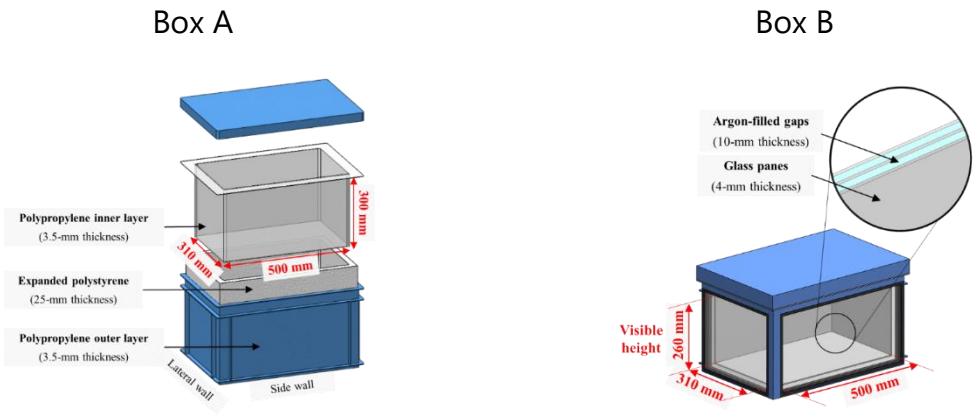

Figure 3.7 Boxes used in the study. Box A: a commercial box for temperature measurement and Box B: a box with walls modification by triple-pane windows for velocity measurement.

Table 3.4 Thermo-physical properties of materials

Material	Density ($kg \cdot m^{-3}$)	C_p ($J \cdot kg^{-1} \cdot K^{-1}$)	k ($W \cdot m^{-1} \cdot K^{-1}$)	Reference
Extruded polystyrene	35	1210	0.029	Cengel and Ghajar (2020)
Polypropylene	910	1925	0.120	Cengel and Ghajar (2020)
Tylose	1070	3372	0.510	Icier and Ilicali (2005)
Water (solid)	920	2040	1.880	Cengel and Ghajar (2020)
Air (5°C)	1.269	1006	0.024	Cengel and Ghajar (2020)
Glass	2225	835	1.4	Cengel and Ghajar (2020)
Argon	-	-	0.018	Roder et al. (2000)

2.2 Thermal study

2.2.1 PCM and test product preparation before experiment

Tap water is used as the PCM for this study (melting temperature close to 0°C). It was first filled into a slab of dimensions 500 mm x 310 mm x 50 mm. The PCM slab was then placed horizontally in a freezer set at -2°C for 48 h to ensure homogenous PCM thickness and temperature. Sixteen packs of the test product (dimensions of a pack 200 mm × 100 mm × 50 mm) were placed in a polystyrene box and stored in a domestic refrigerator set at 4°C 24 hours before each experiment to ensure homogeneous initial product temperature.

2.2.2 Instrumentation

The temperature was measured by T-type thermocouples linked to a data acquisition unit (Agilent 34972A, CA, USA). These thermocouples were previously calibrated at -10°C, 0°C, 10°C, 20°C and 30°C with a precision of ±0.2°C.

2.2.3 Temperature measurement in an unloaded box

Figure 3.8a presents an empty box with PCM on a sidewall. The air temperature was measured on the middle plane (x = 250 mm) at different y and z positions using two stands, and each one was equipped with 12 thermocouples spread over the height (z-axis). Three thermocouples were placed inside the PCM (at mid-thickness) and on the surface of the PCM container.

The installed thermocouples were then placed in the box. 90 minutes after the box was closed (when a steady state was reached), temperatures were recorded every 15

seconds for 5 minutes. After these 5 minutes, the box was opened, and the stands were displaced rapidly (to avoid disturbances by external air) before closing the box again. 15 minutes later (when a steady state was reached again), temperatures were recorded every 15 seconds for 5 minutes. Measurements were repeated by changing the positions of the stands, allowing 200 measurement points in total. A temperature contour map was plotted by MATLAB with interpolation from these measurements following the experiment.

2.2.4 Temperature measurement in a loaded box

The loaded box was prepared using the same methodology for two different types of materials. The first material was four XPS slabs (extruded polystyrene 200 mm × 400 mm × 50 mm), and the second was sixteen test product packs previously stored in a domestic refrigerator for 24 hours. Each material was placed in the center of the box. After closing the box, temperatures in the middle plane (x = 250 mm) were measured at 33 positions (Figure 3.8b) every 30 seconds for 4 hours without opening the box.

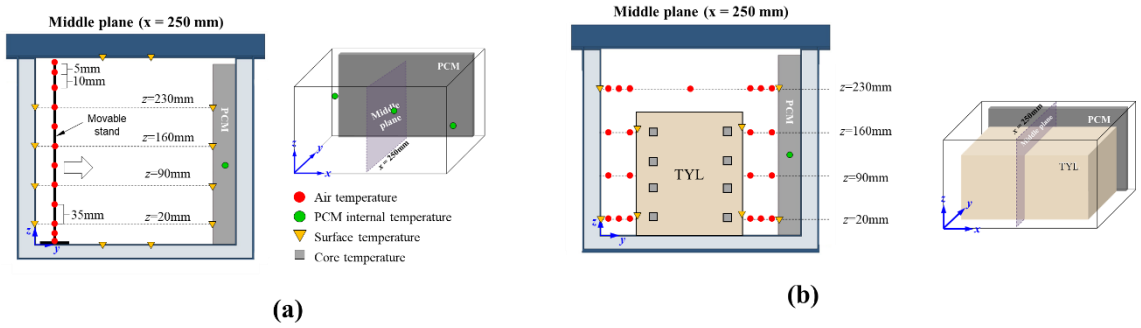

Figure 3.8 Diagram showing the experimental setup for temperature measurement for PCM located on the side wall of (a) empty box, and (b) loaded box. TYL = Tylose packages.

2.3 Airflow study

Figure 3.9 shows the experimental setup for the air velocity measurement using Particle Image Velocimetry (PIV). A smoke machine (Antari, F-80Z) generated an oil-based smoke tracer (mean diameter 0.3 µm); the smoke tracer was precooled in a container with four PCM packs to decrease its temperature from 50°C to 10°C. The smoke was then diffused into Box B through a connecting duct using a small fan.

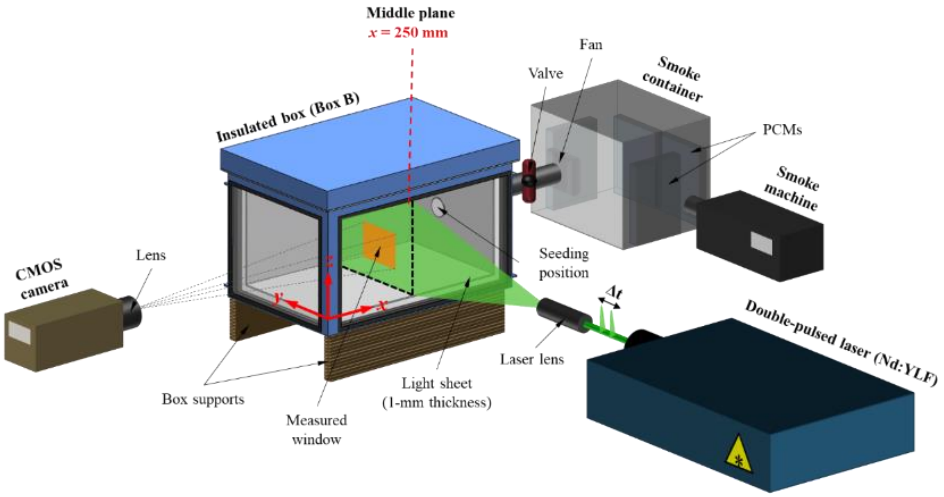

Figure 3.9 Diagram showing the PIV setup.

The 2D-PIV system (LaVision, FlowMaster 2D) included three main components (Figure 3.9): a double-pulsed Nd:YLF laser (527 nm wavelength, 10 mJ pulse energy), a high-speed 12-bit CMOS video camera (Photron, FASTCAM SA3; 1024 × 1024 pixels in resolution) fitted with a lens (Sigma; 105 mm, f/1:2.8). A programmable timing unit (PTU-X) allowed the synchronization between the laser pulse and the camera. Visualization of the airflow pattern was possible by the smoke particle scattering during laser pulses. Image acquisition and post-processing to obtain the air velocity field were achieved using DaVis 10.0.5 software. The camera and the laser were mounted on a three-dimensional displacement system (precision of displacement ±1 mm); both items were aligned to allow the perpendicularity between the camera view and the light sheet (1-mm thickness).

PIV measurements were performed on the middle plane (x = 250 mm). 500 pairs of images were recorded for each measured window every 20 ms, with a time interval of 900 µs between two images of the same pair (between two laser pulses). More details on image acquisition and post-processing can be found in Leungtongkum et al. (2023a).

The measurement was conducted for the box with two PCM positions (top and sidewall) and under three loading conditions: no load, loaded with inert material (extruded polystyrene slabs, XPS), and with test product (Tylose slabs). The second condition demonstrates the effect of the load as an airflow obstacle only (i.e., without heat exchange with air), whereas the third condition demonstrates the effect of the load in a realistic food transport scenario (i.e., where there is heat exchange with air).

3. NUMERICAL STUDY

3.1 Model assumptions

Airflow is laminar, as its Rayleigh number is lower than 10^9 (calculation not shown). The Boussinesq approximation is used (density is assumed constant except in the gravity term). Viscous dissipation into heat is neglected.

The PCM is assumed to be in a melting phase during the whole simulation, so the temperature of its external face is considered constant at 0°C. The convection in melted ice is neglected.

3.2 Governing equations

For air, laminar flow caused by natural convection is considered:

Continuity: $\nabla \cdot (\rho \vec{v}) = 0$ (3.42)

Momentum: $\frac{\partial}{\partial t}(\rho \vec{v}) + \nabla \cdot (\rho \vec{v} \vec{v}) = -\nabla P + \nabla \cdot (\mu \nabla \vec{v}) + \rho_{ref} \beta \left(T - T_{ref}\right) \vec{g}$ (3.43)

Energy: $\frac{\partial}{\partial t}\left(\rho c_p T\right) + \nabla \cdot \left(\rho \vec{v} c_p T\right) = \nabla \cdot (\lambda \nabla T)$ (3.44)

For the load (test product or XPS), only conduction is considered:

Energy: $\frac{\partial}{\partial t}\left(\rho_p c_{p.p} T\right) + \nabla \cdot \left(\rho_p c_{p.p} T\right) = \nabla \cdot \left(\lambda_p \nabla T\right)$ (3.45)

where ρ is the density [kg·m^{-3}]
$\vec{v}$ is the fluid velocity [m·s^{-1}]
P is the pressure [N·m^{-2}]
μ is the dynamic viscosity [kg·s^{-1}·m^{-1}]
ρ_{ref} is the density at reference temperature [kg·m^{-3}]
β is the thermal expansion coefficient [K^{-1}]
T is the temperature [°C or K]
T_{ref} is the reference temperature = 5°C
$\vec{g}$ is the gravitational acceleration = 9.81 m·s^{-2}
c_p is the specific heat capacity [J·kg^{-1}·K^{-1}] and
λ is the thermal conductivity [W·m^{-1}·K^{-1}].

The parameters with index p are for the product (without index is for air).

3.3 Boundary conditions

At PCM wall in contact with internal box walls, constant temperature at 0°C was applied:

T = 0°C (3.46)

At PCM wall in contact with internal air, the coupled thermal boundary condition was used with 2.5 mm wall thickness with no slip boundary condition.

At the internal box walls, the following momentum and thermal conditions were applied:

No slip boundary condition: $\vec{v} = 0$ (3.47)

Cauchy type thermal boundary condition: $U(T_{amb} - T) = \lambda \nabla T \cdot \vec{n} + q_{rad}$ (3.48)

where U is the overall heat transfer coefficient, T_{amb} = 20°C

and $q_{rad} = \varepsilon \sigma T^4 + (1 - \varepsilon)\, q_{in}$ (3.49)

with ε is the wall emissivity

Surface-to-surface radiation was activated, and the radiative flux entering the surface *j* coming from all the other surfaces *i* was calculated from

$q_{in,j} = \sum_i F_{ij} q_{rad,i}$ (3.50)

where F_{ij} is the view factor of the surface *i* relating to the surface *j*

The external area of the box is higher than the internal one; thus, for a global heat balance, the geometric mean of an external and internal area must be used. Since the boundary condition applies on the internal wall, in governing equations for the CFD approach, U is corrected by a factor of $\sqrt{A_{ext}/A_{int}}$.

3.4 Numerical simulation

The geometry was drawn by using SpaceClaim and meshed with ANSYS FLUENT meshing. A mesh independence study was first conducted, which led to considering around 2 x 10^5 cells. The study domain contained between 191850 and 256211 polyhedral cells depending on PCM position and loading conditions.

The numerical study was performed with ANSYS FLUENT 2021 R1 in a transient state. According to a time step independence study, the time step of 1 s was used. For an empty box and a box loaded with XPS, the simulation was performed for 10 min. For a box loaded with Tylose, the simulation was performed for 4 h.

4. RESULTS AND DISCUSSIONS

To highlight the natural convection, first, the experimental and numerical velocity and temperature fields are presented for unloaded boxes with PCM (cold wall) on the side and at the top (Figures 3.10 to 3.13). Then, these fields are presented in the presence of a load in a box with PCM on a sidewall (Figures 3.14 to 3.18) and with PCM at the top (Figure 3.19 to 3.21).

4.1 Air velocity and temperature profiles in an unloaded box with PCM on a sidewall

Figures 3.10a and 3.10b present the observed airflow patterns and temperature fields on the middle plane of the box (x = 250 mm) with PCM on a sidewall. Downward airflow close to the PCM occurs because the air temperature decreases and the air density increases when the air exchanges heat with PCM (Figure 3.10a). Upward airflow close to the opposite vertical wall is caused by heat exchange with the vertical warm wall; here, air temperature increases while air density decreases. Air flows from the right to the left near the bottom of the box. PIV measurement was impossible at the top of the box because the laser sheet could not be projected into this zone. However, the law of mass conservation proves that air flows from the left to the right, leading to an airflow recirculation loop. The maximum measured air velocity was around 0.10 $m \cdot s^{-1}$. The corresponding temperature field (Figure 3.10b) agrees with the airflow pattern, i.e., the coldest air (0.5°C) was observed at the bottom-right corner after air was cooled down by exchange with PCM. The warmest air (10°C) was observed at the top after it was warmed up by exchange with the box walls.

Simulation results at 10 minutes gave similar air velocity flow patterns (Figure 3.10a') and temperature fields (Figure 3.10b'). In this simulation, the velocity and temperature fields did not vary from 7 minutes to 10 minutes, implying that a steady state was reached. Figure 3.11 compares the experimental and numerical air velocity values in the z-direction and temperature at z = 160 mm. A good agreement between predicted and measured values was observed with a maximum difference in air velocity and temperature of 0.02 $m \cdot s^{-1}$ and 1.2°C, respectively.

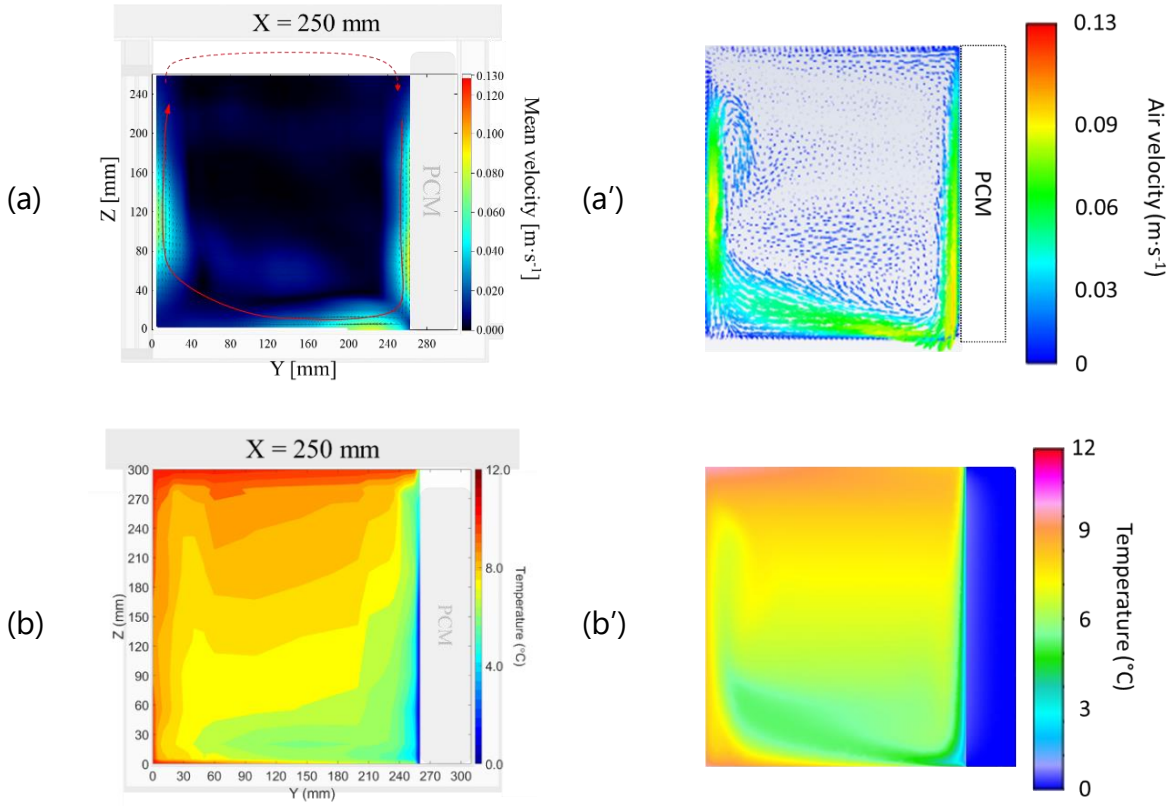

Figure 3.10 (a) Experimental air velocity field and (b) experimental temperature field on the middle plane of an unloaded box with PCM on a sidewall. (a') Corresponding numerical air velocity field and (b') Corresponding numerical temperature field.

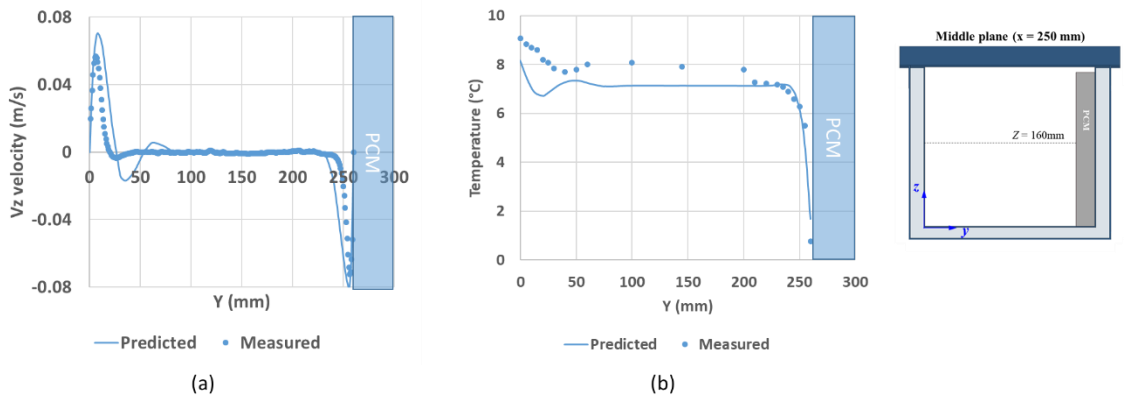

Figure 3.11 Comparison between experimental and numerical results at the middle plane and z = 160 mm in an unloaded box with PCM on a sidewall (a) air velocity in the z-direction and (b) air temperature

4.2 Air velocity and temperature profiles in an unloaded box with PCM at the top

Figure 3.12 shows the observed airflow patterns (Figure 3.12a) and temperature fields (Figure 3.12b) on the middle plane of the box (x = 250 mm) with PCM at the top. Two

airflow loops are observed, with a downward flow in the middle of the box and an upward flow close to each side wall. Air becomes colder and flows downwards when it exchanges heat with the PCM at the top. The air moves toward the warmer side walls, as its density decreased after reaching the bottom of the box, and it flows upwards until approaching the PCM at the top again. The maximum measured air velocity was about 0.08 $m \cdot s^{-1}$. The visual observation of smoke flow with time showed that the downward flow in the central region was oscillating (result not shown). The corresponding experimental temperature field (Figure 3.12b) confirms this flow explanation with the coldest air (4.1°C) at the center of the box just below the PCM surface and the warmest air (8.1°C) near the mid-height of the side walls after the air was warmed up by exchange with the box walls. It is to be highlighted that the velocity shown in Figure 3.12a was averaged over 10 seconds, and the temperature in Figure 3.12b was averaged over 5 minutes.

The simulation confirms the instability of air velocity: the velocity field varied with time (Figure 3.12a') even when the boundary conditions were steady, and the flow was laminar due to the nonlinearity of the Navier-Stokes equations. The temperature field was also unstable (Figure 3.12b'). The simulations at 5, 7, and 10 minutes did not give the same air velocity field and temperature distribution; however, it seems that the result at 5 minutes provided good agreement with the measured air velocity field and temperature distribution. Figure 3.13 shows a comparison between the experimental and numerical values (at 5, 7, 10 minutes and average between 5 minutes and 10 minutes) of air velocity in the z-direction and temperature at z = 125 mm. On average, the simulation can capture the trends and the order of magnitude but comparing instantaneous predicted data with time-averaged measured data is difficult.

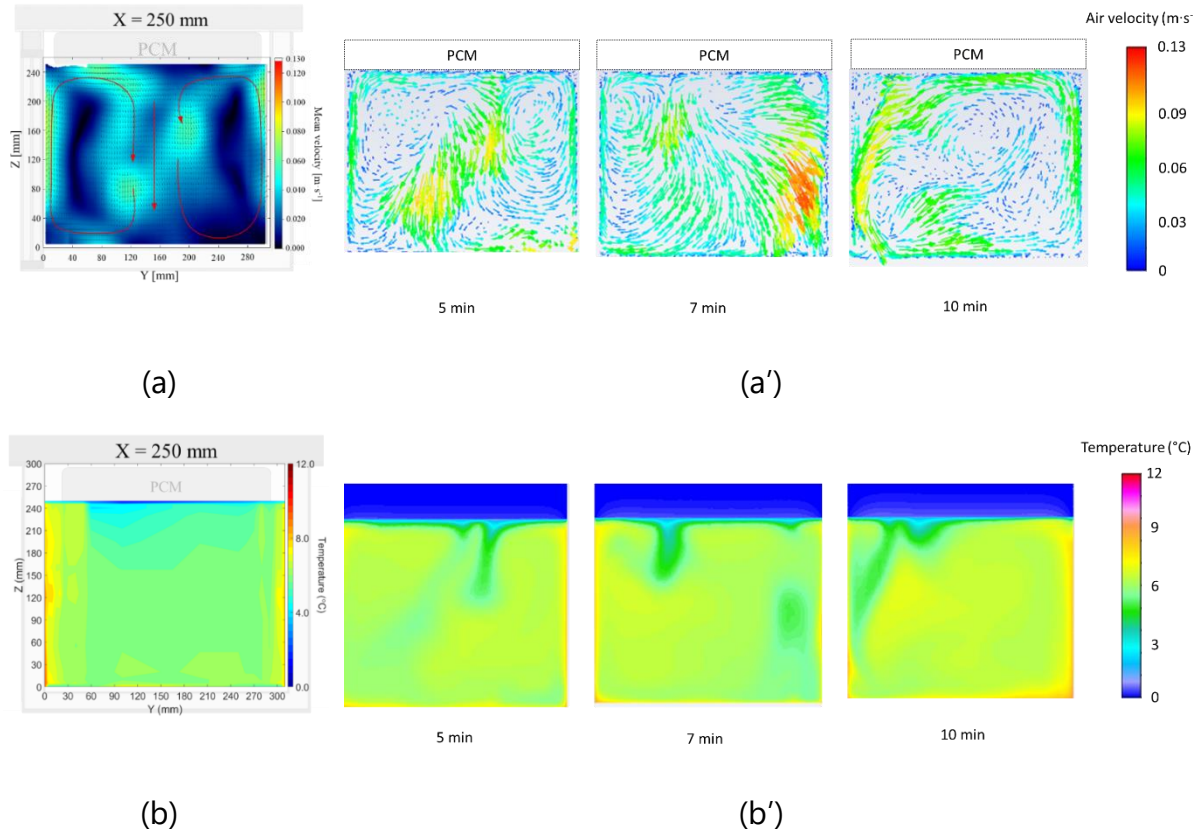

Figure 3.12 (a) Experimental air velocity field and (b) experimental temperature field on the middle plane of an unloaded box with PCM at the top. (a') and (b') are corresponding numerical results at 5 min., 7 min. and 10 min.

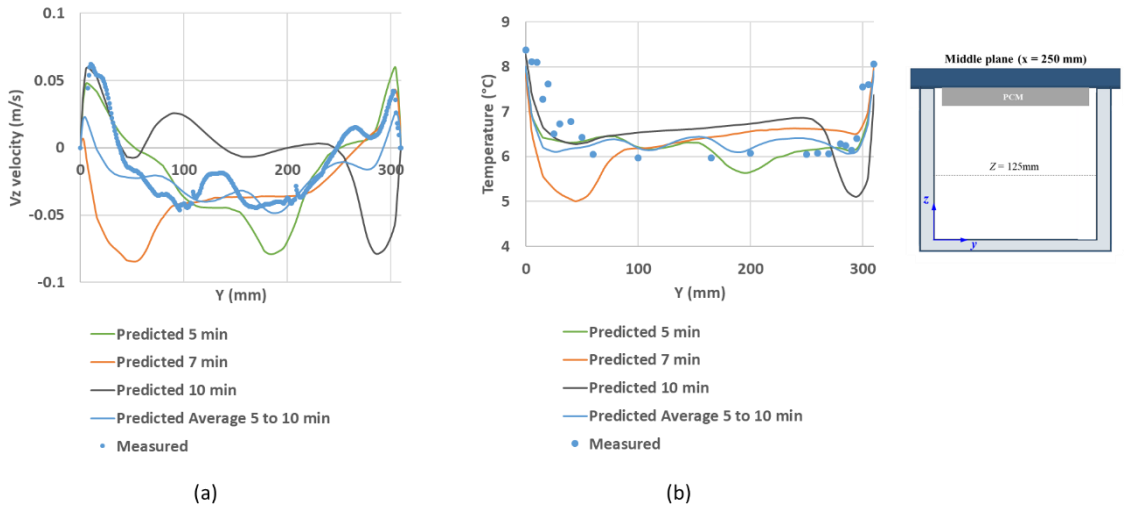

Figure 3.13 Comparison between experimental and numerical results at t = 5 min., 7 min., 10 min. and average between 5 min. and 10 min. in an unloaded box with PCM at the top at the middle plane and z = 125 mm of (a) air velocity in the z-direction and (b) air temperature

4.3 Air velocity and temperature profiles in a loaded box with PCM on a sidewall

Figures 3.14a and 3.15a present the observed airflow patterns on the box's middle plane (x = 250 mm) with PCM on a sidewall and loaded with XPS and Tylose, respectively. In both cases, air flew upwards in the left gap and flew downward in the right gap. The impossibility of laser sheet access into this gap explains the lack of PIV measurements at this position. The maximum measured air velocity was around 0.10 $m \cdot s^{-1}$. Figures 3.14b and 3.15b present the experimental temperature field for the box loaded with XPS and Tylose slabs, respectively. In both cases, the temperature results agreed with the air velocity field, i.e., increasing temperature along the air-circulation loop after air was cooled down by exchange with PCM.

The numerical simulation gave similar air velocity fields (Figure 3.14a' and 3.15a'), but the predicted temperatures (Figures 3.14b' and 3.15b') were slightly lower than the measured values. The airflow was then analyzed in 3D since air flew around the load, as illustrated in Figure 3.16. Air flew downwards and toward the lateral walls in the gap between PCM and load (Figure 3.16a) and from the left (near PCM) to the right in the lateral walls (Figure 3.16b). Figure 3.16c shows the complete air circulation loop.

Figure 3.17 compares experimental and numerical air velocity values in the z-direction and temperature at z = 230 mm in a box loaded with Tylose (initial temperature 4.4°C). A good agreement between predicted and measured values can be observed with a maximum air velocity difference of 0.03 $m \cdot s^{-1}$ and a maximum temperature difference of 1.5°C.

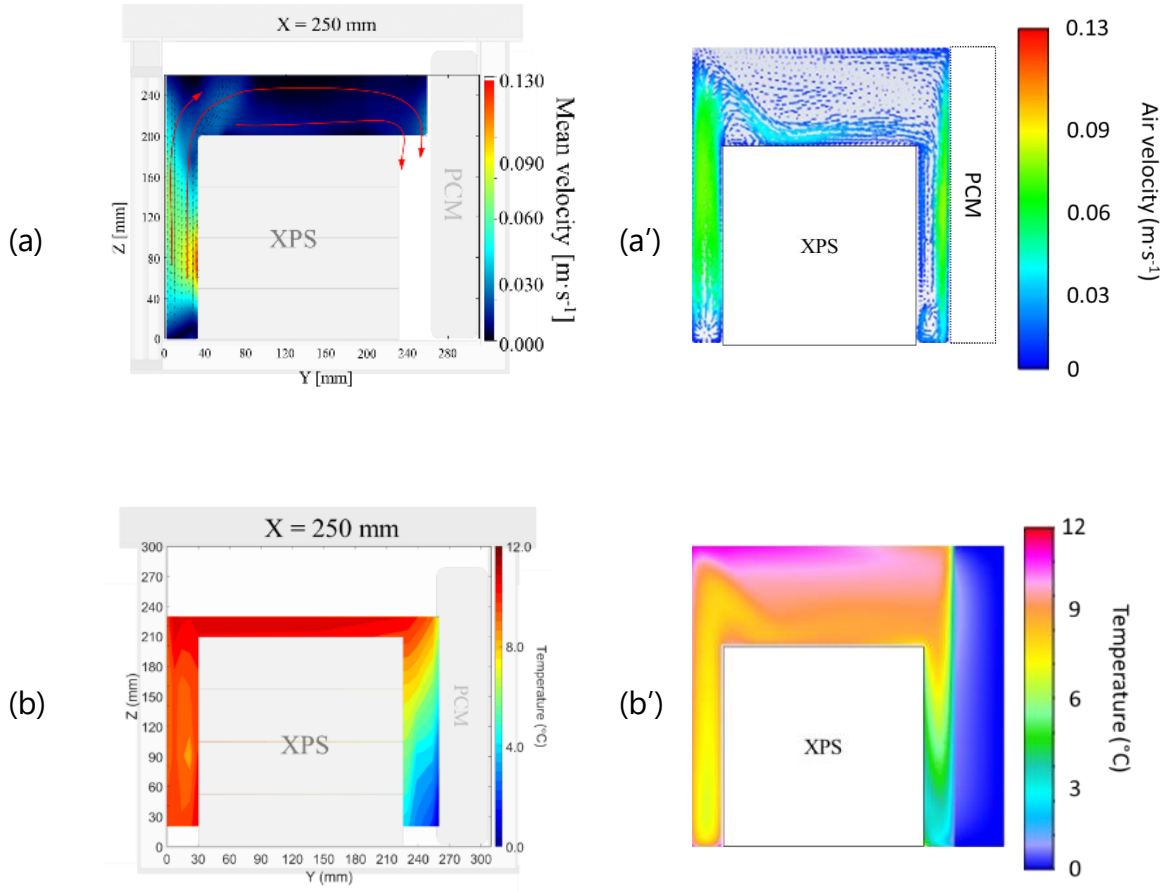

Figure 3.14 (a) Experimental air velocity field and (b) experimental temperature field on the middle plane of a box loaded with XPS with PCM on a sidewall. (a') and (b') are corresponding numerical results

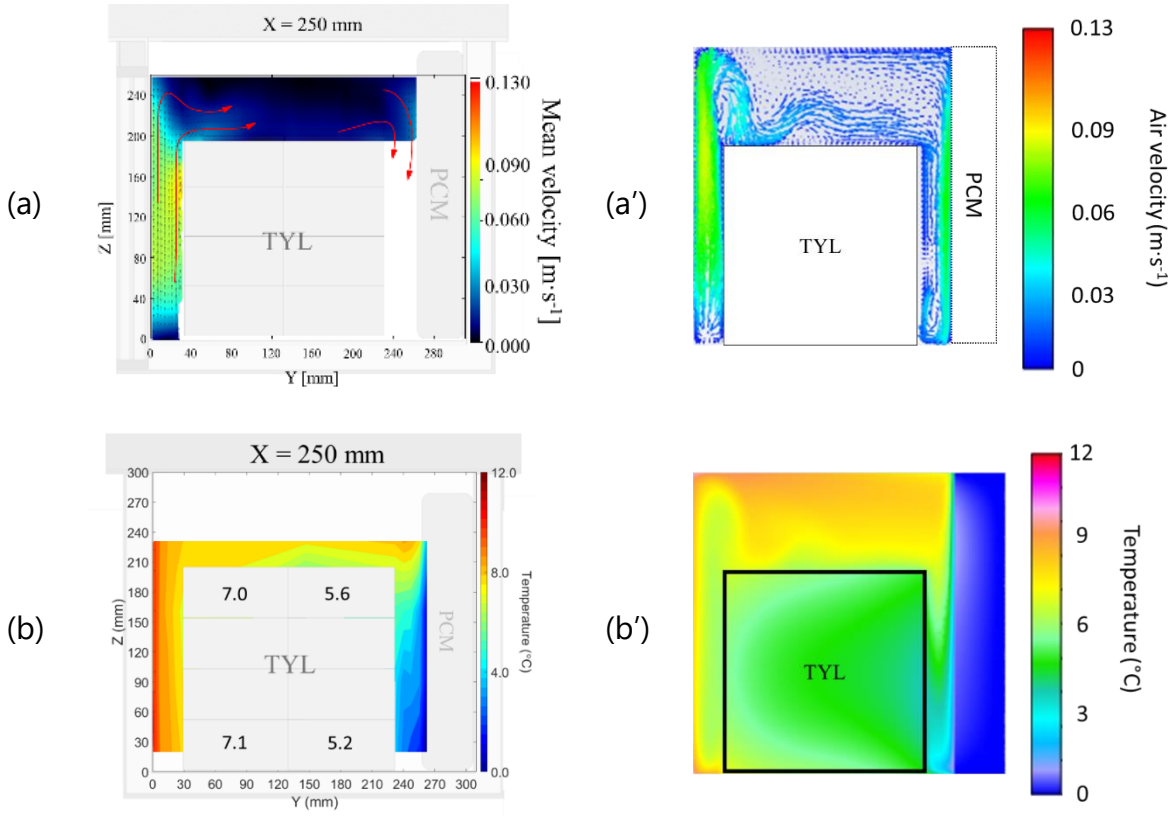

Figure 3.15 (a) Experimental air velocity field and (b) experimental temperature field on the middle plane of a box loaded with Tylose with PCM on a sidewall. (a') and (b') are corresponding numerical results with initial air and Tylose temperature of 20°C and 4.4°C, respectively

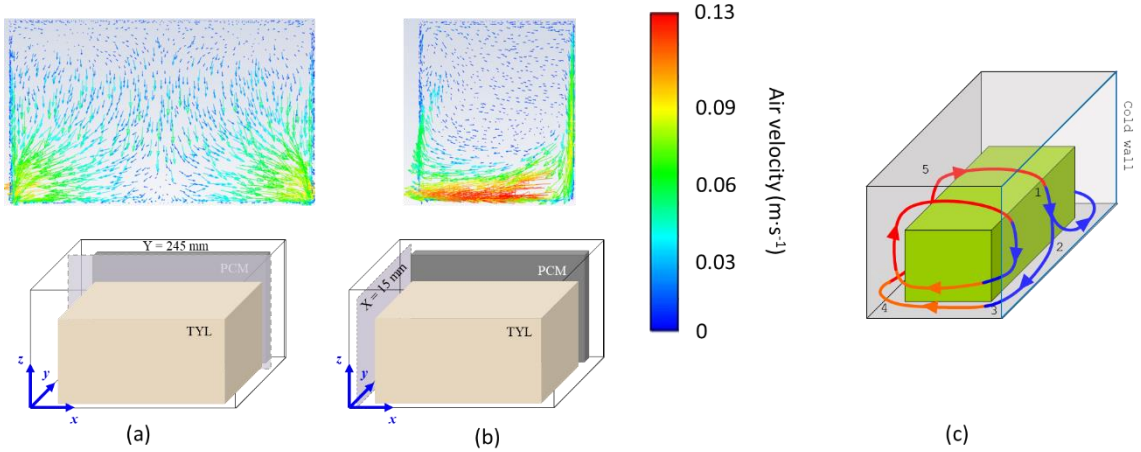

Figure 3.16 Predicted air velocity field at (a) y = 245 mm and (b) x = 15 mm, and (c) 3D airflow illustration in a loaded box with PCM on a sidewall

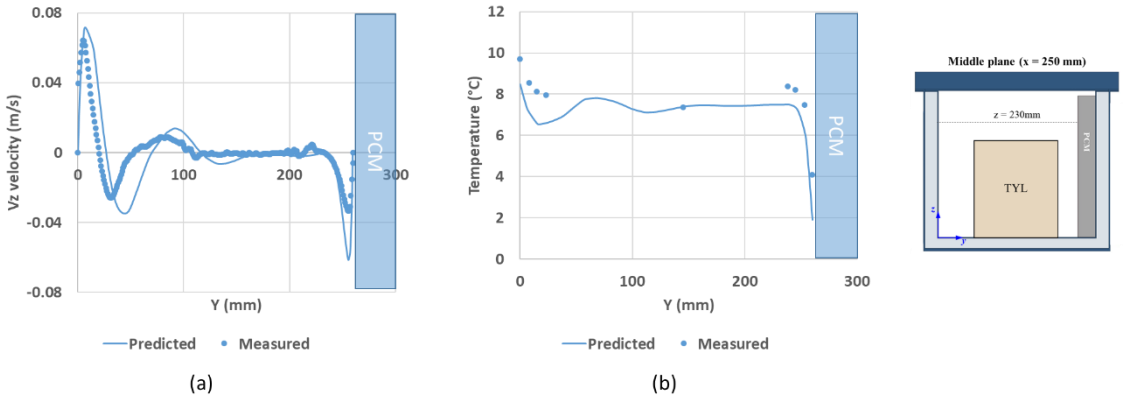

Figure 3.17 Comparison between experimental and numerical results in a box loaded with Tylose with PCM on a sidewall at the middle plane and z = 230 mm of (a) air velocity in the z-direction and (b) air temperature

Figure 3.18 compares the predicted and measured temperature evolution at two positions inside the Tylose slab from the beginning to 4 hours. Temperature slightly decreased at position A (at the bottom near PCM – almost the coldest position) because of convection with colder adjacent air and radiation with colder PCM surface. The temperature continuously increased at position B (at the top near a vertical wall opposite the PCM – almost the warmest position), indicating that a steady state was not reached even after 4 hours. The experimental and numerical results are in good agreement.

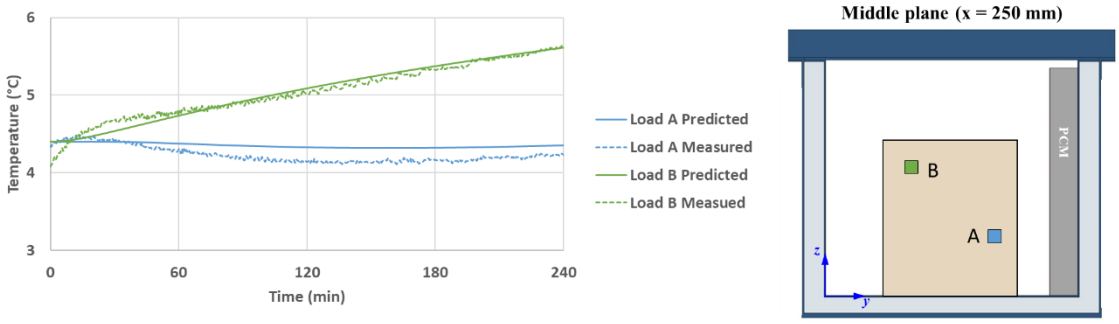

Figure 3.18 Comparison between experimental and numerical results of temperature evolution at two positions in Tylose slab in a box loaded with Tylose with PCM on a sidewall from the beginning to 4 h

4.4 Air velocity and temperature profiles in a loaded box with PCM at the top

Figures 3.19 and 3.20 show the experimental and predicted airflow patterns and temperature fields on the middle plane of the box (X = 250 mm) with PCM at the top loaded with XPS and Tylose, respectively. Cold air from the top (near the PCM) flows upward in the left gap between the side wall and load and downward in the right (PIV measurement was impossible in the right gap). The maximum measured air velocity was around 0.08 $m{\cdot}s^{-1}$ and 0.06 $m{\cdot}s^{-1}$ for the box loaded with XPS and with Tylose slab, respectively.

Since the configuration has a symmetry plane at y = 165 mm, a symmetrical flow pattern, and temperature field could be anticipated. However, from the measurements, the air flew from left to right above the load. There seems to be a clockwise circulation loop explaining the lower measured temperature in the right gap where there was more downward flow from PCM than in the left. The numerical results shows that the airflow was asymmetrical, with a slight temperature difference between the left and right sides. The velocity was unsteady, especially near the PCM, like in the empty case with PCM at the top. In the loaded case, the downward flow chose one or another preferential pathway (through the left or right gap). This behavior is related to the non-linear term in the Navier-Stokes equations, which is responsible for a symmetry rupture (even before turbulence appears).

Simulation results gave a similar air velocity field but a slightly lower temperature than the measured field (Figures 3.19a', 3.19b', 3.20a', and 3.20b'). Figure 3.21 compares experimental data and numerical air velocity values in the z-direction and temperature at z = 230 mm in a box loaded with Tylose. As mentioned previously, comparing averaged velocity measurements with instantaneous velocity predictions is challenging.

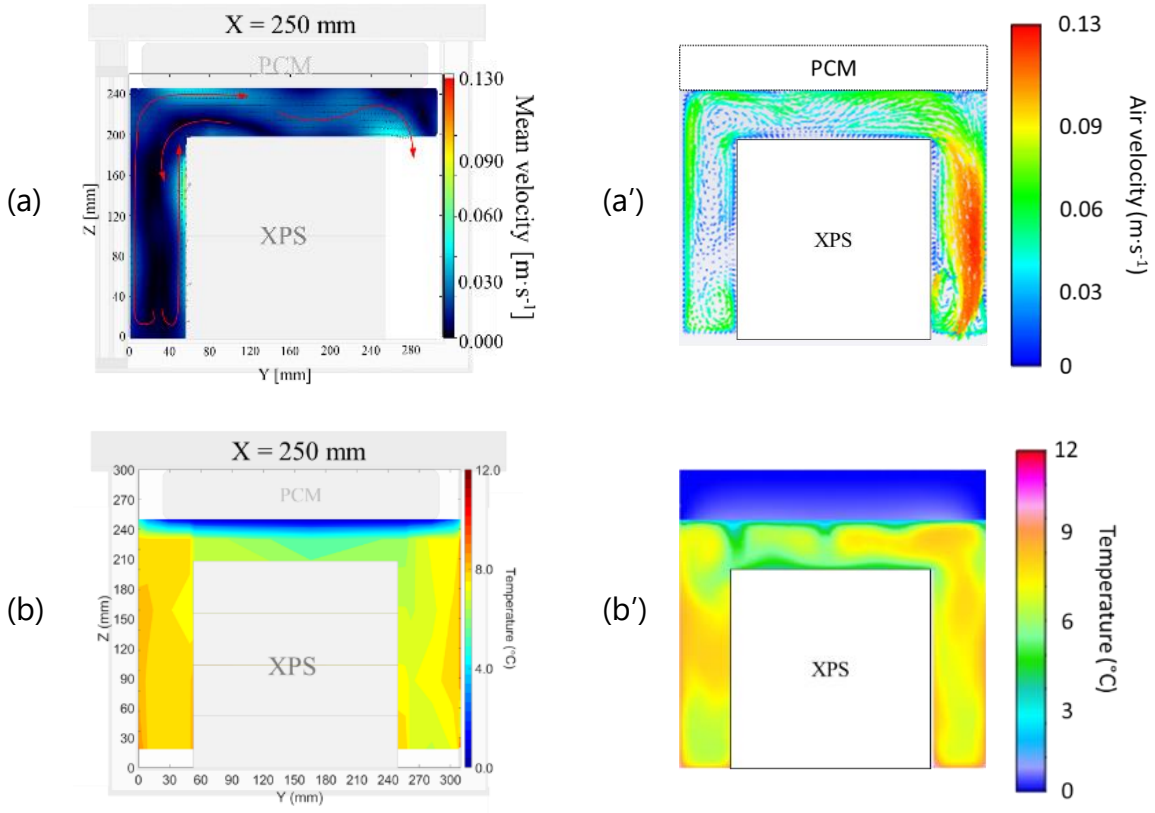

Figure 3.19 (a) Experimental air velocity field and (b) experimental temperature field on the middle plane of a box with PCM at the top loaded with XPS. (a') and (b') are corresponding numerical results

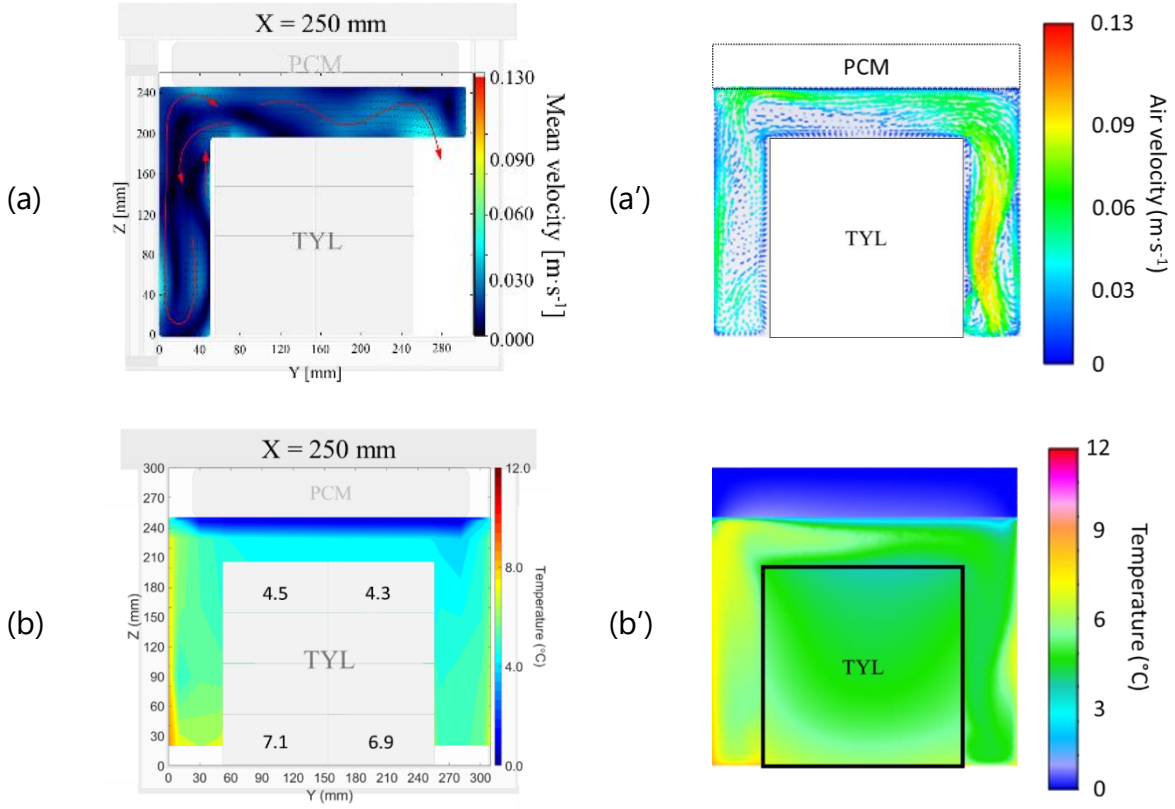

Figure 3.20 (a) Experimental air velocity field and (b) experimental temperature field on the middle plane of a box with PCM at the top loaded with Tylose. (a') and (b') are corresponding numerical results with initial air and Tylose temperature of 20°C and 4.3°C, respectively.

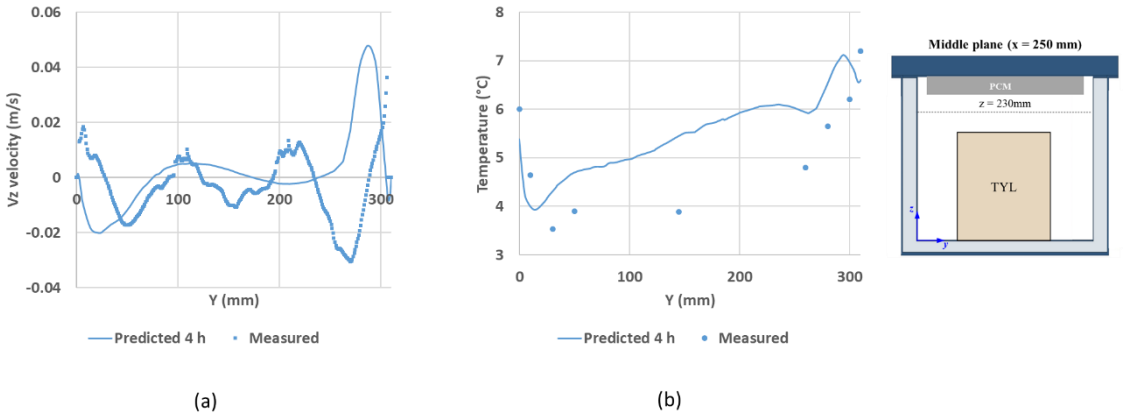

Figure 3.21 Comparison between experimental and numerical results in a box loaded with Tylose with PCM at the top at the middle plane and z = 230 mm of (a) air velocity in z-direction and (b) air temperature

5. CONCLUSIONS

This study implements the CFD model by ANSYS FLUENT in an insulated box equipped with PCM. The model simulates heat conduction, convection and radiation, and airflow inside the box. The model can predict the air velocity, air temperature, and product

temperature evolution in the box with PCM on a sidewall with the maximum difference between predicted and measured values of 1.5°C of air temperature and 0.03 $m \cdot s^{-1}$ of air velocity. However, the model gives less accurate results in the box with PCM at the top due to flow instability and symmetry rupture, making comparisons between measurements (average values) and predictions (instantaneous fluctuating fields) challenging. Nevertheless, this model can be used to better understand variables of box configurations, e.g., box geometry, box insulation and supply chain conditions (ambient temperature).

NOMENCLATURE

c_p	Specific heat capacity ($J \cdot kg^{-1} \cdot K^{-1}$)
F	View factor (-)
$\vec{g}$	Gravitational acceleration (9.81 $m \cdot s^{-2}$)
q_{rad}	Radiative flux ($W \cdot m^{-2}$)
q_{in}	Incoming radiative flux ($W \cdot m^{-2}$)
T	Temperature (°C or K)
U	Overall heat transfer coefficient ($W \cdot m^{-2} \cdot K^{-1}$)
v	Velocity ($m \cdot s^{-1}$)
P	Pressure ($N \cdot m^{-2}$)
λ	Thermal conductivity ($W \cdot m^{-1} \cdot K^{-1}$)
ε	Surface emissivity (-)
σ	Stefan-Boltzmann constant = 5.67 x 10^{-8} $W \cdot m^{-2} \cdot K^{-4}$
ρ	Density ($kg \cdot m^{-3}$)
μ	Dynamic viscosity ($N \cdot s \cdot m^{-2}$)
β	Thermal expansion coefficient (K^{-1})

4 HOW TO CHOOSE A MODEL TO ADDRESS PRACTICAL ISSUES ENCOUNTERED DURING FOOD TRANSPORT IN AN INSULATED BOX EQUIPPED WITH PCM

4.1 SUMMARY

This chapter demonstrates how three validated models (lumped, zonal and Computational Fluid Dynamic – CFD) can be used to deal with technical questions in food transport in an insulated box with Phase change Material - PCM (shown in Article 5). First, the detail of lumped model development and validation is presented. Next, zonal model and CFD model are briefly described here (more details of these model are in chapter III). Afterward, the comparisons of required inputs, provided outputs and the capacity/limitation of each model to answer the technical questions are shown. Then, applications of these models are illustrated with constant or fluctuating ambient temperature. These models are also capable for investigating the effect of box design and operating parameters on product temperature: box insulation and dimension, PCM and product characteristics etc. The importance of internal emissivity is also shown in this chapter. These models can be coupled with predictive quality and safety models to assess the product evolution during transport.

Résumé

Ce chapitre montre comment trois modèles validés (global, zonal et CFD) peuvent être utilisés pour traiter des questions techniques relatives au transport de denrées alimentaires dans un caisson isotherme avec matériau à changement de phase (article 5). Tout d'abord, le détail du développement et de la validation du modèle global (lumped) est présenté. Ensuite, le modèle zonal et le modèle CFD sont brièvement décrits ici (plus de détails sur ces modèles ont été donnés au chapitre III). Une comparaison des entrées requises, des sorties fournies et de la capacité/limite de chaque modèle à répondre aux questions techniques est alors présentée. Puis, des applications de ces modèles sont illustrées avec une température ambiante constante ou variable. Ces modèles sont également capables d'étudier l'effet de la conception de l'équipement et des paramètres de fonctionnement sur la température de produit : isolation et dimension du caisson, caractéristiques du PCM et du produit… L'importance de l'émissivité des parois internes est également montrée dans ce chapitre. Ces modèles peuvent être couplés à des modèles prédictifs de qualité et de sécurité sanitaire pour évaluer l'évolution du produit pendant le transport.

4.2 ARTICLE 5

Comment choisir un modèle pour répondre à des problématiques pratiques rencontrées lors du transport de denrées alimentaires en caisson isotherme équipée de matériaux à changement de phase

Résumé (version française de l'abstract de l'article 5)

Cet article traite des capacités et des limites de trois modèles pour répondre à différentes questions techniques liés au transport des aliments dans un caisson isotherme équipé d'un matériau à changement de phase (Phase Change Material : PCM). Il s'agit d'un modèle global (à une seule zone), d'un modèle à plusieurs zones et d'un modèle de mécanique des fluides numérique (Computational Fluid Dynamics : CFD). Le modèle global prédit l'évolution de la température moyenne et convient pour la conception du caisson en fonction des conditions de fonctionnement lorsque l'hétérogénéité de température n'est une préoccupation majeure. Le modèle zonal décrit les variations spatiales de température, mais nécessite certaines hypothèses concernant le flux d'air et le transfert de chaleur qui sont spécifiques à un agencement de produit et à un emplacement PCM donnés. Le modèle CFD donne les informations les plus complètes sur les phénomènes physiques et les variations de température mais implique un coût de calcul élevé. Cette étude montre la possibilité de combiner ces modèles avec un modèle de qualité. Enfin, les capacités/limites de chaque modèle pour résoudre certains problèmes pratiques sont discutées.

How to choose a model to address practical issues encountered during food transport in an insulated box equipped with PCM

Tanathep Leungtongkum[a, b*], Onrawee Laguerre[a], Steven Duret[a] and Denis Flick[a, b]

[a]Université Paris-Saclay, INRAE, FRISE, 92761 Antony, France
[b]Université Paris-Saclay, INRAE, AgroParisTech, UMR SayFood, 91120 Palaiseau, France

***Corresponding author:** Tanathep Leungtongkum, e-mail: Tanathep.leungtongkum@inrae.fr

Highlights

- Lumped, zonal and CFD models were developed for transport in insulated boxes with PCM
- The lumped model is suitable where the temperature heterogeneity is not a concern
- The zonal model, more complex, provides temperature evolution in different zones
- The CFD model, the most complex, provides temperature and air velocity fields
- Model choice depends on user objectives

Abstract

This article discusses the capabilities and the limitations of three validated models: lumped, zonal and Computational Fluid Dynamics (CFD), to solve several technical issues related to food transport in an insulated box with a Phase Change Material (PCM). The lumped model predicts the average temperature evolution and is suitable for investigating the effect of box design and operating conditions where the temperature heterogeneity is not the main concern. The zonal model depicts spatial temperature variations but requires some assumptions regarding airflow and heat transfer which are specific for a given product arrangement and PCM location. The CFD model gives the most extensive information on physical phenomena and temperature variations but involves a high computational cost that is inevitable. This study shows the possibility of combining these models with a quality model. Finally, the abilities/limitations of each model to solve certain practical issues are discussed.

Keywords: Insulated box, Phase change material, Modelling, Heat transfer, Airflow, Temperature prediction

Nomenclature

A Area [m^2]
B_{mush} Mushy zone constant [$kg \cdot m^{-3} \cdot s^{-1}$]
C Length of the cross-section of the product block for the zonal model [m]
C_p Specific heat capacity [$J \cdot kg^{-1} \cdot K^{-1}$]
E Physiological state of microorganisms [-]

F_{jk} View factor of the surface *j* relating to the surface *k*
$\vec{g}$ Gravitational acceleration = 9.81 $m \cdot s^{-2}$
h Convective heat transfer coefficient [$W \cdot m^{-2} \cdot K^{-1}$]
H Height of the box [m]
K Overall heat transfer coefficient [$W \cdot m^{-2} \cdot K^{-1}$]
L Length of the product block or wall [m]
L_f Latent heat of fusion [$J \cdot kg^{-1}$]
m Mass [kg]
$\dot{m}$ Mass flow rate [$kg \cdot s^{-1}$]
MC_p Thermal inertia [$J \cdot K^{-1}$]
$\vec{n}$ Normal unit vector [-]
P Pressure [Pa]
$\hat{q}_{in}$ Incoming radiative flux [$W \cdot m^{-2}$]
$\hat{q}_{rad}$ Radiative flux from the surface [$W \cdot m^{-2}$]
q_r Radiative heat exchange [W]
R Heat transfer resistance [$K \cdot W^{-1}$]
$\vec{S}$ Momentum source term [$kg \cdot m^{-2} \cdot s^{-2}$]
t Time [s]
t_{max} Maximum storage period [s]
t_{melt} PCM melting time [s]
T, T' Temperature [°C or K]
T_m Melting temperature of PCM [°C or K]
T_{max} Maximum storage temperature [°C]
u Internal energy [$J \cdot kg^{-1}$]
V Volume [m^3]
$\vec{v}$ Velocity [$m \cdot s^{-1}$]
W Width [m]
$\vec{x}$ Position [-]
Y Number of microorganisms [$\log_{10}$ CFU $\cdot g^{-1}$]
x, y, z Coordinate [m]

Greek symbols

ϵ A constant used for Eq. A.11 [-]
μ Dynamic viscosity [$N \cdot s \cdot m^{-2}$]
θ Liquid fraction [-]
α Dimensionless convective heat transfer coefficient [-]
β Thermal expansion coefficient [K^{-1}]
ε Surface emissivity [-]
λ Thermal conductivity [$W \cdot m^{-1} \cdot K^{-1}$]
φ Ice fraction [-]
ρ Density [$kg \cdot m^{-3}$]
σ Stefan-Boltzmann constant = 5.67 x 10^{-8} $W \cdot m^{-2} \cdot K^{-4}$

τ Characteristic time [s]
η Microbial growth rate [h^{-1}]
δ Ratio of air mass flow rate between the secondary and the primary airflow loops for the zonal model (see Figure 4.14b) [-]

Subscripts

0	Initial condition
a	Air
c	Product core
e	External
eq	Equilibrium state
i	Internal
j, k	Surface number for view factor calculation
liq	Liquid state
max	Maximum value
mean	Mean value
melted	Melted
min	Minimum value
n	Zone number of the zonal model (see Figures 4.4 and 4.14)
p	Product
pcm	Phase change material
ref	Reference value
s	Surface of the product block
sh	Product shell
sol	Solid state
tot	Total
w	Internal wall

1. Introduction

Insulated boxes equipped with a Phase Change Material (PCM) has an important role in food cold chain (Nie et al., 2020; Zhao et al., 2020a), particularly for the last mile delivery to consumers (Robertson et al., 2017). The advantages of the insulated box are its simplicity of use, the flexibility related to several box designs available, and the low cost. However, product waste caused by temperature abuse were often observed because of spatial and temporal temperature variations during food transport (Laguerre et al., 2013; Liu et al., 2019; Mercier et al., 2017).

The temperature evolution inside an insulated box equipped with PCM was investigated experimentally and numerically by several authors and summarized in Leungtongkum et al. (2022). For model simplification, several studies considered only heat conduction in the air inside the box, and ignored natural convection and radiation (Du et al., 2020; Kozak et al., 2017; Paquette et al., 2017; Xiaofeng & Xuelai, 2021). Recently, some studies took natural convection of internal air and melted PCM into

account (Burgess et al., 2022; Calati et al., 2023; Rahimi-Khoigani et al., 2023). According to our knowledge, no study has considered radiation between the internal surfaces in the model in spite of the fact that all heat transfer modes are of the same order of magnitude in closed cavities (Laguerre & Flick, 2010).

There are different thermal modelling approaches described in the literature: the lumped models considering the average product temperature and overall heat transfer resistances (Kozak et al., 2017; Laguerre et al., 2019), the zonal models distinguishing warmer and colder regions (East & Smale, 2008), and the Computational Fluid Dynamic (CFD) models describing detailed temperature and velocity fields (Burgess et al., 2022; Laguerre et al., 2018; Margeirsson et al., 2012). Each model needs different types of input data, and thus has a different degree of complexity and provides different outputs. The users of the model (scientists, manufacturers, and stakeholders) have various levels of expertise and different practical questions: the amount of PCM needed to maintain the recommended temperature throughout a supply chain, the product temperature evolution, the warmest/coldest temperatures and their positions, etc.

This article aims to present three different modelling approaches from basic to advance: lumped, zonal and CFD models to answer these questions. The capabilities and limitations of each model related to the insulated boxes with PCM for food transport are discussed. This study is original since it is the first time that three modelling approaches are compared, and their ability to answer certain questions is demonstrated. It is to be emphasized that the zonal and CFD model development was presented in our previous studies (Leungtongkum et al., 2023b; 2023d).

2. Modelling approaches

2.1 Lumped model

2.1.1 Model descriptions and assumptions

An insulated box equipped with PCM loaded with product can be schematized by using electrical analogy (Figure 4.1). The thermal inertia of air is neglected and the product is assumed to be a lumped object.

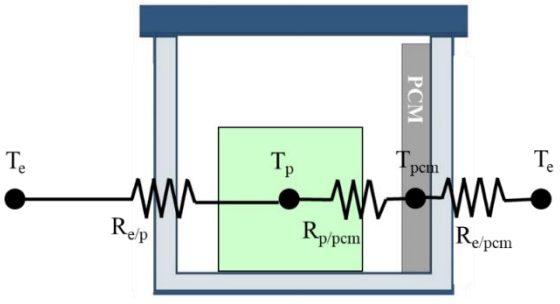

Figure 4.1 Lumped model structure

$R_{e/pcm}$ is the heat transfer resistance (mainly due to the wall insulation of the box) between the external air and the PCM [K·W^{-1}]

$$R_{e/pcm} = \frac{1}{KA_{pcm}} \qquad (4.1)$$

$R_{e/p}$ is the heat transfer resistance (mainly due to the wall insulation of the box) between the external air and the product [K·W^{-1}]

$$R_{e/p} = \frac{1}{KA_{tot-pcm}} \qquad (4.2)$$

where K is the overall heat transfer coefficient of the box [W·m^{-2}·K^{-1}]

$$A_{pcm} = \sqrt{A_{i.pcm}A_{e.pcm}} \qquad (4.3)$$

and $A_{i.pcm}$ is the internal area of the box wall in contact with the PCM [m^2]

$A_{e.pcm}$ is the corresponding external area [m^2]

$$A_{tot-pcm} = \sqrt{(A_{i.tot} - A_{i.pcm})(A_{e.tot} - A_{e.pcm})} \qquad (4.4)$$

and $A_{i.tot}$ is the total internal area of the box walls [m^2]

$A_{e.tot}$ is the corresponding external area [m^2]

$R_{p/pcm}$ is the heat transfer resistance between the product and the PCM [K·W^{-1}]

2.1.2 Product temperature evolution

The energy balance of the product can be written as indicated in Equation 4.5.

$$m_p C_{p.p} \frac{dT_p}{dt} = \frac{T_e - T_p}{R_{e/p}} - \frac{T_p - T_{pcm}}{R_{pcm/p}} \qquad (4.5)$$

where m_p is product mass [kg]

$C_{p.p}$ is specific heat of product [J·kg^{-1}·K^{-1}]

If T_e and T_{pcm} are constant and the characteristic time τ [s] is defined in Equation 4.6

$$\tau = \frac{m_p C_{p.p}}{\frac{1}{R_{e/p}} + \frac{1}{R_{p/pcm}}} \qquad (4.6)$$

Equation 4.5 becomes $$\frac{dT_p}{dt} + \frac{T_p}{\tau} = \frac{T_{p.eq}}{\tau} \qquad (4.7)$$

Thus, $$T_p = T_{p.eq} + (T_{p.0} - T_{p.eq})e^{-\frac{t}{\tau}} \qquad (4.8)$$

At steady state, if PCM is still melting ($T_{pcm} = T_m$), the product temperature (T_p) reaches an equilibrium value ($T_{p.eq}$) related to the unknown thermal resistance $R_{pcm/p}$, which can be represented by Equation 4.9.

$$\frac{T_e - T_{p.eq}}{R_{e/p}} + \frac{T_m - T_{p.eq}}{R_{pcm/p}} = 0 \qquad (4.9)$$

2.1.3 PCM evolution

PCM evolves in 3 states from solid state until it is completely melted. The energy balances of PCM can be written for each state as follows.

State 1: when the PCM is completely solid ($T_{pcm} < T_m$) and $m_{pcm.melted} = 0$;

$$m_{pcm} C_{p.pcm.sol} \frac{dT_{pcm}}{dt} = \frac{T_e - T_{pcm}}{R_{e/pcm}} + \frac{T_p - T_{pcm}}{R_{pcm/p}} \qquad (4.10)$$

State 2: when the PCM is melting ($T_{pcm} = T_m$);

$$L_f \frac{dm_{pcm.melted}}{dt} = \frac{T_e - T_{pcm}}{R_{e/pcm}} + \frac{T_p - T_{pcm}}{R_{pcm/p}} \qquad (4.11)$$

State 3: when the PCM is completely liquid ($T_{pcm} > T_m$) and $m_{pcm.melted} = m_{pcm}$;

$$m_{pcm} C_{p.pcm.liq} \frac{dT_{pcm}}{dt} = \frac{T_e - T_{pcm}}{R_{e/pcm}} + \frac{T_p - T_{pcm}}{R_{pcm/p}} \qquad (4.12)$$

From Equations 4.8 and 4.11, if T_e and T_{pcm} are constant:

$$m_{pcm.melted} = \frac{(T_{p.eq} - T_{pcm})t + \tau(T_{p.0} - T_{p.eq})(1 - e^{-\frac{t}{\tau}})}{R_{pcm/p} L_f} + \frac{T_e - T_{pcm}}{R_{e/pcm} L_f} t \qquad (4.13)$$

Assuming $t \gg \tau$ (asymptotic approximation):

$$m_{pcm.melted} \approx \frac{\tau(T_{p.0} - T_{p.eq})}{R_{pcm/p} L_f} + \left(\frac{T_{p.eq} - T_{pcm}}{R_{pcm/p} L_f} + \frac{T_e - T_{pcm}}{R_{e/pcm} L_f}\right) t \qquad (4.14)$$

2.1.4 Model validation by experiment

2.1.4.1 Materials

The insulated box for model validation is a 45-L commercialized multilayer insulated box (Manutan SA, Gonesse, France) with 500 mm x 310 mm x 300 mm internal dimensions (Figure 4.2). The walls, containing four layers, consisted of three materials: expanded polystyrene (25 mm thickness), polypropylene (inner and outer layers with a thickness of 3.5 mm) and air gap between the expanded polystyrene and the inner layer (estimated thickness: 5 mm). The measured heat transmission coefficient (K) of this box, by internal heating method (ATP, 2020), is 0.90 $W \cdot m^{-2} \cdot K^{-1}$.

To allow uniform heat exchange with the ambient, the box was put on a 50-mm height

wooden support. This box was placed on a 0.7-m height table located in the center of the temperature-controlled test room (Width 3.4 m x Length 3.4 m x Height 2.5 m). The PCM plate (external dimensions 460 mm x 280 mm x 47 mm) with an enclosure made of polypropylene (3.5-mm thickness) and filled with 3.5 kg of tap water (melting point ~ 0°C). 16 kg of Tylose slabs (dimensions 400 mm x 200 mm x 200 mm) is used as test product. It contained 23% methyl hydroxyethylcellulose, 76.4% water and 0.5% NaCl (Refrigeration Development and Testing Ltd., North Somerset, UK).

From the box geometry and the material conductivities, two heat transfer resistances can be determined: $R_{e/pcm}$ = 3.68 K·W^{-1} and $R_{e/p}$ = 1.67 K·W^{-1}.

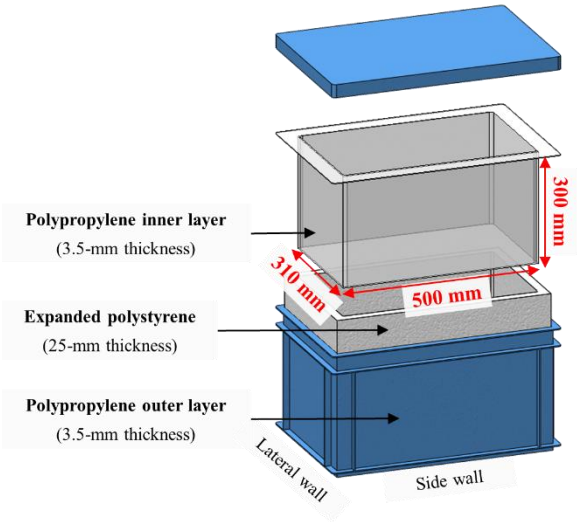

Figure 4.2 Insulated box used in the experimental validation

(Source: Leungtongkum et al. (2023a)).

2.1.4.2 Experimental protocol

The PCM was frozen in a freezer (-2°C) for at least 48 h prior to the experiment. Although it was horizontally placed, the thickness of the PCM slab was not uniform (35 mm to 50 mm). The test products were placed in a polystyrene box and put into a domestic refrigerator with setting temperature of 4°C for at least 24 h. Temperatures inside the PCM, product and air at different positions were measured using calibrated thermocouples with a precision of ± 0.1°C (Leungtongkum et al. 2023b). The average product temperature was determined from 16 measurement positions.

2.1.4.3 Product equilibrium temperature determination

The equilibrium temperature was determined experimentally by replacing the PCM with a completely frozen one every 12 h over a period of 72 h. For the box with PCM on a side wall and 20°C ambient temperature, the average product temperature at equilibrium ($T_{p.eq}$) was 8.6°C. Thus, the thermal resistance between product and PCM ($R_{p/pcm}$) was 1.26 K·W^{-1}.

2.1.4.4 Product temperature evolution validation

The temperature evolution inside the box was measured with a completely frozen PCM slab for the product initial temperature of 4.4°C under 20°C ambient. Figure 4.3a compares the measured and calculated temperature evolution. It can be seen that the lumped model can reliably predict the product average temperature evolution.

2.1.4.5 Validation of the evolution of mass of melted PCM

The amount of melted PCM from 0 h to 24 h was measured immediately after taking it out of the box. Figure 4.3b shows good agreement between the measured and calculated amounts of melted PCM by the lumped model (Equation 4.13). In our experiment, the characteristic time (τ) was about 8.8 h; after this time, the asymptote lumped model (Equation 4.14) gives a good approximation.

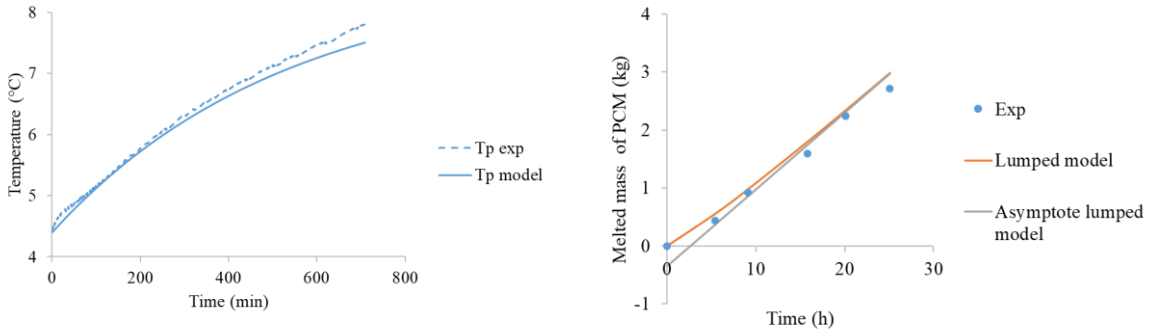

(a) (b)

Figure 4.3 Comparison between the experimental and numerical values (by lumped model) in a box with PCM on a side wall under 20°C ambient: (a) product temperature evolution with $T_{p.0}$ = 4.4°C, and (b) melted PCM mass

2.2 Zonal model

2.2.1 Model description and assumptions

This model applies for an insulated box with PCM on a side wall and a gap below the product. As suggested by our previous experimental study (Leungtongkum et al., 2023c), 2D-airflow path is considered (Figure 4.4). This model assumes that there is a temperature difference between the top and the bottom of the box because of thermal stratification, and between the cold side (near the PCM) and the warm one. By taking conductive and convective heat exchange in account, there is also a temperature difference between product surface and product core. van der Sman (2003) suggested that, when heat conduction and convection occur simultaneously, distinguishing the shell and core temperatures gave more accurate results than assuming a uniform temperature. In our zonal model, the product (parallelepiped shape with a length *L*) was divided into four blocks. Each block had a height and width of *C* with a shell (*C/4*)

and core (*3C/4*).

Figure 4.4 illustrates the control volumes, airflow path and heat fluxes considered. More detail of model description and assumptions can be found in Leungtongkum et al. (2023b).

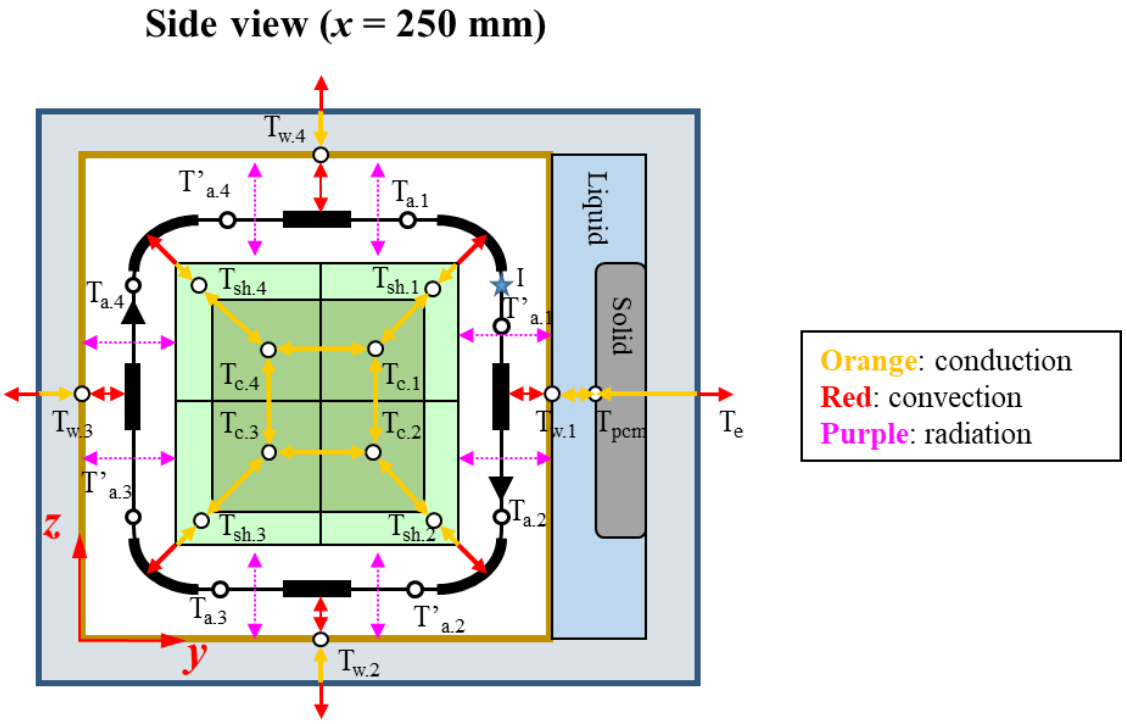

Figure 4.4 Side view of a simplified heat transfer and airflow diagram in the zonal model of an insulated box with PCM on a side wall. Source: Leungtongkum et al. (2023b)

Following state variables describe 12 solid zones at a given time:

- $T_{sh.n}$ when $n \in [1,4]$ represents average temperature in the product shell
- $T_{c.n}$ when $n \in [1,4]$ represents average temperature in the product core
- $T_{w.n}$ when $n \in [1,4]$ represents wall temperature, where $T_{w.1}$ is the surface temperature of PCM and $T_{w.2}$ to $T_{w.4}$ are the temperatures of the internal walls

T_{pcm} and φ are used to characterized PCM which define its temperature and ice fraction, respectively. Air temperature consists of eight values representing the evolution along the airflow path. By exchanging with the product shells, air temperature varies from $T_{a.n}$ to $T'_{a.n}$ when $n \in [1,4]$. While its temperature changes from $T'_{a.n}$ to $T_{a.n+1}$ when $n \in [1,3]$ and from $T'_{a.4}$ to $T_{a.1}$ by exchanging with the internal walls.

More details regarding model development are presented in Leungtongkum et al., (2023b). Appendix 1 presents some equations representing air or product heat balances.

2.2.2 Model validation

Figure 4.5 compares the measured and calculated values (by zonal model) under steady state (Figure 4.5a) and transient state (Figure 4.5b). The model provides a good prediction of the temperature distribution and temperature evolution.

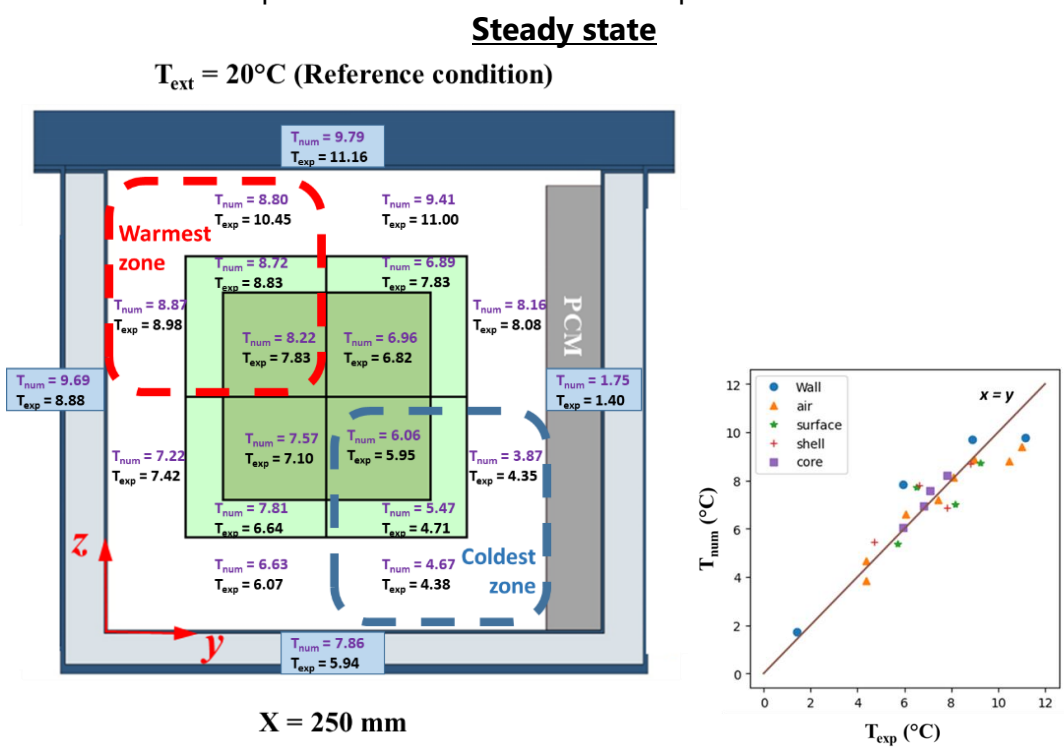

(a)

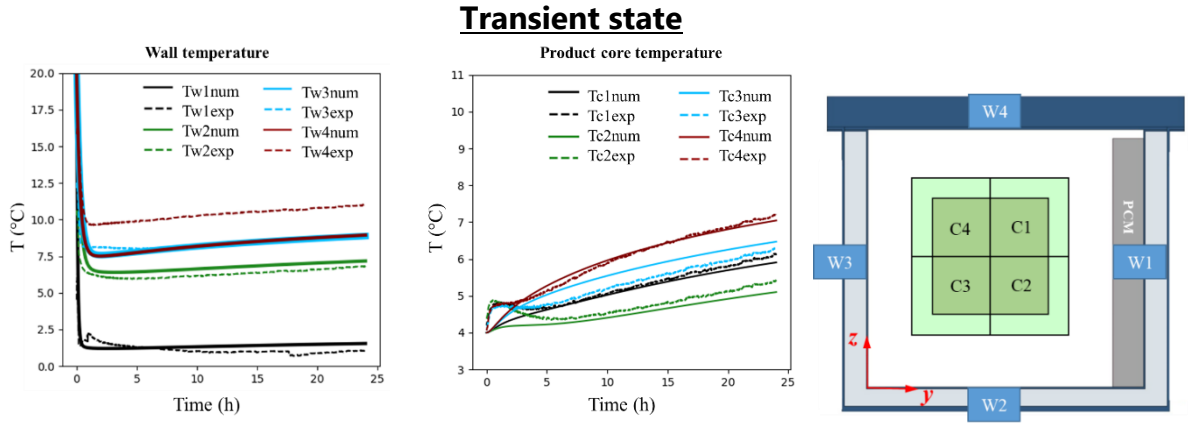

(b)

Figure 4.5 Comparison between the experimental and numerical (by zonal model) temperatures in an insulated box equipped with PCM on one side wall with an initial product temperature of 4°C and ambient temperature of 20°C: (a) steady state, and (b) transient state. Source: Leungtongkum et al. (2023b)

2.3 CFD model

2.3.1 Model description and assumptions

In our CFD model, the following assumptions were applied:

- Laminar airflow as its Rayleigh number is lower than 10^9 (calculation not shown).
- Boussinesq approximation (density is assumed constant except in the gravity term).
- Viscous dissipation into heat is neglected.
- PCM density is assumed to be constant as that of its liquid state.

Appendix 2 presents the governing equations.

2.3.2 Numerical simulation

The geometry was drawn by using SpaceClaim and meshed with Ansys Fluent meshing. A mesh independence study was first conducted by comparing the maximum air temperature difference between the experimental and calculated values for the mesh number varying from 4.3 x 10^3 to 1.4 x 10^6 polyhedral cells. The study domain with 2.6 x 10^5 polyhedral cells was chosen for the reference box (cf. Section 3).

The numerical study was performed with Ansys Fluent 2021 R1 in a transient state. According to a time step independence study (from 0.1 s to 10 s), the time step of 1 s was used as the compromise between the calculation time and the time to reach the first convergence solution (maximum 20 iteration each).

2.3.3 Model validation

Figures 4.6 and 4.7 compare experimental and CFD results of temperature field and temperature evolution in a box with PCM on a side wall. It can be seen that the CFD model gave accurate predictions with a maximum difference of 2.0°C with the experimental value.

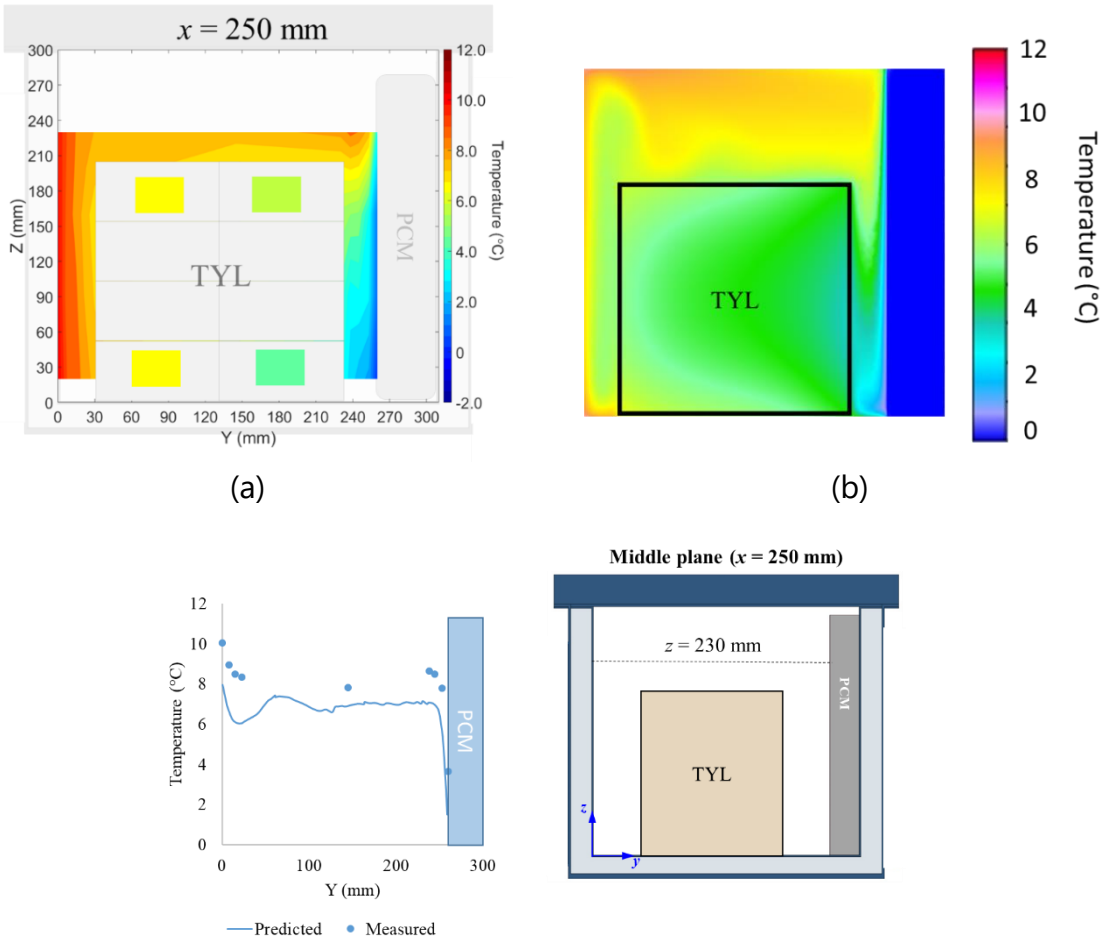

Figure 4.6 Temperature field determined by: (a) measurement, (b) CFD results, and (c) comparison between experimental and CFD results at t = 4 h of air temperature at z = 230 mm on the middle plane. Box loaded with test product (Tylose, TYL) with PCM on a side wall.

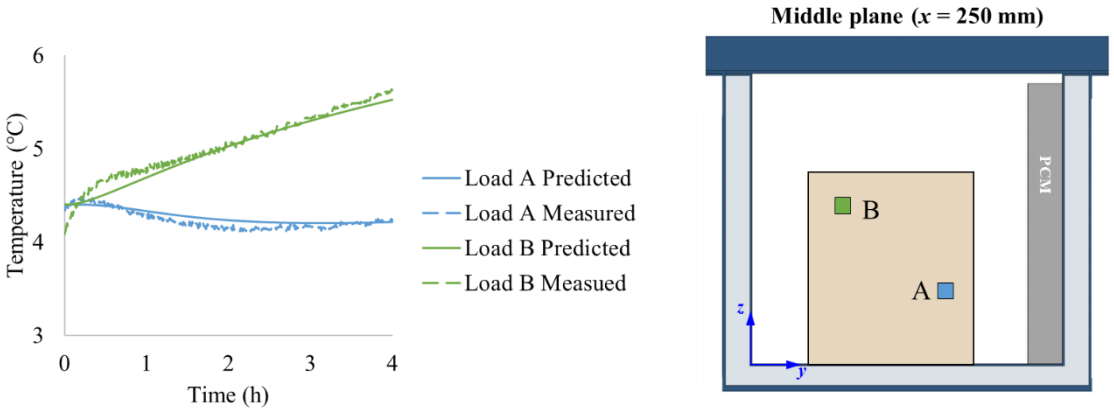

Figure 4.7 Comparison between experimental and CFD determination of the temperature evolution at two positions.

2.4 Summary of input and output parameters

The input parameters needed, and the outputs provided for each model are summarized in Table 4.1. To develop the lumped and zonal models, some measurements and parameter estimations are necessary, but none are required for CFD model development.

Table 4.1 Input and output parameters of each model

Model	Input parameters from box/PCM/product/air characteristics	Input parameters from measurements or correlations	Outputs
Lumped model	Box: - Dimension - Insulation (by conductivity of the material) PCM: - Dimensions - Mass - Specific heat - Melting temperature - Latent heat of melting Product: - Dimensions - Mass - Specific heat	$R_{p/pcm}$ = heat transfer resistance between PCM and product. (determined from product temperature at equilibrium by constantly changing PCM as mentioned in section 2.1.4.4)	Mean product temperature evolution: $T_{p.mean}\ (t)$ Melted PCM evolution: $m_{melted.pcm}\ (t)$
Zonal model	Same parameters required for the lumped model cited above. Additional parameters: - Box wall emissivity - Thermal conductivity of the product - Product emissivity - Specific heat capacity of the air	- h_w and h_p = internal convective heat transfer coefficient (determined from local temperature measurements as described in Leungtongkum et al. (2023a) or free convection correlations) - $\dot{m}_a$ = mass flow rate of air (determined from developed relation with heat transfer coefficient as shown in Leungtongkum et al. (2023b))	Temperature evolution for air, product core and shell in 4 zones (top/bottom; left/right): • $T_{p.i}\ (t)$ • $T_{a.i}\ (t)$ and $T'_{a.i}\ (t)$ Melted PCM evolution: $m_{melted.pcm}\ (t)$
CFD model	Same parameters required as for the zonal model cited above. Additional parameters: - Air viscosity - Air density as a function of temperature	No estimated parameter needed	Detailed 3D temperature of product and air and air velocity fields: • $T_p\ (t, \vec{x})$ • $T_a\ (t, \vec{x})$ • $\vec{v}_a(t, \vec{x})$ Melted PCM evolution: $m_{melted.pcm}\ (t)$

2.5 Model applicability

Since each model is based on different assumptions, Table 4.2 shows the applicability of each model to answer the technical questions.

Table 4.2 Model applicability to answer technical questions

Technical questions	Lumped model	Zonal model	CFD model
How does the product temperature change with time under varying ambient temperatures as in a real supply chain?	✓*	✓	✓
What is the required PCM mass to maintain the average product temperature under the recommended values during a given duration?	✓*	✓	✓
How does the box insulation affect the product temperature?	✓*	✓	✓
How do PCM melting temperature and its latent heat impact the product temperature?	✓*	✓	✓
How do the mass and the thermophysical properties of the product impact its temperature?	✓*	✓	✓
Where are the warmest and coldest positions in the product?	✗	✓**	✓**
How does the emissivity of the internal walls and product surface affect the product temperature?	✗	✓*	✓
How does the PCM position impact the product temperature?	✓±	✓±*	✓*
What are the approximated airflow pattern and temperature distribution?	✗	✓**	✓
Are the 3D airflow pattern and temperature field shown in detail?	✗	✗	✓*
What is the influence of product compactness on its temperature?	✗	✗	✓±
How do the box dimensions affect the product temperature?	✓±	✓±	✓*
What is the effect of box/PCM characteristics under varying ambient temperatures on the organoleptic qualities and sanitary risk?	✓±*	✓	✓

✓ Applicable
✗ Not applicable
✓± Applicable but require modifications/precautions
* To be demonstrated in the Results and Discussions section
** Already shown in the model development or validation

3. Results and Discussions

To demonstrate the model applicability, the conditions/parameters shown in Table 4.3 were used as input parameters unless otherwise indicated. The demonstrated box called the "reference box" was equipped with polyurethane insulation with a thickness of 40 mm; it was shown that it allowed the transport of temperature-sensitive products for periods of up to 96 hours (Kacimi & Labranque, 2011).

Table 4.3 Input parameters for numerical studies

Parameter	Value	Unit
Reference Box		
Internal dimensions of the box (*L* x *W* x *H*)	0.5 x 0.3 x 0.31	m^3
Wall thickness	0.04	m
Heat transmission coefficient of box insulation (*K*)	0.58	$W \cdot m^{-2} \cdot K^{-1}$
PCM (ice) on a side wall		
PCM dimensions (*L* x *W* x *H*)	0.5 x 0.05 x 0.3	m^3
PCM mass	2	kg
Specific heat (solid state)	2070	$J \cdot kg^{-1} \cdot K^{-1}$
Specific heat (liquid state)	4217	$J \cdot kg^{-1} \cdot K^{-1}$
Latent heat of fusion	333,700	$J \cdot kg^{-1}$
Melting temperature range	-0.2 to 0.2 (0°C for the lumped model)	°C
Product (Tylose)		
Product dimensions (*L* x *W* x *H*)	0.4 x 0.2 x 0.2	m^3
Product mass	16	kg
Specific heat	3372	$J \cdot kg^{-1} \cdot K^{-1}$

3.1 Temperature and PCM evolution under varying ambient conditions

The ambience usually varies according to geographical location, the time of day and the season. Thus, taking the variation of ambience into account is necessary for transport design (East et al., 2009; Fioretti et al., 2016; Navaranjan et al., 2013). The numerical models taking into account the variable ambient temperature can be useful for designing the box and for estimating the PCM amount required to preserve food (Kacimi & Labranque, 2019).

Figure 4.8 shows the results obtained with the lumped model used to predict the average product temperature (T_p), PCM temperature (T_{pcm}), and amount of melted PCM ($m_{pcm.melted}$) under varying ambient profiles (T_e) adapted from Fioretti et al. (2016). The model highlights the various temperature changes when the ambient temperature alters. During the first 9.5 h (T_e = 14°C), the product temperature increased slowly until it reached 4.3°C (product equilibrium temperature 4.6°C, initial temperature 4.0°C) and

the melting rate of the PCM was 0.06 kg/h. Then, the product temperature increased to 7.3°C during the following 12 h (T_e = 28°C) with a product equilibrium temperature of 9.2°C, and the PCM melting rate was 0.11 kg/h. This rate is almost twice that observed during the first period as the temperature difference between the ambient and the PCM doubled from 14°C to 28°C. The product temperature decreased slightly during the following 1.5 h (T_e = 20°C), while the product equilibrium temperature was 6.6°C. However, when the PCM was completely melted (23 h and thereafter), the PCM and the product temperatures increased. Despite the decreasing ambient temperature which dropped to 14°C during the final 8 h, the product temperature constantly increased, unlike during the first period, because the PCM temperature rose continuously after it was completely melted.

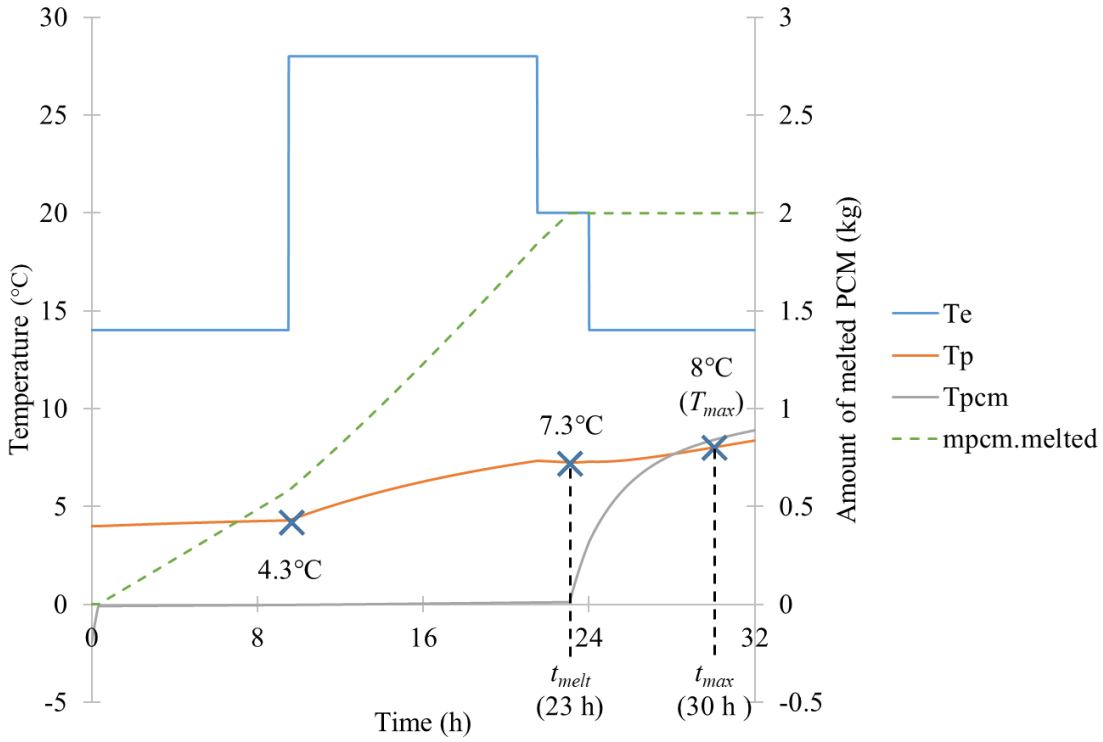

Figure 4.8 Product (T_p) and PCM (T_{pcm}) temperatures, melted PCM mass evolution ($m_{pcm.melted}$) under varying ambient conditions (T_e) predicted by the lumped model; the product and PCM initial temperatures were 4°C and -2°C, respectively, PCM mass 2 kg.

3.2 PCM melting time and maximum storage period

Section 3.1 demonstrates the determination of the PCM melting time (t_{melt}) and maximum storage period (t_{max}) so that the product temperature remains below the maximum storage temperature (T_{max}) for given PCM mass, product initial temperature and external temperature. As shown in Figure 4.8, the PCM melting time for m_{pcm} = 2 kg is 23 h, and the maximum storage period for T_{max} = 8°C is 30 h. However, in practice, stakeholders usually have information regarding the targeted transport duration (t_{max}), the maximum storage temperature not to be exceeded, and the external temperature.

Thus, they need to determine the PCM amount required for each transport operation.

Here, we considered a constant ambient temperature. First, we examined the case where $T_{p.eq} < T_{max}$. The melting time (t_{melt}) can be estimated from Equation 4.13 by adding the sensible heat of the PCM from $T_{pcm.0}$ to T_m as shown in Equation 4.15.

$$m_{pcm}\left(L_f + C_{pcm.sol}\left(T_m - T_{pcm.0}\right)\right) + m_p C_{p.p}\left(T_{p.eq} - T_{p.0}\right)\frac{\left(1-e^{-\frac{t_{melt}}{\tau}}\right)}{1+\frac{R_{pcm/p}}{R_{e/p}}} \approx \left(\frac{T_{p.eq}-T_m}{R_{pcm/p}} + \frac{T_e-T_m}{R_{e/pcm}}\right)t_{melt} \quad (4.15)$$

One could consider that the transport duration should not exceed the melting time. Therefore, it can be assumed that t_{melt} as t_{max} gives the first estimation of the necessary mass of PCM; but this leads to an overestimation of the PCM mass because the thermal inertia of the product and the PCM is underestimated. Thus, a better estimation can be obtained by including product thermal inertia from $T_{p.0}$ to T_{max} and the sensible heat of melted PCM from T_m to T_{max} as described in Equation 4.16.

$$m_{pcm}\left(L_f + C_{pcm.sol}\left(T_m - T_{pcm.0}\right) + C_{pcm.liq}\left(T_{max} - T_m\right)\right) + m_p C_{p.p}\left(T_{max} - T_{p.0}\right) \approx \left(\frac{T_{p.eq}-T_m}{R_{pcm/p}} + \frac{T_e-T_m}{R_{e/pcm}}\right)t_{max} \quad (4.16)$$

Figure 4.9a shows the melting time and maximum storage period for T_{max} = 8°C in the reference box (cited in Table 4.3) under 20°C ambient conditions ($T_{p.eq}$ = 6.6°C). It can be seen that the maximum storage period was longer than the melting period thanks to product and PCM thermal inertia. The estimations of melting time and maximum storage period by Equation 4.15 and 4.16 are very close to that obtained by direct transient simulation as shown in Section 3.1. The advantage of Equation 4.16 is that it gives an analytical expression of the required PCM amount as a function of $T_{p.0}$, $T_{pcm.0}$, T_e, T_{max}, t_{max} and box insulation (through $R_{e/pcm}$). This equation can be applied only when T_{max} is higher than the product equilibrium temperature ($T_{p.eq}$).

In some cases, for example, transport conducted using a poorly insulated box or under high ambient temperatures, $T_{p.eq}$ can be higher than T_{max}. In this case, the product temperature reaches the maximum value (T_{max}) at a given time (t'_{max}) before it reaches equilibrium, and t'_{max} can be determined from Equation 4.17 as follows:

$$T_{max} = T_{p.eq} + \left(T_{p.0} - T_{p.eq}\right)e^{-\frac{t'max}{\tau}} \quad (4.17)$$

If the targeted maximum storage period (t_{max}) is longer than t'_{max}, the product temperature will exceed T_{max} whatever the PCM amount. On the other hand, if t_{max} is lower than t'_{max}, the required PCM amount can still be determined by using Equation 4.16.

Figure 4.9b shows the melting time and maximum storage period for T_{max} = 8°C in the reference box under 30°C ambient temperature ($T_{p.eq}$ = 9.9°C). Since t'_{max} is 14.5 h, it is impossible to maintain T_p below T_{max} after 14.5 h, whatever the PCM mass used. If it is necessary to achieve a longer transport period under this ambient temperature, a

better-insulated box is needed.

Equations 4.15 and 4.16 can be used only under constant external temperature. For varying ambient conditions, the direct approach should be used by solving t_{melt} or t_{max} for various PCM masses, then interpolating to determine the required amount at the targeted period (Figure 4.9).

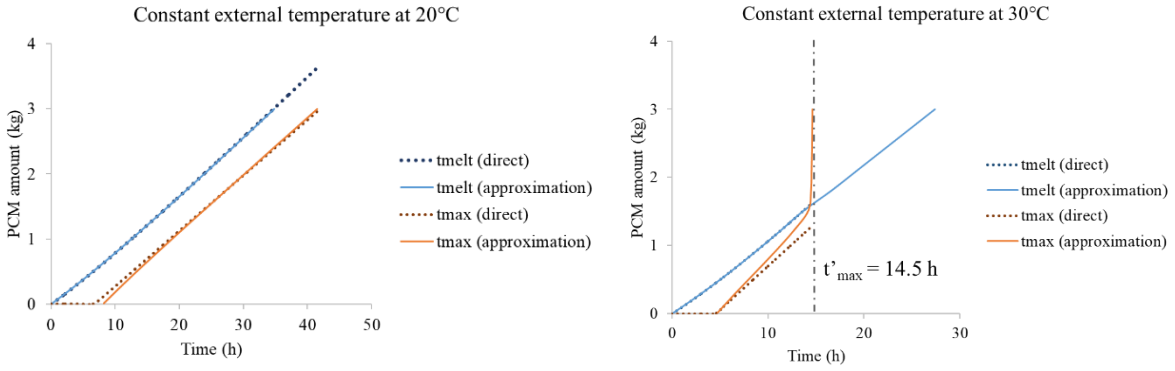

(a) (b)

Figure 4.9 Required PCM amount (orange curves) as a function of the maximum storage period (t_{max}) for a maximum product temperature of 8°C by direct calculation and approximation under (a) constant 20°C ambient temperature, and (b) constant 30°C ambient temperature. The product and PCM initial temperatures were 4°C and -2°C, respectively. The blue curves also indicate the melting period (t_{melt}).

3.3 Effect of the box insulation

Box insulation is the main criterion for transport performance in an insulated box with PCM as emphasized by several studies (Du et al., 2020; Leungtongkum et al., 2023b; Margeirsson et al., 2011; Paquette et al., 2017). Equations 4.5, 4.9 and 4.11 describe the relationship between the box insulation (via thermal resistances) and product temperature evolution, product temperature at equilibrium and PCM melting rate, respectively.

Figure 4.10 shows the impact of different types of box insulation on the product temperature evolution and the amount of melted PCM. The demonstrated boxes are: reference box (polyurethane with a thickness of 40 mm, K = 0.58 $W{\cdot}m^{-2}{\cdot}K^{-1}$), box with a vacuum-insulated panel (VIP box, vacuum-insulated panel with a thickness of 20 mm, and polyurethane with a thickness of 20 mm, K = 0.17 $W{\cdot}m^{-2}{\cdot}K^{-1}$) (Kacimi & Labranque, 2011), and our experimental box shown in Figure 4.2 (Exp box, K = 0.90 $W{\cdot}m^{-2}{\cdot}K^{-1}$).

From Figure 4.10, box insulation exerted a significant impact on temperature change in an insulated box. The box with less effective insulation (higher K value) led to a higher rate of temperature rise since the characteristic time (τ) was lower (12.6 h and 10.6 h for the reference box and the experimental box, respectively) and the

equilibrium temperature ($T_{p.eq}$) was higher (6.6°C and 8.6°C for the reference box and experimental box, respectively) (Figure 4.10a). The product temperature was reduced in the box with better insulation (VIP) as the equilibrium temperature ($T_{p.eq}$ = 2.5°C) was lower than the initial product temperature (4°C). A higher PCM melting rate was also observed in a box with a higher K value (Figure 4.10b).

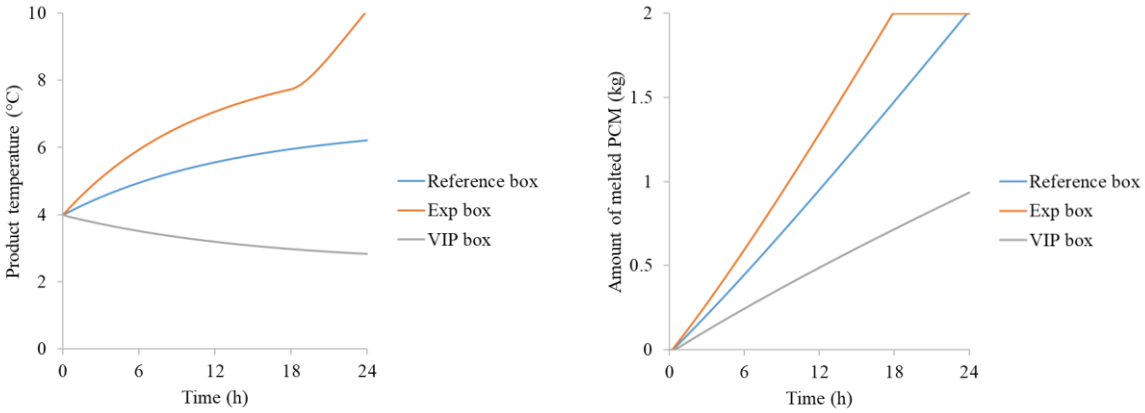

(a) (b)

Figure 4.10 Effect of box insulation on: (a) average product temperature evolution; and (b) the amount of melted PCM estimated by the lumped model. The initial product and PCM temperatures were 4°C and -2°C, respectively

3.4 Effect of melting temperature and latent heat of PCM

Cold energy storage by the PCM is another key factor enabling a low temperature to be maintained in an insulated box (Yang et al., 2021). There are numerous PCM materials to choose from, e.g., water, salt solution, salt hydrate, paraffin, commercially available PCM (Oró et al., 2012a). Each one has different thermophysical and chemical properties. The main concerns for transport are the PCM melting temperature and its latent heat. The melting temperature determines the equilibrium temperature inside the box (Equation 4.9) and the latent heat determines the time interval during which the PCM can provide cold (Equation 4.11).

Figure 4.11 demonstrates, by simulation, the impact of the PCM material on the product temperature ($T_{p.0}$ = 4°C) and the melted PCM mass evolution assuming that the PCM is not completely melted. Three PCM materials were chosen for comparison: ice (T_m = 0°C and L_f = 333700 J·kg^{-1}), an eutectic Mg_2SO_4 solution (T_m = -3.9°C and L_f = 264400 J·kg^{-1}) and K_2HPO_4 salt hydrate (T_m = 4°C and L_f = 109000 J·kg^{-1}) (Cengel & Ghajar, 2020; Li et al., 2013; Sharma et al., 2009). It can be seen that using ice and K_2HPO_4 salt hydrate led to a product temperature increase since the equilibrium temperature for each PCM was 6.6°C and 9.3°C for ice and salt hydrate, respectively. Despite the same characteristic time in each case, the temperature rise in the box with salt hydrate was the highest. The box filled with eutectic PCM did not show a temperature change as $T_{p.eq}$ = 4°C, i.e. the same value as the initial product temperature.

The increase in melted PCM mass is inversely related to its latent heat, e.g., ice melts at the lowest rate compared with the other two.

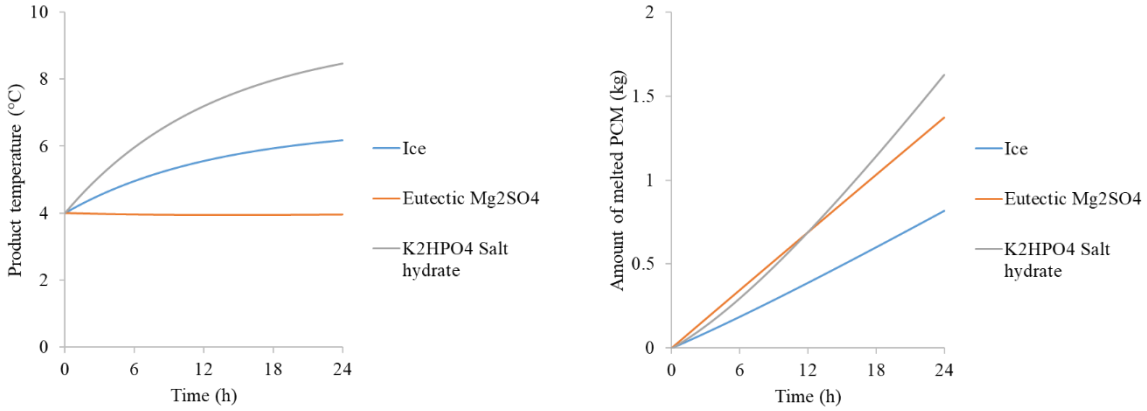

(a) (b)

Figure 4.11 Effect of the PCM type on: (a) product temperature evolution; and (b) PCM melted mass evolution calculated by the lumped model; the product initial temperature was 4°C

3.5 Effect of product mass and thermophysical properties

As explained previously, the thermal inertia of the product plays an important role in the temperature evolution and PCM melting rate. Two aspects can be considered: product mass and the thermophysical properties of the product.

Figure 4.12a shows the influence of salmon mass (4, 8 and 16 kg) on the product temperature evolution, and Figure 12b shows the influence of the nature of the product (salmon, butter and milk); thus, the specific heat varied: salmon (C_p = 3360 $J{\cdot}kg^{-1}{\cdot}K^{-1}$), butter ($C_p$ = 2080 $J{\cdot}kg^{-1}{\cdot}K^{-1}$), and milk ($C_p$ = 3960 $J{\cdot}kg^{-1}{\cdot}K^{-1}$) (Cengel & Ghajar, 2020). It was found that higher thermal inertia, i.e., a higher mass and/or higher specific heat led to a lower temperature change as it allowed a higher characteristic time (τ) (defined in Equation 4.6). The impact of thermal inertia on the PCM melting rate follows the same trend as that of temperature evolution (results not shown). The conditions with the lowest thermal inertia (4 kg of salmon and 16 kg of butter in Figures 4.12a and 4.12b, respectively) resulted in the lowest PCM melting time, so the product temperature sharply increased at the end of the simulation, implying that the PCM was completely melted.

Changing the product mass also affects the occupied volume in the box, which in turn may impact internal convective heat transfer, hence, the thermal resistance between the product and PCM ($R_{p/pcm}$). Caution must also be taken if the product is too large since in this case it obstructs the internal airflow by natural convection (Leungtongkum et al., 2023a).

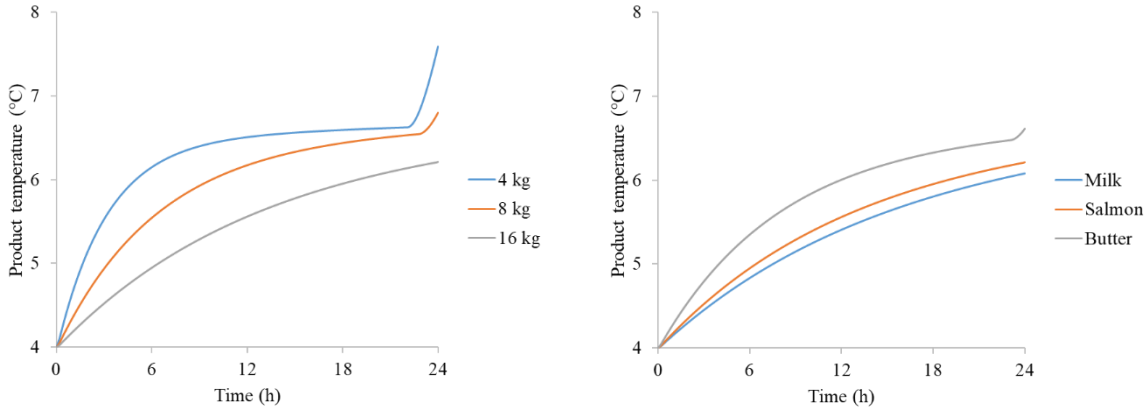

(a) (b)

Figure 4.12 Effect of: (a) a mass of salmon, and (b) the nature of the product (16 kg of salmon, butter or milk) on the product temperature evolution calculated by lumped model for a PCM mass of 2 kg. The product and PCM initial temperatures were 4°C and -2°C, respectively.

3.6 Effect of internal radiation

Since heat exchange by conduction, natural convection and radiation in a cavity with cold and warm surfaces are of the same order of magnitude (Laguerre & Flick, 2010), the inclusion of all these heat transfer modes can improve the accuracy of the thermal model. It is to be highlighted that the lumped model could not take radiation into account as it does not apply the difference between the surface and the internal temperatures. Consequently, only the zonal model is used for demonstration purposes.

Figure 4.13 compares the impact of the internal wall and the PCM surface emissivity on the product core temperature at steady state. Three wall emissivity configurations were numerically studied: case 1: box and PCM walls were bright (ε = 0.03, polished aluminum); case 2: box walls were bright (ε = 0.03) while the PCM wall was not (ε = 0.97, polypropylene); case 3: none of the walls were bright (ε = 0.97). The highest core temperature was observed in case 1; indeed, when every surface was bright, the heat flux from ambient to the product was reduced, but the heat flux from the PCM to the product decreased to a greater extent. The lowest core temperature was observed in case 2; in this manner, the transfer from ambient to product to ambient was reduced but not the transfer from the PCM to the product. These predictions were confirmed by an experiment undertaken by covering different walls with aluminum foil.

The results presented in Figure 4.13 confirm that internal radiation must be taken into account for food transport in an insulated box with PCM to prevent temperature abuse.

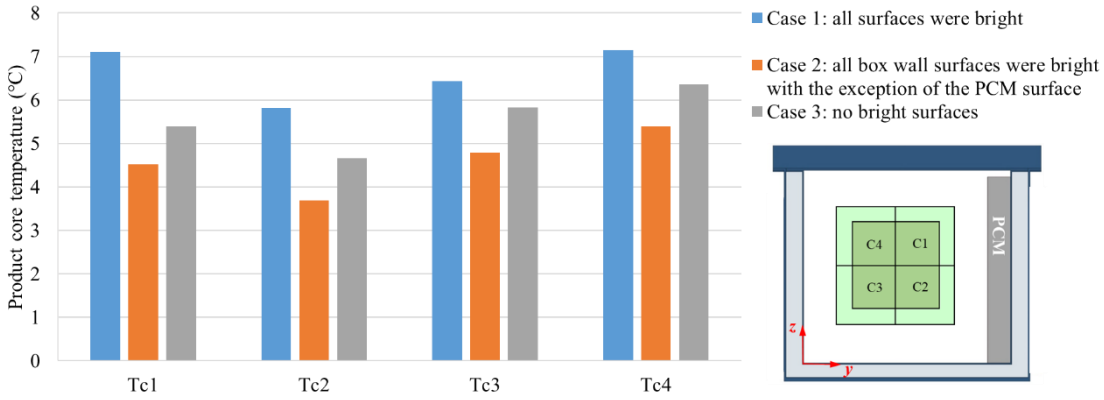

Figure 4.13 Effect of internal emissivity on the product core temperature in an insulated box with PCM on a side wall predicted by the zonal model under steady state

3.7 Modelling approaches for a box with PCM at the top

The position of the PCM is another factor that affect temperatures in an insulated box (Du et al., 2020). However, the lumped model previously developed for the box with PCM on a side wall cannot directly apply when the PCM is at the top. In fact, when the PCM position is changed, thermal resistances are changed as well, and this results in different product temperature equilibria. According to our experiment using the box loaded with the product under 20°C ambient conditions, the product equilibrium temperature decreased from 8.6°C (PCM on a side wall) to 8.2°C (PCM at the top). Hence, the zonal model and the CFD model are used to study the impact of the PCM position in this section.

3.7.1 Zonal model

The assumption of airflow pattern in an insulated box is essential for zonal model development; thus, the model is posteriori. Changing the PCM location and consequently the airflow pattern leads to different heat transfer and heat balance equations.

Our previous experimental data showed that airflow and temperature fields in an insulated box loaded with the product and with PCM at the top are asymmetrical in spite of the geometrical symmetry (Leungtongkum et al., 2023a). Thus, two zonal model approaches are demonstrated and compared in this section. First, we applied the same heat transfer and airflow as those previously developed for the insulated box with PCM on a side wall by redefining the state variables (Figure 4.14a). Another approach was developed from a preliminary result of 2D CFD in a rectangular cavity with a cold surface at the top. The CFD results indicated two airflow loops in a loaded box; thus, the heat transfer and airflow diagram were modified (Figure 4.14b). There is a primary airflow loop (black continuous line in Figure 4.14b) with a mass flow rate of $\dot{m}_a$ and a secondary airflow loop (black dashed line in Figure 4.14b) of $\delta\dot{m}_a$. The air mixing is estimated to be at point 1 located at the mid-height of the box, while the

heat transfer by conduction, convection and radiation were identical to those obtained with the previous model.

The zonal model and the adapted zonal model gave good agreement with the average experimental values obtained at 24 positions (internal walls, internal air and product) with a root mean square error of 0.83°C and 0.79°C, respectively. Figure 4.14c shows the comparison between the experimental product core temperature and that predicted by each model. It was found that the adapted zonal model gave a slightly better prediction of the product core temperature.

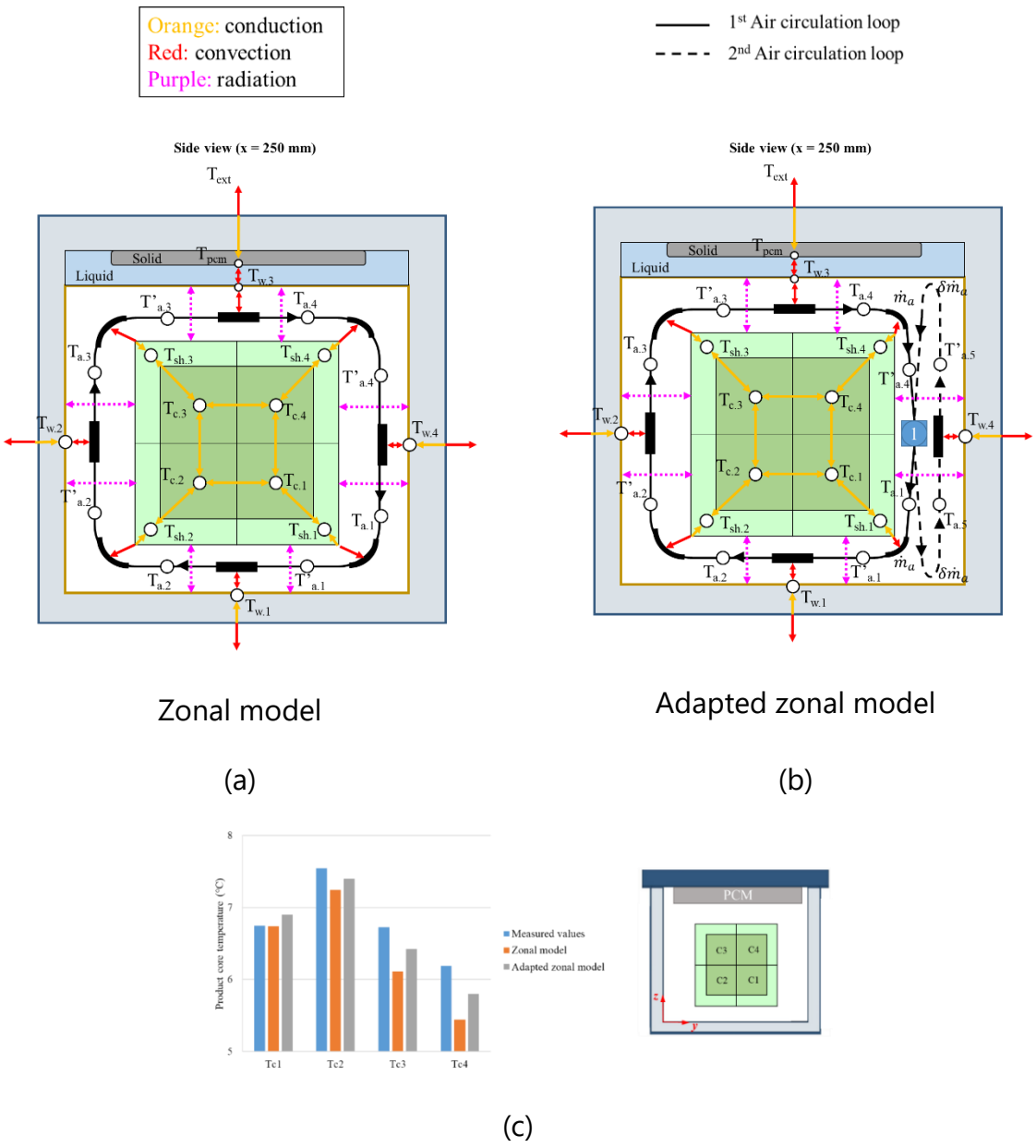

Figure 4.14 Heat transfer and airflow diagram in a 2D insulated box with PCM at the top for (a) the zonal model; (b) the adapted zonal model; and (c) comparison between the average core temperature at 4 measured positions and numerical values under steady state using an experimental box

3.7.2 CFD model

Since CFD model algorithm directly solves Navier-Stokes and energy partial differential equations at each position (Söylemez et al., 2021), so the model is priori, i.e., the users do not need assumptions on physical phenomena to develop this model. Thus, it can directly demonstrate the impact of PCM position in an insulated box in which the airflow is initially unknown, unlike the zonal model.

Figure 4.15 illustrates the CFD results of air velocity and temperature fields on the middle plane of a loaded insulated box with PCM at the top. The air flows from the right to the left above the load. The anti-clockwise circulation loop explains the lower temperature in the left gap because of the downward flow coming from the PCM. It shows that the downward flow takes place in one or another preferential pathway (either the left or right gap). This result confirms that despite symmetrical geometry, the airflow is asymmetrical; hence, it leads to an asymmetrical temperature field. This is due to the non-linear term in Navier-Stokes equations resulting in a symmetry rupture (even before turbulence appears).

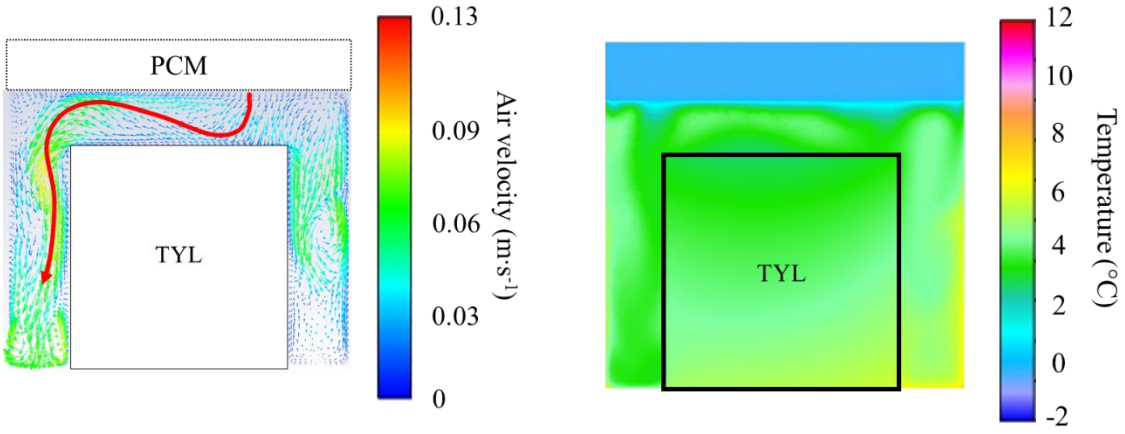

(a) (b)

Figure 4.15 CFD results at t = 6 h of (a) air velocity field; and (b) temperature field on the middle plane of a box loaded with test product (TYL) initially at 4°C and with PCM at the top

3.8 Detailed airflow pattern and effect of product compactness

As previously discussed, the CFD model can provide the detailed airflow and heat transfer phenomena without knowledge of model assumptions. This information is necessary to fully understand the phenomena, especially for complex configurations, e.g. irregular product shape, porous product and PCM on several surfaces.

Figure 4.16a shows the airflow pattern in the air gap near the PCM located on a side wall of an insulated box with PCM (y = 245 mm). Air flows downwards and toward the lateral walls in this gap. Figure 4.16b shows a lateral view (x =15 mm): air flows from the left (near the PCM) to the right (near the lateral walls). These figures confirm that

there is 3D airflow as illustrated in Figure 4.16c: air flows downward near the cold wall (PCM) and toward the side walls; then it flows upward along the opposite wall and returns near the PCM. The CFD model can also be used for more complex configurations by simply changing the input geometry.

The product to be transported in food cold chains can vary in its compactness related to the nature of the product and/or packaging geometry. Since internal convective heat transfer cannot be neglected, different levels of compactness lead to different heat transfer coefficients between the internal air and the product surface. (Laguerre et al., 2008b) conducted CFD simulation for a porous load (spherical fruits or vegetables). They compared the simulation results of two approaches: a direct approach with meshing of all the product items, or a porous media approach. Both approaches gave good agreement with the experimental data.

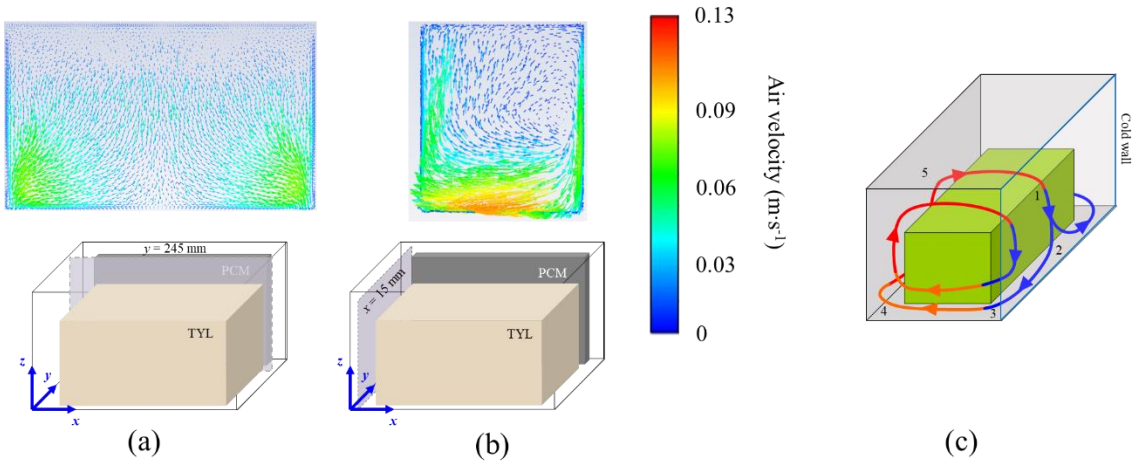

Figure 4.16 CFD results of air velocity field at t = 24 h (a) near an PCM surface, y = 245 mm (b) near lateral wall, x = 15 mm, and (c) 3D airflow illustration (in a loaded box with PCM on a side wall)

3.9 Effect of box dimensions

The boxes used in food transport can vary in volume and aspect ratio (*H/L*). Figure 4.17a shows the effect of different aspect ratios of the box on the average load temperature evolution. In the case of the same percentage of occupied volume inside the box, changing the aspect ratio did not affect the average temperature evolution. Thus, the same characteristic time (τ) was obtained. Figure 4.17b shows the temperature evolution at the cold and warm points for different *H/L*. Increasing *H/L* caused greater thermal stratification with temperature differences between the cold and warm points at 24 h of 1.5°C and 2.3°C for the box with *H/L* = 1.1 and 1.7, respectively (see the warm and cold points in Figure 4.17c).

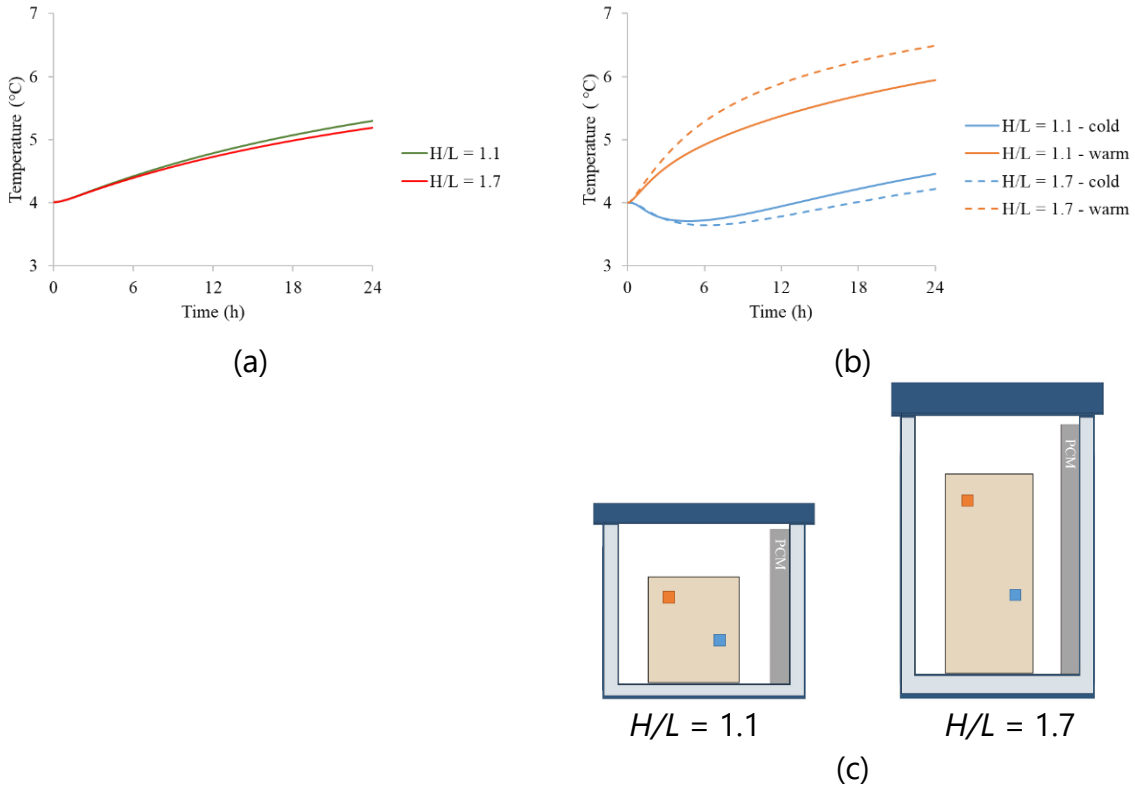

Figure 4.17 The effect of the aspect ratio (*H/L*) of the box on: (a) average load temperature evolution; and (b) load temperature evolution at the coldest and warmest points; (c) position of the coldest (■) and warmest (■) points.

3.10 Prediction of quality change and sanitary risk during transport

Many studies have combined thermal models that predict the temperature evolution in different steps throughout the cold chain with quality and microbial growth models (García et al., 2022; Matar et al., 2020; Onwude et al., 2022; Penchaiya et al., 2020). This section highlights the possibility and limitations governing the use of the thermal models we developed to predict food quality alterations in a cold chain during which the ambient temperature may vary with time. In fact, if the practical objective is to evaluate the influence of the ambient temperature variability in the cold chain on the product through a Monte Carlo process (Duret et al., 2019), a CFD model might not be appropriate because of the high calculation costs. Although some studies combined a quality model with a CFD model, they focused only on certain operating conditions in a given cold facility (Wu & Defraeye, 2018). These studies cannot be applied when the full variability of the operating conditions in the entire cold chain must be taken into account.

In this section, we present the coupling of a predictive *Listeria monocytogenes* growth model (given that such growth may occur during cold storage and transport) with the lumped model for fresh salmon transport in an insulated box with PCM on a side wall. The first-order equation was used to describe the growth of *L. monocytogenes* taking into account the lag time as follows (Baranyi & Roberts, 1994; Jia et al., 2020).

$$\frac{dY}{dt} = \frac{1}{1 + e^{-E}} \times \eta_{max} \quad (4.18)$$

where Y is the amount of *L. monocytogenes* [$\log_{10}$ CFU·g^{-1}]

E, the physiological state of the *L. monocytogenes* [-], can be described by Equation 4.19. $$\frac{dE}{dt} = \eta_{max} \quad (4.19)$$

where $\eta_{max} = \eta_{ref}\left(\frac{T - T_{min}}{T_{ref} - T_{min}}\right)^2$ (4.20)

For *L. monocytogenes*: η_{ref} = 0.183 h^{-1}, T_{min} = -2°C and T_{ref} = 25°C (Baranyi & Roberts, 1994; Jia et al., 2020)

At t = 0: E_0 = -1.05 (4.21)

Figure 4.18 shows the evolution of PCM and the product (fresh salmon) temperatures and the growth of *L. monocytogenes* on the average under varying ambient temperatures adapted from Fioretti et al. (2016). This figure indicates that an increase of *L. monocytogenes* corresponded to its temperature evolution. When PCM was melting ($t \leq 23$ h), the product temperature increased slowly even during a drastic change in ambient temperature (10 h < t < 23 h); thus, microbial growth was low (0.11 $\log_{10}$ CFU·g^{-1} increase during the first 23 h). When the PCM was completely melted ($t >$ 23 h), the product temperature increased rapidly, and this led to a sharp increase in *L. monocytogenes*, and growth reached 0.7 $\log_{10}$ CFU·g^{-1} at 48 h. Thus, it is essential to place sufficient PCM mass in the box to prevent microbial growth.

Regarding the sanitary risk, if the objective is to conduct a quantitative microbial risk assessment (QMRA) of fish product, e.g., the risk from *L. monocytogenes*, then the zonal model should be used. Indeed, the results of listeriosis cases in the *L. monocytogenes* QMRA model are linked to the extreme right values of the exposure distribution (Pouillot et al., 2009) corresponding to risky situations. Hence, the thermal model used to predict the risk of listeriosis must indicate the temperature heterogeneity inside the box, since several sensitivity analysis studies highlighted the impact of temperature variability on the risk associated with exposure to *L. monocytogenes* (Duret et al., 2014; Ellouze et al., 2010).

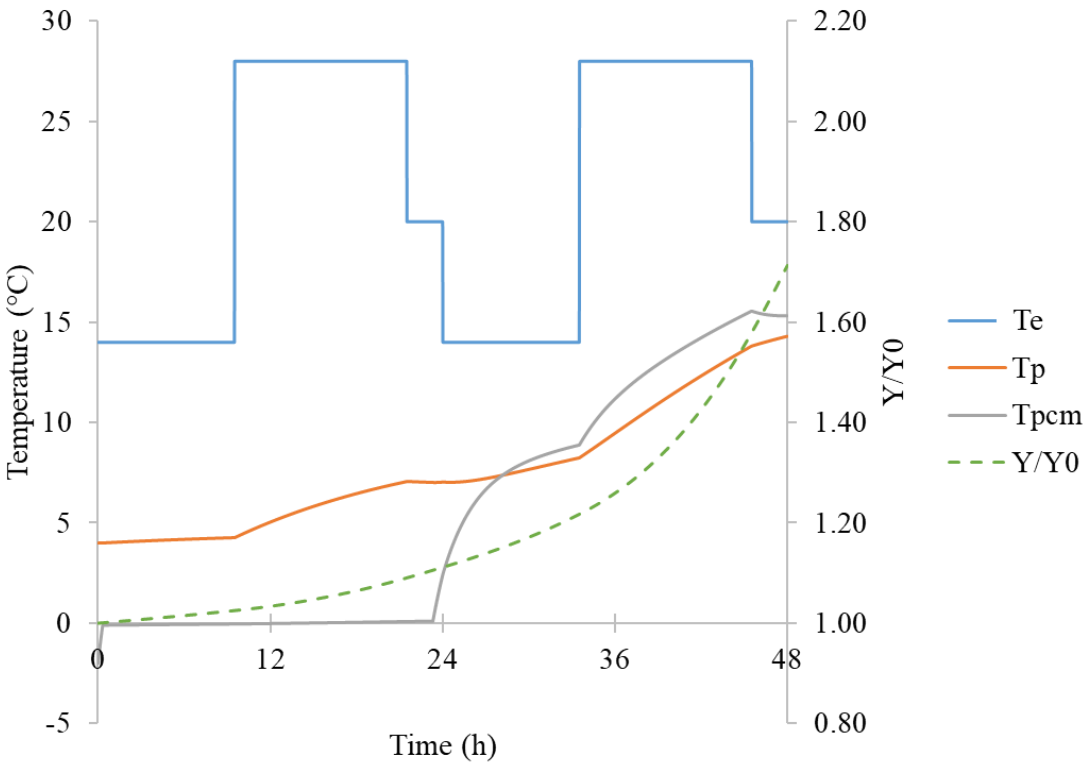

Figure 4.18 Product (fresh salmon), PCM temperature evolution and *L. monocytogenes* (Y/Y_0) increase on the average under varying ambient temperatures (T_e); the initial product and PCM temperatures were 4°C and -2°C, respectively

3.11 Applications and limitations of each thermal model

The demonstrations of thermal model applications to design the box, choose the product and PCM arrangement have been discussed in depth using different models. Table 4.4 summarizes the characteristics of the models presented in this article in terms of input parameters, computational resources, outputs and model flexibility. To develop the model, the users need to establish the airflow and heat transfer assumptions in order to develop a zonal model, whereas this is not the case for CFD model development.

All models require information on the box, PCM and product dimensions and thermophysical properties. An additional experiment (or a CFD simulation) is needed to estimate the thermal resistance between the product and PCM ($R_{p/pcm}$) to develop a lumped model, since this value depends on the PCM and product arrangement inside the box. The zonal model requires an estimation or an experiment to determine the convective heat transfer coefficient (h) and the air mass flow rate ($\dot{m}_a$).

The lumped model and zonal model can be coded and solved with a free-licensed coding program such as Python, and do not require high computing resources; they can be solved in less than 1 minute. On the contrary, solving the CFD model requires a licensed program and experts to operate it. A CFD model also requires a longer

calculation time, so it may not be suitable for investigating in real time the effect of box design combined with the operating conditions.

The lumped model can provide the temporal evolution inside the box but cannot provide spatial variations. The zonal model and the CFD model give more details on temperature heterogeneity during transport.

To summarize, one has to bear in mind that a complex model might not provide more information (Zwietering, 2009). The choice of the model is then dependent on the application and the users.

Table 4.4 Advantages and limitations of each model

Criteria	Lumped model	Zonal model	CFD model
Airflow and heat transfer assumptions	Not applicable	+ (Posteriori)	- (Priori)
Number of input parameters	11	17	16
Preliminary experiments	+	±	-
Number of estimated parameters	1	3	-
Computing resource required*	Less than 1 minute using Python	Less than 1 minute using Python	More than 3 days using Ansys Fluent
Temporal evolution	+	+	+
Spatial temperature variation	-	+	+
Model flexibility	+	++	+++

*For calculating a 24 h transport duration with a reference box (45 L) using a computer with 64GB RAM

4. Conclusion

Three validated thermal models (lumped, zonal and CFD models) demonstrated their ability to answer practical questions arising during food transport using insulated boxes with PCM. The lumped model, which predicts the average product temperature, can be used to illustrate the temporal evolution, to estimate the PCM amount required to maintain the product temperature (on the average) under the recommended values for a given period. This model can also be used to determine the effect of box insulation, PCM material, product mass and nature. The lumped model does not require high computing resources and it can be used as long as the PCM and product

arrangement are identical to that used in the experiment undertaken for model validation. The zonal model can give a greater insight into heat transfer and airflow. This model does not need high computing resources, but it requires estimations of input parameters relating to internal heat transfer and airflow. The model can be adjusted for different PCM and product arrangements by relying on knowledge of heat transfer and airflow phenomena. The CFD model gives the most thorough comprehension of all physical phenomena occurring during transport without any assumptions, but the computational cost is high. To predict quality change and the sanitary risk by coupling predictive models with previously presented models, the practical objectives must be clear, since different models provide different insights and have different limitations. Studies on the application of these models to predict the evolution under real transport conditions can be useful for developing better boxes and guidelines on efficient transport to avoid temperature abuse.

Appendix 1: Governing equations of the zonal model

Estimation of air temperatures from product shell and wall temperatures

The air at position I in Figure 4.4 successively exchanges heat with wall 1 (PCM surface) and its temperature alters from $T'_{a.1}$ to $T_{a.2}$. The heat balance between the adjacent air and wall 1 can be shown as follows.

$$\dot{m}_a C_{p.a} dT_a = h_w (T_{w.1} - T_a) dA$$

By integration: $$(T_{a.2} - T_{w.1}) = \alpha_{w.1} (T'_{a.1} - T_{w.1}) \qquad \text{(A.1)}$$

$$\text{with } \alpha_{w.1} = exp\left(-\frac{h_w A_{w.1}}{\dot{m}_a C_{p.a}}\right)$$

Where $\dot{m}_a$ is the mass flow rate of air [kg·s^{-1}]

$C_{p.a}$ is the specific heat capacity of air [J·kg^{-1}·K^{-1}]

h_w is the heat transfer coefficient between the internal air and the internal wall [W·m^{-2}·K^{-1}]

$A_{w.1}$ is the area of wall 1 [m^2]

$\alpha_{w.1}$ is the dimensionless convective heat transfer coefficient between the internal air and the internal wall 1 [-]

When air exchanges heat with the product shell, the same approach is also applied, for instance from $T_{a.2}$ to $T'_{a.2}$. Thus, eight linear equations involving the eight air temperatures are obtained which make it possible to estimate the air temperatures from the product shell and box wall temperatures. Full details concerning the estimation of the convective heat transfer coefficient and air mass flow rate can be found in (Leungtongkum et al., 2023b).

Transient evolution of product, walls, and PCM

Equation A.2 is the unsteady heat balance equation for the shell of the product block 1 ($T_{sh.1}$).

$$MC_{p.sh}\frac{dT_{sh.1}}{dt} = \dot{m}_a C_{p.a}(T_{a.1} - T'_{a.1}) + \frac{T_{c.1} - T_{sh.1}}{R_{sh.c}} - q_{r.s1.w1} - q_{r.s1.w4} \qquad \text{(A.2)}$$

Where $MC_{p.sh}$ is the thermal inertia of the product shell [J·K^{-1}]

$R_{sh.c}$ is the heat transfer resistance from the shell to the core of the product [K·W^{-1}]

$q_{r.s1.w1} = \varepsilon_{w.1}\sigma\left({T_{s.1}}^4 - {T_{w.1}}^4\right)CL$ is the radiative heat exchange between the surface of product block 1 and wall 1 [W]

$q_{r.s1.w4} = \varepsilon_{w.1}\sigma\left({T_{s.1}}^4 - {T_{w.4}}^4\right)CL$ is the radiative heat exchange between the surface of product block 1 and wall 4 [W]

The same approach was applied to the 12 solid zones: the shells of the product blocks, the cores of the product blocks and box internal walls.

PCM temperature and ice fraction evolution can be written as for the lumped model (Equations 4.10 to 4.12) except that the PCM exchanges heat with wall 1 which is in fact a PCM-plate wall, not directly with the product.

Appendix 2: Governing equations of the CFD model

For air, laminar flow caused by natural convection is applied (the parameters without index in this section are for air and ρ is the air density at the reference temperature):

Continuity: $\nabla \cdot (\rho\vec{v}) = 0$ (A.3)

Energy: $\frac{\partial}{\partial t}\left(\rho C_p T\right) + \nabla \cdot \left(\rho\vec{v}C_p T\right) = \nabla \cdot (\lambda \nabla T)$ (A.4)

Momentum: $\frac{\partial}{\partial t}(\rho\vec{v}) + \nabla \cdot (\rho\vec{v}\vec{v}) = -\nabla P + \nabla \cdot (\mu\nabla\vec{v}) + \rho\beta\left(T - T_{ref}\right)\vec{\mathrm{g}}$ (A.5)

For PCM, the approach proposed by Rahimi-Khoigani et al. (2023) was used. PCM is assumed to be solid below T_{sol}, liquid above T_{liq} and in a mushy state between T_{sol} and T_{liq}. The fraction of melted PCM (θ) is given by Equation A.6. The internal energy (u_{pcm}) of PCM is given by Equation A.7.

$$\theta = \begin{cases} 0 & T_{pcm} < T_{sol} \\ 1 & T_{pcm} > T_{liq} \\ \frac{T_{pcm} - T_{sol}}{T_{liq} - T_{sol}} & T_{sol} \le T_{pcm} \le T_{liq} \end{cases} \qquad \text{(A.6)}$$

$$u_{pcm} = \int_{T_{ref}}^{T} C_{p.pcm}dT_{pcm} + \theta L_f \qquad \text{(A.7)}$$

When PCM is completely melted (θ = 1), standard free convection laminar flow equations apply. In the mushy state (0 < θ < 1), flow is limited by a momentum source term (the opposite to PCM velocity). When PCM is completely solid (θ = 0), this source term becomes very high so that the PCM velocity disappears.

Continuity: $\nabla \cdot \left(\rho_{pcm}\vec{v}_{pcm}\right) = 0$ (A.8)

Energy: $\frac{\partial}{\partial t}\left(\rho_{pcm}u_{pcm}\right) + \nabla \cdot \left(\rho_{pcm}\vec{v}_{pcm}u_{pcm}\right) = \nabla \cdot \left(\lambda_{pcm}\nabla T_{pcm}\right)$ (A.9)

Momentum:

$\frac{\partial}{\partial t}\left(\rho_{pcm}\vec{v}_{pcm}\right) + \nabla \cdot \left(\rho_{pcm}\vec{v}_{pcm}\vec{v}_{pcm}\right) = -\nabla P + \nabla \cdot \left(\mu_{pcm}\nabla\vec{v}_{pcm}\right) + \rho_{pcm}\beta_{pcm}\left(T - T_{ref}\right)\vec{\mathrm{g}} + \vec{S}$ (A.10)

where $\vec{S} = -\frac{(1-\theta)^2}{(\theta^3+\epsilon)}B_{mush}\vec{v}_{pcm}$ (A.11)

ϵ is a small number (0.001) to prevent division by zero
B_{mush} is the mushy zone constant [kg · m^{-3} · s^{-1}] which is 10^5 in our calculation

For the test product (Tylose), conduction alone is applied:

Energy: $\frac{\partial}{\partial t}\left(\rho_p C_{p.p} T\right) + \nabla \cdot \left(\rho_p C_{p.p} T\right) = \nabla \cdot \left(\lambda_p \nabla T\right)$ (A.12)

The following boundary conditions were applied:

At the internal box walls, the following momentum and thermal conditions were applied:

No slip boundary condition: $\vec{v} = 0$ (A.13)

Cauchy type thermal boundary condition: $K(T_e - T) = \lambda\nabla T \cdot \vec{n} + \hat{q}_{rad}$ (A.14)

where K is the overall heat transfer coefficient [W · m^{-2} · K^{-1}]

and $\hat{q}_{rad} = -\varepsilon\sigma T^4 + (1-\varepsilon)\hat{q}_{in}$ (A.15)

with ε is the wall emissivity [-]

Since air is considered as transparent (optical thickness = 0), so surface-to-surface radiation was activated, and the radiative flux entering the surface *k* coming from all the other surfaces *j* was calculated from

$\hat{q}_{in.k} = \sum_j F_{jk}\hat{q}_{rad.j}$ (A.16)

The external area of the box is higher than the internal one; thus, the geometric mean of an external and internal area must be used to obtain the overall heat balance. Since the boundary condition applies on the internal wall, *K* in governing equations is corrected by a factor of $\sqrt{A_e/A_i}$ for the CFD approach.

5 GENERAL CONCLUSIONS AND PERSPECTIVES

5.1 GENERAL CONCLUSIONS

This Ph.D. thesis aimed to characterize experimentally heat transfer and airflow in an insulated box with Phase Change Material (PCM) loaded with product. Three thermal models with different complexity, from basic to advanced, were also developed in order to predict the product temperature evolution in function of box characteristics (wall thermal conductivity and thickness), PCM type (i.e. cold storage capacity and melting point), PCM mass and position, load characteristics (food nature, mass and arrangement), and operating conditions (ambient temperature and duration). The developed experimental and modelling approaches could help the manufacturers to design the box and the stakeholders to preserve food quality during delivery.

5.1.1 Experimental study

To our knowledge, this study is the first which characterizes airflow by natural convection in an insulated box equipped with PCM by Particle Image Velocimetry (PIV) in addition to temperature measurements. Few data about airflow was available in literature in such configuration due to the difficulty of measuring very low velocities in non-isothermal systems. The study was conducted on cases of progressive complexity: empty, loaded with extruded polystyrene (low conductivity and almost no thermal inertia), and loaded with test product (Tylose, thermal properties close to those of meat). The influence of several parameters were studied to investigate the effect of use conditions: aspect ratio of the box (height/width), PCM amount and position, ambient temperature, initial product temperature and spacing beneath the product. A much better understanding of the phenomena could be obtained by analyzing jointly both air velocity and temperature fields.

Whatever the configurations, the highest measured air velocities were around 0.1 $m \cdot s^{-1}$; thus, convection cannot be neglected compared to conduction in air (Peclet number > 100). This experimental observation was useful for the numerical model development by considering natural convection and conduction.

When the PCM was on the side wall, circular airflow was observed: air flows downwards along the PCM surface and upwards along the side walls. In the empty case, the flow pattern can be approximated by a 2D recirculation cell, but the presence of the load leads to a 3D flow pattern whatever the presence or absence of gap beneath the load. The coldest position is at the bottom, close to the PCM surface, and the warmest one is at the top close to the opposite vertical wall. When the PCM is at the top, air stream is cooled down after contacting PCM surface and flows downwards. Unstable airflow was observed in the empty case and preferential pathways (with symmetry breaking) was showed in the loaded case. The lowest product temperature was always located

at the top, while the highest one was at the bottom, and slightly lower air and product temperatures were observed comparing with the box with PCM on the side wall.

In all cases, after cooling down near the PCM, the air temperature increases progressively along the trajectories until returning close to the PCM. The product surface temperatures are close to the temperature of the adjacent air. At steady state, conduction in the load has a minor effect on the flow pattern, thus, the real food load can be replaced by an obstacle of low conductivity allowing simpler manipulation.

From practical point of view, it is recommended that the PCM should be placed at the top of the box for better temperature uniformity and the aspect ratio (height/width) of a box should not be too high. To maintain the product temperature along a supply chain, PCM could be placed on all walls (top, bottom, sidewalls); however, the available volume would be significantly reduced and the logistic cost per kg of product would be higher. Our study demonstrates that it is possible to place PCM only at one wall (top or side) if an appropriate PCM mass is used. The required PCM mass can be estimated in function of ambient temperature based on two simple measurements for a given box.

It is to be highlighted that linear extrapolation of the result obtained from one ambient to another is not recommended because of non-linear behavior. Thus, physical based models taking natural convection into account should be developed.

Adding a 20-mm air space beneath the test product neither reduces the test product temperature nor increases homogeneity although this gap allows slightly better air circulation. It is suggested to leave a space between the PCM and the load (to promote natural convection) and between the side walls and the load (to allow evacuation of heat from the ambient through the walls by conduction). The gap should be of the same order of magnitude as the boundary layer thicknesses i.e. about 2-3 cm.

In practice, there are many box designs and operating conditions and the interactions between the different factors are complex. To avoid numerous experiments under specific conditions, numerical models are necessary for investigating the influence of these factors on the spatial and temporal temperature variations for a wide variety of configurations.

5.1.2 Modelling

Three thermal models (lumped, zonal and Computational Fluid Dynamic – CFD) were developed and validated to obtain spatial and temporal temperature variation of air and load, PCM evolution (temperature and melting process) and air velocity. These models have different complexity, thus, suitable for different users from stakeholders to scientists.

Lumped model

The lumped model is based on global thermal resistances between ambience, product and PCM. It considers that the product has a uniform temperature (lumped object) and provides the average temperature evolution and melted PCM mass under constant and variable external temperatures. It gives the required PCM mass in function of the recommended product temperature, box insulation and PCM characteristics for a given transport condition. It can be used to predict the effects of different parameters such as box insulation (heat transmission coefficient) and PCM melting point.

Zonal model

A zonal model was developed for an insulated box equipped with PCM on a side wall and loaded with a rectangular shape product. The model considered that the product is composed of 4 blocks with a shell and a core in each block. A comparison with experimental results under steady and transient states demonstrated good agreement in terms of spatial and temporal temperature variations. This model shows good practical applicability with a short calculation time (less than 10 s using a computer with 64 GB of RAM). As the lumped model, it can predict the effects of different parameters such as box insulation and PCM melting point. Moreover, it can predict the effect of emissivity of internal walls. The zonal model gives the product temperature evolution at different positions inside the box exposed to time-temperature fluctuations during delivery.

In fact, it is possible to develop a zonal model for other configuration such as a box with PCM at the top but other assumptions of heat transfer and airflow are required to develop such model.

CFD model

CFD model of an insulated box equipped with PCM was developed by using ANSYS FLUENT. The model takes into account airflow, conduction, convection and radiation inside the box. The model predicted well the air velocity, air temperature, and product temperature evolution in the box with PCM on a sidewall. However, it gave less accurate results when PCM was located at the top due to flow instability and symmetry rupture, which makes the comparison between measurements (average values) and predictions (instantaneous fluctuating fields) challenging. Nevertheless, this model allows better understanding of the effect of box configurations, e.g., box geometry, box insulation and supply chain conditions (ambient temperature). By including PCM melting model, it can also predict amount of melted PCM evolution.

Model comparison

The three validated thermal models described above (lumped, zonal and CFD models) demonstrated their ability to answer several practical questions arising during food

transport in an insulated box with PCM. It is possible to link one of this thermal models with food quality or microbiological models enabling the evaluation of product quality and safety evolution along a real supply chain. To predict such evolutions, the practical objectives must be well defined since different models provide different insights and have different limitations.

5.2 PERSPECTIVES

5.2.1 Experimental study

The measurement of air velocity and temperature in an insulated box was undertaken separately to avoid the airflow perturbation by thermocouples. The experimental device and the instrumentation technique to be developed in the future should allow the measurement of these two parameters simultaneously to assure the same experimental conditions.

Using the current experimental setup, the air velocity could not be measured in the gap beneath and at the right side of the load due to the inaccessibility of the laser sheet at these positions. This experimental device should be modified to allow a complete air velocity field, thus, better understanding the physical phenomena, especially when PCM is at the top.

The evolution of melted PCM (temperature and liquid velocity field) should be extensively studied to precisely determine the surface temperature of the PCM slab, thus, product temperature at different positions. The influence of the other air gap thickness should be further investigated: between PCM and load, between lateral and top walls and load.

The studied configuration, allowing heat diffusion through all box walls, represents the worst scenario. In practice, the boxes are stacked together in the transport facility, thus, less exchange surface area with air. Further investigation on the influence of the box position in a stack is proposed since this aspect is interesting for the stakeholders.

5.2.2 Modelling

<u>Lumped model</u>

A lumped model considering also water permeability of box walls would be of interest. Regarding reusable boxes, it could be important to verify if the wall physical properties change over time.

<u>Zonal model</u>

The zonal approach developed in this Ph.D. thesis is a 2D model. From the experimental data, the airflow is generally in 3D, so further 3D model should be developed for more accuracy in temperature prediction. Moreover, the warmest

position is often located at the corner of a rectangular shape product, so, including 3D effect is useful for determining the maximum temperature.

CFD model

In practice, food product shapes are irregular and more or less porous, further study including this factor may be useful. By the aid of alternative CFD approach, e.g. immersed boundary condition, the simulation with these irregularities could be more accurate.

These three thermal models were developed assuming homogeneous heat flux from ambience. As cited previously, the model for a stack of boxes should be developed for more precision in temperature prediction.

Other modeling approach

To assess the sanitary risk, probabilistic models should be combined with the thermal models to predict the occurrences of temperature abuse of the whole lot. This approach would help the operators to make decision of actions to be implemented when temperature abuse occurs.

5.2.3 Other technical aspects

To improve the thermal performance, a box equipped with a fan could be used. To our knowledge, it has not yet been commercialized. This type of box would allow airflow by forced convection inside the box, and the temperature would be more homogeneous. A mobile rechargeable battery should supply power to the fan in order to assure its continuous running along the supply chain. After arrival at the end-user's premises, the box could be returned to the distribution center (or the departure site), then the battery could be recharged with optimal power prior to the following delivery. The rechargeable battery and fan design need future development.

For the sake of cold chain sustainability, the extensive use of polystyrene and polyurethane as insulating materials should be replaced by biodegradable materials (cellulose-based and chitosan-based for example), thus exerting less impact on the environment. Also, reusable boxes and a recycling logistic chain should be developed to a greater extent taking into consideration both the economic cost and the environmental impact.

Apart from the box material, PCM also exerts environmental impacts because of the PCM production itself, the production of the insulating material and the energy consumption required for charging the PCM before each use, along with PCM waste etc. Consequently, additional specific studies on these issues are necessary for the sustainability of the use of PCMs.

Chapitre V : Conclusions générales et perspectives

5.1 Conclusions générales

Cette thèse visait à caractériser expérimentalement le transfert de chaleur et l'écoulement d'air dans un caisson isotherme équipé d'un matériau à changement de phase (PCM) chargé de produits. Trois modèles thermiques, de complexité croissante, ont également été développés afin de prédire l'évolution de la température du produit en fonction des caractéristiques du caisson (conductivité thermique et épaisseur de la paroi), du type de PCM (capacité de stockage de froid et point de fusion), de la masse de PCM et de sa position, des caractéristiques du chargement (nature, masse et disposition des aliments) et des conditions de fonctionnement (température ambiante et durée). Les approches expérimentales et de modélisation développées pourraient aider les fabricants dans la conception des équipements et les professionnels intervenant dans la chaîne du froid à mieux préserver la qualité des aliments.

5.1.1 Etude expérimentale

A notre connaissance, cette étude est la première qui caractérise l'écoulement d'air par convection naturelle dans un caisson isotherme équipé de PCM grâce à la Vélocimétrie par Image de Particules (Particle Image Velocimetry PIV) en plus des mesures de température. Peu de données aérauliques étaient disponibles dans la littérature dans une telle configuration en raison de la difficulté à mesurer des vitesses très faibles dans des systèmes non isothermes. L'étude a été menée sur des cas de complexité progressive : vide, chargé de polystyrène extrudé (faible conductivité et quasi-absence d'inertie thermique), et chargé de produit test (Tylose, propriétés thermiques proches de celles de la viande). L'influence de plusieurs paramètres a été étudiée : conditions d'utilisation, forme géométrique de la boîte (hauteur/largeur), quantité et position du PCM, température ambiante, température initiale du produit et espacement sous le produit. Une bien meilleure compréhension des phénomènes a pu être obtenue en analysant conjointement les champs de vitesse d'air et de température.

Quelles que soit la configuration, les vitesses d'air mesurées les plus élevées étaient de l'ordre de 0,1 $m.s^{-1}$; ainsi, la convection ne peut être négligée par rapport à la conduction dans l'air (nombre de Peclet > 100). Cette observation expérimentale a été utile pour le développement des modèles numériques qui doivent considérer à la fois convection naturelle et conduction.

Lorsque le PCM était sur la paroi latérale, un flux d'air circulaire a été observé : l'air circule vers le bas le long de la surface du PCM et vers le haut le long des parois latérales. Dans le cas vide, le schéma d'écoulement peut être approximé par une cellule de recirculation 2D, mais la présence du chargement conduit à un schéma d'écoulement 3D (en présence comme en absence d'espace sous le produit). La position la plus froide est en bas, près de la surface du PCM, et la plus chaude est en haut, près de la paroi verticale opposée. Lorsque le PCM est en haut, le flux d'air est refroidi après avoir été en contact avec la surface du PCM et s'écoule alors vers le bas. Un flux d'air instable a été observé dans le cas vide et des chemins préférentiels (avec rupture de symétrie) dans le cas chargé. La température de produit la plus basse était toujours située en haut, tandis que la plus élevée était en bas. Les températures d'air et de produit légèrement inférieures ont été observées avec PCM sur le haut plutôt que sur le côté.

Dans tous les cas, après refroidissement à proximité du PCM, la température de l'air augmente progressivement le long des trajectoires jusqu'à revenir à proximité du PCM. Les températures de surface du produit sont proches de la température de l'air adjacent. En régime permanent, la conduction dans le chargement a un effet mineur sur le schéma d'écoulement, ainsi, le chargement alimentaire réel peut être remplacé par un obstacle de faible conductivité ce qui permet une manipulation plus simple.

D'un point de vue pratique, il est recommandé de placer le PCM en haut de la boîte pour une meilleure uniformité de température et la forme géométrique de la boîte (hauteur/largeur) du caisson ne doit pas être trop élevé. Pour maintenir la température du produit tout au long d'une chaîne d'approvisionnement, le PCM peut être placé sur toutes les parois (haut, bas, côtés) ; cependant, le volume disponible est alors considérablement réduit et le coût logistique par kg de produit plus élevé. Notre étude démontre qu'il est possible de placer le PCM sur une seule paroi (supérieure ou latérale) si une masse de PCM appropriée est utilisée. La masse de PCM requise peut être estimée en fonction de la température ambiante sur la base de deux mesures simples pour un caisson donné.

Il est à souligner que l'extrapolation linéaire des résultats obtenus pour une température ambiante à une autre n'est pas recommandée en raison d'un comportement non linéaire. Ainsi, des modèles physiques prenant en compte la convection naturelle devraient être développés.

L'ajout d'un espace d'air de 20 mm sous le produit à tester ne réduit ni la température moyenne du produit ni son hétérogénéité, bien que cet espace permette une meilleure circulation de l'air. Il est suggéré de laisser un espace entre le PCM et le chargement (pour favoriser la convection naturelle) et entre les parois latérales et le chargement (pour permettre l'évacuation de la chaleur de l'ambiance à travers les parois par conduction). L'écart doit être du même ordre de grandeur que les épaisseurs de la couche limite, c'est-à-dire environ 2 à 3 cm.

En pratique, il existe de nombreuses conceptions de caissons et conditions de fonctionnement et les interactions entre les différents facteurs sont complexes. Pour éviter de nombreuses expériences dans des conditions spécifiques, des modèles numériques sont nécessaires pour étudier l'influence de ces facteurs sur les variations spatiales et temporelles de température.

5.1.2 Modélisation

Trois modèles thermiques (global, zonal et CFD : Computational Fluid Dynamic) ont été développés et validés pour prédire la variation spatiale et temporelle de la température de l'air et du produit, l'évolution du PCM (température et taux de fusion) et la vitesse de l'air. Ces modèles ont une complexité différente et conviennent donc à différents utilisateurs.

Modèle global

Le modèle global est basé sur des résistances thermiques entre l'ambiance, le produit et le PCM. Il considère que le produit a une température uniforme (lumped objet) et fournit les évolutions de la température moyenne et de la masse de PCM fondu sous des températures externes constantes ou variables. Il donne la masse de PCM requise en fonction de la température du produit recommandée, de l'isolation de la boîte et des caractéristiques du PCM pour une condition de transport donnée. Il peut être utilisé pour prédire les effets de différents paramètres tels que l'isolation du caisson (coefficient de transmission thermique) et le point de fusion du PCM.

Modèle zonal

Un modèle zonal a été développé pour un caisson isotherme équipé de PCM sur une paroi latérale et chargée d'un produit de forme rectangulaire. Le modèle considère que le produit est composé de 4 blocs avec une partie superficielle et un cœur dans chaque bloc. Une comparaison avec les résultats expérimentaux en régimes permanent et transitoire a démontré un bon accord en termes de variations spatiales et temporelles de température. Ce modèle montre une bonne applicabilité pratique avec un temps de calcul court (moins de 10 s avec un ordinateur avec 64 Go de RAM). Comme le modèle global, il peut prédire les effets de différents paramètres tels que l'isolation du caisson et le point de fusion

PCM. De plus, il peut prédire l'effet de l'émissivité des parois internes. Il donne l'évolution de la température du produit à différentes positions à l'intérieur du caisson.

Modèle CFD

Un modèle CFD d'un caisson isotherme équipée d'un PCM a été développé en utilisant ANSYS FLUENT. Le modèle prend en compte le flux d'air, la conduction, la convection et le rayonnement à l'intérieur du caisson. Le modèle a bien prédit l'évolution de la vitesse de l'air, de la température de l'air et de la température du produit dans le caisson avec du PCM sur une paroi latérale. Cependant, il a donné des résultats moins précis lorsque le PCM était situé en haut en raison de l'instabilité de l'écoulement et de la rupture de symétrie, ce qui rend difficile la comparaison entre les mesures (valeurs moyennes) et les prévisions (champs fluctuants instantanés). Néanmoins, ce modèle permet de mieux comprendre l'effet des configurations des caissons (géométrie). En incluant le modèle de fusion du PCM, il peut également prédire la quantité fondue.

Comparaison de modèles

Les trois modèles thermiques validés décrits ci-dessus (modèles global, zonal et CFD) ont démontré leur capacité à répondre à plusieurs questions pratiques se posant lors du transport de denrées alimentaires en caisson isotherme avec PCM. Il est possible de coupler l'un de ces modèles thermiques avec des modèles d'évolution de certains critères de qualité des aliments ou microbiologique permettant d'évaluer l'évolution de la qualité et de la sécurité des produits tout au long d'une chaîne d'approvisionnement réelle. Pour prédire de telles évolutions, les objectifs pratiques doivent être bien définis car différents modèles fournissent des informations différentes et ont des limites différentes.

5.2 Perspectives

5.2.1 Etude expérimentale

Les mesures de la vitesse de l'air et de la température dans un caisson isotherme ont été entreprises séparément pour éviter la perturbation de l'écoulement d'air par les thermocouples. Le dispositif expérimental et la technique d'instrumentation à développer dans le futur devront permettre la mesure simultanée de ces deux paramètres pour assurer les mêmes conditions expérimentales.

En utilisant la configuration expérimentale actuelle, la vitesse de l'air n'a pas pu être mesurée dans l'espace sous et sur le côté droit du chargement en raison de l'inaccessibilité de la nappe laser à ces positions. Le dispositif expérimental devrait être modifié pour permettre un champ complet de vitesse de l'air, permettant ainsi de mieux comprendre les phénomènes physiques, notamment lorsque le PCM est en haut.

L'évolution du PCM fondu (champ de température et de vitesse du liquide) doit être étudiée de manière approfondie pour déterminer avec précision la température de surface de la plaque de PCM (qui elle-même influence la température du produit).

L'influence de la présence de lames d'air doit être étudiée plus avant : entre le PCM et le chargement, entre les parois latérales et supérieures et le chargement.

La configuration étudiée, permettant la diffusion de la chaleur à travers toutes les parois du caisson, représente le pire scénario. En pratique, les caisses sont empilées dans l'installation de transport, d'où moins de surface d'échange avec l'air. Une étude plus approfondie sur l'influence de la position du caisson dans un empilement est proposée car cet aspect est intéressant pour les utilisateurs.

5.2.2 Modélisation

Modèle global

Un modèle global prenant également en compte la perméabilité à l'eau des parois du caisson serait intéressant. En ce qui concerne les caissons réutilisables, il pourrait être important de vérifier si les propriétés physiques des parois changent avec le temps.

Modèle zonal

L'approche zonale développée dans cette thèse est un modèle 2D. D'après les données expérimentales, le flux d'air est généralement en 3D, donc un modèle 3D devrait être développé pour plus de précision dans la prédiction de la température. De plus, la position la plus chaude est souvent située dans un coin du produit, l'aspect 3D est donc utile pour déterminer la température maximale.

Modèle CFD

En pratique, les formes des produits alimentaires sont irrégulières et plus ou moins poreuses, une étude plus approfondie incluant ce facteur peut être utile. À l'aide d'une approche CFD alternative, par ex. condition aux limites immergées, la simulation avec ces irrégularités pourrait être plus précise.

Ces trois modèles thermiques ont été développés en supposant un flux de chaleur homogène provenant de l'ambiance. Comme cité précédemment, un modèle pour un empilement de caissons serait intéressant à développer

Autre approche de modélisation

Pour évaluer le risque sanitaire, des modèles probabilistes doivent être combinés avec les modèles thermiques pour prédire les occurrences de rupture de la chaîne du froid. Cette approche aiderait les opérateurs à prendre des décisions sur les actions à mettre en œuvre.

5.2.3 Autres aspects techniques

Pour améliorer les performances thermiques, un caisson équipé d'un ventilateur pourrait être utilisé. A notre connaissance, ceci n'a pas encore été commercialisé. Ce type de caisson permettrait une circulation d'air par convection forcée à l'intérieur du caisson, et la température serait plus homogène. Une batterie rechargeable mobile devrait alimenter le ventilateur afin d'assurer son fonctionnement continu tout au long de la chaîne d'approvisionnement. Après l'arrivée dans les locaux de l'utilisateur final, le caisson pourrait être retournée au centre de distribution (ou au site de départ), puis la batterie pourrait être rechargée avant la livraison suivante. La conception de la batterie rechargeable et du ventilateur nécessite un développement futur.

Dans un souci de durabilité de la chaîne du froid, l'utilisation intensive du polystyrène et du polyuréthane comme matériaux isolants devrait être remplacée par des matériaux biodégradables (à base de cellulose et de chitosane par exemple), exerçant ainsi un impact moindre sur l'environnement. De même, des cartons réutilisables et une chaîne logistique de recyclage devraient être davantage développés en tenant compte à la fois du coût économique et de l'impact environnemental.

Outre le matériau du boîtier, le PCM exerce également des impacts environnementaux du fait de la production du PCM lui-même, de la production du matériau isolant et de la consommation d'énergie nécessaire pour recharger le PCM avant chaque utilisation, ainsi que des déchets de PCM, etc. Par conséquent, des études spécifiques supplémentaires sur ces aspects sont nécessaires.

REFERENCE

Ahmed, M., Meade, O., & Medina, M. A. (2010). Reducing heat transfer across the insulated walls of refrigerated truck trailers by the application of phase change materials. *Energy Conversion and Management*, *51*(3), 383–392. https://doi.org/10.1016/j.enconman.2009.09.003

Aitlahbib, F., & Chehouani, H. (2015). Numerical study of heat transfer inside a Keeping Warm System (KWS) incorporating phase change material. *Applied Thermal Engineering*, *75*, 73–85. https://doi.org/10.1016/j.applthermaleng.2014.09.035

Alleyne, A. (2023, March 30). *The State of Global Food Security in 2023 – Global Health Council*. https://globalhealth.org/the-state-of-global-food-security-in-2023/

Alzuwaid, F., Ge, Y. T., Tassou, S. A., Raeisi, A., & Gowreesunker, L. (2015). The novel use of phase change materials in a refrigerated display cabinet: An experimental investigation. *Applied Thermal Engineering*, *75*, 770–778. https://doi.org/10.1016/j.applthermaleng.2014.10.028

Alzuwaid, F., Ge, Y. T., Tassou, S. A., & Sun, J. (2016). The novel use of phase change materials in an open type refrigerated display cabinet: A theoretical investigation. *Applied Energy*, *180*, 76–85. https://doi.org/10.1016/j.apenergy.2016.07.088

Aniello, A., Schuster, D., Werner, P., Boussuge, J. F., Gatti, M., Mirat, C., Selle, L., Schuller, T., Poinsot, T., & Rüde, U. (2022). Comparison of a finite volume and two Lattice Boltzmann solvers for swirled confined flows. *Computers & Fluids*, *241*, 105463. https://doi.org/10.1016/j.compfluid.2022.105463

Ataei-Dadavi, I., Chakkingal, M., Kenjeres, S., Kleijn, C. R., & Tummers, M. J. (2019). Flow and heat transfer measurements in natural convection in coarse-grained porous media. *International Journal of Heat and Mass Transfer*, *130*, 575–584. https://doi.org/10.1016/j.ijheatmasstransfer.2018.10.118

ATP. (2020). *Agreement on the International Carriage of Perishable Foodstuffs and on the Special Equipment to be Used for Such Carriage: (ATP) as amended 6 July 2020*. United Nations. https://doi.org/10.18356/6fa10b27-en

Azzouz, K., Leducq, D., & Gobin, D. (2008). Performance enhancement of a household refrigerator by addition of latent heat storage. *International Journal of Refrigeration*, *31*(5), 892–901. https://doi.org/10.1016/j.ijrefrig.2007.09.007

Azzouz, K., Leducq, D., & Gobin, D. (2009). Enhancing the performance of household refrigerators with latent heat storage: An experimental investigation.

International Journal of Refrigeration, *32*(7), 1634–1644. https://doi.org/10.1016/j.ijrefrig.2009.03.012

Baïri, A. (2008). Nusselt–Rayleigh correlations for design of industrial elements: Experimental and numerical investigation of natural convection in tilted square air filled enclosures. *Energy Conversion and Management*, *49*(4), 771–782. https://doi.org/10.1016/j.enconman.2007.07.030

Bansal, K. (2015). *Exact Implementation of boundary conditions for Immersed Boundary Methods*. Open Access Theses. https://docs.lib.purdue.edu/open_access_theses/1207

Baranyi, J., & Roberts, T. A. (1994). A dynamic approach to predicting bacterial growth in food. *International Journal of Food Microbiology*, *23*(3), 277–294. https://doi.org/10.1016/0168-1605(94)90157-0

Ben-Abdallah, R., Leducq, D., Hoang, H. M., Fournaison, L., Pateau, O., Ballot-Miguet, B., & Delahaye, A. (2019). Experimental investigation of the use of PCM in an open display cabinet for energy management purposes. *Energy Conversion and Management*, *198*, 111909. https://doi.org/10.1016/j.enconman.2019.111909

Berdja, M., Hamid, A., & Sari, O. (2019). Characteristics and thickness effect of phase change material and frost on heat transfer and thermal performance of conventional refrigerator: Theoretical and experimental investigation. *International Journal of Refrigeration*, *97*, 108–123. https://doi.org/10.1016/j.ijrefrig.2018.10.003

Bergman, T. L. (Ed.). (2011). *Introduction to heat transfer* (6th ed). Wiley.

Biopharma cold chain logistic survey. (2019). *What Matters Most and What it Means for the Future*. https://www.pharmalogisticsiq.com/logistics

Bista, S., Hosseini, S. E., Owens, E., & Phillips, G. (2018). Performance improvement and energy consumption reduction in refrigeration systems using phase change material (PCM). *Applied Thermal Engineering*, *142*, 723–735. https://doi.org/10.1016/j.applthermaleng.2018.07.068

Burgess, S., Wang, X., Rahbari, A., & Hangi, M. (2022). Optimisation of a portable phase-change material (PCM) storage system for emerging cold-chain delivery applications. *Journal of Energy Storage*, *52*, 104855. https://doi.org/10.1016/j.est.2022.104855

Calati, M., Righetti, G., Zilio, C., Hooman, K., & Mancin, S. (2023). CFD analyses for the development of an innovative latent thermal energy storage for food transportation. *International Journal of Thermofluids*, *17*, 100301. https://doi.org/10.1016/j.ijft.2023.100301

Catton, I. (1978). *NATURAL CONVECTION IN ENCLOSURES*. International Heat Transfer Conference 6. https://doi.org/10.1615/IHTC6.2350

Cengel, Y. A., & Ghajar, A. J. (2020). *Heat and Mass Transfer: Fundamentals & Applications*. McGraw-Hill Education.

Cesini, G., Paroncini, M., Cortella, G., & Manzan, M. (1999). Natural convection from a horizontal cylinder in a rectangular cavity. *International Journal of Heat and Mass Transfer*, *42*(10), 1801–1811. https://doi.org/10.1016/S0017-9310(98)00266-X

Chakraverty, A., & Singh, R. P. (2001). *Postharvest Technology: Cereals, Pulses, Fruits and Vegetables*. Science Publishers.

Chaomuang, N., Flick, D., Denis, A., & Laguerre, O. (2020). Experimental and numerical characterization of airflow in a closed refrigerated display cabinet using PIV and CFD techniques. *International Journal of Refrigeration*, *111*, 168–177. https://doi.org/10.1016/j.ijrefrig.2019.12.001

Cheng, C., Liu, B., Tian, M., Fang, T., & Li, C. (2023). Application of interaction models in predicting the simultaneous growth of Staphylococcus aureus and different concentrations of background microbiota in Chinese-style braised beef. *Meat Science*, *200*, 109162. https://doi.org/10.1016/j.meatsci.2023.109162

Choi, C., Cho, H. W., Ha, M. Y., & Yoon, H. S. (2015). Effect of circular cylinder location on three-dimensional natural convection in a cubical enclosure. *Journal of Mechanical Science and Technology*, *29*(3), 1307–1318. https://doi.org/10.1007/s12206-015-0246-3

Choi, S.-J., & Burgess, G. (2007). Practical mathematical model to predict the performance of insulating packages. *Packaging Technology and Science*, *20*(6), 369–380. https://doi.org/10.1002/pts.762

Committee, B. C. C. A. (2014). *Food Safety, Sanitation, and Personal Hygiene*. https://books.google.fr/books?id=xzdfnQAACAAJ

Copertaro, B., Principi, P., & Fioretti, R. (2016). Thermal performance analysis of PCM in refrigerated container envelopes in the Italian context – Numerical modeling and validation. *Applied Thermal Engineering*, *102*, 873–881. https://doi.org/10.1016/j.applthermaleng.2016.04.050

Corcione, M. (2003). Effects of the thermal boundary conditions at the sidewalls upon natural convection in rectangular enclosures heated from below and cooled from above. *International Journal of Thermal Sciences*, *42*(2), 199–208. https://doi.org/10.1016/S1290-0729(02)00019-4

Costa, M. (2020, April 28). *Frozen Food Sales Projected to Remain 30% Higher than 2019 Due to COVID-19 Spending*. https://www.refrigeratedfrozenfood.com/articles/99226-frozen-food-sales-projected-to-remain-30-higher-than-2019-due-to-covid-19-spending?v=preview

Dalal, A., & Das, M. K. (2006). Natural Convection in a Rectangular Cavity Heated from Below and Uniformly Cooled from the Top and Both Sides. *Numerical Heat Transfer, Part A: Applications*, *49*(3), 301–322. https://doi.org/10.1080/10407780500343749

De Cesare, A., Vitali, S., Tessema, G. T., Trevisani, M., Fagereng, T. M., Beaufort, A., Manfreda, G., & Skjerdal, T. (2018). Modelling the growth kinetics of Listeria monocytogenes in pasta salads at different storage temperatures and packaging conditions. *Food Microbiology*, *76*, 154–163. https://doi.org/10.1016/j.fm.2018.04.013

Du, J., Nie, B., Zhang, Y., Du, Z., Wang, L., & Ding, Y. (2020). Cooling performance of a thermal energy storage-based portable box for cold chain applications. *Journal of Energy Storage*, *28*, 101238. https://doi.org/10.1016/j.est.2020.101238

Duret, S., Guillier, L., Hoang, H.-M., Flick, D., & Laguerre, O. (2014). Identification of the significant factors in food safety using global sensitivity analysis and the accept-and-reject algorithm: Application to the cold chain of ham. *International Journal of Food Microbiology*, *180*, 39–48. https://doi.org/10.1016/j.ijfoodmicro.2014.04.009

Duret, S., Hoang, H.-M., Derens-Bertheau, E., Delahaye, A., Laguerre, O., & Guillier, L. (2019). Combining Quantitative Risk Assessment of Human Health, Food Waste, and Energy Consumption: The Next Step in the Development of the Food Cold Chain? *Risk Analysis*, *39*(4), 906–925. https://doi.org/10.1111/risa.13199

East, A., & Smale, N. (2008). Combining a hybrid genetic algorithm and a heat transfer model to optimise an insulated box for use in the transport of perishables. *Vaccine*, *26*(10), 1322–1334. https://doi.org/10.1016/j.vaccine.2007.12.055

East, A., Smale, N., & Kang, S. (2009). A method for quantitative risk assessment of temperature control in insulated boxes. *International Journal of Refrigeration*, *32*(6), 1505–1513. https://doi.org/10.1016/j.ijrefrig.2009.01.020

Elliott, M. A., & Halbert, G. W. (2005). Maintaining the cold chain shipping environment for Phase I clinical trial distribution. *International Journal of Pharmaceutics*, *299*(1), 49–54. https://doi.org/10.1016/j.ijpharm.2005.04.032

Elliott, M. A., & Halbert, G. W. (2008). Maintaining a frozen shipping environment for

Phase I clinical trial distribution. *International Journal of Pharmaceutics*, *346*(1), 89–92. https://doi.org/10.1016/j.ijpharm.2007.06.008

Ellouze, M., Gauchi, J.-P., & Augustin, J.-C. (2010). Global sensitivity analysis applied to a contamination assessment model of listeria monocytogenes in cold smoked salmon at consumption. *Risk Analysis: An Official Publication of the Society for Risk Analysis*, *30*(5), 841–852. https://doi.org/10.1111/j.1539-6924.2010.01380.x

Ezan, M. A., Ozcan Doganay, E., Yavuz, F. E., & Tavman, I. H. (2017). A numerical study on the usage of phase change material (PCM) to prolong compressor off period in a beverage cooler. *Energy Conversion and Management*, *142*, 95–106. https://doi.org/10.1016/j.enconman.2017.03.032

FAO. (2018). *The future of food and agriculture – Alternative pathways to 2050*.

FAO. (2019). *The state of food and agriculture 2019. Moving forward on food loss and waste reduction*.

Fioretti, R., Principi, P., & Copertaro, B. (2016). A refrigerated container envelope with a PCM (Phase Change Material) layer: Experimental and theoretical investigation in a representative town in Central Italy. *Energy Conversion and Management*, *122*, 131–141. https://doi.org/10.1016/j.enconman.2016.05.071

García, M. R., Ferez-Rubio, J. A., & Vilas, C. (2022). Assessment and Prediction of Fish Freshness Using Mathematical Modelling: A Review. *Foods*, *11*(15), Article 15. https://doi.org/10.3390/foods11152312

Ge, C., Cheng, Y., & Li, B. (2014). Numerical simulation and experimental study of the heat transition in a foam container. *Journal of Cellular Plastics*, *50*(1), 15–36. https://doi.org/10.1177/0021955X13503846

Geankoplis, C. J. (1993). *Transport Processes and Unit Operations* (Subsequent edition). Pearson College Div.

Gin, B., & Farid, M. M. (2010). The use of PCM panels to improve storage condition of frozen food. *Journal of Food Engineering*, *100*(2), 372–376. https://doi.org/10.1016/j.jfoodeng.2010.04.016

Grandison, A. S. (2011). Postharvest Handling and Preparation of Foods for Processing. In *Food Processing Handbook* (pp. 1–30). John Wiley & Sons, Ltd. https://doi.org/10.1002/9783527634361.ch1

Ha, M., Kim, I.-K., Yoon, H., Yoon, K., Lee, J. R., Balachandar, S., & Chun, H. (2002). Two-dimensional and unsteady natural convection in a horizontal enclosure with a square body. *NUMERICAL HEAT TRANSFER PART A-APPLICATIONS*, *41*, 183–210. https://doi.org/10.1080/104077802317221393

Hollands, K. G. T., Unny, T. E., Raithby, G. D., & Konicek, L. (1976). Free convective heat transfer across inclined air layers. *J. Heat Transfer; (United States)*, *98:2*. https://www.osti.gov/biblio/7361946

Huang, L. (2016). Mathematical modeling and validation of growth of Salmonella Enteritidis and background microorganisms in potato salad – One-step kinetic analysis and model development. *Food Control*, *68*, 69–76. https://doi.org/10.1016/j.foodcont.2016.03.039

Huang, L. (2018). Growth of non-toxigenic Clostridium botulinum mutant LNT01 in cooked beef: One-step kinetic analysis and comparison with C. sporogenes and C. perfringens. *Food Research International*, *107*, 248–256. https://doi.org/10.1016/j.foodres.2018.02.028

ICI Business on behalf of Centre for the Promotion of Imports from developing countries. (2020, October 28). *The European market potential for exotic tropical fruit | CBI*. https://www.cbi.eu/market-information/fresh-fruit-vegetables/exotic-tropical-fruit/market-potential

Icier, F., & Ilicali, C. (2005). The use of tylose as a food analog in ohmic heating studies. *Journal of Food Engineering*, *69*(1), 67–77. https://doi.org/10.1016/j.jfoodeng.2004.07.011

Jami, M., Mezrhab, A., Bouzidi, M., & Lallemand, P. (2007). Lattice Boltzmann method applied to the laminar natural convection in an enclosure with a heat-generating cylinder conducting body. *International Journal of Thermal Sciences*, *46*(1), 38–47. https://doi.org/10.1016/j.ijthermalsci.2006.03.010

Jami, M., Mezrhab, A., & Naji, H. (2008). Numerical study of natural convection in a square cavity containing a cylinder using the lattice Boltzmann method. *Engineering Computations*, *25*(5), 480–489. https://doi.org/10.1108/02644400810881400

Jevnikar, S., & Siddiqui, K. (2019). Investigation of the influence of heat source orientation on the transient flow behavior during PCM melting using particle image velocimetry. *Journal of Energy Storage*, *25*, 100825. https://doi.org/10.1016/j.est.2019.100825

Jia, Z., Bai, W., Li, X., Fang, T., & Li, C. (2020). Assessing the growth of Listeria monocytogenes in salmon with or without the competition of background microflora—A one-step kinetic analysis. *Food Control*, *114*, 107139. https://doi.org/10.1016/j.foodcont.2020.107139

Jiang, S., Zhang, M., Li, M., Zhu, J., Ge, A., Liu, L., & Yu, J. (2021). Cellulose-based composite thermal-insulating foams toward eco-friendly, flexible and flame-

retardant. *Carbohydrate Polymers*, *273*, 118544. https://doi.org/10.1016/j.carbpol.2021.118544

Joshi, K., Tiwari, B., Cullen, P. J., & Frias, J. M. (2019). Predicting quality attributes of strawberry packed under modified atmosphere throughout the cold chain. *Food Packaging and Shelf Life*, *21*, 100354. https://doi.org/10.1016/j.fpsl.2019.100354

Kaale, L. D., Eikevik, T. M., Rustad, T., & Kolsaker, K. (2011). Superchilling of food: A review. *Journal of Food Engineering*, *107*(2), 141–146. https://doi.org/10.1016/j.jfoodeng.2011.06.004

Kacimi, A., & Labranque, G. (2011). Vacuum Insulated panels (VIP) in insulated packaging. *Proceedings of the 23th IIR International Congress of Refrigeration: Prague, Czech Republic, August 21-26, 2011*.

Kacimi, A., & Labranque, G. (2019). Combination of vacuum insulation panels and phase change materials in temperature-controlled containers. *Proceedings of the 25th IIR International Congress of Refrigeration: Montréal, Canada, August 24-30, 2019*. https://doi.org/10.18462/iir.icr.2019.0163

Kamkari, B., Shokouhmand, H., & Bruno, F. (2014). Experimental investigation of the effect of inclination angle on convection-driven melting of phase change material in a rectangular enclosure. *International Journal of Heat and Mass Transfer*, *72*, 186–200. https://doi.org/10.1016/j.ijheatmasstransfer.2014.01.014

Kang, J. S., & Lee, D. S. (1998). A kinetic model for transpiration of fresh produce in a controlled atmosphere. *Journal of Food Engineering*, *35*(1), 65–73. https://doi.org/10.1016/S0260-8774(98)00009-0

Keane, R. D., & Adrian, R. J. (1992). Theory of cross-correlation analysis of PIV images. *Applied Scientific Research*, *49*(3), 191–215. https://doi.org/10.1007/BF00384623

Kedia, P., Kausley, S. B., & Rai, B. (2021). Temperature and humidity based models for the prediction of transpiration rate in potatoes during storage. *Journal of Food Process Engineering*, *44*(3), e13626. https://doi.org/10.1111/jfpe.13626

Khalaf, Y., El Hage, P., Dimitrova Mihajlova, J., Bergeret, A., Lacroix, P., & El Hage, R. (2021). Influence of agricultural fibers size on mechanical and insulating properties of innovative chitosan-based insulators. *Construction and Building Materials*, *287*, 123071. https://doi.org/10.1016/j.conbuildmat.2021.123071

Kim, J., Kim, D., & Choi, H. (2001). An Immersed-Boundary Finite-Volume Method for Simulations of Flow in Complex Geometries. *Journal of Computational Physics*, *171*(1), 132–150. https://doi.org/10.1006/jcph.2001.6778

Kozak, Y., Farid, M., & Ziskind, G. (2017). Experimental and comprehensive theoretical

study of cold storage packages containing PCM. *Applied Thermal Engineering*, *115*, 899–912. https://doi.org/10.1016/j.applthermaleng.2016.12.127

Labihi, A., Aitlahbib, F., Chehouani, H., Benhamou, B., Ouikhalfan, M., Croitoru, C., & Nastase, I. (2017). Effect of phase change material wall on natural convection heat transfer inside an air filled enclosure. *Applied Thermal Engineering*, *126*, 305–314. https://doi.org/10.1016/j.applthermaleng.2017.07.112

Laguerre, O., Ben Aissa, M. F., & Flick, D. (2008). Methodology of temperature prediction in an insulated container equipped with PCM. *International Journal of Refrigeration*, *31*(6), 1063–1072. https://doi.org/10.1016/j.ijrefrig.2007.12.008

Laguerre, O., Ben Amara, S., Alvarez, G., & Flick, D. (2008). Transient heat transfer by free convection in a packed bed of spheres: Comparison between two modelling approaches and experimental results. *Applied Thermal Engineering*, *28*(1), 14–24. https://doi.org/10.1016/j.applthermaleng.2007.03.014

Laguerre, O., Ben Amara, S., & Flick, D. (2005). Experimental study of heat transfer by natural convection in a closed cavity: Application in a domestic refrigerator. *Journal of Food Engineering*, *70*(4), 523–537. https://doi.org/10.1016/j.jfoodeng.2004.10.007

Laguerre, O., Chaomuang, N., Derens, E., & Flick, D. (2019). How to predict product temperature changes during transport in an insulated box equipped with an ice pack: Experimental versus 1-D and 3-D modelling approaches. *International Journal of Refrigeration*, *100*, 196–207. https://doi.org/10.1016/j.ijrefrig.2018.12.022

Laguerre, O., Derens, E., & Flick, D. (2018). Modelling of fish refrigeration using flake ice. *International Journal of Refrigeration*, *85*, 97–108. https://doi.org/10.1016/j.ijrefrig.2017.09.014

Laguerre, O., & Flick, D. (2004). Heat transfer by natural convection in domestic refrigerators. *Journal of Food Engineering*, *62*(1), 79–88. https://doi.org/10.1016/S0260-8774(03)00173-0

Laguerre, O., & Flick, D. (2010). Temperature prediction in domestic refrigerators: Deterministic and stochastic approaches. *International Journal of Refrigeration*, *33*(1), 41–51. https://doi.org/10.1016/j.ijrefrig.2009.09.014

Laguerre, O., Hoang, H. M., & Flick, D. (2013). Experimental investigation and modelling in the food cold chain: Thermal and quality evolution. *Trends in Food Science & Technology*, *29*(2), 87–97. https://doi.org/10.1016/j.tifs.2012.08.001

Lee, H. J., Doo, J. H., Ha, M. Y., & Yoon, H. S. (2013). Effects of thermal boundary conditions on natural convection in a square enclosure with an inner circular

cylinder locally heated from the bottom wall. *International Journal of Heat and Mass Transfer*, *65*, 435–450. https://doi.org/10.1016/j.ijheatmasstransfer.2013.06.031

Lee, S. H., Seo, Y. M., Yoon, H. S., & Ha, M. Y. (2016). Three-dimensional natural convection around an inner circular cylinder located in a cubic enclosure with sinusoidal thermal boundary condition. *International Journal of Heat and Mass Transfer*, *101*, 807–823. https://doi.org/10.1016/j.ijheatmasstransfer.2016.05.079

Lee, T. L., & Lin, T. F. (1996). Transient three-dimensional convection of air in a differentially heated rotating cubic cavity. *International Journal of Heat and Mass Transfer*, *39*(6), 1243–1255. https://doi.org/10.1016/0017-9310(95)00193-X

Leporini, M., Corvaro, F., Marchetti, B., Polonara, F., & Benucci, M. (2018). Experimental and numerical investigation of natural convection in tilted square cavity filled with air. *Experimental Thermal and Fluid Science*, *99*, 572–583. https://doi.org/10.1016/j.expthermflusci.2018.08.023

Leungtongkum, T., Flick, D., Hoang, H. M., Steven, D., Delahaye, A., & Laguerre, O. (2022). Insulated box and refrigerated equipment with PCM for food preservation: State of the art. *Journal of Food Engineering*, *317*, 110874. https://doi.org/10.1016/j.jfoodeng.2021.110874

Leungtongkum, T., Laguerre, O., Flick, D., Denis, A., Duret, S., & Chaomuang, N. (2023a). Experimental investigation of airflow and heat transfer by natural convection in an insulated box with a Phase Change Material using a Particle Image Velocimetry technique. *Journal of Food Engineering*, *336*, 111207. https://doi.org/10.1016/j.jfoodeng.2022.111207

Leungtongkum, T., Laguerre, O., & Flick, D. (2023b). Simplified heat transfer model for real-time temperature prediction in insulated boxes equipped with a phase change material. *International Journal of Refrigeration*, *149*, 286–298. https://doi.org/10.1016/j.ijrefrig.2023.02.009

Leungtongkum, T., Flick, D., Chaomuang, N., Denis, A., & Laguerre, O. (2023c). Influence of use conditions on heat transfer in an insulated box equipped with a phase change material. *Journal of Food Engineering*, *357*, 111644. https://doi.org/10.1016/j.jfoodeng.2023.111644

Leungtongkum, T., Laguerre, O., Chaomuang, N., Denis, A., & Flick, D. (2023d, August 22). *CFD modelling of heat transfer and airflow in an insulated box equipped with Phase Change Material*. 26th International Congress of Refrigeration, Paris, France.

Li, C., Huang, L., Hwang, C.-A., & Chen, J. (2016). Growth of Listeria monocytogenes in salmon roe – A kinetic analysis. *Food Control*, *59*, 538–545. https://doi.org/10.1016/j.foodcont.2015.06.016

Li, G., Hwang, Y., Radermacher, R., & Chun, H.-H. (2013). Review of cold storage materials for subzero applications. *Energy*, *51*, 1–17. https://doi.org/10.1016/j.energy.2012.12.002

Liu, J., Li, F., Li, T., Yun, Z., Duan, X., & Jiang, Y. (2019). Fibroin treatment inhibits chilling injury of banana fruit via energy regulation. *Scientia Horticulturae*, *248*, 8–13. https://doi.org/10.1016/j.scienta.2018.12.052

Liu, M., Saman, W., & Bruno, F. (2012). Development of a novel refrigeration system for refrigerated trucks incorporating phase change material. *Applied Energy*, *92*, 336–342. https://doi.org/10.1016/j.apenergy.2011.10.015

Loria, K. (2021, April 23). *Tropical produce seeing strong sales | Produce News*. https://theproducenews.com/headlines/tropical-produce-seeing-strong-sales

Mahajan, P. V., Oliveira, F. A. R., & Macedo, I. (2008). Effect of temperature and humidity on the transpiration rate of the whole mushrooms. *Journal of Food Engineering*, *84*(2), 281–288. https://doi.org/10.1016/j.jfoodeng.2007.05.021

Maiorino, A., Del Duca, M. G., Mota-Babiloni, A., Greco, A., & Aprea, C. (2019). The thermal performances of a refrigerator incorporating a phase change material. *International Journal of Refrigeration*, *100*, 255–264. https://doi.org/10.1016/j.ijrefrig.2019.02.005

Margeirsson, B., Gospavic, R., Pálsson, H., Arason, S., & Popov, V. (2011). Experimental and numerical modelling comparison of thermal performance of expanded polystyrene and corrugated plastic packaging for fresh fish. *International Journal of Refrigeration*, *34*(2), 573–585. https://doi.org/10.1016/j.ijrefrig.2010.09.017

Margeirsson, B., Pálsson, H., Popov, V., Gospavic, R., Arason, S., Sveinsdóttir, K., & Jónsson, M. Þór. (2012). Numerical modelling of temperature fluctuations in superchilled fish loins packaged in expanded polystyrene and stored at dynamic temperature conditions. *International Journal of Refrigeration*, *35*(5), 1318–1326. https://doi.org/10.1016/j.ijrefrig.2012.03.016

Matar, C., Guillard, V., Gauche, K., Costa, S., Gontard, N., Guilbert, S., & Gaucel, S. (2020). Consumer behaviour in the prediction of postharvest losses reduction for fresh strawberries packed in modified atmosphere packaging. *Postharvest Biology and Technology*, *163*, 111119. https://doi.org/10.1016/j.postharvbio.2020.111119

McQuillan, F. J., Culham, J. R., & Yovanovich, M. M. (1984). Properties of dry air at one atmosphere—Google Scholar. In *Microelectronics Heat Transfer Lab*. https://scholar.google.com/scholar_lookup?title=Properties%20of%20Dry%20Air%20at%20One%20Atmosphere&author=F.%20McQuillan&publication_year=1984

Melone, L., Altomare, L., Cigada, A., & De Nardo, L. (2012). Phase change material cellulosic composites for the cold storage of perishable products: From material preparation to computational evaluation. *Applied Energy*, *89*(1), 339–346. https://doi.org/10.1016/j.apenergy.2011.07.039

Mercier, S., Villeneuve, S., Mondor, M., & Uysal, I. (2017). Time-Temperature Management Along the Food Cold Chain: A Review of Recent Developments: Food preservation along the cold chain…. *Comprehensive Reviews in Food Science and Food Safety*, *16*. https://doi.org/10.1111/1541-4337.12269

Miroshnichenko, I. V., & Sheremet, M. A. (2018). Turbulent natural convection heat transfer in rectangular enclosures using experimental and numerical approaches: A review. *Renewable and Sustainable Energy Reviews*, *82*, 40–59. https://doi.org/10.1016/j.rser.2017.09.005

Moreno, S., Hinojosa, J. F., Hernández-López, I., & Xaman, J. (2020). Numerical and experimental study of heat transfer in a cubic cavity with a PCM in a vertical heated wall. *Applied Thermal Engineering*, *178*, 115647. https://doi.org/10.1016/j.applthermaleng.2020.115647

Mousazade, A., Rafee, R., & Valipour, M. S. (2020). Thermal performance of cold panels with phase change materials in a refrigerated truck. *International Journal of Refrigeration*, *120*, 119–126. https://doi.org/10.1016/j.ijrefrig.2020.09.003

Muley, A. B., Priya, K., Kakoli, P., Kausley, S. B., externe, L. vers un site, fenêtre, celui-ci s'ouvrira dans une nouvelle, & Beena, R. (2022). *Analyzing the physical and biochemical changes in strawberries during storage at different temperatures and the development of kinetic models*. *16*(1), 222–247. https://doi.org/10.1007/s11694-021-01146-8

Navaranjan, N., Fletcher, G. C., Summers, G., Parr, R., & Anderson, R. (2013). Thermal insulation requirements and new cardboard packaging for chilled seafood exports. *Journal of Food Engineering*, *119*(3), 395–403. https://doi.org/10.1016/j.jfoodeng.2013.05.042

Ndraha, N., Hsiao, H.-I., Vlajic, J., Yang, M.-F., & Lin, H.-T. V. (2018). Time-temperature abuse in the food cold chain: Review of issues, challenges, and recommendations. *Food Control*, *89*, 12–21. https://doi.org/10.1016/j.foodcont.2018.01.027

Ndraha, N., Sung, W.-C., & Hsiao, H.-I. (2019). Evaluation of the cold chain management options to preserve the shelf life of frozen shrimps: A case study in the home delivery services in Taiwan. *Journal of Food Engineering*, *242*, 21–30. https://doi.org/10.1016/j.jfoodeng.2018.08.010

Nie, B., Palacios, A., Zou, B., Liu, J., Zhang, T., & Li, Y. (2020). Review on phase change materials for cold thermal energy storage applications. *Renewable and Sustainable Energy Reviews*, *134*, 110340. https://doi.org/10.1016/j.rser.2020.110340

Ohkawara, H., Kitagawa, T., Fukushima, N., Ito, T., Sawa, Y., & Yoshimine, T. (2012). A Newly Developed Container for Safe, Easy, and Cost-effective Overnight Transportation of Tissues and Organs by Electrically Keeping Tissue or Organ Temperature at 3 to 6°C. *Transplantation Proceedings*, *44*(4), 855–858. https://doi.org/10.1016/j.transproceed.2012.02.023

Oliveira, F., Sousa-Gallagher, M. J., Mahajan, P. V., & Teixeira, J. A. (2012). Development of shelf-life kinetic model for modified atmosphere packaging of fresh sliced mushrooms. *Journal of Food Engineering*, *111*(2), 466–473. https://doi.org/10.1016/j.jfoodeng.2012.01.013

Onwude, D., Bahrami, F., Shrivastava, C., Berry, T., Cronje, P., North, J., Kirsten, N., Schudel, S., Crenna, E., Shoji, K., & Defraeye, T. (2022). Physics-driven digital twins to quantify the impact of pre- and postharvest variability on the end quality evolution of orange fruit. *Resources, Conservation and Recycling*, *186*, 106585. https://doi.org/10.1016/j.resconrec.2022.106585

Oró, E., de Gracia, A., Castell, A., Farid, M. M., & Cabeza, L. F. (2012a). Review on phase change materials (PCMs) for cold thermal energy storage applications. *Applied Energy*, *99*, 513–533. https://doi.org/10.1016/j.apenergy.2012.03.058

Oró, E., Miró, L., Farid, M. M., & Cabeza, L. F. (2012b). Thermal analysis of a low temperature storage unit using phase change materials without refrigeration system. *International Journal of Refrigeration*, *35*(6), 1709–1714. https://doi.org/10.1016/j.ijrefrig.2012.05.004

Orozco, D. A., Hinojosa, J. F., & Amaya, K. (2021). The Effect of a Segmented Wall Filled With Phase Change Material on Heat Transfer and Airflow in a Closed Cavity. *Journal of Heat Transfer*, *143*(9). https://doi.org/10.1115/1.4051600

Padet, J. (2010). *Principes des transferts convectifs, Seconde édition révisée: Convection Libre*. https://www.sft.asso.fr/Local/sft/dir/user-3775/documents/Ouvrages/livre%20Padet/PTC%2009%20-%20Chapitre%205.pdf

Pandey, S., Park, Y. G., & Ha, M. Y. (2019). An exhaustive review of studies on natural convection in enclosures with and without internal bodies of various shapes. *International Journal of Heat and Mass Transfer*, *138*, 762–795. https://doi.org/10.1016/j.ijheatmasstransfer.2019.04.097

Paquette, J.-C., Mercier, S., Marcos, B., & Morasse, S. (2017). Modeling the thermal performance of a multilayer box for the transportation of perishable food. *Food and Bioproducts Processing*, *105*, 77–85. https://doi.org/10.1016/j.fbp.2017.06.002

Penchaiya, P., Tijskens, L. M. M., Uthairatanakij, A., Srilaong, V., Tansakul, A., & Kanlayanarat, S. (2020). Modelling quality and maturity of 'Namdokmai Sithong' mango and their variation during storage. *Postharvest Biology and Technology*, *159*, 111000. https://doi.org/10.1016/j.postharvbio.2019.111000

Pham, A. T., Moureh, J., Belaidi, M., & Flick, D. (2021). CFD modelling of a pallet of heat-generating product applied to a cheese product. *International Journal of Refrigeration*, *128*, 163–176. https://doi.org/10.1016/j.ijrefrig.2021.03.011

Phimolsiripol, Y., Siripatrawan, U., Tulyathan, V., & Cleland, D. J. (2008). Effects of freezing and temperature fluctuations during frozen storage on frozen dough and bread quality. *Journal of Food Engineering*, *84*(1), 48–56. https://doi.org/10.1016/j.jfoodeng.2007.04.016

Pinheiro, J., Alegria, C., Abreu, M., Gonçalves, E. M., & Silva, C. L. M. (2013). Kinetics of changes in the physical quality parameters of fresh tomato fruits (Solanum lycopersicum, cv. 'Zinac') during storage. *Journal of Food Engineering*, *114*(3), 338–345. https://doi.org/10.1016/j.jfoodeng.2012.08.024

Pirdavari, P., & Hossainpour, S. (2020). Numerical study of a Phase Change Material (PCM) embedded solar thermal energy operated cool store: A feasibility study. *International Journal of Refrigeration*, *117*, 114–123. https://doi.org/10.1016/j.ijrefrig.2020.04.028

Pirmohammadi, M., & Ghassemi, M. (2009). Effect of magnetic field on convection heat transfer inside a tilted square enclosure. *International Communications in Heat and Mass Transfer*, *36*(7), 776–780. https://doi.org/10.1016/j.icheatmasstransfer.2009.03.023

PlasticsEurope. (2019). *Plastics—The facts 2019. An analysis of European plastics production, demand and waste data*. https://www. plasticseurope. org/en/resources/publications/1804-plastics-facts-2019.

Pouillot, R., Goulet, V., Delignette-Muller, M. L., Mahé, A., & Cornu, M. (2009). Quantitative risk assessment of Listeria monocytogenes in French cold-smoked

salmon: II. Risk characterization. *Risk Analysis: An Official Publication of the Society for Risk Analysis*, *29*(6), 806–819. https://doi.org/10.1111/j.1539-6924.2008.01200.x

Raffel, M., Willert, C., Wereley, S., & Kompenhans, J. (2007). *Particle Image Velocimetry: A Practical Guide*. https://doi.org/10.1007/978-3-540-72308-0

Rahimi-Khoigani, S., Hamdami, N., & Dalvi-Isfahan, M. (2023). Application of an improved latent heat storage system in the food packaging. *Journal of Food Engineering*, *341*, 111351. https://doi.org/10.1016/j.jfoodeng.2022.111351

Raithby, G. D., & Hollands, K. G. T. (1998). Natural convection. In W. M. Rohsenow, J. P. Hartnett, & Y. I. Cho, *Handbook of Heat Transfer* (3rd ed). McGraw-Hill.

Rincón-Casado, A., Sánchez de la Flor, F. J., Chacón Vera, E., & Sánchez Ramos, J. (2017). New natural convection heat transfer correlations in enclosures for building performance simulation. *Engineering Applications of Computational Fluid Mechanics*, *11*(1), 340–356. https://doi.org/10.1080/19942060.2017.1300107

Robertson, J., Franzel, L., & Maire, D. (2017). Innovations in cold chain equipment for immunization supply chains. *Vaccine*, *35*(17), 2252–2259. https://doi.org/10.1016/j.vaccine.2016.11.094

Roder, H., Perkins, R., Laesecke, A., & Nieto de Castro, C. (2000). Absolute Steady-State Thermal Conductivity Measurements by Use of a Transient Hot-Wire System. *Journal of Research of the National Institute of Standards and Technology*, *105*, 221. https://doi.org/10.6028/jres.105.028

Rostami, S., Afrand, M., Shahsavar, A., Sheikholeslami, M., Kalbasi, R., Aghakhani, S., Shadloo, M. S., & Oztop, H. F. (2020). A review of melting and freezing processes of PCM/nano-PCM and their application in energy storage. *Energy*, *211*, 118698. https://doi.org/10.1016/j.energy.2020.118698

Saury, D., Rouger, N., Djanna, F., & Penot, F. (2011). Natural convection in an air-filled cavity: Experimental results at large Rayleigh numbers. *International Communications in Heat and Mass Transfer*, *38*(6), 679–687. https://doi.org/10.1016/j.icheatmasstransfer.2011.03.019

Schalbart, P., Leducq, D., & Alvarez, G. (2013). Frozen products stabilisation by phase change material. *2nd IIR International Conference on Sustainability and the Cold Chain. Proceedings: Paris, France, April 2-4, 2013*. https://iifiir.org/en/fridoc/frozen-products-stabilisation-by-phase-change-material-29311

Shardt, O. (2020). Comparison of finite volume and lattice Boltzmann methods for multicomponent flow simulations. *The Canadian Journal of Chemical*

Engineering, *98*(1), 44–53. https://doi.org/10.1002/cjce.23634

Sharma, A., Tyagi, V. V., Chen, C. R., & Buddhi, D. (2009). Review on thermal energy storage with phase change materials and applications. *Renewable and Sustainable Energy Reviews*, *13*(2), 318–345. https://doi.org/10.1016/j.rser.2007.10.005

Shinoda, J., Kazanci, O. B., Tanabe, S., & Olesen, B. W. (2019). A review of the surface heat transfer coefficients of radiant heating and cooling systems. *Building and Environment*, *159*, 106156. https://doi.org/10.1016/j.buildenv.2019.05.034

Singh, R. P., Heldman, D. R., & Singh, R. P. (2008a). *Introduction to Food Engineering*. Academic Press.

Singh, S.P., Burgess, G. and Singh, J. (2008b), Performance comparison of thermal

insulated packaging boxes, bags and refrigerants for single-parcel shipments.

Packaging Technology and Science, *21*: 25-35. https://doi.org/10.1002/pts.773

Smith, J. S., & Hui, Y. H. (Eds.). (2004). *Food processing: Principles and applications* (1st ed). Blackwell Pub.

Sonnenrein, G., Baumhögger, E., Elsner, A., Fieback, K., Morbach, A., Paul, A., & Vrabec, J. (2015a). Copolymer-bound phase change materials for household refrigerating appliances: Experimental investigation of power consumption, temperature distribution and demand side management potential. *International Journal of Refrigeration*, *60*. https://doi.org/10.1016/j.ijrefrig.2015.06.030

Sonnenrein, G., Elsner, A., Baumhögger, E., Morbach, A., Fieback, K., & Vrabec, J. (2015b). Reducing the power consumption of household refrigerators through the integration of latent heat storage elements in wire-and-tube condensers. *International Journal of Refrigeration*, *51*, 154–160. https://doi.org/10.1016/j.ijrefrig.2014.12.011

Sonnenrein, G., Baumhögger, E., Elsner, A., Morbach, A., Neukötter, M., Paul, A., & Vrabec, J. (2020). Improving the performance of household refrigerating appliances through the integration of phase change materials in the context of the new global refrigerator standard IEC 62552:2015. *International Journal of Refrigeration*, *119*, 448–456. https://doi.org/10.1016/j.ijrefrig.2020.07.025

Söylemez, E., Alpman, E., Onat, A., & Hartomacıoğlu, S. (2021). CFD analysis for predicting cooling time of a domestic refrigerator with thermoelectric cooling system. *International Journal of Refrigeration*, *123*, 138–149. https://doi.org/10.1016/j.ijrefrig.2020.11.012

United Nations Environment Programme. (2021). *Food Waste Index Report 2021*. http://www.unep.org/resources/report/unep-food-waste-index-report-2021

van der Sman, R. G. M. (2003). Simple model for estimating heat and mass transfer in regular-shaped foods. *Journal of Food Engineering*, *60*(4), 383–390. https://doi.org/10.1016/S0260-8774(03)00061-X

Van Dijk, C., Boeriu, C., Peter, F., Stolle-Smits, T., & Tijskens, L. M. M. (2006). The firmness of stored tomatoes (cv. Tradiro). 1. Kinetic and near infrared models to describe firmness and moisture loss. *Journal of Food Engineering*, *77*(3), 575–584. https://doi.org/10.1016/j.jfoodeng.2005.07.029

Vavilov, V., & Burleigh, D. (2020). *Infrared Thermography and Thermal Nondestructive Testing*. Springer Nature.

Vicent, V., Ndoye, F.-T., Verboven, P., Nicolaï, B., & Alvarez, G. (2019). Effect of dynamic storage temperatures on the microstructure of frozen carrot imaged using X-ray micro-CT. *Journal of Food Engineering*, *246*, 232–241. https://doi.org/10.1016/j.jfoodeng.2018.11.015

Vicent, V., Ndoye, F.-T., Verboven, P., Nicolaï, B., & Alvarez, G. (2020). Modeling ice recrystallization in frozen carrot tissue during storage under dynamic temperature conditions. *Journal of Food Engineering*, *278*, 109911. https://doi.org/10.1016/j.jfoodeng.2020.109911

Wieneke, B. (2015). PIV uncertainty quantification from correlation statistics. *Measurement Science and Technology*, *26*(7), 074002. https://doi.org/10.1088/0957-0233/26/7/074002

Wu, W., & Defraeye, T. (2018). Identifying heterogeneities in cooling and quality evolution for a pallet of packed fresh fruit by using virtual cold chains. *Applied Thermal Engineering*, *133*, 407–417. https://doi.org/10.1016/j.applthermaleng.2017.11.049

Xiaofeng, X., & Xuelai, Z. (2021). Simulation and experimental investigation of a multi-temperature insulation box with phase change materials for cold storage. *Journal of Food Engineering*, *292*, 110286. https://doi.org/10.1016/j.jfoodeng.2020.110286

Xiaofeng, X., Xuelai, Z., & Munyalo, J. M. (2017). Simulation Study on Temperature Field and Cold Plate Melting of Cold Storage Refrigerator Car. *Energy Procedia*, *142*, 3394–3400. https://doi.org/10.1016/j.egypro.2017.12.476

Yang, L., Jin, X., Zhang, Y., & Du, K. (2021). Recent development on heat transfer and various applications of phase-change materials. *Journal of Cleaner Production*, *287*, 124432. https://doi.org/10.1016/j.jclepro.2020.124432

Yang, T., Wang, C., Sun, Q., & Wennersten, R. (2017). Study on the application of latent heat cold storage in a refrigerated warehouse. *Energy Procedia*, *142*, 3546–3552. https://doi.org/10.1016/j.egypro.2017.12.243

Yilmaz, D., Mancuhan, E., & Yılmaz, B. (2020). Experimental investigation of PCM location in a commercial display cabinet cooled by a transcritical CO2 system. *International Journal of Refrigeration*, *120*, 396–405. https://doi.org/10.1016/j.ijrefrig.2020.09.006

Zhang, X., Su, G., Yu, J., Yao, Z., & He, F. (2015). PIV measurement and simulation of turbulent thermal free convection over a small heat source in a large enclosed cavity. *Building and Environment*, *90*, 105–113. https://doi.org/10.1016/j.buildenv.2015.03.015

Zhao, X., Xia, M., Wei, X., Xu, C., Luo, Z., & Mao, L. (2019). Consolidated cold and modified atmosphere package system for fresh strawberry supply chains. *LWT*, *109*, 207–215. https://doi.org/10.1016/j.lwt.2019.04.032

Zhao, Y., Zhang, X., & Xu, X. (2020). Application and research progress of cold storage technology in cold chain transportation and distribution. *Journal of Thermal Analysis and Calorimetry*, *139*(2), 1419–1434. https://doi.org/10.1007/s10973-019-08400-8

Zhao, Y., Zhang, X., Xu, X., & Zhang, S. (2020). Research progress of phase change cold storage materials used in cold chain transportation and their different cold storage packaging structures. *Journal of Molecular Liquids*, *319*, 114360. https://doi.org/10.1016/j.molliq.2020.114360

Zwietering, M. H. (2009). Quantitative risk assessment: Is more complex always better?: Simple is not stupid and complex is not always more correct. *International Journal of Food Microbiology*, *134*(1), 57–62. https://doi.org/10.1016/j.ijfoodmicro.2008.12.025

APPENDIX

ARTICLE 6

Article information

Article title

Dataset of experimental study investigation of airflow and heat transfer in an insulated box equipped with a phase change material

Authors

Tanathep Leungtongkum[a, b]*, Onrawee Laguerre[a], Denis Flick[b], Alain Denis[a], Steven Duret[a] and Nattawut Chaomuang[c]

Affiliations

[a]Université Paris-Saclay, INRAE, FRISE, 92761, Antony, France

[b]Université Paris-Saclay, INRAE, AgroParisTech, UMR SayFood, 91120 Palaiseau, France

[c]Department of Food Engineering, School of Engineering, King Mongkut's Institute of Technology Ladkrabang, Bangkok, Thailand 10520

Corresponding author's email address and Twitter handle

Tanathep.leungtongkum@inrae.fr

Keywords

Food Cold Chain, Heat Transfer, Airflow, Insulated Box, Phase Change Material

Abstract

This article contains a detailed description of the experimental protocol of air velocity (by particle image velocimetry - PIV) and temperature measurement (by T-type thermocouples) in an insulated box equipped with a Phase Change Material (PCM). The study was conducted in an empty box and a loaded box with extruded polystyrene slabs (XPS) and methylcellulose slabs (test product). The measurement was conducted at the middle plane and lateral plane. This article contains a complete dataset along with the illustrated figures of conducted experiment. They lead to more understanding of phenomena inside a closed cavity with a cold source and can be useful for validating numerical models, e.g., the results computed by computational fluid dynamic.

Specifications table

Subject	Bioengineering
Specific subject area	Air velocity and temperature fields measured in an empty and loaded insulated box with a cold source generated by Phase Change Material
Type of data	Table Image Graph MATLAB code Dataset
How the data were acquired	Air velocity measured by Particle Imagery Velocimetry (PIV) Temperature measured by calibrated thermocouples T-Type.
Data format	Raw Analyzed
Description of data collection	Air velocity (at the middle plane and lateral plane of YZ plane and XZ plane) and temperature (at the middle plane and lateral plane of YZ plane and half of the middle plane of XZ plane) in insulated boxes equipped with Phase Change Material (PCM) under following factors: PCM position (on a side and at the top) and Loading condition (no load, loaded with XPS and loaded with test product)
Data source location	• INRAE (FRISE Research unit) • Antony • France
Data accessibility	With the article Repository name: Mendeley Data Data identification number: 10.17632/r7gj93tvz9.1 10.17632/yjbpwtx3c4.1 Direct URL to data: https://data.mendeley.com/datasets/r7gj93tvz9/1 https://data.mendeley.com/datasets/yjbpwtx3c4/1 Repository name: GitHub Data identification number:

	10.5281/zenodo.6900688 Direct URL to data: https://github.com/Tanathepl/Temperature-contour.git.
Related research article	Leungtongkum, T., Laguerre, O., Flick, D., Denis, A., Duret, S., & Chaomuang, N. (2022). Experimental investigation of airflow and heat transfer by natural convection in an insulated box with a Phase Change Material using a Particle Image Velocimetry technique. J. of Food Engineering, 111207. https://doi.org/10.1016/j.jfoodeng.2022.111207

Value of the data

- The experimental data of air velocity, temperatures of air, and product enable an understanding of the relation between heat transfer and airflow by natural convection in a closed cavity with a cold source.
- The different loading conditions (no load, load with extruded polystyrene, and load with test product) allow the understanding of the impact of loading and the heat exchange between the load and the internal air.
- These data are rare in literature for food transport in an insulated box because the methodology of low air velocity measurement is complicated, i.e., appropriate tracer, laser lighting power, and the time interval between image acquisitions.
- Data can be used/reused to compare with the CFD (Computational Fluid Dynamic) simulation results.

1 Data description

Data presented in this article include raw data of air velocity and temperature measurement, figures of air velocity field and temperature contour field in an insulated box equipped with a Phase Change Material (PCM) under various PCM position and loading condition. Table 1 describes all experimental conditions, only the corresponding figures of the conditions 1 to 4 are presented in this data paper, the ones of the conditions 5 and 6 can be found in Leungtongkum et. al. [1].

Table 1 Experimental conditions

Condition	PCM position	Loading condition	Corresponding figures
1	Side wall	No load	1 to 3
2	Top	No load	4 to 6
3	Side wall	XPS (4 slabs)	7 to 10
4	Top	XPS (4 slabs)	11 to 14
5	Side wall	Test product (16 packs)	10 and 12 of Leungtongkum et. al. [1]
6	Top	Test product (16 packs)	13 to 14 of Leungtongkum et. al. [1]

XPS = extruded polystyrene slabs

The air velocity component, its magnitude and uncertainty in the insulated box under these conditions are shown in Dataset 1: Experimental investigation in an insulated box (Air velocity) (https://data.mendeley.com/datasets/yjbpwtx3c4/1)

The average temperature in the insulated box under these conditions are shown in Dataset 2: Experimental investigation in an insulated box (Average temperature) (https://data.mendeley.com/datasets/r7gj93tvz9/1)

The temperature contour field was drawn via MATLAB by interpolating the measured temperature at different positions during stable conditions. The codes of this drawing are shown in Tanathepl/Temperature-contour

(https://github.com/Tanathepl/Temperature-contour.git.)

The air velocity field at Y = 145 mm and 15 mm in the unloaded box with PCM on a side are shown in Figure 1 and 2. The temperature field at Y = 145 mm is shown in Figure 3, due to the symmetry of this plane, only a half of the results is shown. Air velocity field at X = 250 mm and 15 mm and temperature field at X = 250 mm are shown in Figures 5a, 5b and 6a of Leungtongkum et.al [1].

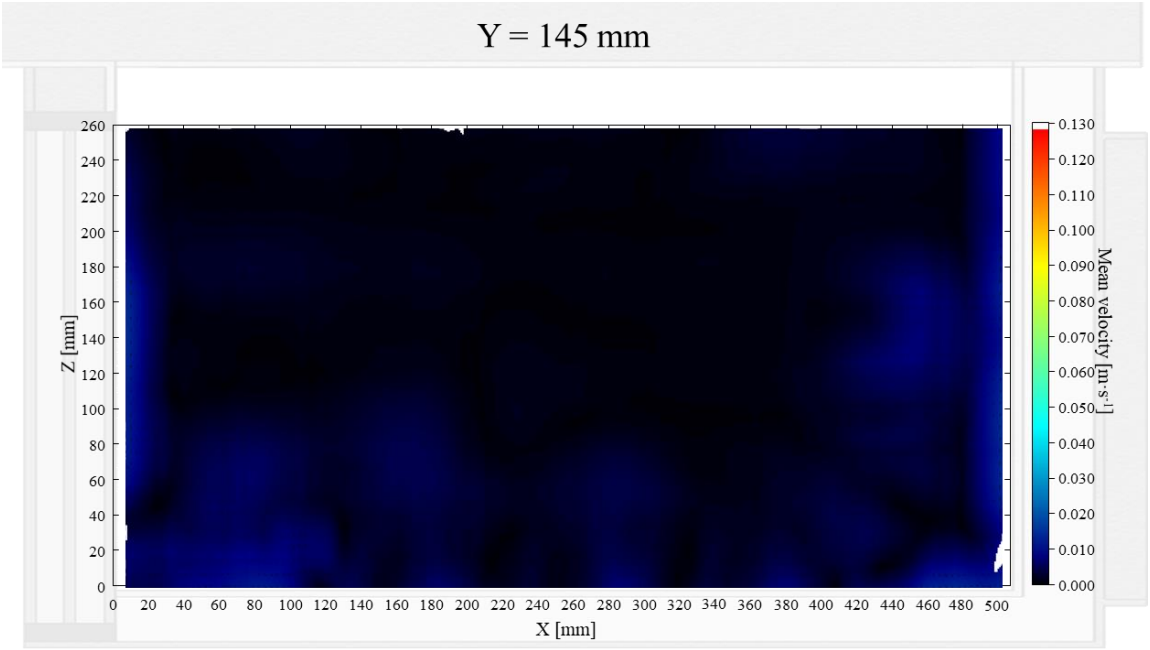

Figure 1: Air velocity field at Y = 145 mm in an unloaded horizontal box with PCM on a side

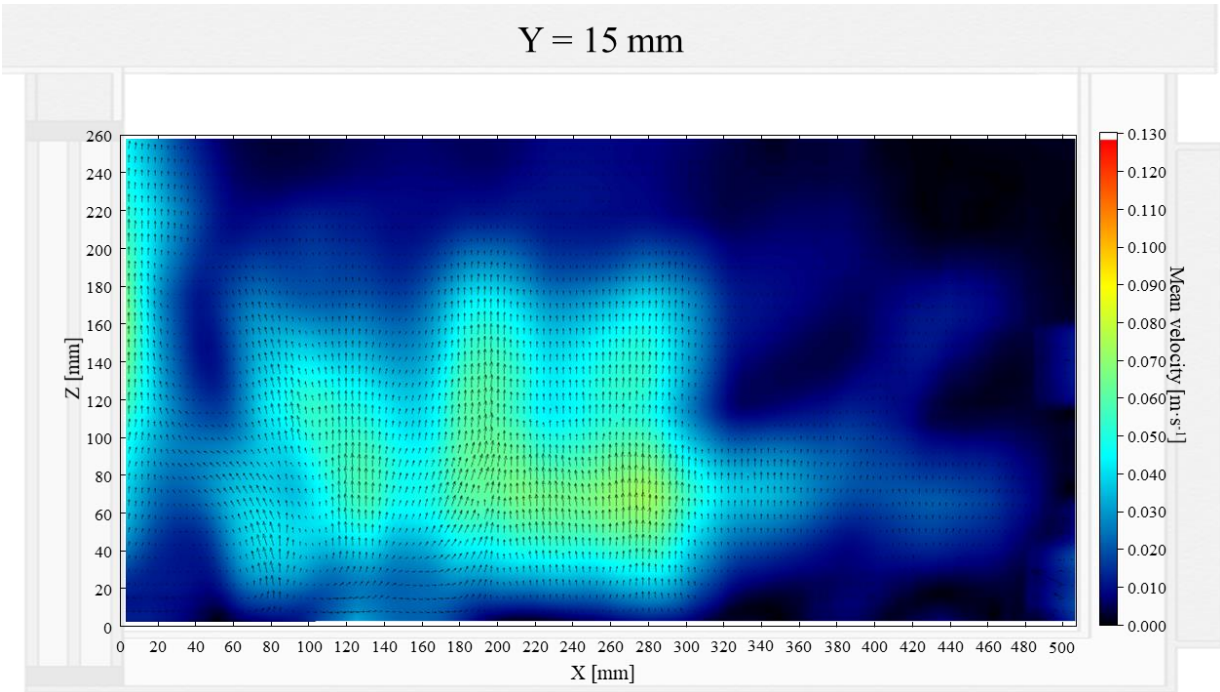

Figure 2: Air velocity field at Y = 15 mm in an unloaded horizontal box with PCM on a side

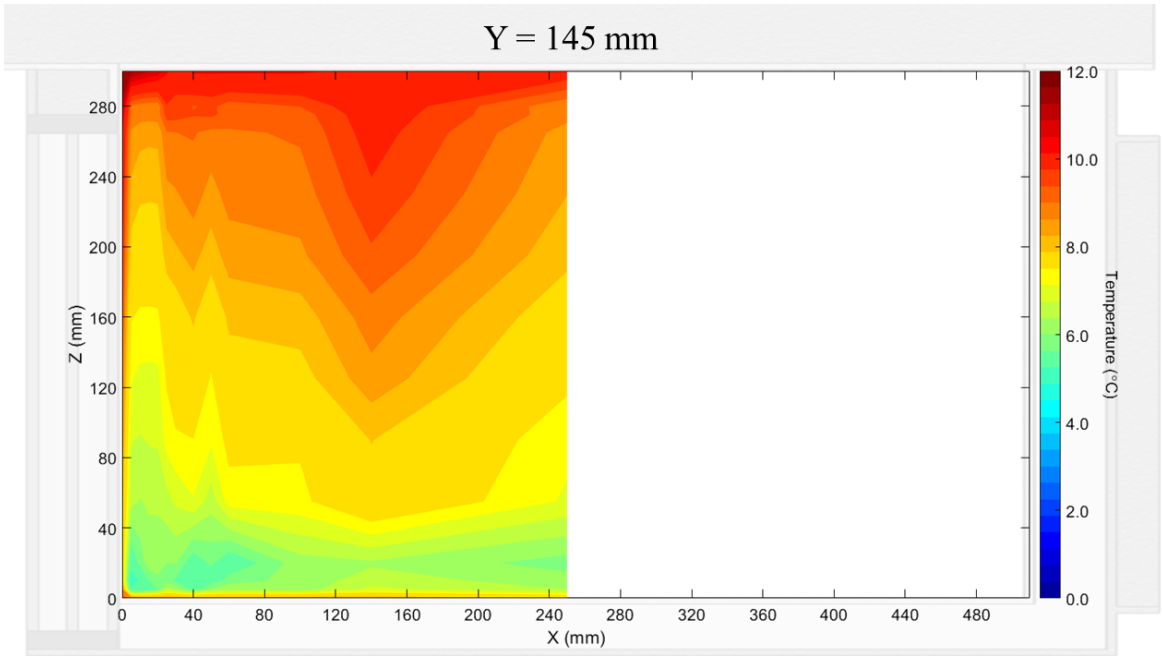

Figure 3: Temperature field at Y = 145 mm in an unloaded horizontal box with PCM on a side

Air velocity field at Y = 165 mm and 15 mm and temperature field at Y = 165 mm (half of the plane) in an unloaded box with PCM at top were shown in Figure 4 to 6. Air velocity field at X = 250 mm and 15 mm and temperature field at X = 250 mm are shown and discussed in Figures 7a, 7b and 8a of Leungtongkum et.al [1].

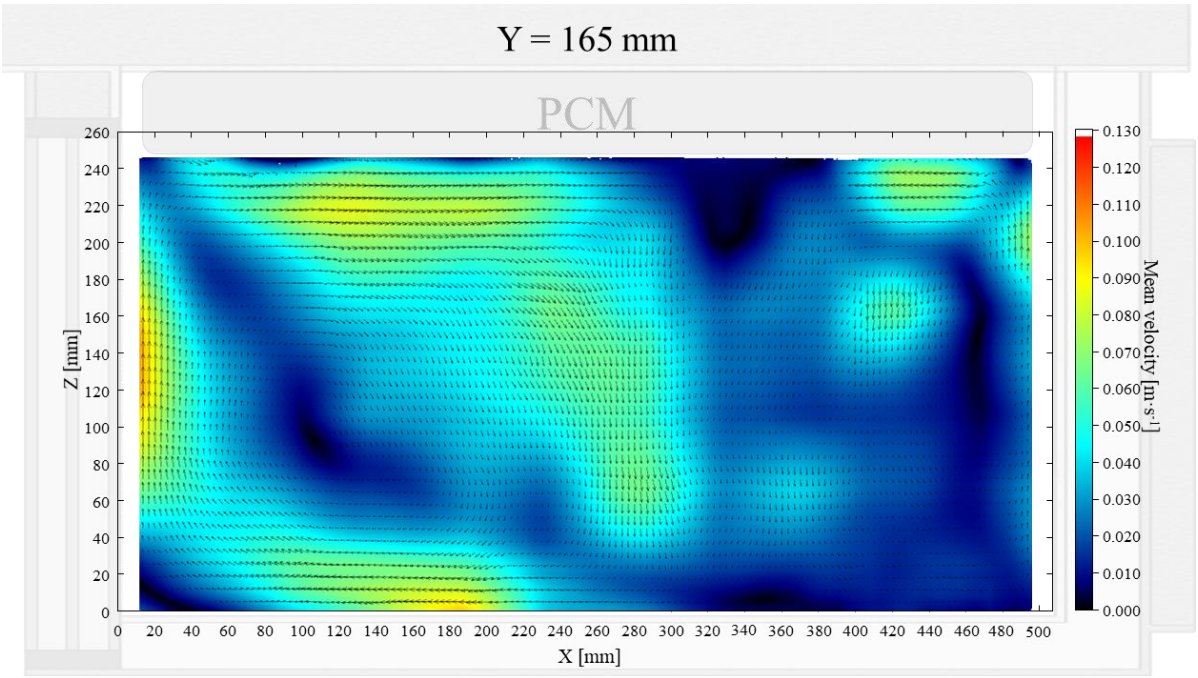

Figure 4: Air velocity field at Y = 165 mm in an unloaded horizontal box with PCM at top

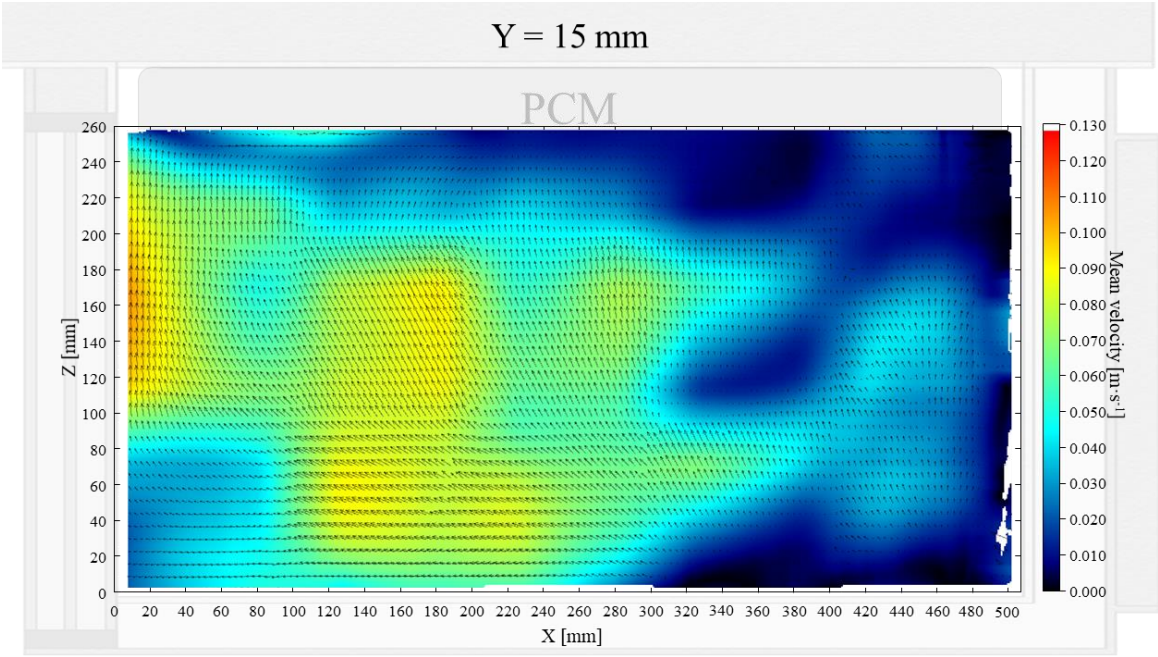

Figure 5: Air velocity field at Y = 15 mm in an unloaded horizontal box with PCM at top

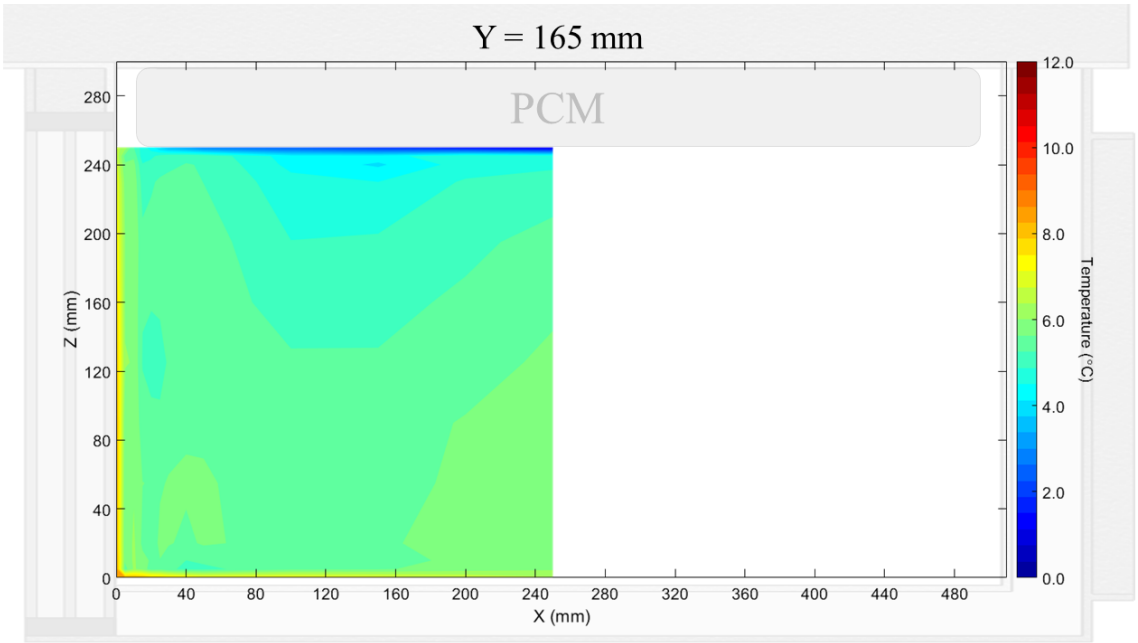

Figure 6: Temperature field at Y = 165 mm in an unloaded horizontal box with PCM at top

Air velocity field at Y = 145 mm and 15 mm and temperature field at X = 250 mm and X = 15 mm in a box loaded with XPS and PCM on a side were shown in Figure 7 to 10. Air velocity field for X = 250 mm and 15 mm are shown and discussed in Figures 10a and 10b of Leungtongkum et.al [1].

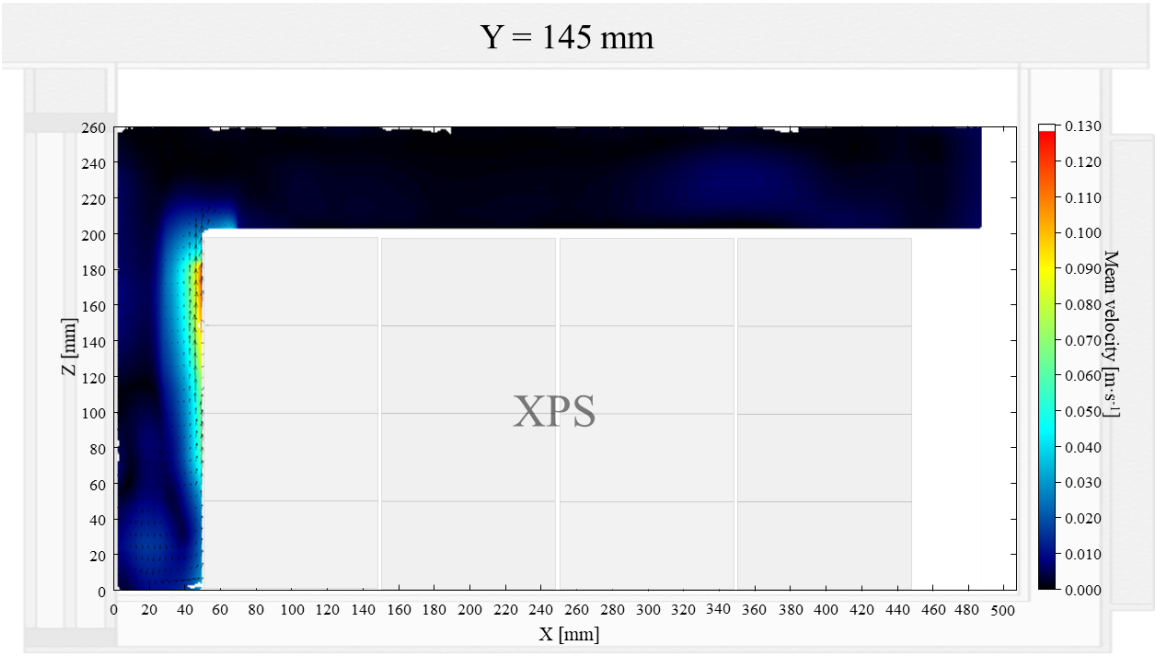

Figure 7: Air velocity field at Y = 145 mm in a box loaded with XPS and PCM on a side. White area on the right represents the unmeasurable zone because of the inaccessibility of laser sheet.

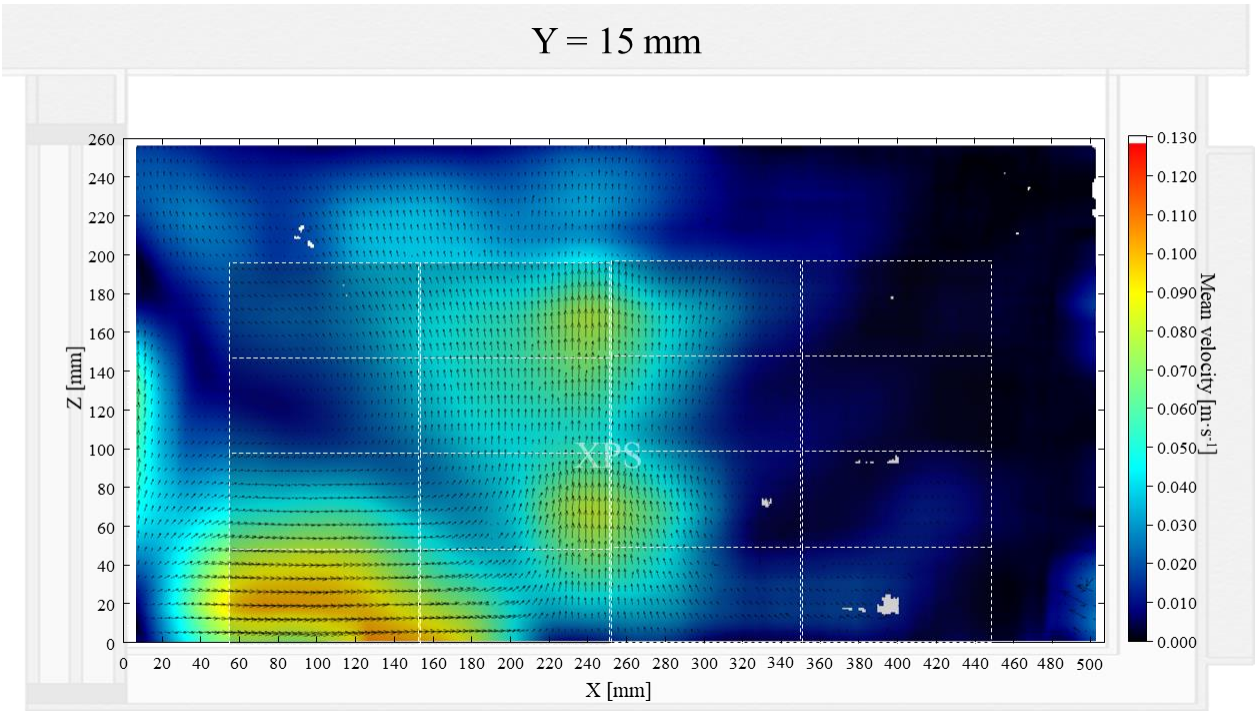

Figure 8: Air velocity field at Y = 15 mm in a box loaded with XPS and PCM on a side

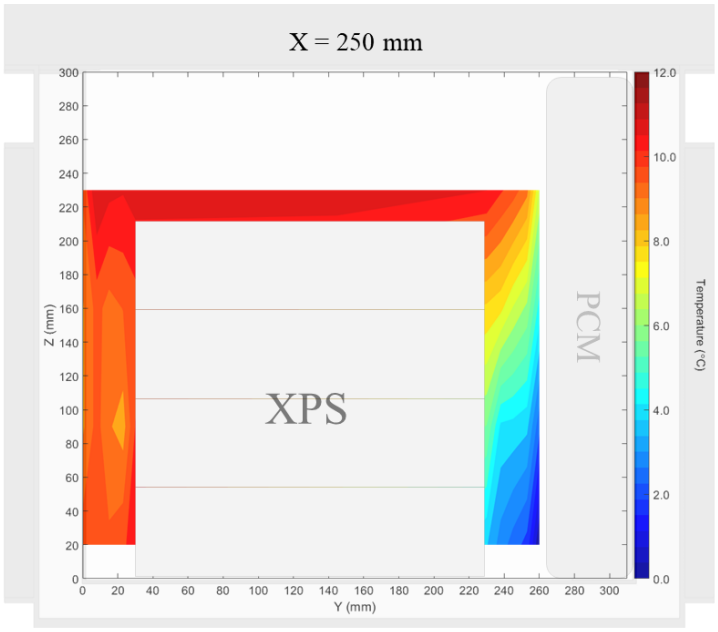

Figure 9: Temperature field at X = 250 mm in a box loaded with XPS and PCM on a side

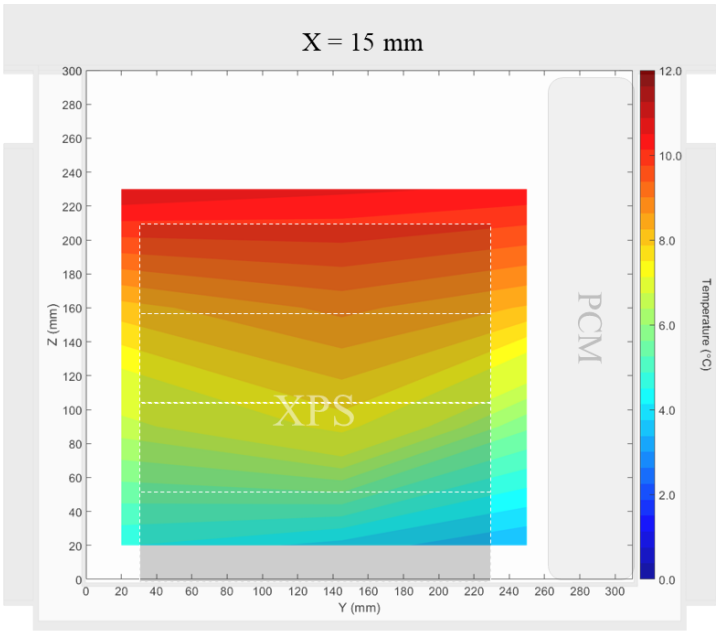

Figure 10: Temperature field at X = 15 mm in a box loaded with XPS and PCM on a side

Air velocity field at Y = 165 mm and 15 mm and temperature field at X = 250 mm and X = 15 mm in a box loaded with XPS and PCM at top were shown in Figure 11 to 14. Air velocity field for X = 250 mm and 15 mm are shown and discussed in Figures 13a and 13b of Leungtongkum et.al [1].

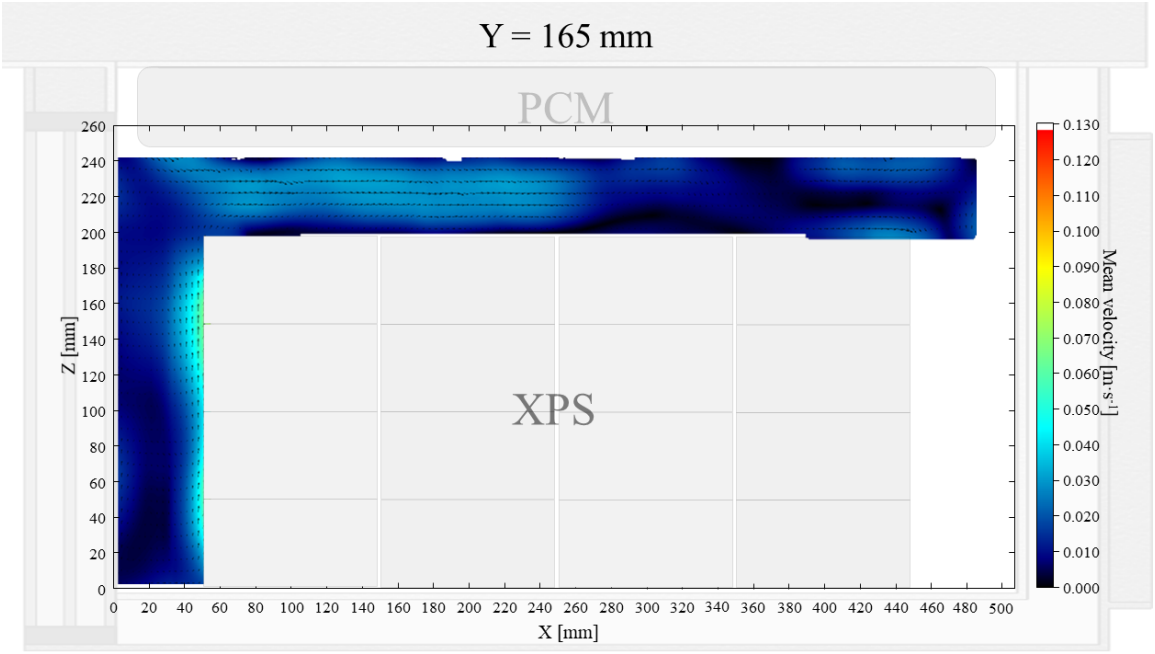

Figure 11: Air velocity field at Y = 165 mm in a box loaded with XPS and PCM at top. White area on the right represents the unmeasurable zone because of the inaccessibility of laser sheet.

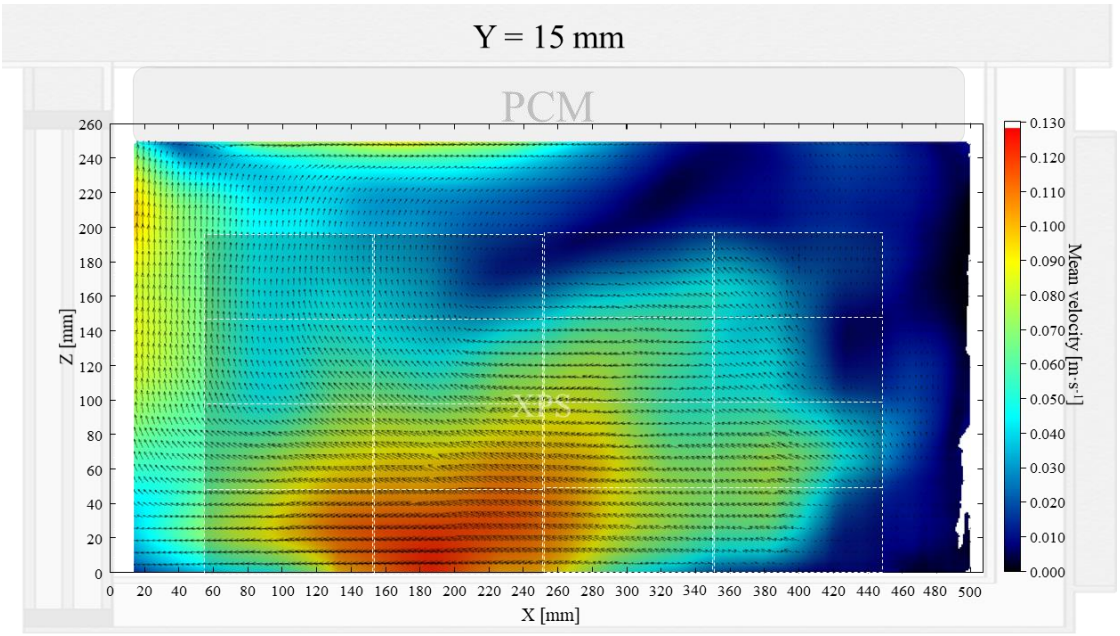

Figure 12: Air velocity field at Y = 15 mm in a box loaded with XPS and PCM at top

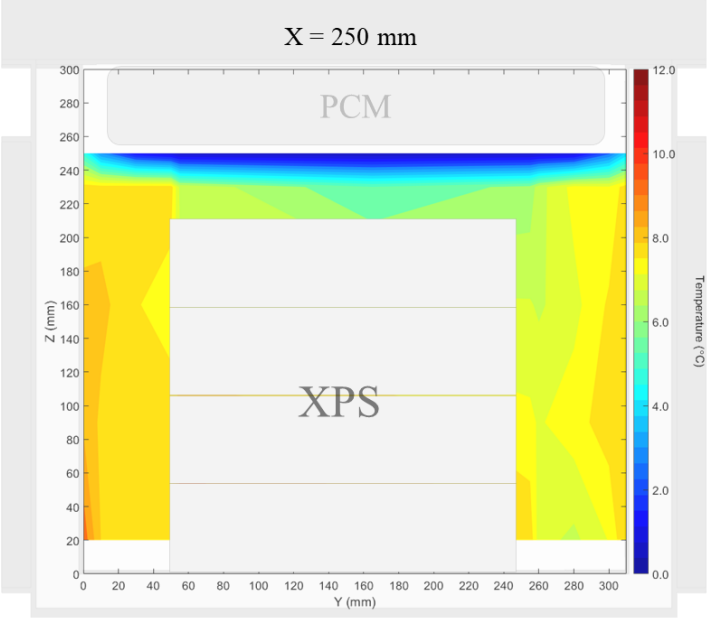

Figure 13: Temperature field at X = 250 mm in a box loaded with XPS and PCM at top

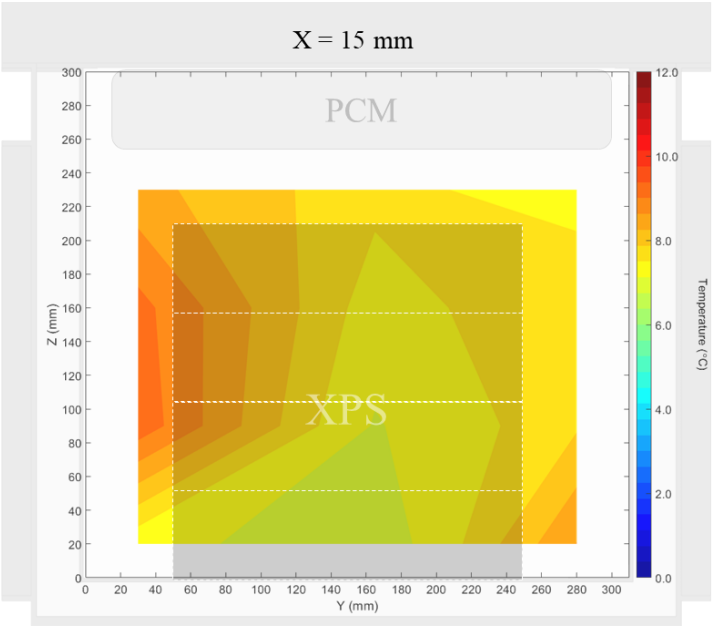

Figure 14: Temperature field at X = 15 mm in a box loaded with XPS and PCM at top

2. Experimental design, materials and methods

2.1 Material

Figure 15 shows the materials and experimental setup. Two boxes were used, for the thermal study, the commercialized multilayer insulated box (Manutan SA, Gonesse,

France) with 500 mm x 310 mm x 300 mm internal dimensions and 570 mm x 380 mm x 370 mm external dimensions is used. The side and bottom walls contain expanded polystyrene (25 mm thickness), polypropylene (inner and outer layers of 3.5 mm thickness), and an air gap is expected between the expanded polystyrene and the inner layer (estimated thickness: 5 mm). The other box is for the airflow study and has the same dimensions and wall structure, but two side walls are replaced by triple-glazed windows (3 glass panes, each with a thickness of 4 mm, two argon-filled 10-mm gaps). The illustration of these two boxes is shown in Figures 1 of Leungtongkum et. al [1]. The box was positioned on a 50-mm height wooden support to ensure homogeneous heat exchange with the ambient air around the box (Figure 15a). This box was placed on a 0.7-m height table in the center of the 3.4 m x 3.4 m x 2.5 m temperature-controlled test room. The PCM container (Figure 15c), made of polypropylene (2.5-mm thickness) and filled with 3.5 kg of tap water (melting point ~ 0°C), has external dimensions of 460 mm x 280 mm x 50 mm. The extruded polystyrene slab (XPS) has a dimension of 400 mm x 200 mm x 50 mm (Figure 15d). The test products (with 200 mm x 100 mm x 50 mm pack dimensions – Figure 15e) contained 23% methylhydroxyethylcellulose, 76.4% water, and 0.5% NaCl (Refrigeration Development and Testing Ltd., North Somerset, UK).

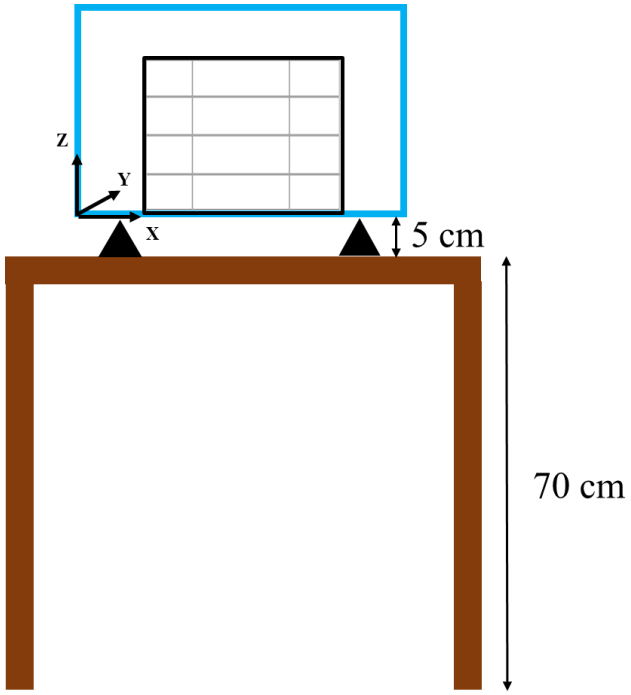

(a)

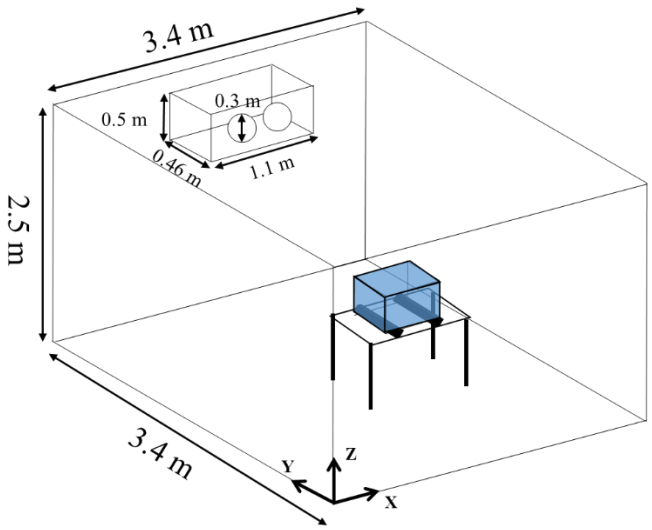

(b)

(c)

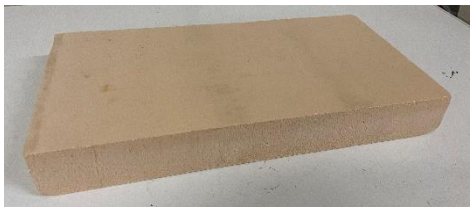

(d)

(e)

Figure 15: Materials and experimental setup (a) the box with wood support on the table, (b) experimental setup, (c) PCM container, (d) extruded polystyrene slab, and (e) test product pack

Thermal conductivity (k) of each box wall was determined by calculation using thermal conductivity and thickness of each layer as in eq.1

$$k = \frac{1}{\sum_{i=1}^{n} \frac{x_i}{k_i}} \quad (1)$$

Wherek is thermal conductivity of material (W m^{-1} K^{-1})

x is thickness (m)

Table 2 shows thermal conductivity at 300 K of each material

Material	k (W m^{-1} K^{-1})	Reference
Polypropylene	0.12	[2]
Expanded polystyrene	0.029	[2]
Air	0.026	[3]
Argon	0.018	[4]
Glass	1.4	[3]

Thus, the thermal conductivity of the insulated wall and the glass-pane wall is 0.90 W m^{-1} K^{-1} and 0.89 W m^{-1} K^{-1}, respectively.

The experiment using the internal heating method (adapted from ATP [5]) was also conducted to measure the heat transmission coefficient (K) with 20 W and 30 W heating. Firstly, 14 thermocouples were placed inside the box (8 at 50 mm from each corner and 6 at 50 mm from the center of each surface). The other 14 were put outside the box in the same manner. The heating unit consisted of adjustable resistance and a fan. After setting the heating power, the system was left until reaching a steady state (temperature fluctuation is less than ±0.3°C for 12 h with less than ±1.0°C during the preceding 6 h.

Data over at least 6 h was averaged to get the mean temperature at each position. Next, mean data of either inside or outside the box was averaged to get internal and external temperature, respectively. The heat transmission coefficient can be calculated by eq.2

$$K = \frac{\dot{Q}}{A\Delta T} \qquad (2)$$

Where K is heat transmission coefficient (W m^{-2} K^{-1})

$\dot{Q}$ is heating power (W)

$A = \sqrt{A_{int}A_{ext}}$ is mean surface area between internal surface and external surface (m^2)

$\Delta T = T_{in} - T_{out}$ is temperature difference between inside and outside of the box (K)

The experimental value of heat transmission coefficient is shown in Table 3.

Table 3 Experimental value of heat transmission coefficient

Box type	**Power (W)**	**A (m^2)**	**T_{in} (°C)**	**T_{out} (°C)**	**K (W m^{-2} K^{-1})**
Box A (Insulated box)	20	1.027	37.52	5.53	0.61
	30	1.027	46.76	5.44	0.71
Box B (Glass-pane box)	20	1.027	36.21	6.13	0.65
	30	1.027	43.9	6.22	0.78

2.2 Thermal study

2.2.1 Experimental setup

The temperature was measured by T-type thermocouples linked to the Agilent 34972A data acquisition unit (Agilent Technologies, CA, USA). These thermocouples were calibrated at -10°C, 0°C, 10°C, 20°C and 30°C with a precision of ±0.2°C.

PCM slab was placed horizontally in a freezer set at -2°C for at least 48 h before each experiment.

Sixteen packs of test product were put in a polystyrene box and stored in a domestic refrigerator set at 4°C or 10°C for at least 24 h before each experiment to assure the homogeneous product's initial temperature.

2.2.2 Temperature measurement in an unloaded box

Firstly, all thermocouples were placed in the box. Air temperature distribution was measured at the middle plane of the YZ plane (X = 250 mm) with various y and z positions and around half of the XZ plane (Y = 145 mm for the box with PCM on the side and Y = 165 mm for that with PCM at the top). Two stands, each equipped with 12 thermocouples spreading over the height (z-axis), were displaced inside the box in x and y direction to obtain the air temperature field. Thermocouples were also put inside the PCM (at half thickness), on the surface of the PCM container, and the box's internal walls. The diagram showing thermocouples positions is in Figure 2a of Leungtongkum et. al. [1].

Ninety minutes after the box was closed (when the steady state was reached), temperatures were recorded for at least 5 min. (acquisition interval 15 s). Then, the box

was opened in order to move the stands prior to closing the box again. This process took less than 1 min. to avoid disturbances caused by external air to the greatest possible extent. Fifteen minutes later (when the steady state was reached again), temperatures were recorded over 5 min. before re-opening the box. Then, the position of the stands was changed in y direction (18 to 21 positions), allowing 200 measurement points in total. A temperature contour map was plotted by MATLAB with interpolation from these measurements.

Figure 16 illustrates the temperature evolution of some locations in an unloaded horizontal box with PCM on a side under 20°C ambient during the first measurement (Figure 16a) and the following measurement (Figure 16b). These figures show the period during which the average temperature was calculated: 135 min. to 140 min. after box closing for the first measurement and 17 min. to 22 min. for the following measurement. Then, these average temperatures were used to present the temperature field in stable condition in the following figures (Figures 1, 2, 4, and 5).

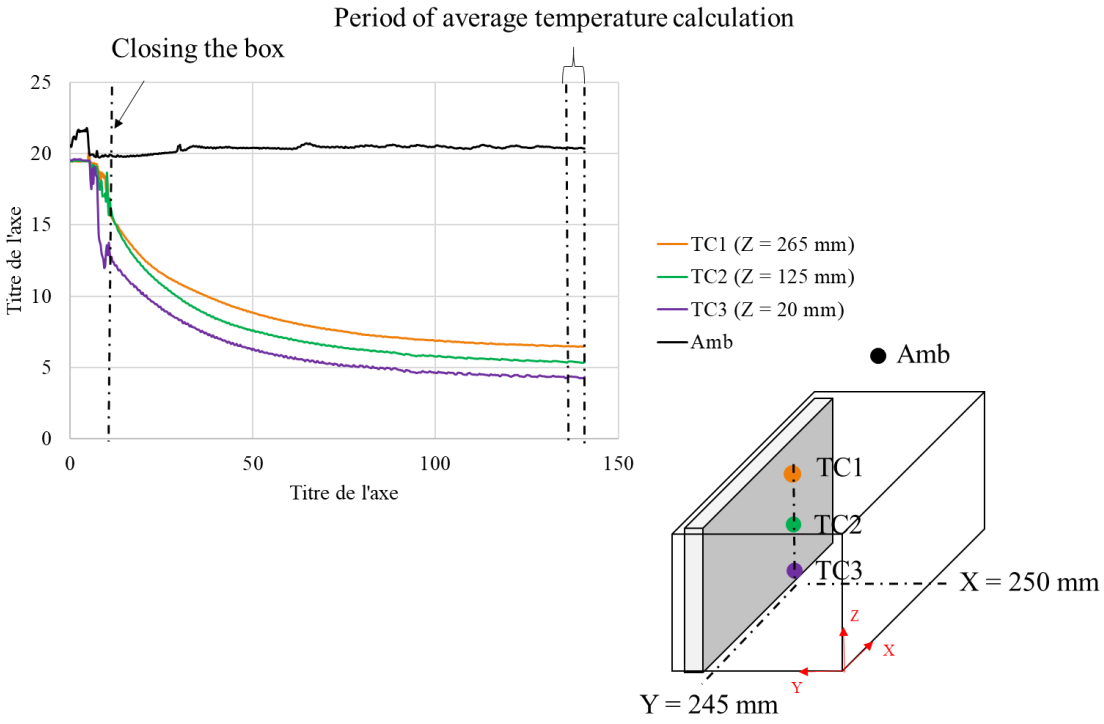

(a)

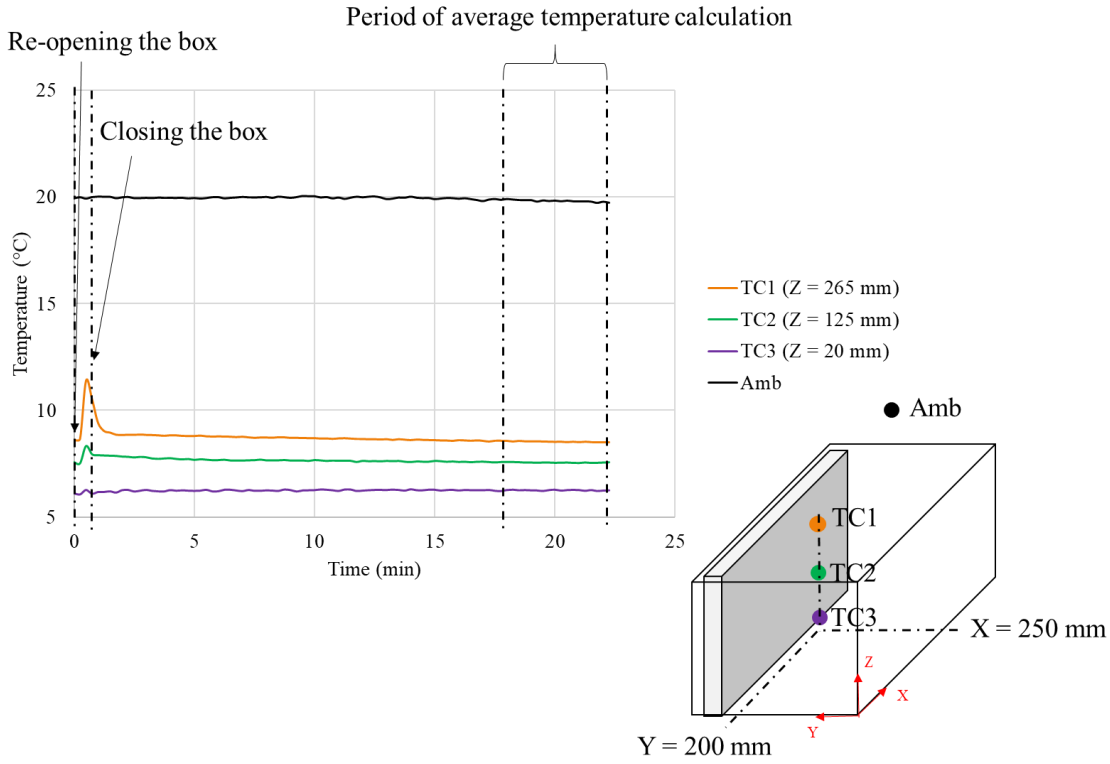

(b)

Figure 16: Temperature evolution of some locations in an unloaded horizontal box with PCM on a side under 20°C ambient) of (a) the first measurement and (b) the following measurement

2.2.3 Temperature measurement in a loaded box

For loaded boxes, it was loaded with four slabs of XPS or 16 test product packs. The temperature measurement was carried out at fixed positions with 29 thermocouples on the surface of the XPS slab, and the test product and core of the test product located at the middle plane (x = 250 mm) and with ten thermocouples at the lateral plane (x = 15 mm). The diagram showing thermocouples positions is in Figure 2b of Leungtongkum et. al. [1]. The measurement started after the box closing until complete PCM melted without the box opening during the experiment. The temperatures at the middle plane (x = 250 mm) were recorded continuously (every 30 s). The results of the period ranging from 400 min. to 600 min. were analyzed and compared. The temperature contour map was drawn by MATLAB with interpolation.

Figure 17 shows temperature evolution at the bottom of a loaded horizontal box with PCM on a side under 20°C ambient, product initial temperature = 4°C. This figure shows the period from 400 min. to 600 min. during which the average temperature

was calculated. Then, these average temperatures were used to present the temperature field in stable condition in the following figures (Figures 7, 8, 11, and 12).

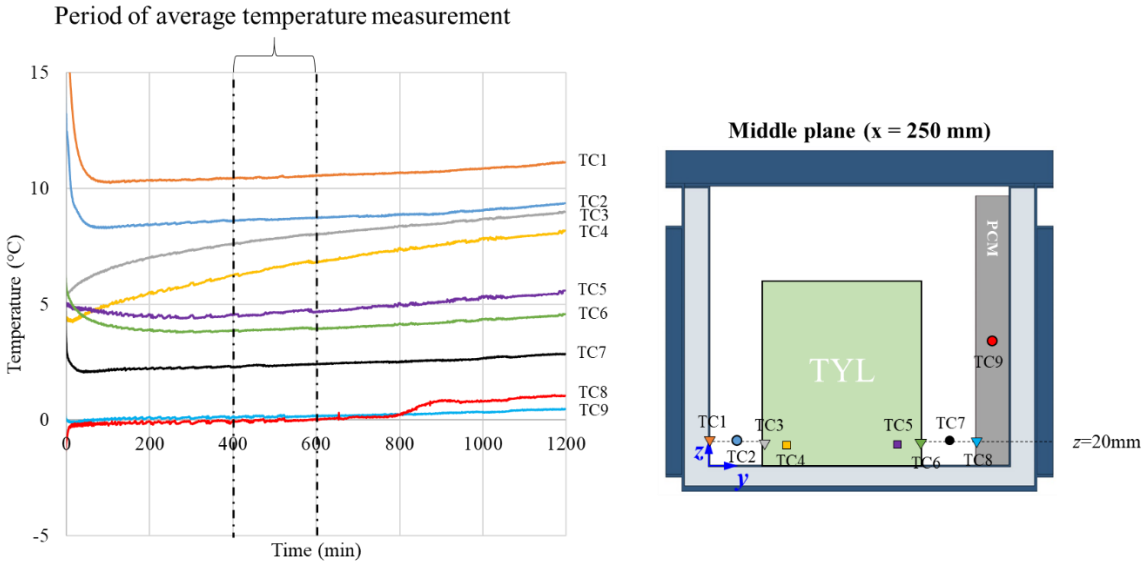

Figure 17: Temperature evolution at the bottom of a loaded horizontal box with PCM on a side loaded with test product

2.3 Airflow study

2.3.1 Instrumentation

The oil-based smoke tracer with a 0.3 µm mean diameter was precooled in a container containing four PCM packs, reducing the smoke temperature from about 50°C to around 10°C. A small fan guided smoke to the box through a connecting duct while a valve controlled its flow rate.

A 2D-PIV system (LaVision, FlowMaster 2D) comprised three main components: a double-pulsed Nd:YLF laser (527 nm wavelength, 10 mJ pulse energy), a high-speed 12-bit CMOS video camera (Photron, FASTCAM SA3; 1024 ×1024 pixels in resolution) connected with a lens (Sigma; 105 mm, f/1:2.8) and a programmable timing unit (PTU-X) for the synchronization of laser and camera. Smoke particle scattering during laser pulses visualized the airflow pattern inside the cavity.

The camera and the laser were mounted on a three-dimensional displacement system (precision of displacement ±1 mm). This system makes the perpendicularity between the camera view and the light sheet (1-mm thickness) possible. The diagram and photograph of the experimental setup for the airflow study are shown in Figure 3 of Leungtongkum et. al. [1].

2.3.2 Image acquisition

For each measured window, 500 pairs of images were recorded every 20 ms with a time interval of 900 μs between two images of the same pair, in other words, between two pulsed laser illuminations. The total duration of measurement was 10 s.

2.3.3 Image post-processing

A multi-pass correlation algorithm was applied to calculate the instantaneous airflow vector. The cross-correlation between each image in the pair was accomplished by decreasing interrogation window sizes: 64 × 64 pixels with 50% overlap for the first pass and 32 × 32 pixels with 75% overlap for the three following passes. In each pass, all interrogation windows at the same position on the paired images were cross-correlated and independently produced a single displacement vector, then were later merged to produce a 2D vector field of the whole image. After 500 instantaneous vector fields had been attained, the mean velocity field of each measured window was calculated by Equation 3.

$$\bar{v} = \frac{1}{N}\sum_{i=1}^{N}\sqrt{v_{y,i}^2 + v_{z,i}^2} \qquad (3)$$

where N is the total number of measured images of the same windows (N = 500 in our study) and v_y and v_z are the horizontal and vertical velocity components in m s^{-1}, respectively.

The mean velocity fields of all measured windows were then combined to construct the velocity field of the entire measurement plane. It should be highlighted that the out-of-plane regions and the regions near the reflection surface in the images (e.g., the surfaces of PCM, walls, and the load) were excluded prior to the vector calculation.

The DaVis software employs the correlation statistics method to estimate the uncertainty of the PIV measurement. As discussed in Wieneke [6], the uncertainty is quantified based on the statistical analysis of the correlation process using differences in the intensity pattern of the two images.

2.3.4 Experimental protocol

Air velocity measurements were conducted under stable conditions: after 90 min. for unloaded boxes, and after 4 hours for loaded boxes. The PIV measurement was started 30 min. afterward. It is to be emphasized that the standard deviations of the air temperatures at different positions in the box did not exceed 0.3°C during PIV measurement.

The PIV measurements were performed on the middle plane of the YZ plane (x = 250 mm), on the lateral plane of the YZ plane (x = 15 mm), on the middle plane of the XZ plane (y = 145 mm for the condition with PCM on a side and y = 165 mm for that with PCM at the top) and a lateral plane of XZ plane (y = 15 mm). Based on the image calibration using a ruler and the DaVis software, a magnification factor of 0.108 mm/pixel was defined, and the image size was 115.5 mm × 115.5 mm. The positions of the measured windows were changed by using the displacement system as explained above. Several measured windows with partial overlapping were applied to cover the whole area of the plane.

Ethics Statement

This work did not involve human subjects, animal experiments and data collected from social media platforms.

CRediT author statement

Tanathep Leungtongkum: Conceptualization, Methodology, Investigation, Validation, Formal analysis, Software, Writing - Original Draft Preparation and Visualization **Onrawee Laguerre:** Validation, Formal analysis, Writing - Review & Editing, Supervision, Project Administration, Funding acquisition **Denis Flick:** Methodology, Validation, Formal analysis, Writing - Review & Editing and Supervision. **Steven Duret:** Validation, Formal analysis, Writing - Review & Editing, Supervision. **Alain Denis:** Investigation and Software **Nattawut Chaomuang:** Conceptualization, Methodology, Investigation, Validation, Formal analysis, Software, Writing - Original Draft Preparation, Visualization and Funding acquisition.

Acknowledgments

King Mongkut's Institute of Technology Ladkrabang, Thailand (contract no. KREF156402), French Embassy in Thailand, and the National Research Institute for Agriculture, Food and Environment, France are gratefully acknowledged for their financial support. The first author, T. Leungtongkum, would also like to thank the Office of the Civil Service Commission of Thailand and Chulalongkorn University, Thailand for the award of his PhD scholarship. Thanks to LaVision for PIV technical support.

Declaration of interests

☒ The authors declare that they have no known competing financial interests or personal relationships that could have appeared to influence the work reported in this paper.

☐ The authors declare the following financial interests/personal relationships which may be considered as potential competing interests:

References

[1] T. Leungtongkum, O. Laguerre, D. Flick, A. Denis, S. Duret, and N. Chaomuang, "Experimental investigation of airflow and heat transfer by natural convection in an insulated box with a Phase Change Material using a Particle Image Velocimetry technique," *Journal of Food Engineering*, vol. 336, p. 111207, Jan. 2023, doi: 10.1016/j.jfoodeng.2022.111207.

[2] Y. Cengel and A. Ghajar, *Heat and Mass Transfer: Fundamentals and Applications*, 5th edition. New York, NY: McGraw-Hill Education, 2014.

[3] T. L. Bergman, A. S. Lavine, F. P. Incropera, and D. P. DeWitt, *Introduction to Heat Transfer*. Hoboken, NJ: John Wiley & Sons, 2011.

[4] B. A. Younglove and H. J. M. Hanley, "The Viscosity and Thermal Conductivity Coefficients of Gaseous and Liquid Argon," *Journal of Physical and Chemical Reference Data*, vol. 15, no. 4, pp. 1323–1337, Oct. 1986, doi: 10.1063/1.555765.

[5] ATP, *Agreement on the International Carriage of Perishable Foodstuffs and on the Special Equipment to be Used for Such Carriage: (ATP) as amended 6 July 2020*. United Nations, 2020. doi: 10.18356/6fa10b27-en.

[6] B. Wieneke, "PIV uncertainty quantification from correlation statistics," *Meas. Sci. Technol.*, vol. 26, no. 7, p. 074002, Jun. 2015, doi: 10.1088/0957-0233/26/7/074002.

ARTICLE 7

Article information

Article title
Dataset of air velocity and temperature fields inside an insulated box equipped with phase change material under several operating conditions

Authors
Tanathep Leungtongkum[a, b]*, Denis Flick[b], Nattawut Chaomuang[c], Alain Denis[a] and Onrawee Laguerre[a]

Affiliations
[a]Université Paris-Saclay, INRAE, FRISE, 92761, Antony, France
[b]Université Paris-Saclay, INRAE, AgroParisTech, UMR SayFood, 91120 Palaiseau, France
[c]Department of Food Engineering, School of Engineering, King Mongkut's Institute of Technology Ladkrabang, Bangkok, Thailand 10520

Corresponding author's email address and Twitter handle
Tanathep.leungtongkum@inrae.fr

Keywords
Heat Transfer, Airflow, Insulated Box, Phase Change Material, Food Cold Chain

Abstract
This article contains a description of protocol to measure air velocity field (by Particle Image Velocimetry - PIV) and temperature field (by T-type thermocouples) in an insulated box equipped with Phase Change Material (PCM) of melting point 0°C. The influence of various conditions was studied: i) PCM position (at sidewall and at top), ii) aspect ratio of the box (height/width ~ 1 and 1.7), iii) ambient temperature (10°C, 20°C and 30°C), iv) test product initial temperature (4°C and 10°C) and vi) spacing beneath the load (0 mm and 20 mm). This article is related to a published research paper, it provides the dataset of all experiments which can be useful for experimenter to understand the phenomena and for expert in numerical model to validate the developed model e.g., by Computational Fluid Dynamic.

Specifications table

Subject	Bioengineering
Specific subject area	Air velocity and temperature fields measured in an empty and loaded insulated box with cold source generated by Phase Change Material

Type of data	Table Image Graph MATLAB code Dataset
How the data were acquired	Air velocity measured by Particle Image Velocimetry (PIV) Temperature measured by calibrated thermocouples T-Type.
Data format	Raw Analysed
Description of data collection	Air velocity (at middle plane and lateral plane) and temperature (at middle plane) in insulated boxes equipped with PCM (melting point 0°C) under various conditions: • PCM position (at sidewall and at top), • aspect ratio of box (height/width = 1 and 1.7), • ambient temperature (10°C, 20°C and 30°C), • test product (Tylose, TYL) initial temperature (4°C and 10°C) • space beneath the load (0 mm and 20 mm).
Data source location	• INRAE (FRISE Research unit) • Antony • France
Data accessibility	With the article Repository name: Mendeley Data Data identification number: 10.17632/ggmkzk634h.1 10.17632/sz5dgkz7k8.1 Direct URL to data: https://data.mendeley.com/datasets/ggmkzk634h/1 https://data.mendeley.com/datasets/sz5dgkz7k8/1 Repository name: GitHub Data identification number: 10.5281/zenodo.6900688 Direct URL to data: https://github.com/Tanathepl/Temperature-contour.git

Related research article	Leungtongkum, T., Flick, D., Chaomuang, N., Denis, A., & Laguerre, O. (2023). Influence of use conditions on heat transfer in an insulated box equipped with a phase change material. Journal of Food Engineering, 357, 111644. https://doi.org/10.1016/j.jfoodeng.2023.111644

Value of the data

- The experimental data of air velocity field, temperatures of air and product at different positions enable the understanding of the relation between heat transfer and airflow by natural convection in a closed cavity with a cold source.
- These data are rare in literature because the methodology of low air velocity measurement as in food transport in an insulated box is complicated i.e., appropriate tracer, laser lighting power and time interval between image acquisitions.
- Data would be useful for understanding phenomena, insulated box design and optimal operating conditions to maintain product temperature at a recommended value along the supply chain.
- Data can be used to compare with the results of CFD (Computational Fluid Dynamic) simulation.

1. Data description

Data presented in this article include raw data of air velocity and temperature measurement, figures of air velocity field and temperature contour field in an insulated box equipped with a Phase Change Material (PCM) under various PCM position, aspect ratio of the box, ambient temperature, initial load temperature (test product, Tylose) and space beneath the load. Table 1 summarizes all experimental conditions presented in this article and their corresponding figures.

Table 1 Experimental conditions

Condition	Pictogram	PCM position	Aspect ratio (height/width)	Ambient temperature (°C)	Initial load temperature (°C)	Spacing beneath load (mm)	Corresponding figures
1	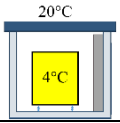	Side wall	1.0	20	4	20	1
2	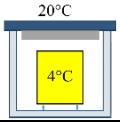	Top	1.0	20	4	20	2
3	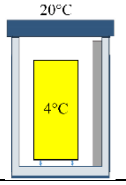	Side wall	1.7	20	4	20	3

4	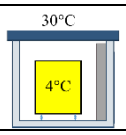	Side wall	1.0	30	4	20	4 and 5
5	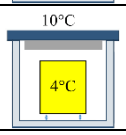	Top	1.0	10	4	20	6
6	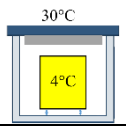	Top	1.0	30	4	20	7
7	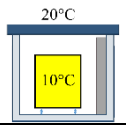	Side wall	1.0	20	10	20	8 and 9
8	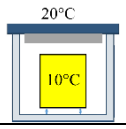	Top	1.0	20	10	20	10
9	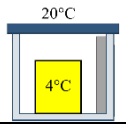	Side wall	1.0	20	4	0	11
10	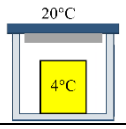	Top	1.0	20	4	0	12

The air velocity component, its magnitude and uncertainty of measurement under these conditions are shown in Dataset 1: Air velocity in an insulated box (https://data.mendeley.com/datasets/ggmkzk634h/1)

The average temperature in the insulated box under these conditions are shown in Dataset 2: Average temperature in an insulated box (https://data.mendeley.com/datasets/sz5dgkz7k8/1)

The temperature contour field was drawn via MATLAB by interpolating the measured temperature at 30 positions during stable conditions. The codes of this drawing are shown in Tanathepl/Temperature-contour (https://github.com/Tanathepl/Temperature-contour.git)

The air velocity field at X = 15 mm in a loaded horizontal box (aspect ratio ~ 1) with PCM on a sidewall under 20°C ambient, product initial temperature = 4°C with 20 mm gap below (condition 1) are shown in Figure 1. Air velocity and temperature fields at X = 250 mm are not shown here, they can be found in Leungtongkum et al. [1] (Figures 2a and 2a').

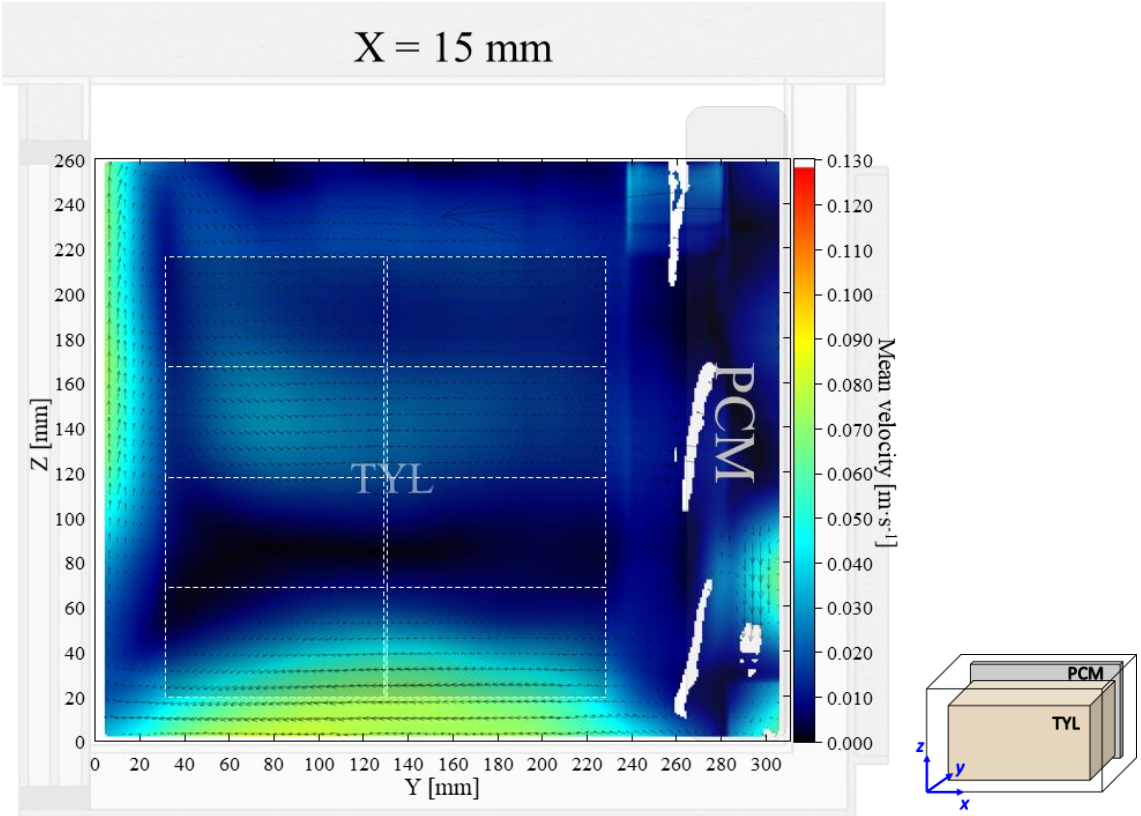

Figure 1: Air velocity field at X = 15 mm in a loaded horizontal box with PCM on a sidewall under 20°C ambient, product initial temperature = 4°C with 20 mm gap below. Note: unmeasured air velocity in white areas on the right can be explained by the refraction from PCM surface behind the laser sheet.

The air velocity field at X = 15 mm in a loaded horizontal box with PCM at the top under 20°C ambient, product initial temperature = 4°C with 20 mm gap below (condition 2) are shown in Figure 2. Air velocity and temperature fields at X = 250 mm are not shown here, they can be found in Leungtongkum et al. [1] (Figures 2b and 2b').

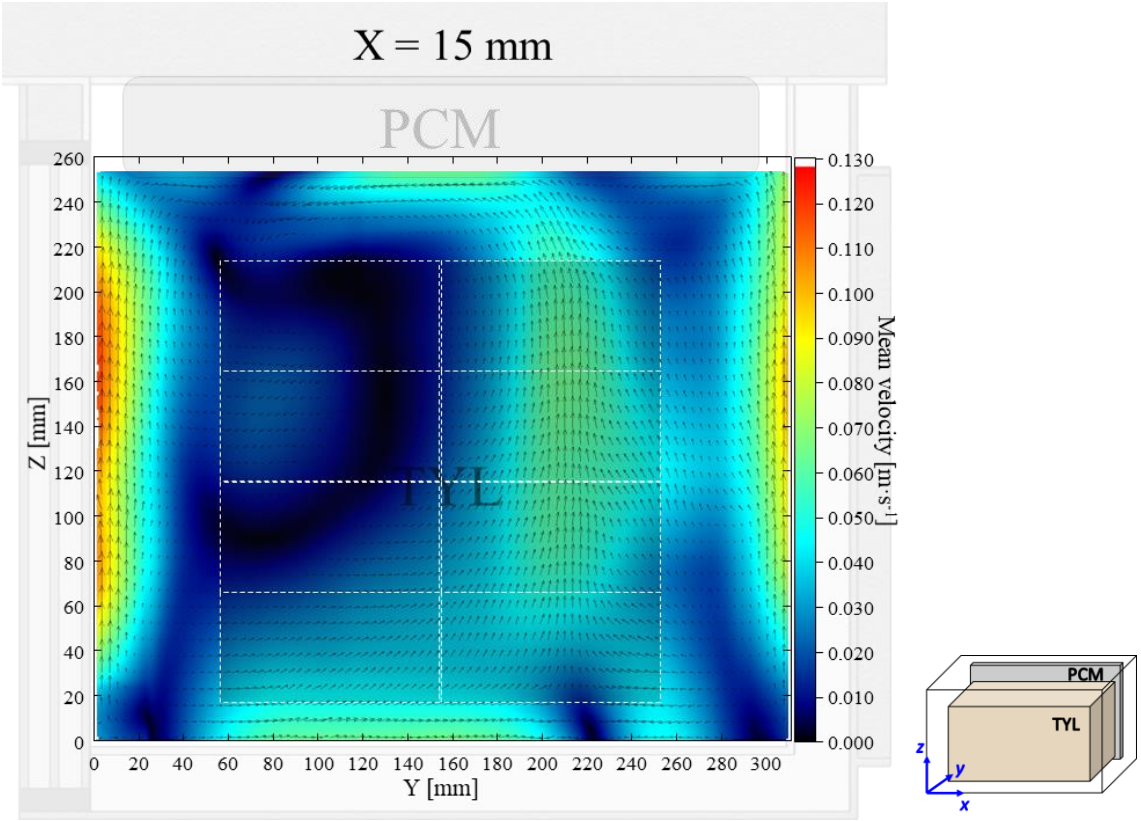

Figure 2: Air velocity field at X = 15 mm in a loaded horizontal box with PCM at the top under 20°C ambient, product initial temperature = 4°C with 20 mm gap below

The air velocity field at X = 20 mm in a loaded vertical box (aspect ratio = 1.7) with PCM on a sidewall under 20°C ambient, product initial temperature = 4°C with 20 mm gap below (condition 3) are shown in Figure 3. Air velocity and temperature fields at X = 250 mm are not shown here, they can be found in Leungtongkum et al. [1] (Figures 2c and 2c').

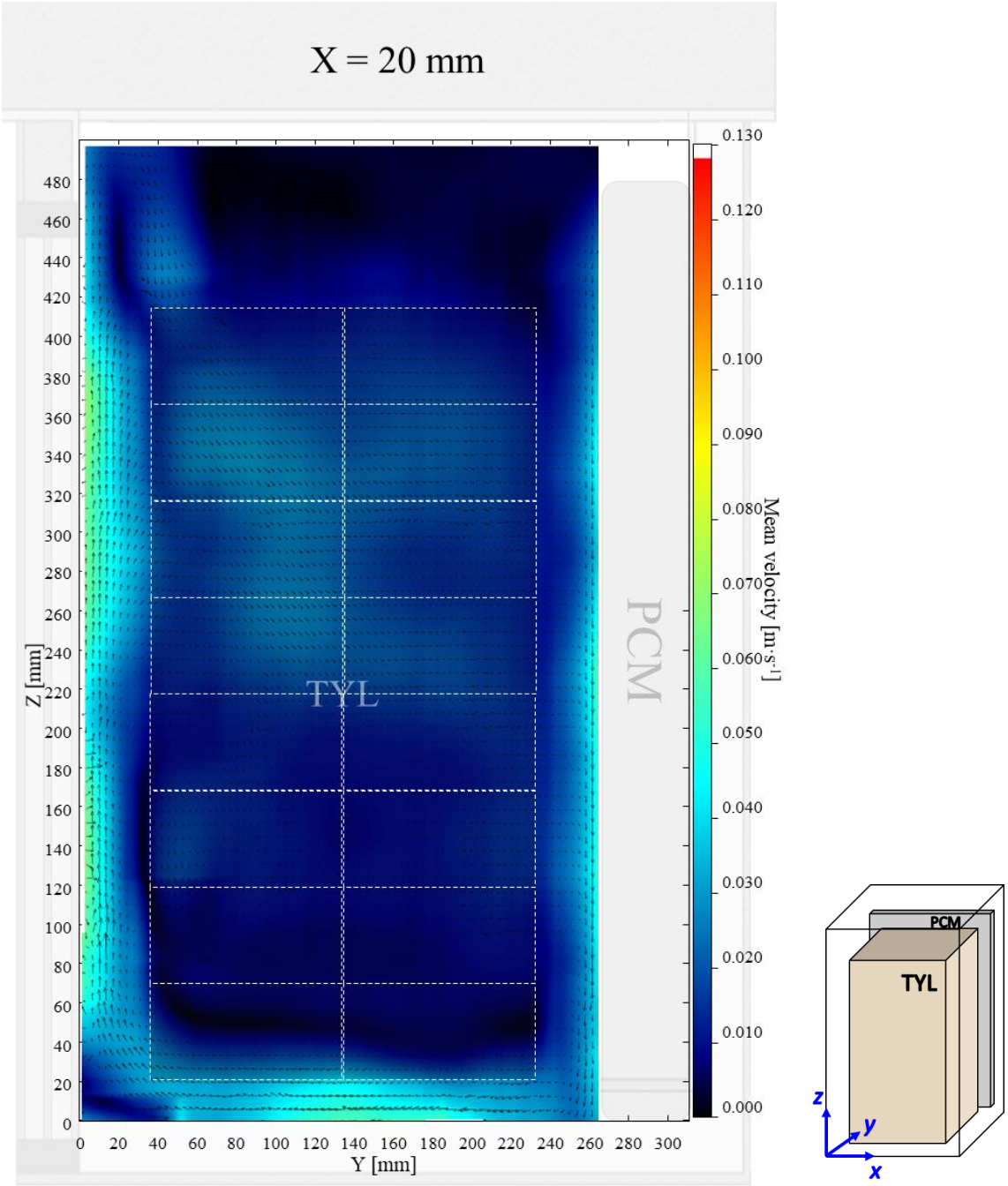

Figure 3: Air velocity field at X = 20 mm in a loaded vertical box with PCM on a sidewall under 20°C ambient, product initial temperature = 4°C with 20 mm gap below

The air velocity and temperature fields at X = 250 mm in a loaded horizontal box with PCM on a sidewall under 30°C ambient, product initial temperature = 4°C with 20 mm gap below (condition 4) are shown in Figure 4 and 5.

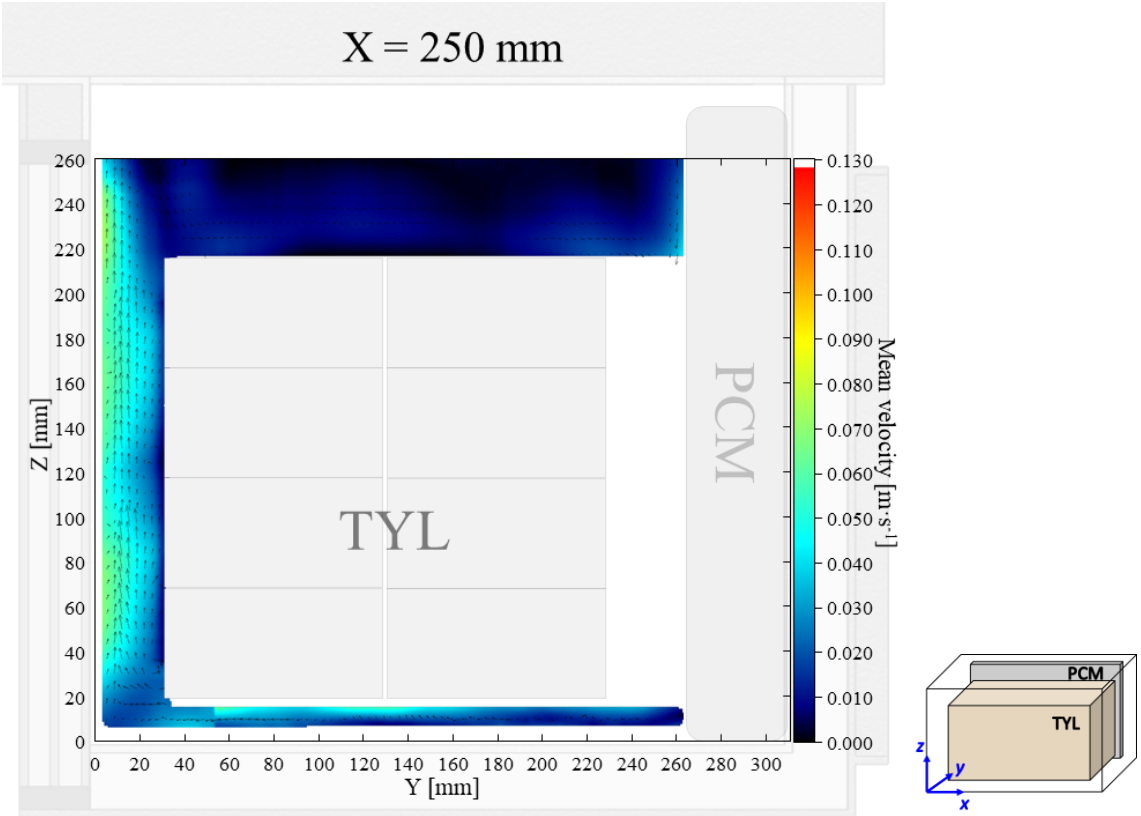

Figure 4: Air velocity field at X = 250 mm in a loaded horizontal box with PCM on a sidewall under 30°C ambient, product initial temperature = 4°C with 20 mm gap below. White area on the right represents the unmeasurable zone because of the inaccessibility of laser sheet.

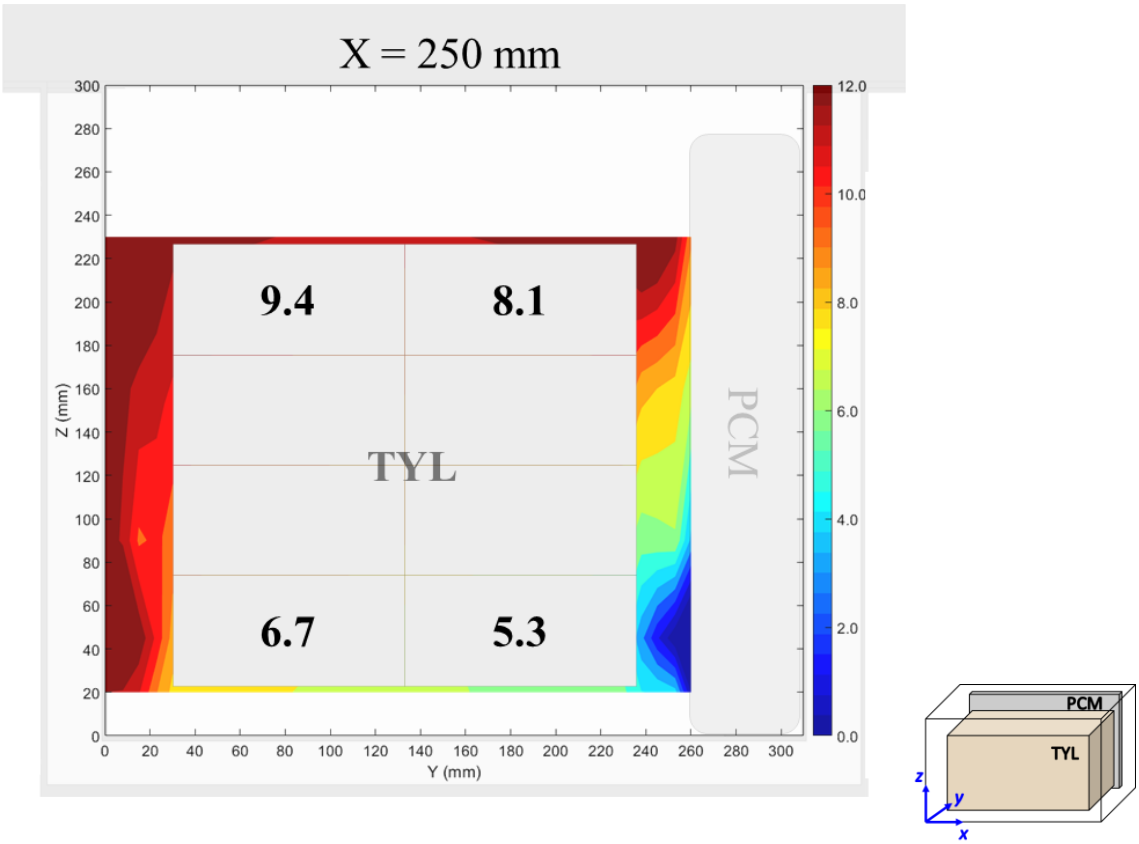

Figure 5: Air temperature field and core temperature of test product (°C) at X = 250 mm in a loaded horizontal box with PCM on a sidewall under 30°C ambient, product initial temperature = 4°C with 20 mm gap below

The air velocity field at X = 250 mm in a loaded horizontal box with PCM at the top under 10°C ambient, product initial temperature = 4°C with 20 mm gap below (condition 5) are shown in Figure 6. Temperature field at X = 250 mm are shown in Figures 3a of Leungtongkum et al. [1].

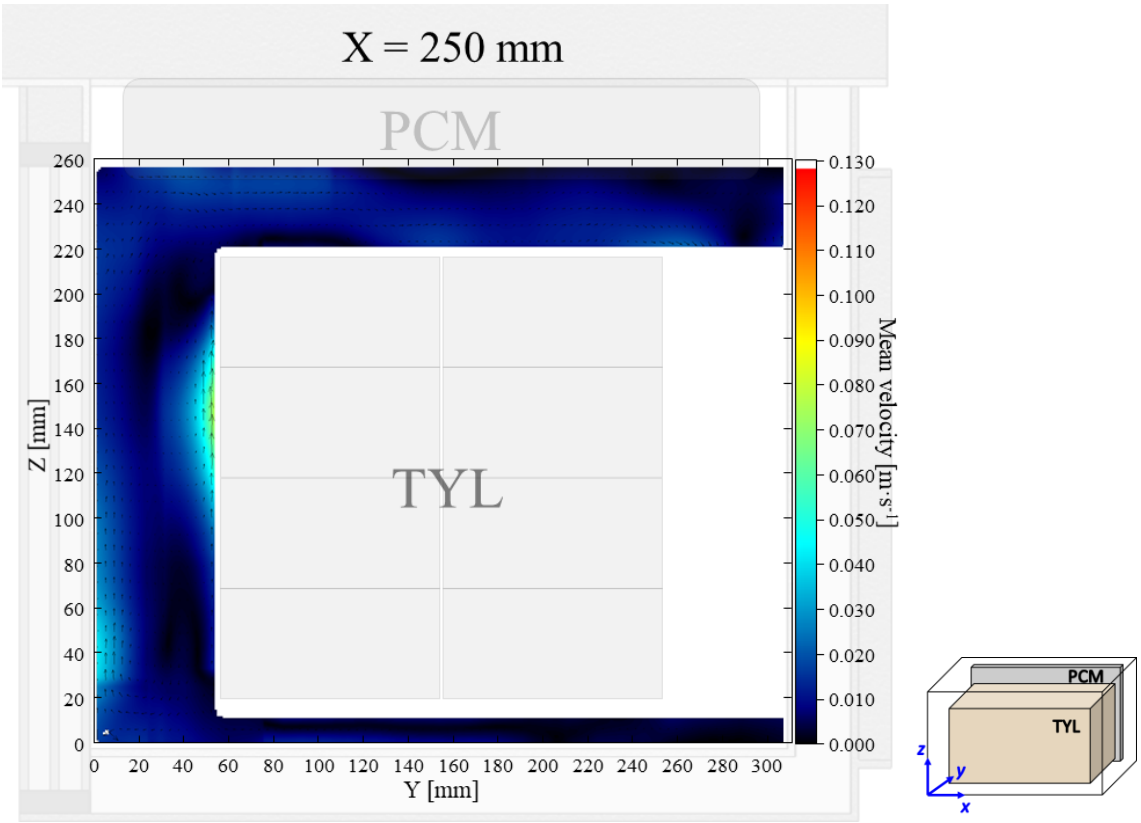

Figure 6: Air velocity field on the middle plane in a loaded horizontal box with PCM at the top under 10°C ambient, product initial temperature = 4°C with 20 mm gap below. White area on the right represents the unmeasurable zone because of the inaccessibility of laser sheet.

The air velocity field at X = 250 mm in a loaded horizontal box with PCM at the top under 30°C ambient, product initial temperature = 4°C with 20 mm gap below (condition 6) are shown in Figure 7. Temperature field at X = 250 mm are shown in Figures 3c of Leungtongkum et al. [1].

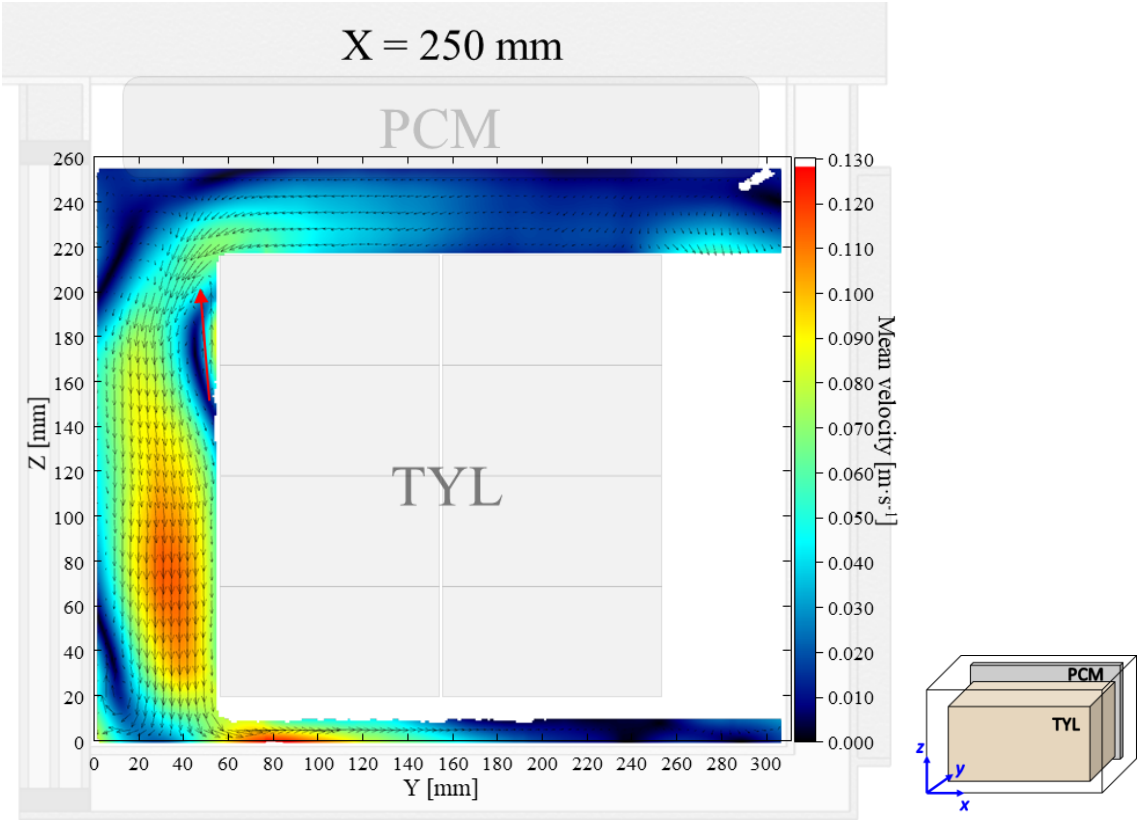

Figure 7: Air velocity field on the middle plane in a loaded horizontal box with PCM at the top under 30°C ambient, product initial temperature = 4°C with 20 mm gap below. White area on the right represents the unmeasurable zone because of the inaccessibility of laser sheet.

The air velocity field and temperature field at X = 250 mm in a loaded horizontal box with PCM on a sidewall under 20°C ambient, product initial temperature = 10°C with 20 mm gap below (condition 7) are shown in Figure 8 and 9.

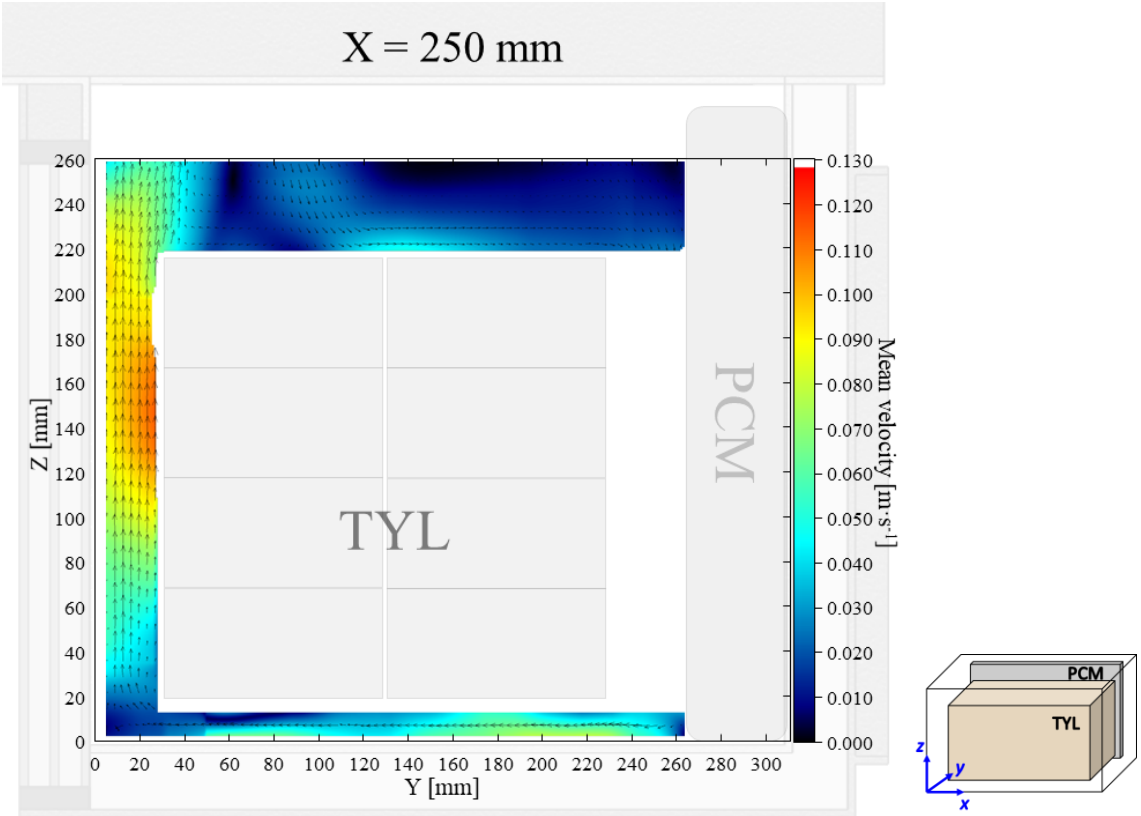

Figure 8: Air velocity field on the middle plane in a loaded horizontal box with PCM on a sidewall under 20°C ambient, product initial temperature = 10°C with 20 mm gap below. White area on the right represents the unmeasurable zone because of the inaccessibility of laser sheet.

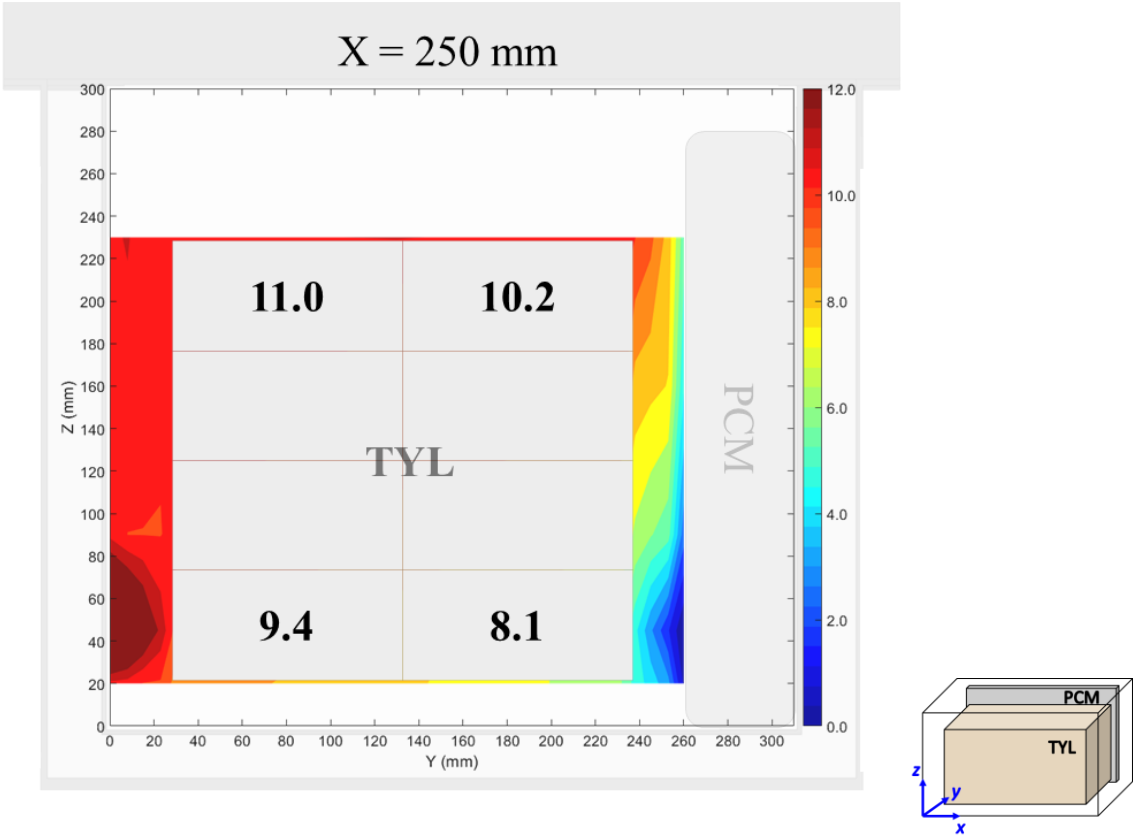

Figure 9: Air temperature field and core temperature of test product (°C) on the middle plane in a loaded horizontal box with PCM on a sidewall under 20°C ambient, product initial temperature = 10°C with 20 mm gap below

The air velocity field at X = 250 mm in a loaded horizontal box with PCM at the top under 20°C ambient, product initial temperature = 10°C with 20 mm gap below (condition 8) are shown in Figure 10. Temperature field at X = 250 mm are not shown here, it can be found in Leungtongkum et al. [1] (Figures 3d).

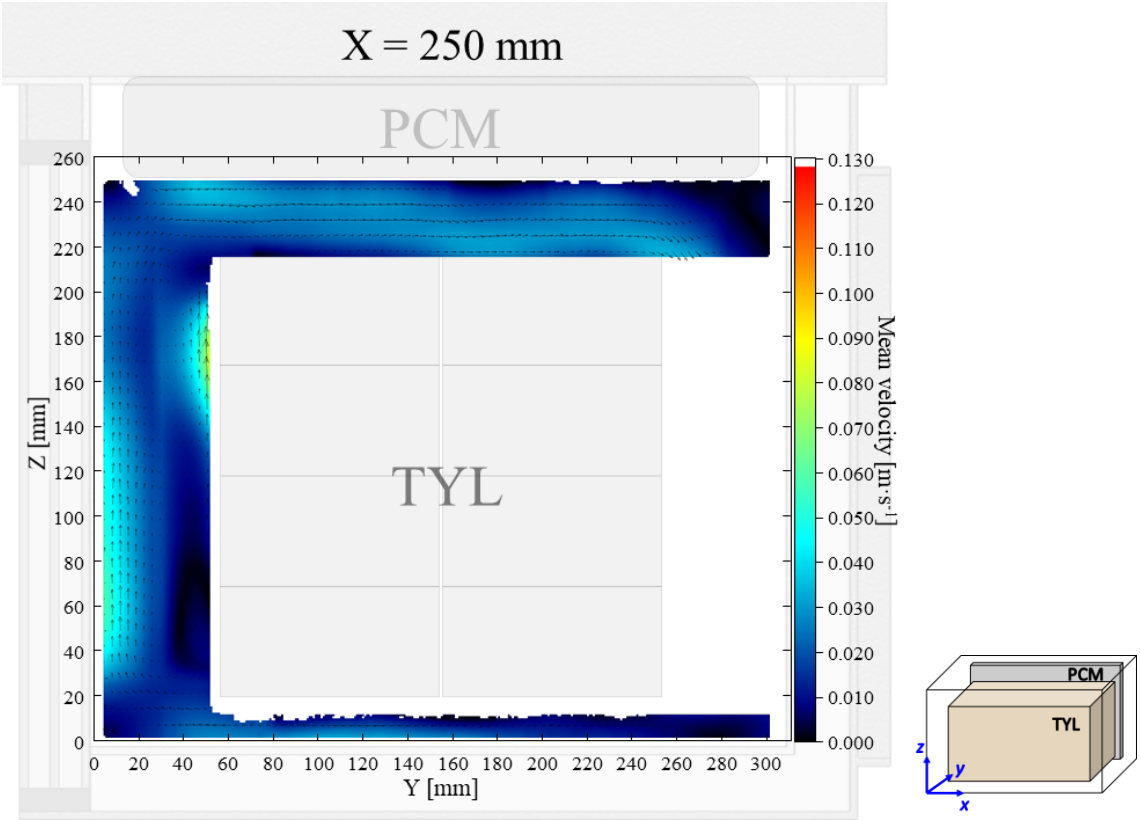

Figure 10: Air velocity field on the middle plane in a loaded horizontal box with PCM at the top under 20°C ambient, product initial temperature = 10°C with 20 mm gap below. White area on the right represents the unmeasurable zone because of the inaccessibility of laser sheet.

The temperature field at X = 250 mm in a loaded horizontal box with PCM on a sidewall under 20°C ambient, product initial temperature = 4°C without gap below (condition 9) are shown in Figure 11. Air velocity field at X = 250 mm are shown not shown here, it can be found in Leungtongkum et al. [1] (Figures 4d).

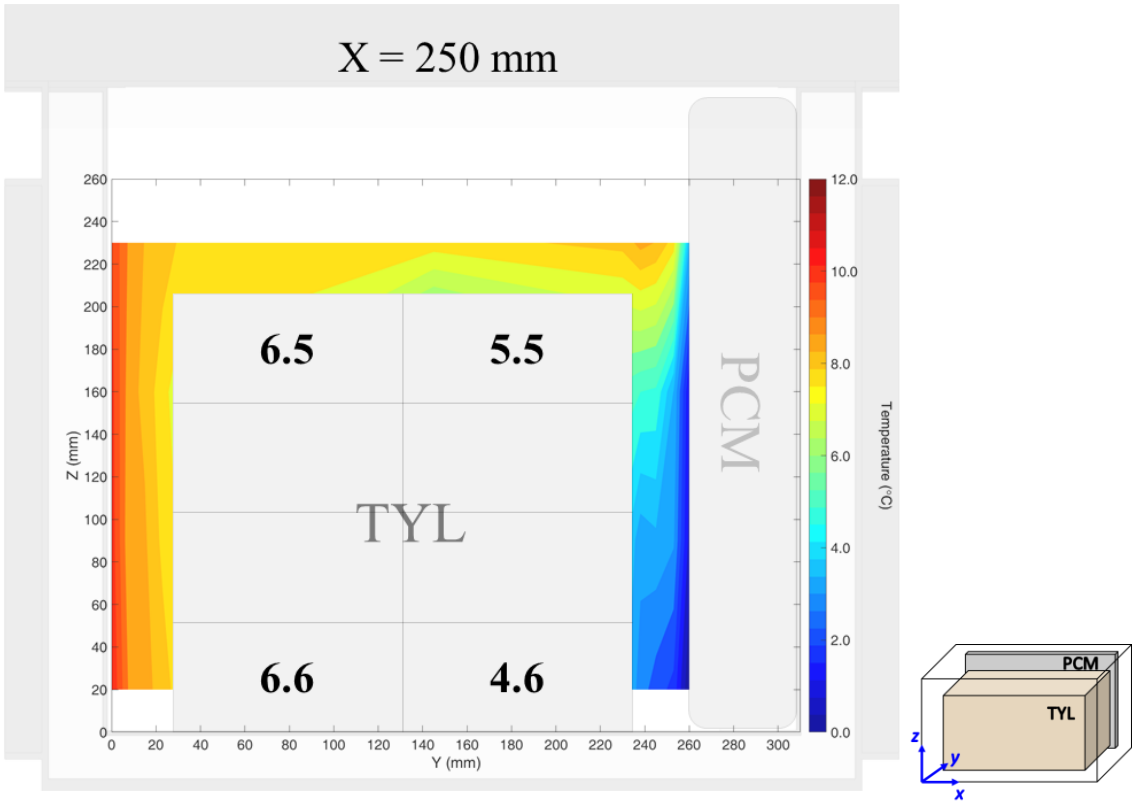

Figure 11: Air temperature field and core temperature of test product (°C) on the middle plane in a loaded horizontal box with PCM on a sidewall under 20°C ambient, product initial temperature = 4°C without gap below

The temperature field at X = 250 mm in a loaded horizontal box with PCM at the top under 20°C ambient, product initial temperature = 4°C without gap below (condition 10) are shown in Figure 12. Air velocity field at X = 250 mm are not shown here, it can be found in Leungtongkum et al. [1] (Figures 4b).

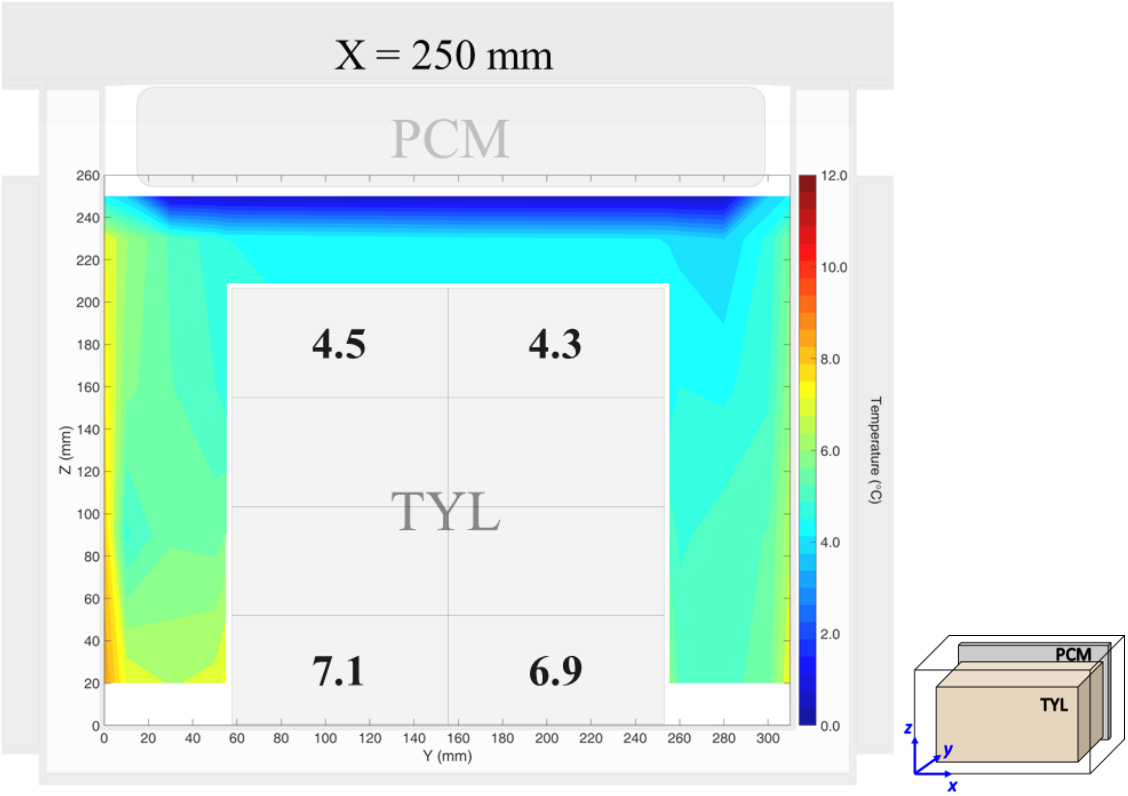

Figure 12: Air temperature field and core temperature of test product (°C) on the middle plane in a loaded horizontal box with PCM at the top under 20°C ambient, product initial temperature = 4°C without gap below

2. Experimental design, materials and methods

The material and methods described in detailed in Leungtongkum et al. [2] are shown succinctly below.

2.1 Material

The details of material and experimental setup description can be found in Leungtongkum et al. [2].

2.2 Thermal study

The box was loaded with 16 test product packs previously conditioned at 4°C or 10°C and a PCM slab whose initial temperature was at -2°C. The temperature measurement was carried out with 34 thermocouples (T-type thermocouples) on the surface and core of product located at the middle plane (x = 250 mm). The diagram showing thermocouples positions is in Figure 1 of Leungtongkum et al. [1]. The measurement started after the box closing until complete PCM melted without the box opening during the experiment during which the temperatures were recorded

continuously (every 30 s) using Agilent 34972A data acquisition unit (Agilent Technologies, CA, USA). The results of the stabilization period ranging from 400 min. to 600 min. were analyzed and compared. The temperature contour map was drawn by MATLAB with interpolation. More details of experimental setup for temperature measurement can be found in Leungtongkum et al. [2].

Figure 13 shows an example of temperature evolution at the bottom of a loaded horizontal box with PCM on a sidewall under 20°C ambient, product initial temperature = 4°C (condition 1). The average temperatures calculated from 400 min to 600 min were shown in Figures 5, 9, 11 and 12 to present the temperature field in stable condition.

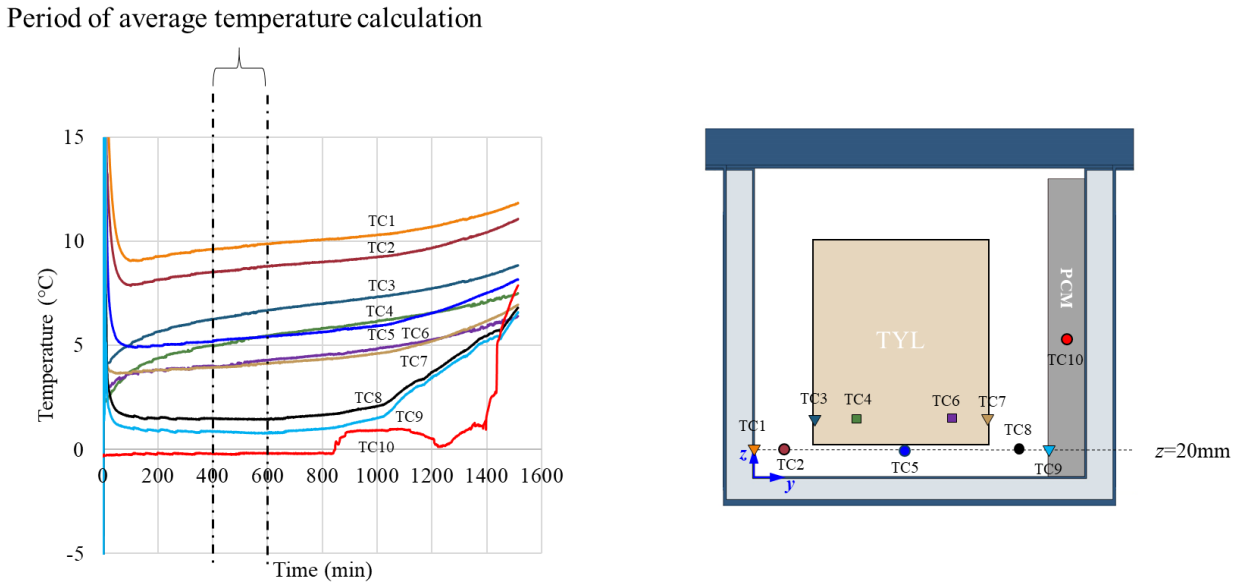

Figure 13: Temperature evolution at the bottom of a loaded horizontal box with PCM at sidewall under 20°C ambient, product initial temperature = 4°C with 20 mm gap below.

2.3 Airflow study

2.3.1 Instrumentation

The PIV device is constituted of three components: a double-pulsed Nd:YLF laser (527 nm wavelength, 10 mJ pulse energy), a high-speed 12-bit CMOS video camera (Photron, FASTCAM SA3; 1024 × 1024 pixels in resolution) fitted with a lens (Sigma; 105 mm, f/1:2.8) and a programmable timing unit (PTU-X) to ensure synchronization of the laser and the camera. Visualization of the airflow pattern is possible by the scattering of smoke particle during laser pulses. Oil-based particles (mean diameter 0.3 μm) were generated using a smoke machine (Antari, F-80Z). More detail on PIV system can be found in Leungtongkum et al. [2].

More details of image acquisition, image post-processing and experimental protocol can be found in Leungtongkum et al. [2].

Ethics Statement

This work did not involve human subjects, animal experiments and data collected from social media platforms.

CRediT author statement

Tanathep Leungtongkum: Conceptualization, Methodology, Investigation, Validation, Formal analysis, Software, Writing - Original Draft Preparation and Visualization **Denis Flick:** Methodology, Validation, Formal analysis, Writing - Review & Editing and Supervision **Nattawut Chaomuang:** Conceptualization, Methodology, Investigation, Validation, Formal analysis, Software, Writing - Original Draft Preparation, Visualization and Funding acquisition **Alain Denis:** Investigation and Software **Onrawee Laguerre:** Validation, Formal analysis, Writing - Review & Editing, Supervision, Project Administration, Funding acquisition.

Acknowledgments

King Mongkut's Institute of Technology Ladkrabang, Thailand (contract no. KREF156402), French Embassy in Thailand, and the National Research Institute for Agriculture, Food and Environment, France are gratefully acknowledged for their financial support. The first author, T. Leungtongkum, would also like to thank the Office of the Civil Service Commission of Thailand and Chulalongkorn University, Thailand for the award of his PhD scholarship. Thanks to LaVision for PIV technical support.

Declaration of interests

☒ The authors declare that they have no known competing financial interests or personal relationships that could have appeared to influence the work reported in this paper.

☐ The authors declare the following financial interests/personal relationships which may be considered as potential competing interests:

References

[1] T. Leungtongkum, D. Flick, N. Chaomuang, A. Denis, and O. Laguerre, "Influence of use conditions on heat transfer in an insulated box equipped with a phase change material," *J. Food Eng.*, vol. 357, p. 111644, Nov. 2023, doi: 10.1016/j.jfoodeng.2023.111644.

[2] T. Leungtongkum, O. Laguerre, D. Flick, A. Denis, S. Duret, and N. Chaomuang, "Dataset of experimental study investigation of airflow and heat transfer in an insulated box equipped with a phase change material," *Data Brief*, vol. 45, p. 108696, Dec. 2022, doi: 10.1016/j.dib.2022.108696.

[3] Y. Cengel and A. Ghajar, *Heat and Mass Transfer: Fundamentals and Applications*, 5th edition. New York, NY: McGraw-Hill Education, 2014.

[4] T. L. Bergman, A. S. Lavine, F. P. Incropera, and D. P. DeWitt, *Introduction to Heat Transfer*. Hoboken, NJ: John Wiley & Sons, 2011.

[5] B. A. Younglove and H. J. M. Hanley, “The Viscosity and Thermal Conductivity Coefficients of Gaseous and Liquid Argon,” *J. Phys. Chem. Ref. Data*, vol. 15, no. 4, pp. 1323–1337, Oct. 1986, doi: 10.1063/1.555765.

[6] ATP, *Agreement on the International Carriage of Perishable Foodstuffs and on the Special Equipment to be Used for Such Carriage: (ATP) as amended 6 July 2020*. United Nations, 2020. doi: 10.18356/6fa10b27-en.

[7] B. Wieneke, “PIV uncertainty quantification from correlation statistics,” *Meas. Sci. Technol.*, vol. 26, no. 7, p. 074002, Jun. 2015, doi: 10.1088/0957-0233/26/7/074002.

ARTICLE 8

The code of simplified heat transfer model for temperature prediction in an insulated box equipped with phase change material

Tanathep Leungtongkum[a,b*], Onrawee Laguerre[a] and Denis Flick[b]

[a]Université Paris-Saclay, INRAE, FRISE, 92761 Antony, France

[b]Université Paris-Saclay, INRAE, AgroParisTech, UMR SayFood, 91120 Palaiseau, France

*Corresponding author: Tanathep Leungtongkum, e-mail: tanathep.leungtongkum@inrae.fr, tel: (+33) 1 40 96 61 48

Abstract

This code presents a simplified heat transfer model based on zonal approach. It allows the temperature prediction (air and product) inside an insulated box with PCM (Phase Change Material as cold source) to maintain product at low temperature during food transport to assure its quality. The model involves airflow, conduction, convection and radiation. The studied geometry is a rectangular insulated box, with PCM on a sidewall and loaded with test product. The code requires a short calculation time and can be useful to researchers and stakeholders to study the effect of box design, PCM/product properties and mass and ambient temperature.

Keywords

Insulated box, Phase change material, Simplified model, Heat transfer, Temperature

Code metadata

Nr	Code metadata description	Please fill in this column
C1	Current code version	V1
C2	Permanent link to code/repository used for this code version	https://github.com/Tanathepl/temp-predict-box-pcm-side
C3	Permanent link to reproducible capsule	https://codeocean.com/capsule/1172946/tree
C4	Legal code license	MIT License
C5	Code versioning system used	None
C6	Software code languages, tools and services used	Python

C7	Compilation requirements, operating environments and dependencies	Package manager needed: conda Package needed: numpy and matplotlib.pyplot
C8	If available, link to developer documentation/manual	-
C9	Support email for questions	tanathep.leungtongkum@inrae.fr

1. Motivation and significance

Insulated boxes equipped with a phase change material (PCM) are commonly used to transport temperature-sensitive products. They are often used in the last-mile delivery of small product quantities when refrigeration equipment is unavailable. However, temperature abuse (spatial and temporal temperature variation) in the product loaded in an insulated box equipped with PCM is often observed mainly due to poor insulation, insufficient PCM mass and inappropriate PCM positioning.
An empirical approach is still mainly used in practice. To understand the real phenomena in the system, Computational Fluid Dynamic models can be used to predict the temperature field and its evolution with time. However, this requires significant calculation time and expertise in fluid mechanics. As an alternative, the simplified thermal model relating to this code can provide spatial and temporal temperature variation in an insulated box equipped with PCM with a short calculation time (less than 10 s using a computer with 64 GB of RAM). This short calculation time is vital to detect temperature abuse when it occurs in the cold chain. The stakeholders can immediately determine the impact on product temperature; thus, quality and safety and the appropriate actions can be implemented to reduce the damage. This code paper is linked with the research paper (Leungtongkum et al. 2023).

2. Simplified thermal model description

This model can be applied to an insulated box loaded by the product with PCM located at a side wall. During PCM melting, it releases cold and this allows to maintain low temperatures inside the box and assure sanitary quality throughout the supply chain. The code allows the prediction of air and product temperature evolution with time at different positions inside the box. The code can be used to study the effect of box dimension, insulation, product mass and its physical properties, PCM mass and its properties and ambient temperature in the supply chain.
The model considers a temperature heterogeneity inside the box, i.e., the difference between air, product surface and core, top and bottom, cold side (near the PCM), and warm side (near opposite wall). The product is considered as four blocks of length C with shell (C/4 length) and core (3C/4 length), Fig. 1. Airflow and heat transfer (conduction, convection, and radiation) in two dimensions (y and z directions) were considered. The model was validated by comparing the predicted air and product temperatures with the ones measured in a rectangular box loaded with test product (Tylose).

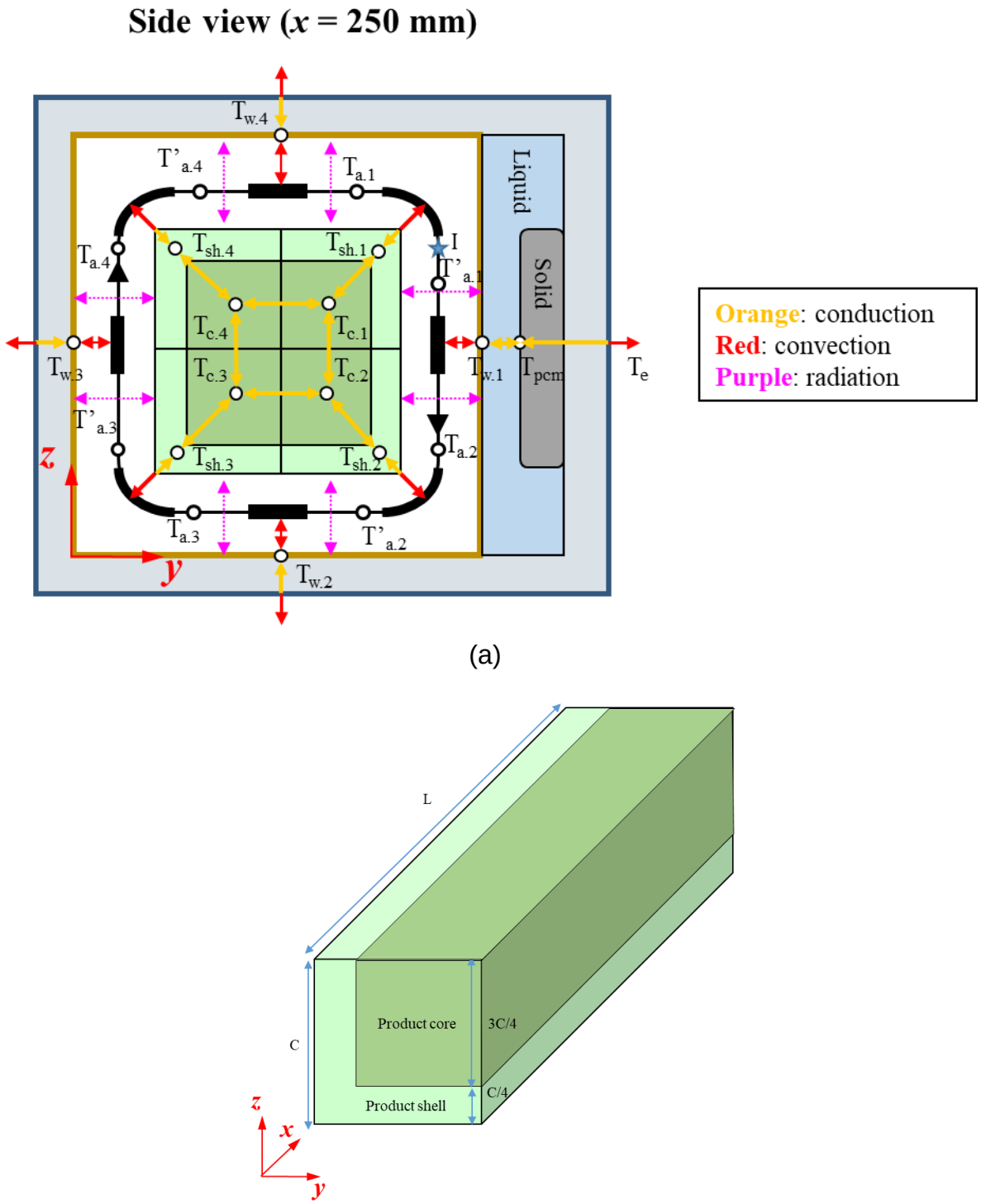

Fig. 1: Simplified 2D heat transfer and airflow diagram in an insulated box with PCM on a side wall (a) Front view and (b) Perspective view of a quarter of product

The model is based on the following assumptions:

- Heat transfer coefficient between internal air and solid surfaces (box walls, PCM container wall, product surface) is constant and is applied for the whole simulation period
- Air flows downward along the PCM container wall and then circulates in a clockwise loop along the other box walls. A mass flow rate of air is assumed as approximately proportional to the heat transfer coefficient.
- Thermal inertia of air (mass multiplied by the heat capacity) is assumed as negligible.

There are 12 solid zones and the following state variables describe the system at a given time:

- Average temperature in product shell: $T_{sh.n}$ when $n \in [1,4]$
- Average temperature in product core: $T_{c.n}$ when $n \in [1,4]$
- Wall temperature: $T_{w.n}$ when $n \in [1,4]$ where $T_{w.1}$ is the PCM surface temperature and $T_{w.2}$ to $T_{w.4}$ are of the internal walls

PCM is characterized by its temperature (T_{pcm}) and its ice fraction (φ). Air temperature evolves along the air circulation loop from $T_{a.n}$ to $T'_{a.n}$ when $n \in [1,4]$ by exchanging with the product shells and from $T'_{a.n}$ to $T_{a.n+1}$ when $n \in [1,3]$ and from $T'_{a.4}$ to $T_{a.1}$ by exchanging with the internal walls.

Some of the equations representing air or product heat balances and radiative heat exchanges are presented here.

Air temperature estimation from product shell and wall temperatures

The air at the top of the box (position I in Figure 1a) exchanges heat with wall 1 (PCM surface) and its temperature changes from $T'_{a.1}$ to $T_{a.2}$. The equation governing the heat balance between the adjacent air and wall 1 can be written in the same manner as that in a heat exchanger.

$$\dot{m}_a C_{p.a} dT_a = h_w (T_{w.1} - T_a) dA$$

$$ln\left(\frac{T_{a.2} - T_{w.1}}{T'_{a.1} - T_{w.1}}\right) = -\frac{h_w A_{w.1}}{\dot{m}_a C_{p.a}}$$

Finally, $$(T_{a.2} - T_{w.1}) = \alpha_{w.1}(T'_{a.1} - T_{w.1}) \text{ with } \alpha_{w.1} = exp\left(-\frac{h_w A_{w.1}}{\dot{m}_a C_{p.a}}\right) \quad (1)$$

where $\dot{m}_a$ is the mass flow rate of air [$kg \cdot s^{-1}$]

$C_{p.a}$ is the specific heat capacity of air [$J \cdot kg^{-1} \cdot K^{-1}$]

h_w is the heat transfer coefficient between air and internal wall [$W \cdot m^{-2} \cdot K^{-1}$]

$A_{w.1}$ is the area of wall 1 [m^2]

This approach is also used when air exchanges heat with the product shell, for example from $T_{a.2}$ to $T'_{a.2}$. This leads to eight equations involving the eight air temperatures. They can be expressed in a matrix form.

$$A \cdot T_a = B \Rightarrow T_a = A^{-1} \cdot B \qquad (2)$$

Where $A = \begin{bmatrix} -\alpha_p & 1 & 0 & 0 & 0 & 0 & 0 & 0 \\ 0 & -\alpha_{w.1} & 1 & 0 & 0 & 0 & 0 & 0 \\ 0 & 0 & -\alpha_p & 1 & 0 & 0 & 0 & 0 \\ 0 & 0 & 0 & -\alpha_{w.2} & 1 & 0 & 0 & 0 \\ 0 & 0 & 0 & 1 & -\alpha_p & 1 & 0 & 0 \\ 0 & 0 & 0 & 0 & 0 & -\alpha_{w.3} & 1 & 0 \\ 0 & 0 & 0 & 0 & 0 & 0 & -\alpha_p & 1 \\ 1 & 0 & 0 & 0 & 0 & 0 & 0 & -\alpha_{w.4} \end{bmatrix}$

$T_a = \begin{bmatrix} T_{a.1} \\ T'_{a.1} \\ T_{a.2} \\ T'_{a.2} \\ T_{a.3} \\ T'_{a.3} \\ T_{a.4} \\ T'_{a.4} \end{bmatrix}$ and $B = \begin{bmatrix} (1-\alpha_p)T_{sh.1} \\ (1-\alpha_{w.1})T_{w.1} \\ (1-\alpha_p)T_{sh.2} \\ (1-\alpha_{w.2})T_{w.2} \\ (1-\alpha_p)T_{sh.3} \\ (1-\alpha_{w.3})T_{w.3} \\ (1-\alpha_p)T_{sh.4} \\ (1-\alpha_{w.4})T_{w.4} \end{bmatrix}$

where α_p is the dimensionless convective heat transfer coefficient between internal air and product shell [-]

This allows to estimate the air temperatures from the product shell and box's wall temperatures.

Convective heat transfer coefficient can be estimated from free convection correlations or local temperature measurements. Air mass flow rate can be determined from a developed relation with heat transfer coefficient. More detail can be found in Leungtongkum et al. (2023).

Radiative heat exchange

The radiative heat exchange between the lateral surface of product block 1 ($T_{s.1}$ in K) and wall 1 (PCM surface, $T_{w.1}$ in K) is shown in Eq. 3.

$$q_{r.s1.w1} = \varepsilon_{w.1}\sigma\left({T_{s.1}}^4 - {T_{w.1}}^4\right)CL \qquad (3)$$

Where $q_{r.s1.w1}$ is the radiative heat exchange between surface of product block 1 and wall 1 [W]
$\varepsilon_{w.1}$ is the surface emissivity of wall 1 [-]
σ is the Stefan-Boltzmann constant = 5.67 x 10^8 W·m^{-2}·K^{-4}
C is the length of the cross-section of the product block [m]
L is the length of the product block [m]

More details can be found in Leungtongkum et al. (2023).

Temperature evolution of product, walls, and PCM, and PCM ice fraction evolution

Eq. 4 is the unsteady heat balance equations for the shell of product block 1 ($T_{sh.1}$).

$$MC_{p.sh}\frac{dT_{sh.1}}{dt} = \dot{m}_a C_{p.a}(T_{a.1} - T'_{a.1}) + \frac{T_{c.1}-T_{sh.1}}{R_{sh.c}} - q_{r.s1.w1} - q_{r.s1.w4} \qquad (4)$$

where $MC_{p.sh}$ is the thermal inertia of product shell [J·K^{-1}]

$R_{sh.c}$ is the heat transfer resistance from shell to core of product [K·W^{-1}]

$q_{r.s1.w1}$ is the radiative heat exchange between surface of product block 1 and wall 1 [W]

$q_{r.s1.w4}$ is the radiative heat exchange between surface of product block 1 and wall 4 [W]

More details can be found in Leungtongkum et al. (2023).

The same approach was applied to the 12 solid zones: shell of product blocks, core of product blocks and box internal walls.

Energy balance of PCM can be written for three different PCM states starting from solid state when its initial temperature is lower than melting temperature to liquid state after PCM is completely melted as follows.

- if PCM is completely frozen ($T_{PCM} < T_m$ and $\varphi = 1$) or completely melted ($T_{PCM} > T_m$ and $\varphi = 0$);

$$MC_{p.pcm}\frac{dT_{pcm}}{dt} = \frac{T_{w1}-T_{pcm}}{R_{pcm.w1}} + \frac{T_{ext}-T_{pcm}}{R_{w.ext.1}} \qquad (5)$$

- if PCM is partially melted ($T_{pcm} = T_m$ and $0 < \varphi < 1$);

$$M_{pcm}\frac{d\varphi}{dt}\Delta H_{fus} = \frac{T_{w1}-T_{pcm}}{R_{pcm.w1}} + \frac{T_{ext}-T_{pcm}}{R_{w.ext.1}} \qquad (6)$$

Where $MC_{p.pcm}$ [J·K^{-1}] is the thermal inertia of PCM (different for frozen or melted state)
$R_{pcm.w1}$ is the heat transfer resistance from PCM to its container wall [K·W^{-1}]
$R_{w.ext.1}$ is the heat transfer resistance from internal wall to the external [K·W^{-1}]
φ is the ice fraction of PCM [-]
ΔH_{fus} is the Latent heat of fusion [J·kg^{-1}]

Numerical solving

At a given time t, firstly, the eight air temperatures were deduced from the wall and product shell temperatures (Eq. 2). To solve the eight linear algebraic equations, the (8x8) matrix A was inverted with the numpy.linalg library. Then, the eight radiative heat

exchanges (example in Eq. 3) were calculated. Finally, the thirteen heat balance equations, i.e., 4 wall temperatures, 4 product shell temperatures, 4 product core temperatures (example in Eq. 4) and 1 PCM (temperature or ice fraction, Eq. 5 and 6, respectively) were applied with an explicit scheme with 5 s time intervals (shorter time intervals led to the same results).

3. Code application

This code serves two purposes, first, for a simulation under a transient state, i.e., temperature evolution with time which is the case from the beginning of delivery (PCM partially melted) to its end (PCM completely melted). Second, for a simulation under steady state, i.e., when temperatures in the box reach equilibrium values while PCM is not entirely melted.

The code allows the users to adjust the input parameters as follows:

- Box dimension and thermal conductivity
- PCM dimension, mass and fusion temperature
- Product dimension and physical properties
- Supply chain conditions, i.e., ambient temperature and duration

This code can be applied to a rectangular box loaded with the product of the same form and a PCM slab on a side wall. It can be applied to other configurations, but some modifications of the code are necessary.

The developed code was validated by comparing with the air and product temperatures measured (1-minute intervals) in an insulated box loaded with a test product made of methylcellulose. The experiment was undertaken in a test room with several controlled ambient temperatures. More detail on constitutive equations and experimental validation can be found in Leungtongkum et al. (2023).

4. Impact and conclusions

Food safety and security has become an urgent issue for several years. A way to maintain food quality is to store it under low temperature along the cold chain. Transportation using insulated boxes with Phase Change Material (PCM) can play an important role, particularly when cooling devices are not available (Robertson et al., 2017). Although food transport in an insulated box is practical and cost-effective, spatial and temporal temperature variations were observed (Laguerre et al., 2013; Mercier et al., 2017) and may cause temperature abuse. This is due to insufficient PCM mass or inappropriate PCM positioning while an empirical approach is still mainly used in practice.

This software paper presents a code of simplified thermal model to predict air and load temperatures in an insulated box equipped with PCM and exposed to different time-temperature profiles as in a supply chain. This simplified model based on a zonal approach and coded in Python language, is original comparing to the finite elements or finite volumes CFD models. This model gives good precision as it involves all three heat transfer modes, i.e., conduction, convection, radiation, and airflow inside the box. The simulation takes less than 10 s using a computer with 64 GB of RAM comparing with more than 3 days by CFD for the box with the same configuration. This model

can be easily used as a real-time prediction tool to estimate the food temperature inside an insulated box in a real supply chain. This code also allows the researchers and the stakeholders to investigate the effect of box configurations and operating conditions on spatial and temporal temperature variations. It is possible to couple this model with microbial growth models to quantify the contamination load in a supply chain until consumption. It can help stakeholders to limit food loss and waste and assure food safety.

Acknowledgements

The authors would like to thank Royal Thai Government Scholarship and Chulalongkorn University, Bangkok, Thailand for T. Leungtongkum's PhD scholarship. This research did not receive any specific grant from funding agencies in the public, commercial, or not-for-profit sectors.

References:

Laguerre, O., Hoang, H. M., & Flick, D. (2013). Experimental investigation and modelling in the food cold chain: Thermal and quality evolution. *Trends in Food Science & Technology*, *29*(2), 87–97. https://doi.org/10.1016/j.tifs.2012.08.001

Leungtongkum, T., Laguerre, O., & Flick, D. (2023). Tanathep / temp-predict-box-pcm-side (Version 1.0) [Software]. Available from https://github.com/Tanathepl/temp-predict-box-pcm-side.

Leungtongkum, T., Laguerre, O. & Flick, D. (2023) Simplified-model-for real-time-temperature-prediction-in-insulated-boxes-equipped-with-a-PCM [Source Code]. https://doi.org/10.24433/CO.1221916.v1

Leungtongkum, T., Laguerre, O., & Flick, D. (2023). Simplified heat transfer model for real-time temperature prediction in insulated boxes equipped with a phase change material. *International Journal of Refrigeration*. https://doi.org/10.1016/j.ijrefrig.2023.02.009

Mercier, S., Villeneuve, S., Mondor, M., & Uysal, I. (2017). Time-Temperature Management Along the Food Cold Chain: A Review of Recent Developments: Food preservation along the cold chain…. *Comprehensive Reviews in Food Science and Food Safety*, *16*. https://doi.org/10.1111/1541-4337.12269

Robertson, J., Franzel, L., & Maire, D. (2017). Innovations in cold chain equipment for immunization supply chains. *Vaccine*, *35*(17), 2252–2259. https://doi.org/10.1016/j.vaccine.2016.11.094